Experimental Investigation of the Suitability of the Track Structure Theory in Describing the Relative Effectiveness of High-LET Irradiation of Physical Radiation Detectors

Hansen, Johnny

Publication date:
1984

Document Version
Publisher's PDF, also known as Version of record

Risø-R-507

RISØ

Risø-R-507

Experimental Investigation of the Suitability of the Track Structure Theory in Describing the Relative Effectiveness of High-LET Irradiation of Physical Radiation Detectors

Johnny W. Hansen

Risø National Laboratory, DK-4000 Roskilde, Denmark
November 1984

Risø-R-507

EXPERIMENTAL INVESTIGATION OF THE SUITABILITY OF THE TRACK STRUCTURE THEORY IN DESCRIBING THE RELATIVE EFFECTIVENESS OF HIGH-LET IRRADIATION OF PHYSICAL RADIATION DETECTORS

Johnny W. Hansen

Abstract. The radiation effectiveness of heavy charged particles relative to radiations of fast electrons, x-rays, and gamma rays has been studied experimentally as well as theoretically for detectors of a thir nylon-based radiation-sensitive film and for the amino acid alanine. Experimental data have been compared with calculated data derived from a theoretical model describing the track structure of heavy charged particles.

The experimental work comprises dose-response characteristics from ^{60}Co γ-rays, 4- and 16-MV x-rays, 6-, 10-, and 20-MeV electrons, and 3-, 6-, and 16-MeV protons, 10- and 20-MeV α-particles, 21-MeV ^{7}Li ions, 42-MeV ^{14}N ions, 64-MeV ^{16}O ions, and 80-MeV ^{32}S ions.

The theoretical work presented here concerns an investigation and modification of parameters involved in the calculations, based on results obtained through the present experiments and published results from other investigators.

This report summarizes results already published or accepted for publication, attaches an appendix, and includes results not previously presented.

November 1984

Risø National Laboratory, DK 4000 Roskilde, Denmark

INIS-Descriptors: ALANINES; COLORIMETRIC DOSEMETERS; COMPUTER CALCULATIONS; DOSE-RESPONSE RELATIONSHIPS; DYES; EFFECTIVE CHARGE; ELECTRON BEAMS; ELECTRON DOSIMETRY; GAMMA RADIATION; HEAVY IONS; IONIZING RADIATIONS; LET; MATHEMATICAL MODELS; MICRODOSIMETRY; PARTICLE TRACKS; PROTON BEAMS; RADIATION DETECTORS; RADIATION DOSE DISTRIBUTIONS; RADIATION QUALITY; RBE; STOPPING POWER; X RADIATION.

This report is based on a thesis submitted to the Faculty of Science of the University of Copenhagen in partial fulfilment of the requirements for the licentiate degree (Ph.D).

ISBN 87-550-1049-0
ISSN 0106-2840

Risø Repro 1984

Forord

Denne rapport er udført som led i de betingelser, der skal opfyldes ved erhvervelsen af den naturvidenskabelige licentiatgrad på Københavns Universitet.

Projektet er udført under det Naturvidenskabelige Fakultet med lektor Leif Sarholt-Kristensen, Fysisk Laboratorium II, H.C. Ørsted Institutet, og lic.scient. Kjeld J. Olsen, Radiofysisk Afdeling, Københavns Amts Sygehus, Herlev, som videnskabelige vejledere. Arbejdet er imidlertid foregået i Acceleratorafdelingen, Forsøgsanlæg Risø, som ligeledes har ydet den finansielle støtte til projektet. Bestrålingerne med tunge partikler er foretaget på Niels Bohr Institutets Tandem Laboratorium, Risø.

Rapporten er skrevet på engelsk, fordi hovedparten af resultaterne allerede er publiceret eller indgivet til publikation i internationale tidsskrifter.

Dansk resumé

Experimentel undersøgelse af sporstruktur-teoriens anvendelse ved beskrivelse af fysiske detektorers effektivitet over for høj-LET stråling.

Projektet indebærer måling og beregning af den relative effektivitet af høj-LET stråling (LET = Linear Energy Transfer) over for gamma- og elektron stråling af to fysisk-kemiske detektorer, dye film og alanin. De eksperimentelle målinger er sammenlignet med teoretisk beregnede værdier udført på grundlag af en sporstruktur-model for tunge ioner, der oprindeligt er udviklet af Professor Robert Katz, University of Nebraska, USA.

Gennem arbejder af R. Katz og medarbejdere er det blevet påvist, at høj-LET stråling er et relativt begreb, som afhænger af uadskillige parametre for strålingens art og detektorens strålingsfølsomhed. Strålingen beskrives ved partiklens elektriske ladning og hastighed, mens detektorens følsomhed beskrives ved en ækvivalent størrelse af det strålingsfølsomme element i detektoren og ved størrelsen af den karakteristiske D_{37}-dosis, som er den dosis, hvorved 63% af detektorens maksimale respons er opnået. Sporstruktur-modellen beregner den relative effektivitet af høj-LET stråling ved at antage, at forskellen på høj-LET og fx gammastråling skyldes den inhomogene dosisfordeling omkring sporet af den tunge partikel, og at denne partikel påvirker detektoren gennem sekundær elektroner, delta-stråler, udsendt fra partikelsporet.

Som en del af beregningsgrundlaget indgår en eksperimentel måling af detektorens dosis-respons karakteristik for gamma- eller høj-energi elektronstråling. Denne karakteristik sammen med den beregnede dosisfordeling omkring en enkelt partikels spor omregnes til en fordeling i aktiveringssandsynlighed, der ved en integration over hele sporets diametrale udstrækning giver et aktiveringstværsnit. Partikelsporets laterale udstrækning i detektoren opdeles i en række tynde segmenter, for hvilke et middel-aktiveringstværsnit beregnes. Herefter beregnes et totalt tværsnit for partiklen i hele detektoren som et vægtet gennemsnit af aktiveringstværsnittene i forhold til den afsatte dosis i segmenterne. Aktiveringstværsnittet er et udtryk for detektorens strålingsfølsomhed over for den pågældende type stråling.

I det foreliggende arbejde er modellen anvendt på to typer detektorer, dye-film og alanin, der benyttes som dosimetre i høj-dosis området fra ca. 1 Gy til 1 MGy. Dye-film dosimetret består af en nylon matrice, hvori er indlejret

pararosanilin, der ved bestråling bliver farvet. Mængden af dannet farvestof måles i et spektrofotometer og er et udtryk for den tilførte dosis. Filmen fremstilles kommercielt i tykkelser på nominelt 5- og 50 µm. Alanin dosimetret er en aminosyre i fast form, som ved bestråling danner et yderst stabilt radikal. Radikaludbyttet, der er et mål for dosis, bestemmes ved elektron spin resonans spektroskopi. Alanin er et kommercielt tilgængeligt og billigt materiale.

Dye-filmen er undersøgt i et LET-område fra 2- til 6700 MeVcm^2/g, hvilket er middel LET i detektoren, med følgende typer af stråling: ^{60}Co γ-stråling, 10-MeV elektroner, 3- og 16-MeV protoner, 10-MeV α-partikler, 21-MeV ^{7}Li ioner, 42-MeV ^{14}N ioner og 64-MeV ^{16}O ioner. Alanin er undersøgt i et LET-område fra 2- til 20200 MeVcm^2/g, middel LET i detektoren, med følgende typer af stråling: ^{60}Co γ-stråling, 4- og 16-MV bremsestråliing, 6-, 10-, og 20-MeV elektroner, 6- og 16-MeV protoner, 20-MeV α-partikler, 21-MeV ^{7}Li ioner, 64-MeV ^{16}O ioner og 80-MeV ^{32}S ioner.

Der er i dette arbejde indført forbedringer i den af Katz foreslået beregningsprocedure. Der er således indført en eksponentiel rækkevidde-energi relation for sekundær elektronerne samt et forbedret udtryk for disse elektroners stoppeevne (stopping power). Dette har betydning for beregning af den radiale dosisfordeling omkring sporet af den tunge partikel og i bedre overensstemmelse med publicerede eksperimentelle data. Der er endvidere ændret i beregningen af "extended target dosis" og således i beregningen af aktiveringstværsnittet, som er blevet opdelt i et udtryk for tværsnit i "core" og i et udtryk for tværsnit i "track". "Core" betegner det strålingsfølsomme element, som tænkes ramt centralt af den indkomne ion, mens "track" betegner den del af mediet uden for core, som dækkes af sekundær elektronerne fra en enkelt ion. Det strålingsfølsomme element betragtes som en cylinder med aksen parallelt med ionens spor. Denne beregningsprocedure tillader på en nem måde, at også excitationsenergier fra sekundær elektronerne og den afsatte energi fra Auger elektronerne medregnes i dosisfordelingen, hvilket især har betydning for detektorer, som er følsomme over for excitationsenergier. Endvidere har en tilpasning af udtrykket for ionens effektive ladning betydet større overensstemmelse mellem beregnet stopping power for ionerne og publicerede eksperimentelle data. Disse ændringer har tilsammen medført en bedre overensstemmelse mellem beregnede og eksperimentelle værdier for ionernes relative effektivitet.

Arbejdet har vist, at dye-filmen har sublinear dosis-respons karakteristik, og er således ikke en ideel detektor for sporstruktur-modellen. Resultaterne er dog gode og inden for den eksperimentelle usikkerhed, sålænge filmen er en tynd detektor i forhold til ionens rækkevidde. Stoppes ionen imidlertid helt i filmen, er overensstemmelsem mellem beregnede og eksperimentelle værdier mindre god. Forsøg med nedbremsning af litium- og ilt ioner i en stak af tynde film har vist, at beregningerne er i relativ stor uoverensstemmelse med eksperimentelle data i området omkring ionens Bragg-peak, d.v.s. for energier under 1 MeV/amu. Resultater med alanin dosimetret, som er en ideel detektor for modellen, er meget tilfredsstillende, også selvom ionerne stoppes helt i detektoren. Dette viser, at beregningsmodellen giver gode resultater, når detektoren er ideel, men at modellen delvis mangler evnen til at regne på systemer, som ikke er i fuld overensstemmelse med kravene til en ideel detektor.

Det foreliggende arbejde viser, at modellen på trods af visse mangler er velegnet til at beregne den relative effektivitet og til at forudsige dosis-respons for en fysisk-kemisk detektor bestrålet med tunge ioner. Andre arbejder har vist, at modellen er velegnet til beskrivelse af cellulære systemers response på dosis fra tunge ioner og fra neutroner, hvorved modellen får betydning ved stråleterapi med høj-LET stråling og i helsefysiske sammenhænge, især da effekten af små doser kan beregnes.

Modellen benytter på visse områder unødvendigt grove tilnærmelser, fx vedrørende vinkelfordeling af sekundær elektronerne og Poisson fordelingsfunktionen for aktiveringssandsynlighed som funktion af dosis. Disse tilnærmelser bør ændres, hvorved modellen vil opnå en større fleksibilitet og give bedre resultater. Som helhed betragtet er modellen baseret på et sundt grundprincip og er den eneste beregningsprocedure, der på nuværende tidspunkt er i stand til at forudsige den relative effektivitet for høj-LET stråling.

CONTENTS

1. INTRODUCTION

Generally radiation dosimetry concerns the use of low-LET radiation of fast electrons, x-ray or γ-ray photons for which the absorbed dose is a sufficient description of the radiation field in terms of response to the radiation action. In the case of high-LET radiation of, e.g., neutrons or heavy charged particles a completely different situation exists. The radiation field within the absorbing medium now consists of different kind of radiations, such as primary and secondary ions, secondary electrons and electromagnetic radiation all of which will interact differently with the medium and thus contribute to the total radiation action in a very complex way. The result is that the measurement of absorbed dose no longer suffices to describe the effect we are seeking, as the correspondence between absorbed dose and its effect is without immediate coherence.

A few models based on microdosimetric considerations have been put forward in order to correlate experimental data from high-LET irradiations of biological[1,2] and physico-chemical[3-6] systems with calculations. The aim has been to predict the radiation effectiveness as a function of the linear energy transfer, LET, of high-LET particles. In this work LET is equivalent to LET_{∞}. The delta-ray theory of track structure originaly developed by Katz[7-12] seems to be a promising model, which at present is the only theory being able to predict a relative effectiveness of high-LET radiation for most physical and chemical radiation-sensitive media, once a few parameters obtained from low-LET radiation are known. For biological systems additional parameters obtained from experiments with high-LET radiation must be known as well.

The present work deals with the theoretical model of Katz et al., which predicts the radiation effectiveness of heavy charged particles and as such the dose-response relationship once certain characteristics are known about the absorbing medium irradiated with low-LET radiation. The model is investigated experimentally as well as theoretically and the procedures of calculating the radial dose distribution have been improved. The procedure of calculating the dose to the core is different from the one used in the original work of Katz.

The conceptual theory will shortly be outlined in an introductory manner in order to facilitate a general survey before a detailed description is given in the following section. The track structure theory is fundamentally based

upon the observation that track effects in different detector systems indicate that secondary and higher-order electrons, ejected from the path of an energetic heavy charged particle, are chiefly responsible for the radiation effects. Radiation effects of, e.g., γ-rays and high-energy electrons are as well caused by low-energy electrons generated through interactions of the primary radiation with the medium. But while the dose imparted by high-energy photons and electrons, low-LET radiation, is homogeneously distributed in the medium, the dose from heavy charged particles, high-LET radiation, is highly inhomogeneously distributed around the path of the individual emerging particle. Hence, by taking these observations into account the theory proposes that the difference in radiation effect between low- and high-LET radiation is due to differences in dose distribution, and that the response of a detector to high-LET radiation can be calculated from parameters of low-LET radiation. The problem then of determining the effectiveness of high-LET radiation concentrates on finding the dose distribution around the particle track and on determining the dose-response characteristic of the detector from experiments with low-LET radiation.

The track structure theory assumes that any detector consists of radiation sensitive elements in the shape of cylinders or spheres, the size of which is characteristic for the individual detector. The radiation sensitive element responds to the average dose absorbed in the element in accordance with a probability function fitted to mimic the dose-response curve for low-LET radiation. This function is convoluted into the function of radial dose distribution thus forming a function of radial distribution of probability for the radiation effect surrounding a single particle. Hence, to consider the total effect from a particle at all distances from the particle's path, an integration of the probabilities must be made over the detector volume being affected by the secondary electrons generated by the particle. This integration yields the total cross section for an effect which, when normalized to the total energy deposited by the particle, leads to the radiation sensitivity of a detector to high-LET radiation. The radiation sensitivity of a detector to low-LET radiation is given by the reciprocal of the characteristic D_{37}-dose obtained from the low-LET dose-response curve, where D_{37} is the dose at which 63% of the maximum achievable response has been obtained. The relative effectiveness of high-LET radiation to a detector is then obtained by the ratio between the radiation sensitivities for high-LET radiation and low-LET radiation.

The shape of the low-LET dose-response curve is of great importance for determining the dose response for various types of high-LET radiation. If the dose-response curve for low-LET radiation is purely exponential, the dose response for any ionizing radiation will be exponential as well, and the effectiveness relative to low-LET radiation will, according to the theory of Katz, never exceed unity. In biological systems the dose-response curve obtained for low-LET radiation mainly exhibits a shoulder. This is why the shape of the dose-response curve may be different for high-LET radiations and the relative effectiveness may become greater than unity.

In the following section 2 the concept of relative effectiveness of ionizing radiation is described as is the δ-ray theory of track structure used in theoretical treatment of the radiation detectors dealt with in this work. Section 3 describes the radiation detectors, and section 4 the experimental equipment. Section 5 describes the procedures of measuring the dose-response functions and the uncertainties involved in these measurements. Section 6 deals with the experimental and theoretical results, parts of which are already published[13-20]. In section 7 the results are discussed, and finally in section 8 concluding remarks summarize arguments for and against the theory in its present state and outline alternative suggestions for a future trend towards the ideal model. Section 10 is an appendix, which includes detailed calculational procedures and a description and listing of the Algol computer program "REINT" used in the present calculations of relative effectiveness. Published and submitted articles[16-20] are attached to this work.

2. DESCRIPTION OF THE TRACK STRUCTURE THEORY

2.1 The concept of relative effectiveness of radiation

When speaking of the response of a medium to ionizing radiation of various kinds we use a concept called the relative effectiveness, RE, or (in the case of biological systems) relative biological effectiveness, RBE, and express it as a function of the linear energy transfer, LET. The relative effectiveness of high- to low-LET radiation is defined as the ratio of the doses of the radiations being compared, which produce the same response under identical target conditions[21,22]. Different biological systems display a marked varia-

tion in their RBE-LET characteristic with the value of LET for maximum RBE varying by an order of magnitude from one system to another, Fig. 1. Furthermore, cells show initially an increase in RBE with increasing LET followed by a decrease at very high LET, whereas bacteria systems like most physical and chemical radiation detectors display a monotonic decrease in relative effectiveness with increasing LET and with RE always equal to or less than unity. High-LET radiation is often arbitrary defined as a radiation quality having LET well above that of electrons. But in view of the above mentioned it should rather be defined as a radiation quality that in a given medium results in a radiation effectiveness relative to that of high-energy photons and electrons differing from unity. This definition, however, may include electrons below 500 eV as being defined as high-LET particles (see the following section 2.2).

As a fast heavy charged particle slows down in a medium the LET increases to a maximum at the far end of the particle range, the Bragg peak, whereafter the LET decreases again. The relative effectiveness is a function of LET and particle velocity and depends further on the stopping medium. For most physico-chemical media the relative effectiveness, RE, decreases monotonically with increasing LET. But as the stopping particle beyond the Bragg peak has lost most of its energy and only moves very slowly, RE decreases with decreasing LET. Hence, RE is a double-valued function of LET. For biological systems, however, where the survival curve as a function of dose has a shoulder at low doses due to the repair mechanism, the relative biological effectiveness, RBE, at first increases monotonically with LET to a maximum and then decreases monotonically for increasing LET. As for physico-chemical media biological systems as well show a decrease in RBE beyond the Bragg peak of the penetrating particle. Thus RBE is a multi-valued function of LET for biological systems.

Even where it is merely a question of correlating dose and response proportionately the situation quickly gets complicated, since one must correct for the particle type, energy- and slowing down spectrum of the penetrating particles, as well as for the type of medium. The use of RE or RBE as simple conversion factors for calculating the response of a given dose is not a particularly useful method and in most cases it will give the wrong result.

2.2. The action of low- and high-LET radiation

The response of ionizing radiation on physical and chemical radiation detectors as well as on biological systems results from excitations and ionizations from secondary and higher-order generations of electrons, which are ejected from the atoms and molecules of the medium by the incident primary radiation. The energy deposited in the medium causes bond rupture, radical formation, and physico- and chemical changes, which are detectable in different ways.

It has been known for a long time that the differences in observed effect mainly arises from the time scale with which the secondary electrons are generated and their spatial distribution, and to a much lesser extent from the nature of the events themselves[24] (e g. radical formation, breaking of DNA), as long as the energy of the primary radiation remains above 10 keV. Gamma-ray photons and high-energy electrons distribute their energy homogeneously in the medium because of multiple scattering (Compton processes) and the relatively long range of the secondary electrons, the maximum energy of which based on the definition can be half of that of the primary electrons. Heavy charged particles essentially move in straight lines losing only a small fraction of their energy per collision; they distribute their energy very inhomogeneously in the medium through the ejected low-energy electrons, the δ-rays. The maximum energy and range of the δ-rays, however, are only small fractions of that of the primary particle.

The track of a heavy ion is constituted by a core of clusters, which consist mainly of very low-energy Auger electrons, excited atoms and ions, and a penumbra of more energetic δ-rays clearly separated from the core. The energy of the heavy ion is transferred mainly through inelastic collisions with the atomic electrons of the medium generating ionizations and excitations[25]. At particle energies below 10 keV/amu (atomic mass unit) elastic collisions begin to have some influence and are dominant at energies below 1 keV/amu, where the energy is dissipated mainly through displacement of the atoms of the medium and through vibrational motion[25,26] The δ-rays deposit their energy through coulomb interactions by ionization and excitation of the molecules of the medium.

The response of various detectors to different kinds of low-LET radiation, e.g. electrons and photons of different initial energy spectra, has been widely studied by many investigators[8,9], and differences in response seem to

be relatively infrequent in physico-chemical media. For many physical detectors the dose-response function is approximately linear at low doses and saturates exponentially at high doses, and the response is a single-valued function of dose within a large range of initial photon and electron energies. Detailed Monte Carlo calculations[24] of slowing-down spectra and yields of different kind for electrons in water at initial energies from 1 keV to 1 MeV have shown that the energy spectrum of electrons at energies less than 1 keV is essentially independent of the initial energy of the primary electron. Further, the number of interactions per unit energy deposited is essentially independent of the primary energy. This may lead to the conclusion that differences in relative effectiveness for different radiations cannot be ascribed to differences in secondary electron spectra, as long as the primary energy of the electrons is above 1 keV. Recent investigations, however, have shown that secondary electrons generated by x-rays of energy below 1 keV are more efficient in producing effects in some biological systems[27,28] than are electrons of higher energies. Observations[29] of Auger electrons in some amino acids have revealed a lowered efficiency as compared with electrons of higher energies. It must be noted here that high-LET irradiation of biological multihit systems, see section 2.3, may lead to an RBE above unity, whereas the RE of one-hit systems always is below unity. As a first approximation, however, the effect of electrons and photons is considered to be the same for all energies. The effort then has been concentrated on calculations of the energy distribution around a heavy charged particle and on relating this distribution in energy to a distribution in induced effect, which primarily concerns generation of radicals.

2.3 The stochastic process of radiation action

As present work comprises investigations of two radiation detectors for which the radiation action can be considered as single-hit processes, the theoretical considerations will be concentrated on single-hit processes. A "hit" is defined[30] as a quantized interaction which implies that one event under consideration takes place in the sensitive element of the medium and initiates an effect. It is assumed that the medium consists of identical sensitive elements, which may be either atoms or molecules embedded in a more or less passive matrix acting as an energy transfer medium. Once the sensitive element has been activated it will in principle stay activated despite being hit several times. The amount of excitation and ionization energy deposited by secondary electrons is taken to be a measure of the density of hits in the

hits in the irradiated medium.

The radiation action may be considered as a stochastic process, i.e. a succession of random events, and can thus be described in terms of a probability for activation of a sensitive element. The probability function describing the fractional number of sensitive elements being hit can be expressed by a Poisson distribution[30] as

$$P = 1 - \exp(-\bar{D}/D_{37}) \qquad 2\text{-}1$$

where $\bar{D}$ is the average dose deposited and D_{37} is a characteristic dose for the medium corresponding to each element receiving one hit on the average. D_{37} is the dose at which 37% (or 1/e) of the sensitive elements are not being activated by the radiation. If the medium is uniformly irradiated to the dose $\bar{D}$, then the average number of hits per sensitive elements is $\bar{D}/D_{37}$. The normalized dose-response of a one-hit detector follows the expression given by eq. 2-1.

According to the definition[30] an ideal one-hit detector has the following properties: a) a linear dose-response up to doses comparable to D_{37}, the characteristic dose; b) absence of dose-rate effects since the sensitive element may be activated by a single electron, and fading or recombination is disregarded; c) in a double-logarithmic plot all dose-response curves will be 45°-lines at low doses no matter if the radiation is low- or high-LET; and d) the relative effectiveness, RE, will decrease nonlinearly with increasing z^2/β^2, and LET, and be multi-valued, i.e. exhibit more values of RE for the same value of LET. The relative effectiveness of a medium will be uniquely described only through a combination of z^2/β^2, or LET, and β, where z and β are the effective charge and relative velocity of the penetrating ion, respectively. Throughout this work z is to be considered as the effective charge of the moving ion. Further, for a one-hit detector where activation may be brought about by a single electron passing through the sensitive element, RE must always be less than or equal to unity. This will be shown in the following section 2.4.

One-hit detector response has been shown to have quite general applicability to various kinds of ionizing radiation detecting systems[9,31,32]. One-hit response is found in many systems and includes a) enzyme and virus inactivation[7], b) single-strand breaks in DNA[9], c) free radical production in, e.g., the ferrous sulphate Fricke dose meter[33] and several amino acids[32],

d) colour center formation in cobalt glass and in dye film[34], scintillation counters[9], some peaks in thermoluminescent dose meters[9], and e) photographic emulsions[9,35]. In these systems the detector response is characterized by two macroscopic parameters, namely the characteristic D_{37}-dose obtained for high energy photons or electrons, and the radius a_0 of the radiation-sensitive element. In all cases the response to dose declines with increasing values of LET of the incident radiation, is multivalued and non-linear in LET, the latter becoming more pronounced for the more sensitive radiation detecting systems, i.e. for decreasing characteristic D_{37}-dose. As the one-hit response to beams of photons or electrons is interpreted as an observed effect after passage of a single electron through the sensitive element, then some physical detectors (e.g. most glow peaks in TL dose meters[36] and some nuclear emulsions[9,37]) and biological cells[9,31] require the passage of more than one electron through the sensitive element site in order to create an observed effect. The sensitive element site of these systems consists either of several targets each of which have to be hit once (e.g. inactivation of a cell nucleus), or the element must be hit several times (e.g. TL dose meters) before the effect is observed. A single-hit multi-target system or a multi-hit system may in a certain dose range be described by eq. 2-1 raised to the power of m, where m is a quantized number reflecting the number of targets in the sensitive element site, or the number of hits necessary to achieve an observed effect. Such a system has a supra-linear dose-response characteristic with m being the slope of the linear part of the double logarithmic curve. These systems will not be dealt with in this work.

The size of the sensitive element is to a certain extent a fitted parameter, which can be more precisely determined once a few dose-response data from high-LET irradiation of the medium are known. An approximate estimate, however, may be derived from greatly simplified calculations from target theory[30], which, from a knowledge of the radiation sensitivity of the medium and the mean energy necessary to create an ion pair, determines the volume of the sensitive element considered as a sphere. This will be dealt with in section 7.3. For a physico-chemical detector the approximate size of the sensitive element may simply be the size of the sensitive molecule. The structure, however, of the sensitive element may not necessarily be clearly defined, but only considered as a target for the radiation.

2.4 Activation cross section and RE

The dose deposited to the sensitive elements of the medium after irradiation with heavy charged particles is calculated by grouping these elements into volumes which lie along iso-dose contours as cylindrical volumes whose axis is the path of the ion. Such an iso-dose shell is shown in Fig. 2. According to the track structure theory the elements between these shells will respond to the local dose deposited there by the generated δ-rays, as if the elements were part of a larger system uniformly irradiated with low-LET radiation to the same dose. In other words the dose-response characteristic, which is experimentally obtained for the medium irradiated with low-LET radiation, is used to correlate the calculated dose in the shells with a produced effect. Thus the dose-response obtained for low-LET radiation is convoluted into a calculation of dose from the δ-rays to give a distribution in effect.

The probability that a sensitive element is activated by an ion is given by the Poisson distribution function of eq. 2-1 as

$$P(z,\beta,t,a_0,D_{37}) = 1 - \exp(-\bar{D}(z,\beta,t,a_0)/D_{37}) \qquad 2\text{-}2$$

where $P(z,\beta,t,a_0,D_{37})$ represents the fraction of sensitive elements of radius a_0 activated by the incoming ion, and which are lying between adjacent cylindrical shells at a distance t from the track axis. z is the effective charge of the ion, β its velocity relative to that of light, and D_{37} is the characteristic dose of the medium. $\bar{D}(z,\beta,t,a_0)$ is the average dose deposited in the sensitive element at a distance t from the track axis, and is found from a calculation of the dose distribution around the ion's path.

To find the total effect produced by a single particle or a beam of particles with effective charge z and velocity β, an integration of $P(z,\beta,t,a_0,D_{37})$ must be performed over all distances t from the axis of the ion's path to the maximum range of the δ-rays. This integration yields the total activation cross section $\sigma(z,\beta,a_0,D_{37})$, which is the probability that a single particle activates a single sensitive element in a medium containing one such element per unit area perpendicular to the path of the particle. The cross section is expressed as

$$\sigma(z,\beta,a_0,D_{37}) = \int_{t_{min}}^{t_{max}} 2\pi P(z,\beta,t,a_0,D_{37})\,t\,dt \qquad 2\text{-}3$$

The upper limit of integration, t_{max}, which is the maximum range of the

δ-rays, will be determined in section 2.7. The lower limit of integration, t_{min}, may be defined as a distance from the track axis at which there still is a physical entity with which the δ-rays can react, and at which there will be evidence for reasonable calculations of the dose deposition. From these considerations we have chosen an integration cut-off at 10^{-10} m, while other investigators[38] have been using a cut-off at 10^{-12} m (see section 2.7).

The sensitivity of a medium towards low-LET radiation is given by $1/D_{37}$, while the sensitivity towards high-LET radiation is defined[30] as the ratio of the total cross section to the average energy deposited by the moving ion. This leads to

$$\text{sensitivity to low-LET radiation: } k_\gamma = 1/D_{37} \qquad 2\text{-}4$$

$$\text{sensitivity to high-LET radiation: } k_i = \sigma/E \qquad 2\text{-}5$$

where E is the average energy deposited per unit path length in a unit density material. This energy may be obtained from the collision stopping power of the moving ion, which for a heavy charged particle at energy above 10 keV/amu is equal to LET_∞. With the definition of the relative effectiveness, RE, in mind an expression for RE can thus be derived from the radiation sensitivities (eqs. 2-4 and 2-5) of the radiations involved.

$$RE = k_i/k_\gamma = \sigma D_{37}/E = k\rho\sigma D_{37}/LET \qquad 2\text{-}6$$

For D_{37} in Gy and LET in MeV/m the conversion constant k equals $6.24 \cdot 10^{12}$ $MeVGy^{-1}kg^{-1}$. ρ is the mass density of the medium in kg/m^3.

When considering a thick medium in which the ion either loses a major part of its energy or is brought to a complete stop, a track segment calculation is performed. The RE for the ion in the medium is found from an integration over the path of the ion, and the RE for each segment of integration is weighed with the energy deposited in the segment in proportion to the total energy deposited. Thus the individual segment RE's contribute to the total RE proportionately to the energy lost with a certain effectiveness.

Considering eq. 2-3 one find that the cross section depends both on parameters of the medium, a_0 and D_{37}, and of the penetrating ion, z and β. This makes it evident that particle and medium parameters are not separable variables when speaking about the relative effectiveness of a radiation field.

2.5 Effective charge of heavy ions

A heavy charged particle passing through a stopping medium changes its charge state continuously due to electron capture and loss processes in interactions with the atomic electrons of the medium. Bohr[39] proposed that the probability of capture or loss of an orbital electron by an ion is determined by the ratio of the ion velocity in the medium to the orbital velocity of the electron of the ion. On this background several authors have established improved analytical expressions for a quantitative determination of the effective charge of the ion as a function of its velocity. Much of this work is based on empirical considerations and fitting of parameters through measurements of stopping power, resulting in expressions valid for a certain range of ion energy and atomic number. In general the published expressions for the effective charge are independent of the atomic number of the medium and contain only parameters of the penetrating ion.

A few analytical expressions[40-45] have been investigated showing rather large deviations at energies below 1 MeV/amu, Fig. 3. At higher energies, where the ion is almost stripped of all its electrons, a better agreement was found. In this work four different analytic expressions, as given by Ziegler[45], have been used to determine the effective charge of protons, α-particles, lithium ions, and all other kinds of heavy ions. These expressions are fitted with numerical results of theory and various experiments and cover the energy range from 0.2 to 1000 MeV/amu. The expressions for the effective charges are as follows:

Protons:

$$z_p = 1 - \exp(-0.2E^{1/2} - 1.2\cdot10^{-3}E - 1.443\cdot10^{-5}E^2) \qquad 2\text{-}7$$

α-particles:

$$z_\alpha/z_p = 2\gamma\left[1 - \exp(-0.7446 - 0.1429\cdot\ln E - 0.01562(\ln E)^2 + 2.67\cdot10^{-3}(\ln E)^3 - 1.325\cdot10^{-6}(\ln E)^6\right] \qquad 2\text{-}8$$

Li-ions:

$$z_{Li}/z_p = 3\gamma\left[1 - \exp(-0.7138 - 2.797\cdot10^{-3}E - 1.348\cdot10^{-6}E^2)\right] \qquad 2\text{-}9$$

where

$$\gamma = 1 + (7\cdot10^{-3} + 5\cdot10^{-5}Z_2)\exp\left[-(7.6 - \ln E)^2\right]$$

other ions:

$$z_i/z_p = Z_1[1- (\exp(-A))\cdot(1.034 - 0.1777\cdot\exp(-0.08114Z_1))] \qquad 2\text{-}10$$

where

$$A = 0.1772E^{1/2}\cdot Z_1^{-2/3} + 0.0378 \sin(0.2783\cdot E^{1/2}\cdot Z_1^{-2/3})$$

E is the particle energy in keV/amu, Z_1 and Z_2 are the atomic numbers of the particle and medium, respectively.

In this work the above expressions have been used at energies down to 1 keV/amu, but the validity of the expressions have to some degree been tested by comparing experimental stopping power data of α-particles and lithium ions with data generated by means of proton stopping power and effective charge calculations down to an energy of 10 keV/amu. This will be dealt with in the following section 2.6. The application of the procedure of effective charge is rather problematic since there are different effective charges to discriminate from. This is further discussed in section 7.1.

2.6 Stopping power of heavy ions

The collision stopping powers of the ions in the media under investigation were calculated from published proton stopping power data[46] and the expressions for effective charge described in section 2.5 as

$$S(z,\beta) = S(z_p,\beta)\cdot(z^2/z_p^2) \qquad 2\text{-}11$$

$S(z,\beta)$ is the stopping power of the ion with atomic number Z moving at a velocity β relative to that of light, $S(z_p,\beta)$ is the stopping power of a proton moving at the same velocity, and z and z_p are the effective charges of the ion and proton, respectively, calculated from eqs. 2-7 through 2-10.

The two media under investigation are compounds constituted from hydrogen, carbon, oxygen, and nitrogen, and the bombarding ions have been protons, α-particles, ^{7}Li-, ^{14}N-, ^{16}O-, and ^{32}S ions. The proton stopping power data have been obtained through an interpolation procedure from tabulated data[45] with 1 keV as the lowest energy. The stopping power data of α-particles have been obtained by means of proton data and eqs. 2-8 and 2-11, except for α-particles in hydrogen where eq. 2-10 was found to fit better with experi-

mental results[47] in the energy range of 10 to 150 keV/amu. The stopping power data of lithium ions have been obtained by means of proton data and eqs. 2-9 and 2-11, except for lithium ions in hydrogen where eq. 2-10 was found to fit better with experimental results[48,49] in the energy range of 10 to 200 keV/amu. The stopping power data of oxygen-, nitrogen-, and sulphur ions have been obtained by means of proton data and eqs. 2-10 and 2-11.

In the theory of track structure it is assumed that only excitation- and ionization processes give rise to activation of a sensitive element, whereas elastic nuclear collisions do not. In the computation of the amount of energy lost by inelastic electronic collisions and for determination of the actual slowing down of the particles, the stopping power due to nuclear collisions has been calculated as well. In the calculations of heavy charged particle stopping powers the energy lost by radiation has been neglected. The following formula[45,50] has been used in the calculations:

$$S_{nucl.} = s_n \cdot 5.098 \cdot 10^3 Z_1 \cdot A_1 \cdot Z_2 \cdot A_2^{-1} \cdot \left[(A_1+A_2)(Z_1^{2/3}+Z_2^{2/3})^{1/2}\right]^{-1} \qquad 2\text{-}12$$

$$s_n = 0.5\left(\ln(1+\varepsilon)\right)\left(\varepsilon+0.10718\cdot\varepsilon^{0.37544}\right)^{-1}$$

$$\varepsilon = 32.53 \cdot 10^3 \cdot E \cdot A_1 \cdot A_2 \cdot \left[Z_1 \cdot Z_2 \cdot (A_1+A_2)(Z_1^{2/3}+Z_2^{2/3})^{1/2}\right]^{-1}$$

where s_n and ε are the reduced stopping power and reduced energy[51], respectively. With E in MeV/amu the nuclear stopping power $S_{nucl.}$ is expressed in $MeVcm^2g^{-1}$. The proton stopping power data includes only inelastic collisions, so that the total stopping power is the sum of the collision and nuclear interactions. The nuclear interactions become significant at energies below 10 keV/amu.

For particles penetrating complex media, e.g. compounds, the normally used method has been to employ simple additivity of the stopping powers of the constituent elements for the penetrating particle at a given energy. This method is based on Bragg's additivity rule[52], which states that the stopping power of a compound medium is the sum of the stopping powers of the constituent elements weighted by their relative abundance in the medium. From this formulation an expression for stopping power of a compound medium may be given by

$$S_{comp} = \frac{1}{N} \sum_i n_i \cdot S_i \qquad 2\text{-}13$$

where N is the number of atoms or molecules per unit volume in the medium, and n_i and S_i are the number of atoms per unit volume and stopping power of the i'th element in the compound, respectively. Deviations from this rule may occur due to chemical binding of atoms into molecules and the physical phase of the stopping medium, but it is generally assumed[53,54] that these effects have little influence on the average energy loss. The largest deviations, however, in actual stopping power from that obtained from eq. 2-13 may occur at energies in and below the transition region, i.e. below approximately 0.2 MeV/amu, and for organic media containing hydrogen. For organic media the measured and calculated stopping power may deviate as much as 50%[53] at the lowest energies.

2.7 The radial dose distribution around a heavy ion

Calculation of the radial dose distribution $D(z,\beta,t,a_0)$ around the path of a penetrating ion is one of the basic functions in the track structure theory. This function relates the inhomogeneous distribution of absorbed energy to a distribution of radiation effects, an integration of which over the whole irradiated volume expresses the average response of the medium. Extensive measurements of cross sections for δ-ray production in ion-molecule interactions have been made and various models for calculating the radial dose distribution have been proposed[7,56-59].

In this work the energy and angular distribution of δ-rays ejected, when the ions undergo ionizing collisions with the atoms and molecules of the medium, are fundamentally based on the Rutherford scattering formulation, where the electrons of the medium are considered as free and the binding energies are neglected. The number distribution differential in energy of the δ-rays is calculated from Bethe theory[55], and the energy distribution calculations for the δ-rays are based on fitted parameters from published range-energy relations for electrons below 10 keV. Some assumptions have been made, and simplifications are introduced for ease of calculation and in order to reduce the computer time for track segment calculations, which are very time consuming. These assumptions are: 1) δ-ray calculations are continuous instead of stochastic; 2) energy deposition by δ-rays alone have been considered; 3) the Bethe formulation for the δ-ray energy distribution is used also for energies below electron binding energies, where the Bethe theory clearly contradicts experimental evidence and present theoretical predictions[60], and 4) the δ-rays are assumed to be ejected perpendicular to the ion's path. Apart from

smaller differences due to the chemical composition of the medium, there exists fairly good agreement between the absolute electron energy distribution found from the Bethe formulation and experiments[61-63] at electron energies down to 100 eV. According to the Bethe theory of δ-ray distribution most of the electrons are emitted at large angles with the direction of the incident ion but with low energies, whereas a diminishing number of electrons of high energy are emitted in the forward direction, e.g. the maximum angle being 90° for zero energy and 0° for the maximum electron energy (see Appendix I). Recent investigations[64] of angular distribution of δ-rays produced by protons of 0.3 to 2 MeV show that electrons ejected with low energy (< 50 eV) are nearly isotropically distributed especially for high-energy protons. As the energy of the primary ion increases the angular distribution becomes peaked at an angle of approximately 45° with the incident direction, and at the maximum obtainable energy the electrons are preferentially ejected in the forward direction. It has further been shown[64] that the spectrum of δ-ray energies does not depend on the specific chemical composition of a low-Z medium for δ-ray energies above 30 eV, but only on the electron density. That these approximations are plausible appear from the following, where a comparison is made of calculated dose distributions with experiments and distributions obtained from continuous slowing down calculations involving stochastic processes.

From the above considerations an expression for the radial dose distribution around the path of a penetrating ion is derived for which a detailed description is given in Appendix 1. The dose distribution calculations have been performed first, by means of a linear (projected) range-energy relation for the δ-rays as used by Butts and Katz[7] in their original work, and secondly by means of a power-law range-energy relation, which is a superior fit to experimental data. A comparison of these two calculations and the influence on the final data of relative effectiveness are described in an article[18] attached (section 12). The linear relation $r = k_1 \rho^{-1} \omega$ with r equal to the range and ω equal to the energy leads to a dose distribution formula given by

$$D(z,\beta,t) = \frac{Ne^4}{mc^2} \cdot \frac{z^2}{\beta^2} \cdot \rho \cdot \frac{1}{t^2} \cdot \left[1 - \frac{t}{t_{max}}\right] \qquad 2\text{-}14$$

This formula is in the track structure theory called the point target dose distribution and describes the dose to sensitive elements of infinitesimal size as a function of the effective charge z and relative velocity β of the ion and of the distance t from the path of the ion. N is the number density of electrons of charge e and mass m in the medium of density ρ, and t_{max} =

$k_1 \cdot \rho^{-1} \cdot \omega_{max}$ is the maximum range of the δ-rays. $\omega_{max} = 2mc^2\beta^2(1-\beta^2)^{-1}$ is the maximum energy of the δ-rays.

The power-law relation $r = k_2\rho^{-1}\omega^{\alpha}$ leads to a point target dose distribution given by

$$D(z,\beta,t) = \frac{Ne^4}{mc^2} \cdot \frac{z^2}{\beta^2} \cdot \rho \cdot \frac{1}{\alpha} \cdot \frac{1}{t^2} \cdot \left[1 - \frac{t}{t_{max}}\right]^{1/\alpha} \qquad 2\text{-}15$$

and a maximum range of the δ-rays given by

$$t_{max} = \frac{1}{\rho} \cdot k_2 \cdot \omega_{max}^{\alpha} = \frac{1}{\rho} \cdot k_2 \cdot (2mc^2\beta^2/(1-\beta^2))^{\alpha} \qquad 2\text{-}16$$

where $\alpha = 1.67$ and $k_2 = 5.2 \cdot 10^{-10}$ $kgm^{-2}eV^{-\alpha}$ are found by fitting to published data. Many range quantities have been defined either from experiments[65-72] or from theoretical approaches[73-76], where the experiments have dealt with projected range or transmission range, and theoretical path lengths have been derived from Monte Carlo calculations of a continuous slowing-down approximation model. In Fig. 4 are shown published data of mass-range as a function of energy for electrons in water as well as the fitted power-law curve used in this work. The published data, which are obtained for various low-Z materials, are corrected for electron density by $r_{H_2O} = r_{medium} \cdot (A_{medium}/A_{H_2O}) \cdot (Z_{H_2O}/Z_{medium})$, where A and Z are atomic mass and atomic number, respectively.

The radial dose distributions calculated from eqs. 2-14 and 2-15 have been tested by comparison with experimental data[77] and continuous slowing down model calculations[77] for 42 MeV ^{79}Br ions in a tissue-equivalent unit-density gas (Rossi-type). The results are shown in Fig. 5 and in Table I. The percentage deviation of calculated values using eq. 2-14 from those experimentally obtained varied from +267 to +7% with root mean square deviation of 39% over the range of distances from the ion path of 0.5 to 70 nm. Results obtained by using eq. 2-15 varied from +77 to -36% with a root mean square deviation of 12%. It should be noted, however, that according to the reference 77 a too low energy deposition is observed in the experimental case at very small distances ($< 1.35 \cdot 10^{-9}$ m) from the ion's path. This could be due to an increase in $\bar{W}$-value at lower radii and/or to a lack of charge equilibrium in the ionization chamber with which the energy deposition was measured. The authors[77] assume that 60% of the total energy should be deposited within the stated range in contradiction to a measured value of 23%. Accuracy of experimental data was not stated.

Radial dose distribution calculations by means of eqs. 2-14 and 2-15 have further been compared with experimental data and continuous slowing down model calculations for 1 MeV protons in a tissue-equivalent unit-density TE-gas. The data were read from published[57] curves.The results shown in Fig. 6 show calculations of eq. 2-15 to confirm with results obtained from the continuous slowing down approximation, but disagree with the experimental data to a higher extent than the comparisons made in Fig. 5 with the bromine ions. The root mean square deviation is 14% of calculated values from eq. 2-15 compared to experimentally obtained values. The accuracy of the experimental data was not stated.

The radial dose distribution calculations from eq. 2-15 have been compared to experimental data[78] for 0.262 MeV/amu ^{127}I and 2.4 MeV/amu ^{16}O ions. The ratio of experimental-to-calculated doses as a function of the distance from the particle track is shown in Fig. 7. In the experiments the effective charge was calculated from the formula of Nikolaev and Dmitriev[44]. The formula given by Ziegler[45] gives almost identical z for 2.4 MeV/amu ^{16}O ions but about 10% lower z for ^{127}I. This difference has been corrected for in the calculations shown in Fig. 7. The larger discrepancy for the 2.4 MeV/amu ^{16}O data is due partly to the experimental data being approximately 20% too high due to too high an assumed value for W as discussed by Baum et al.[78]. W is the energy required to create an ion pair. Below 1 nm experimental data are too low due to lack of charge equilibrium.

Radial dose distributions in water calculated from eq. 2-15 agree with published theoretical data[56] for 2 MeV/amu C-ions, 8 MeV/amu Ne-ions, and 90 MeV/amu Fe-ions with a root mean square deviation of 10, 8, and 6%, respectively, over the range of distances from 0.3 to 10^5 nm. Results are shown in Table II. The root mean square deviations for the radial dose distributions calculated by means of the linear range-energy relation are 29, 22, and 14%, respectively.

In the calculation of the activation cross section σ for a medium, an average dose deposited in the sensitive element must be used. As described in section 2.4 the medium is assumed to be made up of sensitive elements in the shape of cylinders with radius equal to a_0, and with the axis of symmetry parallel to and positioned at a distance t from the ion's path (Fig. 8). Though different parts of the cylinder experience different doses in the strongly varying field around the ion's path, the dose-response is determined by the average

dose delivered to the element. This dose is called the extended target dose and is given by

$$\bar{D}(z,\beta,t,a_0) = \frac{1}{\pi a_0^2} \int_{t-a_0}^{t+a_0} D(z,\beta,t) \cdot A(t,a_0) dt \qquad 2\text{-}17$$

where $A(t,a_0)$ is a geometry function determined by the shape of the sensitive volume element (Fig. 9). For a cylinder this function is given by

$$A(t,a_0) = 4 \text{ Arctg } \sqrt{[a_0^2-(t_0-t)^2]/[(t_0+t)^2-a_0^2]} \quad \text{for } (t_0+t) > a_0$$

$$A(t,a_0) = 2\pi \quad \text{for } (t_0+t) \leq a_0 \qquad 2\text{-}18$$

where t is the variable distance in the calculation of the extended target dose to the sensitive element, the center of which is placed at a distance t_0 from the ion's path. In the computer calculation of the extended target dose t_0 is used for ease as the variable distance from the ion's path to the center of the sensitive element, whereas t is kept as the variable distance within the sensitive element. (see Appendix 1).

The extended target dose distribution calculations from eq. 2-17 are shown in Fig. 10 for the 64 MeV ^{16}O ions investigated in this work and for an infinitesimal thick segment of the dye film. It is characteristic that the dose distribution profiles have a flat top extending to a distance from the ion's path corresponding to the radius a_0 of the sensitive element. The ion's path is assumed to penetrate the sensitive element at its center, and the plateau of the dose distribution profile equals the average dose to that element, which is considered separately from the rest of the medium. The total energy of the δ-rays with energy large enough to have ranges greater than a_0 is calculated by an integration of the point target dose profile (eq. 2-15) from the distance $t = a_0$ to the maximum range t_{max} of the δ-rays. This distance from a_0 to t_{max} is called the track. The energy deposited in the central element, the core, can then be calculated as a subtraction of the energy deposited in the track by the δ-rays outside the central core from the total energy deposited by the penetrating ion. The total energy is found from the collision stopping power. From this procedure of calculating the dose to the central core excitation energy deposited by the penetrating ion is taken also into account, whereas the energy to the track is due only to δ-rays.

The dose distribution profile of a heavy charged particle may be divided schematically into three concentric zones as shown in Fig. 11. The central

zone is characterized by an area of high energy density where saturation of activation is dominant. A large part of the particle energy may be deposited within this area, but the contribution to the total effect is negligible because the area is comparatively small. In the intermediary region surrounding the central area saturation diminishes .The energy density is high and may be above the characteristic D_{37}-dose, which means that the dose-response is sublinear. Finally, there follows a large peripheral zone with low energy density where the dose-response is linear. The total effect of activation will be determined by the distribution of energy among these three zones, where low effectiveness is highly probable in the central and intermediate zones leading to a decreased total effectiveness of the ion as compared to the effect for the same absorbed dose from low-LET radiation.

Looking at the dose distribution profile in Fig. 10, the effectiveness of radiation from a heavy charged particle may be explained qualitatively from a horizontal line drawn at a dose equal to D_{37}. If this line lies above the plateau of the extended-target dose profile, the average integral dose relative to the characteristic dose, $\bar{D}/D_{37}$, will always be less than 1 for all sensitive elements affected by the ion with only a small loss in effectiveness. This leads to RE = 1. If the horizontal line is below the plateau, $\bar{D}/D_{37}$ will be greater than unity with resulting saturation and waste of energy in a part of the sensitive elements. This leads to RE < 1. A Taylor expansion of the exponential term in the expression for $P(z,\beta,t,a_0)$ (eq. 2-2) shows that for values of $D \ll D_{37}$ the cross section (eq. 2-3) to a good approximation is given by $\sigma_T = \bar{D}/D_{37}$, which leads to a value of RE (eq. 2-6) equal to unity.

2.8 Why experimental testing of the track structure theory?

The track structure theory was originary developed to predict dose-response characteristics and radiosensitivies of enzymes and viruses irradiated with high-LET radiation. The theoretical work by Katz has mostly been tested against experimental data derived from the work of other investigators. Except for investigations with biological systems the theory has been tested against the following experiments with: enzymes and viruses[7], photographic emulsions[31,35,37,80], etchable tracks in dielectrics[81], thermoluminescent dose meters[5,6,36,82], the radiochromic dye film[13,34], radical formation in amino acids[83,84], the Fricke dose meter[32], and NaI scintillators[9]. Since very few of these experimental investigations were carried out over a suffi-

ciently broad spectrum in LET or z and β, it has not been possible to make a detailed test of the predictions of the theory.

In order to test and improve the theory in details the theoretical work could with advantage be followed up by systematic experiments designed to test certain parameters and procedures of calculation. Conversely, experimental data could give rise to improvements in theory, because the experiments were performed only in order to yield information about a certain detector in the context of the development of the model.

3. THE RADIATION DETECTORS

3.1 The radiochromic dye film

One radiation detector used in this work is the nylon-based FWT-60 dye film, commercially available from Far West Technology Inc., 330 Kellogg, Goleta, California, USA. This thin radiochromic dye film dose meter contains a leuco-cyanide, hexahydroxyethyl pararosaniline cyanide $[C_6H_4N(C_2H_4OH)_2]_3C\text{-}CN$, which is transformed into a coloured state, the dye, by absorption of energy from ionizing or exiting radiation. The radiochromic leucocyanide, 10-15% by weight, is dissolved in a nylon matrix $(C_{12}H_{22}N_2O_2)_n$. Upon irradiation the C-CN bonds are heterogeneously broken and the triarylmethane groups become the highly coloured carbonium ion. This reaction takes place upon irradiation with particle energies exceeding the C-CN bond strength which is about 3.8 eV[85].

The dye has a broad absorption band in a part of the visible spectrum with a maximum at 604 nm. In this work the response to radiation is mostly measured at the wavelength of 510 nm, which is on the edge of the absorption peak, and expressed as an increase of optical density per unit film thickness, ΔOD/mm. The dose meter is supplied in pieces of 1×1 cm^2 with an approximate thickness of 55-μm. For some of the experiments a very thin FWT-60 film has been used with a thickness of 5 μm, but with the same material and content of leuco-cyanide. These very thin films have been measured at 604 nm.

A thorough investigation, described in details in a published article[19] attached in section 12, has been made of the problems involved in using a dye film dose meter for precision dosimetry. This investigation includes: the optical absorption spectrum at various dose levels and radiation qualities, kinetics of build-up and fading of coloration after exposure to high and low doses, the saturation dose-response level, bleaching at very high doses, comparison of dose-response after irradiation in air and vacuum, dose rate effects at high doses, and temperature dependence of the dose-response. These investigations of the dye film were a necessary supplement to previous investigations[85-98].

The light absorption spectrum of the dye film irradiated with low- and high-LET radiation (Fig. 12) shows that irradiation with different radiation qualities to the same medium-range light absorption level causes the same shape of the spectrum. This shows that the formation of dye is independent of how the energy is deposited in the film, either by homogeneously distributed ionizations and excitations as from γ-ray photons and fast electrons or by highly inhomogeneously distributed δ-rays from high-LET particles, or by excitation alone as from UV-light.

The leucocyanide does not change into the coloured state immediately upon irradiation, but intermediate species are formed with an absorption maximum at 412 nm. These rather short-lived species decay and the blue coloured dye is formed with an absorption maximum at 604 nm (Fig. 13). The build-up of coloration takes place within the first 10-20 hours after irradiation. Thereafter a decline in response is observed until about 100 hours after irradiation (Fig. 14). The rate of build-up is dose and dose-rate dependent and the build-up depends further on the content of oxygen and water in the film material during irradiation. Despite these differences in the time-course of build-up no significant difference in dose-response was found, if the readings of response were made at the time for maximum coloration. Neither did irradiation in vacuum versus that in open air influence the final response.

The wavelength of 494 nm is an isosbestic point[99] (Fig. 13) which is stable in time within the first 24 hours after irradiation and thus independent of build-up of colour. The sensitivity, however, of the film to irradiation is reduced by a factor of 2.5 as compared to measurements at 510 nm. The manufacturer of the film recommends measurements at 604 nm for γ-ray and electron doses below 30 kGy and at 510 nm at higher doses. These wavelengths of measurements have been used as well in order to compare our findings with the

ones of other investigations.

Previous investigations[87-89] have shown the film to be dose rate independent at low to medium doses except at very low dose rates[96,97], < 1 Gy s^{-1}. The present work shows (Figs. 15 and 26) differences in saturation optical density, which may be due to dose rate effects at high doses. This effect is discussed in section 7.2.

The dependency of dose-response on temperature during irradiation of the dye film has been monitored at the spectrophotometer wavelength of 510 nm. The temperature effect was found to be dependent on dose having an average increase of 0.6%/°C and 0.9%/°C for the dose levels of 10 and 100 kGy in the temperature interval of 20 to 50°C[19] (Fig. 16).

For purposes of calculating the effective charge and stopping power of charged particles penetrating into the dye film, equivalent atomic number and atomic weight for the compound material have been found to have the values of 5.94 and 11.77, respectively. The equivalent molecular weight M_W and average number of electrons per molecule n_e have been found to be 261.2 and 142.6, respectively. M_W and n_e are used in the calculation of the radial dose distribution due to δ-rays ejected from the path of a heavy charged particle, and the constant $C = 2\pi Ne^4/mc^2$, used in section 2.7 and in Appendix 1, gets the value of $1.343 \cdot 10^{-12} \cdot \rho$ joule/m for the dye film. $\rho = 1.13 \cdot 10^3$ kg/m^3 is the mass density of the dye film. The above values are calculated for the dye film consisting of 10% dye and 90% Nylon 66 by means of Bragg's additivity rule[52].

The radiation sensitive element is the leuco dye molecule, the radius of which is approximately 10^{-9} m. The energy deposited in the molecule will migrate within the molecular structure and break the weakest bond, which is the C-CN bond. This means that an interaction process involving energy deposition above a certain threshold will turn the leuco dye into the coloured state independent of where the event takes place within the molecule.

The dye film must be handled and kept in dark as it is sensitive to daylight and fluorescent light. Normal handling procedures may be made in incandescent light.

Dose-response curves of the radiation qualities under investigation will be dealt with in section 6.1.

3.2 The alanine radiation detector.

Commercially available purified crystalline amino acid L-α-alanine has been investigated for use in radiation detection. The chemical composition of alanine (CH_3-$CHNH_2$-COOH) is close to that of tissue, thus providing similarity to biological systems in absorption of radiation energy. The microcrystalline powder is compressed into pills, 4.5 mm in diameter by 2 mm in thickness, with 5% by weight cellulose ($C_6H_{10}O_5$) added as a binding material[36]. The cellulose binding material was found to have a negligible effect on the ESR signal after irradiation to doses above 10 Gy. The covalent bonds of the amino acid formed by a pair of valence electrons with opposite spin offer a zero magnetic momentum. Ionizing radiation exposed to the system causes a rupture of these bonds resulting in two paramagnetic species each having an unpaired electron. Through a series of reactions these species are converted into a free radical which is highly stable in time and may be detected by means of electron spin resonance (ESR) spectroscopy[100,101]. This radical has the chemical composition of (CH_3-$\dot{C}H$-COOH). By this measuring technique the free radicals may be detected qualitatively as well as quantitatively and represents a measure of the amount of energy imparted to the material[102].

The spectrum of alanine irradiated with low- and high-LET radiations (Fig. 17) shows that irradiation with different radiation qualities to the same ESR-signal causes the same shape of the spectrum. The formation of the detected radicals is thus independent of how the energy is deposited, either homogeneously distributed as from γ-rays and fast electrons or inhomogeneously as from δ-rays ejected by the passage of heavy charged particles.

In this work the ESR signal is not measured until 5 minutes after irradiation at which time the radical formation in the alanine has stabilized. No build-up of radicals has been observed after exposure to low or high doses at room temperature, nor has fading of the ESR signal been observed for doses below the D_{37}-dose, even 1-1/2 year after irradiation. At doses above the D_{37}-dose fading increases with dose to approximately 20% at saturation dose measured 7 months after irradiation. A detailed investigation of fading has not been performed in this work, but other investigators[83,84,103-106] claim that no fading occurs over several years for L-α-alanine irradiated to medium-range doses and stored at room temperature and under normal laboratory humidity conditions. One investigator[107] has found DL-α-alanine to fade by approxi-

mately 18% up to 100 hours after irradiation, whereafter the ESR signal was constant for at least 700 hours. The irradiation dose, however, was not stated.

Previous investigations[103-106] have shown L-α-alanine to be dose-rate independent even at high doses (350 kGy) to a maximum dose rate of 10^8 Gy s^{-1}. This work confirms these findings at doses below the $D_{3,7}$-dose, but shows, as also observed[107] for ^{210}Po α-particles, a decline in the ESR signal at saturation doses for irradiation with heavy charged particles of increasing LET. This effect is ascribed to a high ionization density caused by either a high dose rate in the track of a heavy charged particle or crossing tracks[107]. The same authors, however, observe a change in the hyperfine structure of the ESR signal for irradiation with ^{210}Po α-particles, which we do not observe at irradiations with heavy charged particles. At saturation we find a ~ 10% increase in the ESR signal for irradiation with 10-MeV electrons with a dose rate of $5 \cdot 10^7$ Gy s^{-1} compared to irradiation with ^{60}Co γ-rays with a dose rate of 14 Gy s^{-1}.

The dependency of dose-response on temperature during irradiation of L-α-alanine has been thoroughly investigated[103-106], and it has been found that the ESR signal increases linearly with irradiation temperatures between -10°C and +90°C. The increase in ESR signal is 0.18%/°C at doses below 10^4 Gy and 0.31%/°C at a dose level of approximately 10^5 Gy. The temperature during irradiation and measurement have been kept at room level in this work, and this is why the temperature effect has not been taken into account.

Dose-response curves of the radiation qualities under investigation will be dealt with in section 6.3.

The alanine dose meter pills have been manufactured in the Accelerator Department at Risø and kept under normal humidity and room temperature conditions and in the dark during storage. This is in regard to both unirradiated and irradiated samples. An influence of daylight or fluorescent light to the ESR signal before and after irradiation for normal handling procedures of the dose meter has been found to be undetectable.

For calculating the effective charge and stopping power of charged particles penetrating into the compressed alanine pills, equivalent atomic number and atomic weight for the compound material have been found to be 6.49 and 12.91, respectively. The equivalent molecular weight M_W and average number of elec-

trons per molecule n_e have the values of 92.65 and 49.9, respectively. The constant $C = 2\pi Ne^4/mc^2$ used in section 2.7 and in Appendix 1 for calculation of the radial dose distribution around the ion's path attains the value of $1.324 \cdot 10^{-12} \cdot \rho$ joule/m for alanine. $\rho = 1.21 \cdot 10^3$ kg/m^3 is the mass density of the alanine pill. These values are calculated for a compound consisting of 95% pure alanine and 5% cellulose by means of Bragg's additivity rule[52].

The radiation-sensitive element, which is the target for the present ESR spectroscopy, is the carboxyl-amino group of the L-α-alanine system; its size is approximately 10^{-9} m. The energy deposited in the alanine macromolecule generates several radicals[108]. Hence, it is assumed that the imparted energy is able to migrate within the molecule and the generation of the stable, dominant radical is independent of where the event takes place within the macromolecule.

4. IRRADIATION FACILITIES

4.1 ^{60}Co γ-ray source

The γ-ray irradiations have been carried out at the Risø $3.7 \cdot 10^{15}$ and $1.1 \cdot 10^{15}$ Bq ^{60}Co facilities[109] both of which are calibrated with Fricke dosimeters with $G(Fe^{+++}) = 15.6$ [110]. The dose rate of the $3.7 \cdot 10^{15}$ Bq facility was 14 Gy s^{-1} and 1 Gy s^{-1} for the $1.1 \cdot 10^{15}$ Bq facility.

Irradiations of dye film and alanine were carried out under the same irradiation conditions as was the calibration, namely in a nylon container of wall thickness of 1 cm ensuring electron equilibrium. The dose calibration is accurate to within ± 2%.

4.2 Electron linear accelerators

Irradiations with fast electrons have been carried out on the Risø 10-MeV electron linear accelerator[111] in a bent beam and straight ahead beam mode. The bent-beam mode is accurately dose calibrated for single step doses of maximum $5 \cdot 10^4$ Gy, whereas the straight-ahead beam mode is uncalibrated but

can be used for irradiation of single-step doses to any dose level and under different environmental conditions.

In the bent-beam mode (Fig. 18) the samples to be irradiated are placed in a tray on a conveyor belt and transported to the irradiation zone, which is a 10-MeV electron beam scanned in the transverse direction of the conveyor belt movement. The beam is pulsed with 200 pulses per second each having a pulse length of 4 μs. The dose rate in the pulse is $5 \cdot 10^7$ Gy s^{-1}. The dose to the sample is controlled through the speed of the conveyor. The energy of the electrons is determined by the current in the bending magnet. Maximum dose given to the sample at each run is $5 \cdot 10^4$ Gy as higher doses will cause excessive heating (2.5°C per 10^4 Gy in water). The samples are irradiated in open air. The radiation field is calibrated by water calorimetry[112-114]. The water calorimeter is a 1.5-cm thick petri dish filled with water, the temperature increase of which is measured with a built-in thermistor. The calorimetric body is encapsulated in styrofoam in order to prevent heat exchange with the surroundings.

Irradiations of dye film and alanine in the bent beam mode were carried out in a Perspex block of the same thickness in kg/m^2 as the calorimetric body, and the samples were placed in the block at a depth corresponding to average dose in the water calorimeter. This depth was determined from the depth-dose curve of 10-MeV electrons in water (Fig. 19).

In the straight-ahead beam mode the samples to be irradiated were placed in a chamber connected to a beam tube of the accelerator beam-handling system (Fig. 20). This chamber was also used for irradiations on the tandem Van de Graaff accelerator. The chamber is separated from the accelerator vacuum system by a 0.2-mm aluminum foil window allowing the chamber either to be evacuated or filled with a gas at different temperatures. The electron beam is pulsed with a pulse rate of 25 pulses per second and a pulse length of 4 μs. The electron energy can be controlled in an energy-analyzing spectrometer connected to the beam-handling system.

Before the electron beam enters the irradiation chamber it is dispersed in the vertical plane by a doublet quadrupole magnet. A spreading of the beam in the horizontal plane occurs in the switching magnet of the beam handling system due to energy inhomogeneity of the electron beam leaving the accelerator. A double set of beam-defining slits are mounted in front of the sample in order to collimate the beam. This collimator set-up is constructed such

that the bremsstrahlung generated by the stopping electrons in the slits is attenuated appropriately. The dispersed and collimated beam produced a homogeneous irradiation field in which the target was placed. To ensure homogeneity an irradiated film was scanned across the irradiated area by means of a scanning spectrophotometer. Most of the electrons penetrating the target sample were picked up by a Faraday cup thus diminishing the influence from back scattered electrons. As the pulse-to-pulse variation of the current in the beam is small (< 1.8%), the energy fluence is proportional to the number of pulses which are counted for dosimetry purposes. The dose calibration is performed by comparing the sample response for a given number of pulses with the dose-response of the same kind of sample irradiated in the bent-beam mode to a dose of less than $2 \cdot 10^{4}$ Gy. The dose rate in the straight-ahead beam mode corresponds to the dose rate in the bent beam-mode.

The dose calibration in the bent-beam mode is accurate to within ± 2%, while the dose in the straight ahead beam mode is accurate to within approximately ± 4%.

For intercomparison of doses given at the Risø linear accelerator and doses given at the University Hospital in Herlev, irradiations were performed with a 4-MeV and a 20-MeV radiation therapy linear accelerators. These accelerators are pulsed operated as well with a pulse repetition rate of 300-600 pulses per second and a pulse length of 2 μs giving a dose rate of 80 Gy s^{-1} in the pulse. The homogeneously irradiated area is 10 cm×10 cm.

The dose calibration was performed in a Perspex phantom with an ion chamber placed at the maximum of the depth dose curve. The ion chamber was then replaced by the samples fixed into the proper position in a small block of Perspex. The dose calibration is within ± 2%.

4.3 Tandem Van de Graaff accelerator

The ion-beam irradiations were carried out on the tandem Van de Graaff accelerator at the Niels Bohr Institute. This accelerator has a maximum terminal voltage of 9-MV with a stability of the final beam energy exceeding 10-keV independent of the kind of particle with atomic mass less than approximately 16. The energy and charge state of the accelerated ions were kept constant after a 90° analyzing magnet which was controlled by nuclear magnetic resonance detection. The average dose rate for most of the experiments

was approximately 10^3 Gy s^{-1}, and unlike the linear accelerator the beam current in the Van de Graaff accelerator is continuous dc. A layout of the accelerator and the beam handling system is shown in Fig. 21.

The experimental equipment, mounted on to beam tube 7, was an aluminum chamber in direct connection with the vacuum of the beam handling system. The equipment was designed and constructed in cooperation with Mads Wille at the Accelerator Department. In front of the equipment was a vacuum valve for closing off the beam tube, when the chamber was opened for change of target samples. An oil diffusion pump together with a roughing pump were used to evacuate the chamber to a pressure of 10^{-3} Pa before opening the valve.

To ensure beam homogeneity on the irradiated area, the particle beam was dispersed by a magnetic field from a triplet quadrupole magnet. Subsequent collimation was carried out by two sets of thin collimators constructed and positioned such that secondary electrons and scattered ions originating from the slit edges were prevented from reaching the target. A pair of slits, 3×3 mm^2, was later changed to slits having an aperture of 1×6.6 mm^2, with the largest dimension in the vertical plane. To limit effects arising from secondary electrons escaping from the Faraday cup, a magnetic field of 0.5 T perpendicular to the beam axis was applied at the entrance to the cup. The strength of this field was determined from the magnetic rigidity of the secondary electrons of maximum energy and the dimension of the Faraday cup opening. Additionally an electron shield ring with a potential of +5 kV was mounted between the target sample and Faraday cup.

The absorbed dose in the sample was calculated from particle fluence and stopping power values. The particle fluence was determined from an integration of the ion current to the Faraday cup, and the energy and charge state of the ions were measured in the analyzing spectrometer of the beam-handling system. During the irradiation three target samples were mounted around the periphery of a rotating wheel carrying them through the beam path. When the samples were in the beam path the integration of the current from the Faraday cup was interrupted, thus avoiding corrections for the change in charge state of those ions penetrating the target and uncontrolled interruptions of the beam for total absorbing targets. Further, corrections are avoided for particle number attenuation, scattering from the film edges, large-angle scattering, and secondary electrons escaping from the back side of the detector. The interruption was controlled by cutting off the light path in an optical coupler by another wheel running synchronously to the wheel on which the target

samples were mounted (Fig. 22). The wheel was rotated with approximately 200 rpm which made the intervals between irradiation of the samples and measurement of the beam current very short, thus diminishing the influence from fluctuations in beam current with time. Irradiation of three samples at each run prevented random spread in measured response of the irradiated sample and in the measured charge.

The electric charge, Q_{beam}, transported by the ion beam into the irradiation chamber is obtained from a measurement of integrated current to the Faraday cup, charge Q_{cup}, as

$$Q_{beam} = Q_{cup} \frac{2\pi}{p\phi} = \frac{1}{k'} \cdot Q_{cup} \qquad 4\text{-}1$$

where ϕ is the pulse length in terms of radians of the signal from the optical coupler, and p=4 is the number of pulses per revolution of the wheel (Figs. 22 and 23). The ratio of particles hitting the target sample to those entering the irradiation chamber is $\ell/2\pi r$, where ℓ is the width of the collimating slit and r the radial distance to the target center when the target sample is mounted on the rotating wheel.

The particle fluence Φ hitting the target sample was determined by

$$\Phi = \frac{Q_{cup}}{k' \cdot n \cdot e \cdot h \cdot 2\pi \cdot r} \qquad 4\text{-}2$$

where n is the charge state of the ions, e the charge of the electron, and h the vertical dimension of the collimating slit. From measurement of the size of the irradiated area on a film fixed at the target sample position, beam divergence was found to be negligible. The absorbed dose in the sample was then calculated from the track average electronic stopping power in the sample S_{av} and the particle fluence Φ as

$$D = \frac{1}{k} \cdot S_{av} \cdot \Phi = \frac{S_{av} \cdot Q_{cup}}{k \cdot k' \cdot n \cdot e \cdot h \cdot 2\pi \cdot r} \qquad 4\text{-}3$$

with $k = 6.24 \cdot 10^{12}$ MeV $kg^{-1}Gy^{-1}$ as a conversion constant. A detailed derivation of the dose calculation is given in Appendix 3.

The charge measurements have an uncertainty of 2% found from repeated measurements of an integrated discharge current from a 1.5 V battery through a 200 MΩ resistor. This discharge current is of the same order of magnitude as the beam current into the Faraday cup. The current meter was a "Keithley

Instrument 414A Picoammeter", the output of which was 1 volt for full scale deflection. The integrator was a "Dymec Integrating Digital Voltmeter, Model 2401B", the integration of which could be stopped by a +5 volt input pulse and the integrated signal stored during stop.

5. PROCEDURES OF DOSE-RESPONSE MEASUREMENTS

5.1 Measurements on the dye film

The response of the irradiated film samples was measured by means of a scanning spectrophotometer[115] with a nigh spatial resolution. Variations in the optical density, either due to variations in film thickness or inhomogeneity in the radiation field, can thus be detected very precisely by the scanning technique. The effective slit height and width is 50×10 μm determined by the dimensions of the analyzing light beam on the surface of the film sample. Special care has been taken to avoid interference of the light reflected from the film surface and to take scattering of the transmitted light into account. The output from the spectrophotometer is plotted on an x-y recorder, and the complete read-out system has a very short rise time ensuring photometric measurements of light changes occurring over small distances. The complete instrument is calibrated to an optical density of maximum 3.5 by means of a photographic step tablet supplied by the U.S. National Bureau of Standards. The light-absorption spectra, as shown in Figs. 12 and 13, were carried out on a Pye Unicam SP8-400 spectrophotometer.

In Fig. 24a is shown a scan across a whole film sample homogeneously irradiated with γ-rays. Small spikes on top of the optical density signal are due to film irregularities, dust, and electrical noise. In Fig. 24b a scan across the whole film sample irradiated with 16-MeV protons is shown. The irradiated area is in the middle of the scan and the optical density signal on both sides of the irradiated area is the background optical density of the unirradiated film. In situations where the irradiated area on the film is inhomogeneously irradiated, the maximum optical density for a certain part of the area was used, and the measured dose was corrected accordingly. This procedure, of course, easily involves inaccuracies, but was applied only at saturation doses where the maximum optical density is of interest and where the

optical density is a slow function of dose. At lower doses the optical density reading of an inhomogeneously irradiated film was averaged by an integration technique by means of a planimeter.

The thickness of each film sample was carefully measured by means of an electronic gauge unit. To prevent a random inhomogeneity in the film casting being decisive, the thickness was measured at different places on the irradiated area.

The film response to radiation is expressed as an increase of optical density per unit film thickness, ΔOD/mm, measured at the spectrophotometer wavelength of 510 nm for the 55-μm thick film and at 604 nm for the 5-μm film.

5.2 Uncertainty in dose-response measurements on the film

The uncertainty on dose-response data for the dye film consists of a random uncertainty and a systematic error. The overall uncertainty at 95% confidence level as defined by The International Atomic Energy Agency[116] is calculated from

$$U = \sqrt{\sum_j x_j^2 + 1.13 \sum_i x_i^2} \qquad 5\text{-}1$$

where x_j is the random uncertainty and x_i is the estimated maximum systematic error of the individual data points. For the 55-μm and the 5-μm thick dye film these figures are as follows:

Random uncertainty:

	55 μm	5 μm
measurement of optical density	: ± 5%	± 10%
measurement of background optical density	: ± 2%	± 10%
measurement of film thickness	: ± 1%	± 2%
charge measurements of high-LET irradiations	: ± 2%	± 2%

Systematic error:

dose calibration	± 2%	± 2%
spectrophotometer calibration	± 1%	± 1%
stopping power of high-LET irradiation (E > 0.4 MeV/amu):	± 1%	± 1%
inaccuracy on stopping power data due to compound material	± 10%	± 10%

The inaccuracy on stopping power data is only relevant for those ions not fully absorbed by the medium. For ions totally stopped in the medium the imparted energy equals the kinetic energy of the ion.

The overall uncertainty on a 95% confidence level on dose-response measurements for low-LET irradiations of the 55-μm film is

$$U = \sqrt{5^2 + 2^2 + 1 + 1.13(2^2+1)} = 6\%$$

and for high-LET irradiations of the 55-μm film with ion energies above 400 keV/amu and including inaccuracy due to compound material

$$U = \sqrt{5^2 + 2^2 + 1 + 2^2 + 1.13(1 + 1 + 10^2)} = 12.2\%$$

The overall uncertainty on a 95% confidence level on dose-response measurements for low-LET irradiations of the 5-μm film is

$$U = \sqrt{10^2 + 10^2 + 2^2 + 1.13(2^2 + 1)} = 14.5\%$$

and for high-LET irradiations of the 5-μm film with ion energies above 400 keV/amu and including inaccuracy due to compound material

$$U = \sqrt{10^2 + 10^2 + 2^2 + 2^2 + 1.13(1 + 1 + 10^2)} = 18\%$$

The dose calibration of the ^{60}Co γ-ray source[109] and the 10-MeV electron accelerator[112,113] is accurate to within ± 2% and the precision at a 95% confidence level of the response interpretation is ± 5.5% for the 55-μm film determined from the uncertainty of the individual measurements involved in an experimental data point.

The accuracy of the particle fluence data is difficult to determine, because a contamination of the ion beam with secondary electrons and scatter of the

ion charge state, due to collisions with the beam defining slit edges, may introduce a systematic failure though precautions against these sources of error have been taken. The precision at a 95% confidence level of the measurements including statistic scatter amounts to ± 5.8% for the 55-μm film irradiated with ions, but the accuracy of the dose determination depends on the tabulated proton stopping power data and the influence from the calculation procedure of heavy-ion stopping power and of a compound material. The uncertainty on the proton stopping power data ranges from 1 to 15%, highest for the lower energies [45-47], and the uncertainty on the heavy ion stopping power in a compound material is of the same order of magnitude[53,54].

The precision of the experimental RE for particles penetrating the 55-μm film is 13.6% calculated as the root mean square of the precisions on the low- and high-LET dose-response characteristics. The precision on the theoretical RE is 11.7% calculated as the root mean square of the precision on D_{37} and the uncertainties on stopping power data. For particles penetrating the 5-μm film the precision on experimental and theoretical RE is 23.1% and 17.6%, respectively, determined as above and for energies above 400 keV/amu. At energies below 400 keV/amu and for particles penetrating the 5-μm film the precision on experimental and theoretical RE is 25.2% and 20.3%, respectively.

5.3 Measurements on alanine

The ESR spectra were all recorded at room temperature using a Varian E 3 spectrometer operating at the frequency of 9.395 GHz and at a constant microwave power level of 8 mW. For those samples homogeneously irradiated to doses above 10^5 Gy, the microwave power level is set at 11 mW in order to achieve an optimal ESR signal. The magnetic field setting is 340 mT, the field scan-range is 25 mT, and the magnetic modulation frequency and amplitude are 100 kHz and 10^{-4} T, respectively, for all measurements. The receiver gain for detection of the microwave absorption signal, the scan time, and the filter time constant are changed in accordance with the signal strength in order to have a proper size of the signal on the x-y recorder. Attention must be paid to the detector bias current, which strongly influences the recorded signal. This bias current is before any measurement adjusted to exactly 200 μA. The temperature and humidity conditions in the laboratory are continuously monitored and registered.

The alanine pills are placed on top of a vertically mounted quartz tube; on lowering the tube the pill is placed accurately and reproducibly in the ESR cavity. Before and after a series of measurements the ESR spectrometer sensitivity is checked by introducing a calibrating pitch into the cavity on top of the quartz tube. This standard pitch consists of a stable-free radical, 2.2 diphenyl-1-picrylhydrazyl (DPPH), contained in a sealed quartz tube.

The ESR measuring technique performs the first derivative of the paramagnetic microwave absorption signal by scanning a magnetic modulation signal. The detected and amplified microwave signal is recorded on the x-y recorder as shown in Figs.17 and 25. Despite the large dose range there is only a small difference in the shape and width of the spectra in Fig. 25, showing that possible secondary reactions are negligible.

A double integration over the total scan range of the recorded ESR signal yields the area under the microwave absorption curve. This area is directly proportional to the concentration of free radicals, and can be related to an absolute concentration through a known standard such as the DPPH or other stable radicals. As the shape and width of the spectrum are constant at these signal strengths of interest, a measure of the peak-to-peak value of the highest peaks will be proportional to the double integrated spectrum and thus proportional to the number of free radicals. In this work the peak-to-peak value of the largest peak measured in millimeters serves as the measure for the number of radiation-induced free radicals.

A single pill does not fill the ESR cavity completely. This is why the weight of the irradiated part of the pill must be taken into account in the evaluation of the dose-response. For those pills being fully penetrated by the radiation the total weight of the pill is used. The weight of the irradiated fraction of a pill is determined by the calculated range of the radiation being completely stopped in the pill.

Due to the existence of a small number of unpaired electrons in the unirradiated alanine and to the signal-to-noise ratio of the ESR spectrometer, there is a lower detection limit, which at present corresponds to an absorbed dose of 2 Gy from a low-LET radiation source.

The response for alanine to radiation is expressed as an increase in ESR signal measured in millimeters per unit mass of irradiated alanine, ΔESR/m.

5.4 Uncertainty in dose-response measurements on alanine

The uncertainty in dose-response data for alanine consists of a random uncertainty and a systematic error. The overall uncertainty at 95% confidence level, as defined by The International Atomic Energy Agency[116], is calculated from eq. 5-1 in section 5.2. The data to be used for the alanine pills are the following:

Random uncertainty:

measurement of ESR signal	:	± 0.3%
measurement of weight	:	± 0.2%
charge measurement of high-LET irradiations	:	± 2%

Systematic error:

dose calibration	:	± 2%
ESR spectrometer calibration	:	± 1%
stopping power of high-LET irradiation (E > 0.4 MeV/amu)	:	± 1%
inaccuracy in stopping power data due to compound material	:	± 10%

The overall uncertainty at 95% confidence level on dose-response measurements for low-LET irradiation of alanine is

$$U = \sqrt{0.3^2 + 0.2^2 + 1.13(2^2 + 1)} = 2.4\%$$

and for high-LET irradiations of alanine with ion energies above 400 keV/amu and including inaccuracy due to compound material

$$U = \sqrt{0.3^2 + 0.2^2 + 2^2 + 1.13(1 + 1 + 10^2)} = 10.9\%$$

Uncertainties in the ^{60}Co γ-ray source strength, the 10-MeV electron accelerator, and the proton stopping power data are described in section 5.2.

The accuracy of the particle fluence data is difficult to determine, because a contamination of the ion beam with secondary electrons and scatter of the ion charge state due to collisions with the beam-defining slit edges may

introduce a systematic failure though precautions against these sources of error have been taken. The inaccuracy in stopping power data is only relevant for those ions not fully stopped in the medium. For ions stopped in the medium the imparted energy equals the kinetic energy at the ion. The response, ΔESR/g, and the average dose, energy imparted per unit mass, are both inversely proportional to the penetration depth of the ion and as such dependent on the stopping power calculations. This uncertainty, however, influences only the position of the actual data point on the dose-response curve at low doses but not its position relative to that of low-LET radiation, i.e. the experimental relative effectiveness is unaffected by the precision on stopping power data. At saturation doses the level of response will be inversely proportional to the weight, and hence dependent on the penetration depth and stopping power. This leads to a precision of 2.3% on the dose-response characteristics for high-LET particles determined as a total random uncertainty at 95% confidence level. The precision of the experimental RE is 3.3% calculated as the root mean square of the precisions on the low- and high-LET dose-response characteristics. For the 16 MeV protons the precision of the experimental RE at 95% confidence level is 11.1%.

The theoretical evaluation of RE makes use of both the characteristic D_{37}-dose obtained from the low-LET radiation and the stopping power of the ions, and is as such subject to uncertainties from these two factors. The precision on the theoretical RE is 10.3% calculated as the root mean square of the precision on D_{37} and the uncertainties on stopping power data.

6. RESULTS

6.1 Dose-response and relative effectiveness of the 55-μm thick dye film

Dose-response characteristics of the dye film have been obtained for the following radiation qualities: ^{60}Co γ-rays, 10-MeV electrons, 3- and 16-MeV protons, 10-MeV α-particles, 21-MeV ^{7}Li-, 42 MeV ^{14}N-, and 64-MeV ^{16}O ions covering a range in initial LET of 2-5430 MeVcm^2/g corresponding to an average LET in the film of 2-6740 MeVcm^2/g. The dose-response characteristics measured at the wavelength of 510 nm are shown in a double logarithmic plot in Fig. 26. Each data point consists of measurements of at least three irra-

diated samples, and the bars indicate the uncertainty at 95% confidence level.

All curves are parallel at low doses with the same slope up to approximately $\Delta OD/mm = 10$, but the saturation optical densities are different. At doses below $5 \cdot 10^4$ Gy the curves for the low-LET radiations, i.e. ^{60}Co γ-rays and 10-MeV electrons, are identical, but the maximum optical density per unit film thickness is considerably higher for the 10-MeV electrons than for ^{60}Co γ-rays. These observations have been confirmed by other authors[94]. Accordingly the $D_{3,7}$ values are $3.3 \cdot 10^5$ and $1.7 \cdot 10^5$ Gy, respectively. The saturation optical density per unit film thickness for the 42 MeV ^{14}N- and 64 MeV ^{16}O ions is the same as for the 10-MeV electrons, whereas the saturation optical density per unit film thickness for the 3- and 16-MeV protons and the 10-MeV α-particles is between the saturation optical density per unit film thickness for ^{60}Co γ-rays and 10-MeV electrons.

The parallel displacement of the curves relative to the curves for ^{60}Co γ-rays and 10-MeV electrons reflects the relative effectiveness, RE, of the different radiation qualities. For determination of RE only the linear part of the curves in the double logarithmic plot should be used.

The slope of the curves in the double logarithmic plot is approximately 43° indicating sublinearity of the dose-response. This indicates that the Poisson distribution function, eq. 2-2 in section 2.4, should be modified with an exponent $m = 0.94$ in the theoretical evaluation of RE though this exponent in the hit theory conceptually is a quantized number. The dose-response curves for the dye film are fitted by the expression

$$\Delta OD/mm = (\Delta OD/mm)_{max} \cdot (1 - \exp(-D/D_{3,7}))^{0.94} \qquad 6\text{-}1$$

for which variations in maximum optical density and $D_{3,7}$ are not taken into account, but $m = 1$ is used in the theoretical calculations of RE.

Because of sublinearity the relative effectiveness of the different radiations can be found with higher accuracy from a change in the initial slope of the dose-response curves plotted in a linear scale, Fig. 27. The difference between the two sets of results is insignificant as long as RE is measured at the linear part of the log-log curves. Experimentally obtained values of RE based on the linear plot are shown in Table III, together with theoretical values based on the track structure theory as outlined in section 2 using the

Poisson distribution function as expressed in equation 2-2. Theoretical RE-values based on D_{37} equal to $1.7 \cdot 10^5$ Gy and $3.3 \cdot 10^5$ Gy are also compared in Table III. For the heavy charged particles the 55-μm dye film is investigated here for a thick detector (with the exception of 16-MeV protons), i.e. the bombarding particle is either stopped or has lost a considerable amount of its initial energy in the detector, hence the measured REs are average values. The calculated RE has to be an average value as well and is obtained by dividing the 55-μm thick film into a number of segments, and for each segment average values of z, β, σ, and RE are determined. The number of segments used must be large enough for the RE to converge.

The uncertainty in stopping power data influences the determination of absorbed dose to the film and consequently the dose-response characteristics of the ions and measured RE. The measured RE decreases with increasing stopping power. The influence on the theoretical RE from uncertainties in stopping power is most noticeable at those values of stopping power causing an RE much less than unity. A 10% increase in stopping power causes a 2% decrease in theoretical RE for the 16-MeV protons, 6% for the 3-MeV protons, and 10% for the 64-MeV ^{16}O ions. A comparison between experimental and theoretical RE is then unaffected by the uncertainty in stopping power data for small RE.

Two different range-energy relations for low-energy electrons have been used in the radial dose distribution calculations: linear relation, as used in the work of Katz et al., and a power-law relation as described in section 2.7. The power-law relation is used in the calculations leading to the results presented here. The two sets of results are shown in Table IV and detailed described in a published article[18] attached to this work.

The relative effectiveness of the investigated particles in the dye film has been calculated as a function of the size of the sensitive element, a_0, in the range from 10^{-10} to 10^{-7} m, and with D_{37} equal to $3.3 \cdot 10^5$ Gy (Fig. 28). In the calculations the characteristic dose, D_{37}, for 10-MeV electrons is used, since the dose rates for the heavy particle beams and the 10-MeV electron beam are comparable (see section 3.1 and Fig. 15). By comparing the results with experimentally obtained RE-values it is found that $a_0 = 1.3 \cdot 10^{-9}$ m is an optimum value. The calculated values, however, are within the experimental uncertainty of the measured values by using a sensitive element size of $a_0 = 10^{-9}$ m, except for the results of the nitrogen ions. $a_0 = 10^{-9}$ m has subsequently been used in all calculations for the dye film.

It is seen, however, that the results for the nitrogen ions deviate from the general picture by having a calculated RE, which deviate from the measured RE by more than the experimental uncertainty. In contrast to the other investigated radiations the nitrogen ions were completely stopped in the film, thus including the Bragg-peak with δ-rays of very low energies. As the theory of δ-ray distribution and absorption to a certain extent is untenable at the lowest energies, larger differences between experiments and theory must be anticipated. Further, the theoretical assumption of equivalence of the slowing down spectrum of electrons from low-LET radiation and the δ-ray spectrum of low-energy electrons generated by the penetrating ion may be invalid.

6.2 Stacked thin-film experiments

With background in the results presented in the foregoing section 6.1 it was decided to investigate the slowing down of heavy charged particles in a thick detector consisting of a stack of 5-μm thick dye film samples of the same material as the 55 μm ones[20]. By measuring the individual samples after irradiation and calculating the absorbed dose to each element by means of average stopping power and particle fluence, the difference between measured and calculated RE was registered at different energies of the slowing down particle.

The dose-response characteristics of the 5-μm thick FWT 60-20 radiochromic dye film to low-LET radiations of ^{60}Co γ-rays and 10 MeV electrons are shown in Fig. 29, measured at the spectrophotometric wavelength of 604 nm. At doses below $3 \cdot 10^5$ Gy the response is identical for the two radiation qualities, while at higher doses the response to 10-MeV electrons is higher than to ^{60}Co γ-rays. This is in correspondence with observations made for the 55 μm thick film measured at 510 nm. The low-LET dose-response curves of the 5-μm and 55-μm thick films measured at 604 and 510 nm, respectively, are parallel, but the sensitivity in terms of ΔOD/mm per unit dose is increased by a factor of approximately 6.5 for read-out at 604 nm. The $D_{3,7}$-dose for 10-MeV electrons is $3.3 \cdot 10^5$ Gy.

The average absorbed dose in the thin dye films irradiated in stacks with 21 MeV ^{7}Li- and 64 MeV ^{16}O ions is shown in Figs. 30 and 31 as a function of depth and ion energy. Curve number 1 shows the dose determined from the measured optical density and the low-LET calibration curve for electrons in Fig. 29. For comparison, the dose calculated from the stopping power and particle

fluence is also shown (curve number 2). The error bars indicate 95% confidence level on experimental values. The penetration depth calculated from the continuous slowing down of the ions taking nuclear stopping into account is 107- and 77-μm for 3-MeV/amu ^{7}Li- and 4-MeV/amu ^{16}O ions, respectively. The measured range determined as the depth at the center of the last film in the stack giving a response significantly different from zero is 108- and 73-μm for ^{7}Li-and ^{16}O ions, respectively.

Theoretical values of the relative effectiveness (RE) of the two ion beams with respect to 10-MeV electrons have been calculated using $D_{37} = 3.3 \cdot 10^{5}$ Gy and a radius of the radiation sensitive element, a_0, equal to 10^{-9} m. Experimental and theoretical values are shown in Figs. 32 and 33 for the two ions as a function of the average LET in the individual stacked dye film, and indicate deviations between experimental and theoretical RE values at low ion energies. For ease of comparison the ratio of calculated to experimental RE values is given in Fig. 34, both for ^{7}Li and ^{16}O ions as a function of the specific energy of the ions. The solid lines indicate the 95% confidence level for a ratio of unity independent of the energy.

Due to the longer penetration range of the ^{7}Li ions a 53-μm thick dye film was interspersed in the beginning of the dye film stack irradiated with 21-MeV ^{7}Li ions. The measured and calculated RE value for this film agreed within 5% with the results presented in section 6.1 taking a slight change of RE into account as due to a difference in stopping power values used in the two investigations. Similarly for the first 53 μm of the stack irradiated with ^{16}O ions the experimental and theoretical RE agreed both with previous data and with each other within 5%.

The two parameters in the theory, D_{37} and a_0, have been varied from the stated values of $3.3 \cdot 10^{5}$ Gy and 10^{-9} m, respectively. A reduction of D_{37} will lead to a decrease in calculated RE values. The decrease in RE will be slightly lower at high specific energies (> 2 MeV/amu) than at low energies (< 1 MeV/amu), but the difference was not sufficient to obtain a significantly better correlation between experiment and theory than shown in Fig. 34. By changing the size of the sensitive element a_0 it has not been possible to obtain better overall agreement between theory and the present experimental results.

6.3 Dose-response and relative effectiveness of alanine

Dose-response characteristics of L-α-alanine have been obtained for the following radiation qualities: ^{60}Co γ-rays, 4- and 16-MV x-rays, 6-, 10-, and 20-MeV electrons, 6- and 16-MeV protons, 20-MeV α-particles, 21-MeV ^{7}Li-, 64-MeV ^{16}O-, and 80-MeV ^{32}S ions covering a range in initial LET of 2-20201 MeVcm^2/g. Response expressed as change in ESR-signal per unit weight of irradiated alanine as a function of absorbed dose is shown in a double logarithmic plot in Fig. 35. For those particles completely stopped in the sample the weight of irradiated alanine is found from the calculated penetration depth in the continuous slowing down approximation. The calculated range is relied upon for the dose calculations, since it very accurately corresponded to the measured range for 21-MeV ^{7}Li- and 64-MeV ^{16}O ions in the FWT 60 dye film as shown in section 6.2. Each data point consists of measurement of three samples irradiated simultaneously under the same irradiation conditions and measured individually in the ESR spectrometer. The bars indicate uncertainty at 95% confidence level.

All curves are parallel up to a level of approximately ΔESR/g ≈ 0.5, where saturation sets in for those particles having the lowest response at saturation. As for the dye film measurements the saturation ΔESR-response is different for the used radiation qualities, but in contradiction with the dye film the saturation level is in general a decreasing function of the LET of the penetrating particle. For the 10-MeV electrons, however, the saturation response is above that of ^{60}Co γ-rays. This is ascribed to the big difference in dose rate for the two radiations, as a pronounced fading (approx. 6% in 20 hours) of the saturation response is observed after irradiation with the 10 MeV electrons. The same amount of fading of the saturation response has been observed for the ion irradiations, why all measurements of the saturation response is referred to a response immediately after irradiation. Dose-response characteristics for the 4- and 16-MV x-ray and for the 6- and 20-MeV electron irradiations have been performed only at doses, $\leq$ 200 Gy, because of a "low" dose rate, 80 Gy s^{-1}, of the radiation therapy linear accelerators at the University Hospital at Herlev. The radiation sensitivity, however, of alanine for these radiations is the same as the one obtained with ^{60}Co γ-rays. These radiations all fully penetrate the alanine sample.

The parallel displacement of the curves relative to the curves for ^{60}Co γ-rays or fast electrons reflects the relative effectiveness, RE, of the different radiation qualities. As the saturation ESR-signals are changing with

the radiation quality, only the linear part of the log-log plot curves should be used. The slope of the curves is exactly 45° indicating linearity at doses below D_{37} and that alanine mimic an ideal one-hit detector with regard to the shape of the dose-response curve. Experimentally obtained values of RE are shown in Table V together with theoretical values calculated from track structure theory as described in section 2. The power-law range-energy relation for the secondary electrons has been used in the calculations.

The 0.2 cm thick alanine pill is a thick detector which, except for the 16-MeV protons, completely stops the investigated heavy charged particles. The penetration depth of the 80-MeV ^{32}S ions is $4 \cdot 10^{-5}$ m, i.e. only a small fraction of the alanine pill is irradiated. The measured RE is an average of a whole spectrum of RE-values generated as the particle slows down in the medium. The calculated RE must be an average as well, and is obtained by dividing the range of the particle in a number of segments and for each segment to determine average values. As the particles are completely stopped in the detector and the calculations of RE around the Bragg-peak are uncertain, a relatively big divergency between measured and calculated RE-values is anticipated.

The relative effectiveness of the investigated particles in alanine has been calculated as a function of a_0, the size of the sensitive element, in the range from 10^{-10} to 10^{-7} m and with $D_{37} = 1.05 \cdot 10^5$ Gy (Fig. 36). By comparing the results with measured values it is found that $a_0 = 3 \cdot 10^{-9}$ m is an appropriate size which then is used for the results shown in Table V. In the calculations the calibration curves for ^{60}Co γ-rays and 10 MeV electrons have been used giving a characteristic D_{37}-dose of $1.05 \cdot 10^5$ Gy.

7. DISCUSSION

7.1 Radial dose distribution and effective charge

The power-law range-energy relation of low-energy electrons (eq. A1-4) leads to a radial dose distribution (eq. 2-15) around the ion's path in reasonable agreement with published data[56,57,77,78].

The radial dose distributions calculated from eq. 2-15 are compared with experimental data for 0.262 MeV/amu $^{127}I^-$ and 2.4 MeV/amu ^{16}O ions[78] in Fig. 7, and for 0.563 MeV/amu $^{79}Br^-$ ions[77] in Fig. 5 and Table I. The large discrepancy for the 2.4 MeV/amu ^{16}O data is partly due to the experimental data being approximately 20% too high due to an overestimate of W, the mean ionization energy, as discussed in reference 78. Below 10^{-9} m experimental data of the iodine and oxygen ions are too low due to lack of electron equilibrium, which might also be the case for the bromine ions. It is observed that the calculated values obtained from eq. 2-15 oscillate around the experimentally obtained data as do the data for the bromine ions calculated in a continuous slowing down approximation[77]. The same observations are made when comparing calculated data from eq. 2-15 with data found in reference 56, see Table II. The disagreement below 10^{-9} m, which corresponds to an electron energy of 50 eV, may as well be due to a possible underestimate of the range in eq. A1-4 and to uncertainty in the Bethe energy distribution formula, eq. A1-3, at low energies[60-64]. These discrepancies, however, at low electron energies have a limited influence on the calculation of RE, because of the splitting of the dose to the central core and the dose to the track as described in section 2.7, and because the contribution to dose in the track from electrons of lowest energy is small.

The radial dose distribution formula 2-15 includes the effective charge of the incident ion, which as well is used in the published experimental[57,77,78] and theoretical[56-58,77] data. The referenced experimental data make use of an effective charge based on a formula of Nikolaev et al.[44], which for bromine, iodine, and oxygen ions yields an effective charge of 14.7, 16.1, and 7.03 compared to an effective charge from Ziegler[45], eq. 2-10, of 9.8, 8.8, and 7.1, respectively. Calculated data in references 56 and 58 make use of an effective charge of Barkas[40], which yields 10.2, 8.8, and 7.2, respectively. A comparison of the effective charge calculated from different formulas is shown in Fig. 3.

The uncertainty about the effective charge of the heavy ion is the major cause of divergencies when comparing results of, e.g., the stopping power and dose deposition of ejected δ-rays. The usual assumption in the formulas of effective charge is that the probability of attachment of an electron to an ion is a function of the ion velocity relative to the orbital velocity of the electron when bound to the ion[39]. The expressions for effective charge in references 40-44 are based on this assumption.

Despite the frequent application the procedure of using the effective charge is rather problematic[117], since there are several effective charges to be discriminated in this context, e.g. effective charge for stopping power calculations, charge distribution after passage of the ion through a medium, and effective charge for emission of secondary electrons. The effective charge of an ion is not necessarily a parameter based on a sound physical background, but rather a parameter fitted to describe differences in the interaction between different ions and media for the same ion velocity. The effective charge as defined by Ziegler[45] is based upon a fit of a numerous number of experimental stopping power data to a general formula describing the stopping power of an ion by means of an expression for the effective charge and the proton stopping power data. At ion energies, however, above approximately 1 MeV/amu eq. 2-10 can be rewritten into a term similar to that referenced in 40 and 41.

The empirical expression, eq. 2-10, has been used in this work because of being a versatile description of effective charge independent of the kind of ion and stopping medium. α-particles and lithium ions form an exception. The expression, however, has been developed in order to describe stopping power of a penetrating ion and may not necessarily describe accurately the effective charge to be used in the expression for dose deposition from δ-rays ejected by the ion.

The good agreement between calculated and experimental dose distributions indicates that the various approximations involved in calculations in this work have only a minor effect. The angular distribution has been observed[61-64] to be nearly isotropic for low-energy δ-rays, while higher-energy δ-rays are ejected preferentially in the forward direction. This observation is equivalent to an increase in dose close to the ion's path relative to the calculations. For the very low-energy (< 50 eV) δ-rays the chemical composition of the target material plays a role in the ability to stop and scatter the δ-rays. This is why a theory describing energy distribution in a pure material will be inaccurate in any event. This uncertainty, however, in energy distribution of these very low-energy electrons has only a small impact on the dose distribution. An underestimate of the range of low-energy δ-rays implies a too high calculated dose close to the track. The reasonable agreement between the calculated dose distribution in this work and published experimental data indicates that these effects mentioned here taken together to a certain extent cancel each other.

7.2 Dose-response of the dye film

The experimental results in Fig. 26 show that the dye film is not an ideal detector with a dose-response characteristic in accordance with eq. 2-2. The response is slightly sublinear and does not have a constant saturation level for the different investigated radiation qualities. This may be due to several factors. It has been observed[118] that saturation occurs long before all the latent event sites in a medium have been converted into free radicals, e.g. coloured state of the dye molecules. The concentration of leucocyanide molecules in the film is $1.1 \cdot 10^{26}$ m^{-3}, which corresponds to an average distance between these molecules of approximately $2.5 \cdot 10^{-9}$ m when the molecules are considered as spheres. The distance between coloured dye molecules at saturation dose is approximately $4.5 \cdot 10^{-9}$ m because the measured saturation optical density is only 20% of the theoretically achievable value. This means that the coloured dye molecules are not stabilized closer together than about $4.5 \cdot 10^{-9}$ m in the film material. Radicals trapped in organic solids are reported[119] to stabilize not closer together than approximately 10^{-8} m, which is very close to our findings. Thus, it might seem that saturation in the dye film arises by the interaction of dye molecules that are closer to each other than a certain minimum distance, and furthermore, any interaction between nearest neighbours would be expected to be independent of the type of radiation. Considering Fig. 12, showing the light absorption spectra of the film irradiated to about the same level of coloration by γ-rays, UV-light, and 3 MeV protons, it is found that different radiations lead to the same shape of the spectrum and as such to the production of the same radical species. As the dose-response characteristics for the different radiations show the same shape as well, it would seem probable that the same mechanism of saturation would be present. Figure 26 shows, however, large differences in the level of saturation optical density, which then could be explained by dose-rate effects.

The content of leuco cyanide in the film is approximately 10% by weight (information from manufacturer). With an extinction coefficient of approximately 10^7 $\ell\ mol^{-1}m^{-1}$ 85,120) a theoretical saturation optical density at the wavelength of 604 nm is calculated to have an OD ~ 120 for a 50 μm thick film. Such a high optical density cannot be measured at any spectrophotometer. From measurements, however, of the 5 μm thick film at 604 nm, Fig. 29, a saturation optical density of 2.25 is obtained, which for a 50 μm thick film corresponds to an OD = 22.5. This is a factor of approximately 5 below the theo-

retical value, corresponding to that only 20% of the leucocyanide molecules are converted into the coloured dye at saturation. At a 10% content by weight the concentration of leucocyanide molecules is $1 \cdot 10^{23}$ molecules/kg if they are homogeneously distributed in the film. With an estimated average energy deposition per event, event size, of 60 eV[121], the number of event sites per kg of film is $2.1 \cdot 10^{23}$ at a saturation dose of 2 MGy. This consideration leads to that all existing leucocyanide molecules experience 2 hits in average if all the energy is absorbed by the leucocyanide molecules and, that the maximum obtainable optical density theoretically should be achieved. If the energy is homogeneously distributed on both leucocyanide and nylon molecules, calculations show that only 20% of the existing leucocyanide molecules are hit once at a dose of 2 MGy. If this is the case, no saturation in dye formation would be observed in the investigated dose range.

The chemical reactions leading to the final dye formation have not yet been established in detail. It has been shown, however, in section 3.1 that the reaction leading to the dye formation takes place in two steps, the latter being fairly slow[19,93]. An intermediate product may react with the primary radicals and ions in an as yet unknown fashion and simultaneous bleaching may compete slightly with the dye formation. The bleaching may be due to an effect which anneals the otherwise-formed coloured carbonium ion[122] resulting in the sublinearity and bleaching above saturation doses. Another possible explanation for sublinearity and premature saturation is the destruction of latent colour centers[123-126] and of already-formed colour centers[127,128] by the radiation. Likewise, the nylon matrix may be seriously deformed at the high doses employed, and if this deformation takes place at the same time as irradiation proceeds, the effectiveness of the irradiation may change as well.

Attempts[94] to accomplish linearity by adding a dose-response curve for bleaching to the dose-response curve for colour formation fail. This is because the saturation optical density and bleaching as a function of dose are not constant for different radiation qualities and dose rates (Figs. 26 and 15). A detailed investigation, however, of the mechanisms controlling the dye formation and bleaching effects is beyond the scope of the present work. Any of the suggested mechanisms seem to be possible as an explanation for the premature saturation effect and sublinearity at low doses. The rather strong dose-rate dependency of the saturation optical density may be related to the relatively low rate constant for the second-order process together with an annealing effect.

The difference in saturation optical density can be due to dose-rate effects at high doses. Previous publications[97] and investigations in this work, section 6.1, have shown the film to be dose-rate independent at low to medium doses except at very low dose rates, < 1 Gy s^{-1} 96). The dose rate for ^{60}Co γ-rays is 14 Gy s^{-1}, but $5 \cdot 10^7$ Gy s^{-1} for the 10 MeV electrons. The dose rate for the ions expressed as an average dose rate calculated from absorbed dose and irradiation time is approximately 10^3 Gy s^{-1}. Taking the highly inhomogeneous dose distribution for high-LET particles into account by considering an average dose rate in microvolumes around the ion path, a more appropriate dose rate is obtained. A 64 MeV ^{16}O ion penetrating the film has an effective average dose rate in the track of approximately 10^7 Gy s^{-1}, if the energy is absorbed within 1 μs corresponding to the length of the linac electron pulse and the formation time of the primary radicals and radiation induced species. This dose rate is comparable to that of the 10 MeV electrons. Similar calculations for the 16 MeV protons give an effective average dose rate of 500 Gy s^{-1}, which is only an order of magnitude higher than for ^{60}Co γ-rays. These considerations agree with the experimental findings, which show the saturation optical density to be an increasing function of dose rate (Fig. 15).

7.3 Relative effectiveness of high-LET irradiation of the dye film

In the prediction of relative effectiveness the size, a_0, of the radiation-sensitive element must be known as well as the characteristic dose, D_{37}, for low-LET radiation and the hittedness of the irradiated medium. Hittedness is the number of ionizing events, hits, necessary to activate the radiation sensitive element. The hittedness, which is a quantized number and for the idealized dye film equals unity, and the characteristic dose are obtained from the measured dose-response characteristic for low-LET radiation (Fig. 26). The size of the sensitive element, however, is to a certain extent a fitted parameter, which can be determined only roughly in advance from the knowledge of D_{37}. The classical target theory[30,129,130] yields a procedure for determination of the inactivation cross section of biological molecules. The values obtained are in general consistent with those found by means of physico-chemical methods[131,132] and the procedure may be an approach for estimating the sensitive site size of smaller organic molecules. If it is assumed that the radiation-induced events are deposited randomly in the medium, and that the elements are considered spherical in shape, the volume of the sensitive element can roughly be calculated from the measured character-

istic dose. Having an event size of 60 eV, 1 Gy yields $6.24 \cdot 10^{18}/60$ hits per kg material. $6.24 \cdot 10^{18}$ eV/kg is a conversion constant (the reciprocal of the elementary charge). At the characteristic dose, D_{37}, all elements have experienced one hit on the average. This is why 1 kg of material contains $6.24 \cdot 10^{18} \cdot D_{37}/60$ elements being hit once. The radius, a_0, of the sensitive element is then equal to $(3 \cdot 60/(6.24 \cdot 10^{18} \cdot 4\pi\rho D_{37}))^{1/3}$ m. Taking $D_{37} = 3.3 \cdot 10^5$ Gy a radius of $1.8 \cdot 10^{-9}$ m is obtained for the sensitive element in the dye film, compared to an optimal value of $1.3 \cdot 10^{-9}$ m obtained from a parameter study of the theoretical model (see section 6.1, Fig. 28, and Table VI). $a_0 = 1.3 \cdot 10^{-9}$ m is of course based upon a subsequent rationalization, and a rounded-off value of 10^{-9} m has been used for the calculated results. The size of the sensitive element derived through this procedure from target theory points to an approximate value of a_0, which can be used in a preliminary prediction of the effectiveness for a given kind of particle radiation in a material for which the low-LET dose-response is known.

The relative effectiveness strongly depends on the average dose deposited in sensitive elements close to the ion's path. While the point-target dose distribution mainly depends on the charge and velocity of the penetrating ion, the extended target dose distribution further depends on the size of the sensitive element in the medium and varies inversely with the square of the radius a_0. When a_0 increases an increasing amount of dose from a high-LET particle is deposited at a level below saturation, i.e. below the characteristic D_{37}-dose for γ-rays, with a subsequent increase in total cross section for activation and relative effectiveness.

Taking $D_{37} = 3.3 \cdot 10^5$ Gy and $a_0 = 10^{-9}$ m, theory and experiment agree within experimental uncertainty (Table V), which is remarkable when taking the wide range in LET into account. Considering, however, the relative effectiveness as a function of either initial or average LET as shown in Table VII, no monotonic decrease in RE is found with increasing LET. Similar results have been observed by other investigators[5,9,133,134]. The 64 MeV ^{16}O ions have both higher initial and average LET than the 42 MeV ^{14}N ions, and also a higher RE. This may be explained by reference to the curves in Fig. 38. In the case of 42 MeV ^{14}N ions the Bragg-peak lies within the 55 μm thick dye film, and since z^2/β^2 increases smoothly through the Bragg-peak, whereas LET starts to decrease, the nominal value of average z^2/β^2 in the film will be much higher than the nominal value of average LET. With 64 MeV ^{16}O ions the Bragg-peak is not reached in the 55 μm thick dye film (see Fig. 31) and LET and z^2/β^2 increases continuously during passage of the film.

That RE also depends on β [9] is illustrated by curves 1 and 2 in Fig. 39, where two ions, a 42 MeV ^{14}N ion and a 0.66 MeV α-particle, with the same average $z^2/\beta^2 = 6630$, but with different average relative velocity, $\beta = 8.02 \cdot 10^{-2}$ and $1.85 \cdot 10^{-2}$ have a calculated RE of 0.39 and 0.20, respectively.

When the ion slows down, the range of the δ-rays decreases, and relatively more energy is deposited in a region of saturation close to the ion's path with a resulting decrease in RE. Thin films irradiated in stacks (Figs. 30-33) give experimental evidence for this explanation. At energies, however, below 1.5 MeV/amu, Fig. 34 shows that the calculated RE deviates considerably from that obtained experimentally.

Variations of the two parameters D_{37} and a_0 are unable to reconcile the calculations with the experimental data. Calculated RE at low ion energies (< 1.5 MeV/amu) cannot be decreased by choosing appropriate values of D_{37} and a_0 without decreasing RE at higher ion energies, where theory and experiments are in very good agreement.

The discrepancy in the stacked film experiments between the calculated and measured RE is highest for the 21 MeV ^7Li ions compared to the results for the 64 MeV ^{16}O ions. This can be due to the use of too high a D_{37} value for the lithium ions. As shown in section 6.1 the dye film is dose-rate dependent at saturation doses, which causes that a lower value of $D_{37} \approx 2.2 \cdot 10^5$ Gy should be used in calculating RE for the lithium ions. Hence D_{37} is considered as a fitted parameter not related to the radiation sensitivity of the detector at low doses. A decrease in D_{37} yields a decrease in calculated RE as well over the whole range of LET, but the overall agreement between theory and experiment will be improved only slightly.

Considering the calculated radial dose distributions in Figs. 5, 6, and 7 it is observed that compared to experimental data calculations underestimate doses at distances close to the ion's path. When the ion slows down, the energy and range of the δ-rays decrease and relatively more energy is deposited very close to the ion's path in regions of saturation doses. By underestimating the dose in saturation regions the RE gets overestimated, which might be an explanation for the discrepancy between calculated and experimental RE at low ion energy. Figure 39 explains clearly what happens to the radial dose distribution when the ion slows down.

The good agreement between the calculated and measured range of the ions implies that no large errors are present in the stopping power calculations though the Bragg additivity rule is used for the determination in a compound material. Above 200 keV/amu the stopping power of the individual material components is stated to be accurate to within 5%[45]. A larger uncertainty below 200 keV/amu will have little influence on the total range, but will have a large effect on the calculated and experimental RE values. A shift in position of 1 μm for a 5 μm film placed with the center corresponding to 180 keV/amu of a ^{7}Li ion will change the calculated RE by 20%. Such a shift may be introduced both by the stopping power calculations and by measurements of the film thicknesses.

Another reason for deviations between theory and experiment at low energies of the heavy charged particles is believed to be due to the assumption in the theory that the response of the detector to the δ-ray spectrum is equivalent to the response from the slowing-down spectrum of high-energy electrons from low-LET radiations of either fast electrons or ^{60}Co γ-rays. Ettinger[29] reported an RE of 0.88 and 0.92 for ^{3}H- and ^{14}C β-rays in sucrose compared to ^{60}Co γ-rays, while the low energy Auger electrons from the ^{125}I isotope had an even lower RE of 0.66. At low energies W increases[72], which will lead to a decrease in effectiveness for a detector more sensitive to ionizations than to excitations.

These explanations for discrepancies between measured and calculated RE-values are not unambiguous and cannot be considered to be valid for detectors in general. This has been proved through the results with heavy charged particles completely stopped in alanine, where good agreement between experiments and theory is achieved. The discrepancies in the dye film results are very difficult to explain, but may be ascribed to the general deviations of the dye film parameters from those of the ideal one-hit detector.

D_{37} expresses the radiation sensitivity of a detector and in the theory[7-12,30] is related to the response at saturation dose for low-LET radiation. When the response at saturation is dose-rate dependent, D_{37} appears to be dose-rate dependent as well. By expanding the Poisson distribution function (eq. 2-1) in a Taylor series, P will be equal to $\bar{D}/D_{37}$ at low doses indicating that D_{37} is related to the average energy required to create a dye molecule. Since ^{60}Co γ-rays and 10 MeV electrons have the same effectiveness at low doses D_{37} must be the same for the two radiation qualities, and the apparent difference in D_{37} is only due to dose-rate effects of the maximum

optical density. At present, however, the theory cannot compensate for dose-rate effects, and the D_{37}-value should be chosen from a low-LET radiation with a dose rate corresponding to that of the investigated radiation quality. This reasoning indicates that the D_{37}-value for the 10 MeV electrons is the most appropriate, and the agreement between calculations and experiments is then very good indeed, within -6.2% and +14.3%. These arguments invoked for the D_{37}-value also suggest that the initial slope of the dose-response characteristics (Fig. 27) should be used when determining the experimental values of RE.

7.4 Dose-response of alanine

The experimental results in Fig. 35 show that alanine may be considered as an ideal one-hit detector with respect to the shape of the dose-response function, which appears to be pure exponential in accordance with eq. 2-2. The absence of sublinearity in dose-response, as is seen for the dye film, may be explained by an apparent first-order process of radical production and the high long-time stability of these radicals. Fast formation of radicals in alanine, e.g. investigated by means of a pulsed-radiolysis technique, has so far not been investigated to the author's knowledge, but in the time frame of minutes after irradiation no change in radical concentration has been observed. The destruction or annealing, if present, of the already formed radicals at low- and medium-range doses must be negligible compared to the production of radicals. No dose-rate dependency is observed for low- and medium-range doses for dose rates between 14 and $5 \cdot 10^7$ Gy s^{-1} in accordance with previous investigations[83,84,103-106] at lower dose rates.

The flattening-off of the response at high doses may be explained by the same mechanisms as discussed in section 7.2[126]. The saturation level may correspond to the net production of only one radical per 10^2 to 10^6 molecules[126], depending on the particular solid material being investigated. As for the dye film, however, a change in the saturation level for alanine is observed for different radiation qualities. It is found that the saturation level is slightly higher for the 10 MeV electrons having a dose rate of $5 \cdot 10^7$ Gy s^{-1} than for the ^{60}Co γ-rays having a dose rate of 14 Gy s^{-1}. This difference is ascribed to an observed fading of the response at saturation doses, leading to a relatively smaller saturation response for irradiation with a low dose rate. At saturation doses the level of response will be inversely proportional to the weight of irradiated alanine, and hence dependent on the pene-

tration depth and stopping power of the ions. Uncertainties in calculated penetration depths and corrections for fading strongly influence the experimental values of response at saturation doses. This may be responsible for discrepancies in the general tendency of decreasing saturation level with increasing atomic number and/or average LET of the heavy charged particles, which corresponds to an increase in dose rate in the track of the heavy ion. Decreasing saturation level with increasing LET of the penetrating ion contradicts the observations made for the dye film. However, due to differences in the kinetics of radical formation in the dye film and alanine, there may as well be differences in how the final radical concentration is achieved for various dose rates.

Quantitative measurements of the unpaired electrons by calibration with a known amount of DPPH (2.2-diphenyl-1-picrylhydrazyl) may possibly be able to explain some of the differences observed at saturation doses. The first derivative of the ESR absorption spectra obtained at low- and saturation doses for the same radiation quality shows differences (Fig. 25). Similar phenomena have also been reported by other investigators[107]. A comparison, however, between spectra obtained at saturation doses for different radiation qualities does not reveal changes which could be responsible for these observations.

7.5 Relative effectiveness of high-LET irradiation of alanine

In the prediction of relative effectiveness the size, a_0, of the radiation-sensitive element must be known as well as the characteristic dose, D_{37}, for low-LET radiation and the hittedness of the irradiated medium. The hittedness, which for alanine equals unity, and the characteristic dose are obtained from the measured dose-response characteristic for low-LET radiation, Fig. 35. The size of the sensitive element is found by means of the same procedures as outlined for the dye film in section 7.3. By taking $D_{37} = 1.05 \cdot 10^5$ Gy an estimated radius of a_0 equals $2.6 \cdot 10^{-9}$ m, which should be compared to an optimal value of $3 \cdot 10^{-9}$ m obtained from a parametric study of the theoretical model (see section 6.3, Fig. 36, and Table V). The size of the sensitive elements derived through the procedure from target theory yields an approximate value which can be used in preliminary predictions of the relative effectiveness. The physical consequences of varying a_0 are outlined and discussed in section 7.3.

The results in Table V show good agreement between calculations and experiments. For $D_{37} = 1.05 \cdot 10^5$ Gy and $a_0 = 3 \cdot 10^{-9}$ m theory and experiment agree within the experimental uncertainty, even for the 80 MeV ^{32}S ions having an average LET of 20200 MeVcm^2/g, which is four orders of magnitude higher than LET for the electrons. The divergence between calculated and experimental data is numerically smaller for alanine than for the dye film, which is also reflected in the experimental uncertainty expressed at a 95% confidence level being 12.4 and 10.5 for film and alanine, respectively. The better agreement between experiments and calculations is surprising when taking into account that all but the 16-MeV protons are stopped in the alanine, which means that the Bragg-peak of the stopping particle is within the detector except for the 16-MeV protons. This contradicts the results from the stacked film experiments. Similar experiments with alanine are much more difficult to perform; their results, however, would be very interesting.

Previous investigations[83] with 4 MeV α-particles in alanine have shown a decreasing RE with dose. The reference radiation was ^{60}Co γ-rays. This corresponds to non-parallel dose-response characteristics of the low- and high-LET radiations, and may lead to a lower response at saturation for the 4 MeV α-particles compared to the ^{60}Co γ-rays in agreement with the observations in this work. The measured RE-values were 0.50, 0.46, 0.47, and 0.39 with increasing dose compared to our calculated value of 0.45 for a sensitive element size of $3 \cdot 10^{-9}$ m, and determined at a low dose. The D_{37}-value was found[83] to be $11.2 \cdot 10^4$ Gy compared to our value of $1.05 \cdot 10^5$ Gy. This explains the difference in measured and calculated RE, 0.50 and 0.45, respectively. The difference in the D_{37} dose for ^{60}Co γ-rays cannot be explained at present. Other investigators[36,135] have published a D_{37}-dose for ^{60}Co γ-rays of $7.5 \cdot 10^4$ Gy.

A comparison between experimentally obtained RE-values and values calculated by Katz for 650 MeV α-particles stopped in alanine[83] shows calculated values that are too small (-15%), especially in track segments penetrated by particles of high energy. In these calculations a sensitive element size of $a_0 = 1.1 \cdot 10^{-9}$ m was used, which is one-third of the value obtained in this work giving too low RE-values as RE increases with a_0. In the theoretical data of Katz too big ranges of the generated δ-rays are used which leads to too high doses in the calculation of radial dose distribution[48]. This as well contributes to too small values of RE. The experiments with 650 MeV α-particles also revealed that the effectiveness did not differ significantly from unity, until the LET was above approximately 50 MeVcm^{2}g^{-1}. The average LET of the

16-MeV protons used in this work is 38 $MeVcm^2g^{-1}$, and experimentally no deviation in relative effectiveness from unity is observed.

From knowledge of the spectrum of secondary charged particles from neutron irradiation of alanine, the relative effectiveness has been calculated by Katz over a broad spectrum (2-14 MeV) in primary neutron energy and compared with experimental results[83]. The maximum deviation was approximately 15%. The relative radiation sensitivity of alanine irradiated with neutrons is rather high and varies slowly with energy from 0.5 to 0.74 in the energy range of 2-14 MeV. This makes alanine a useful detector in neutron dosimetry.

8. CONCLUDING REMARKS

The theoretical considerations outlined in the first sections of this work aim to describe by means of a model in quantitative terms the physical phenomena and the consequent effects associated with the radiation action. Based on definitions and experimental dose-effect relations the track structure theory attempts the understanding and prediction of the primary physical events leading to physico-chemical reactions, which are the end points for the action of the different ionizing radiation qualities. While the theory focuses on the description of the physical events for the determination of effects, the physico-chemical reactions are considered as qualitative events, "black-boxes". The internal mechanisms of these events are considered to be affected from influences of nothing but average absorbed dose in the volume of the sensitive element and the number of hits or targets (in biological systems). Experiments make it evident, however, that the mechanisms in media due to the radiation action are not fully described by mathematical models based on radiation physics, probability functions, and approaches from classical target theory. Numerous effects such as kinetics of radical formation, radical-radical interactions, annealing effects, radiation-induced destruction of latent event sites, and the influence from the rate of energy deposition also account for the measured dose-effect relation. Unfortunately, there is a significant lack of information describing the virtual mechanisms to be incorporated into a model, which details and predicts the final effect precisely for a given dose of ionizing radiation.

The subject of this work is to investigate a theoretical model, which on the basis of experimental knowledge from low-LET irradiation of a medium predicts the dose-effect curves for the medium irradiated with high-LET particles. This theory of track structure, however, does not attempt to identify the particular interactions that are reflected in the processes, neither does it specify the nature of the sensitive element, though the size of the element is an important parameter for the model. In spite of these shortcomings the experimental and theoretical results show that remarkable good results can be obtained with a model that separates physical stochastics from radiation-induced physico-chemical events in a mathematical treatment by incorporation of a few experimentally obtained data for the particular medium under investigation.

The success of the model of track structure is without doubt due to the conception of the distribution of the imparted energy. This profound sound physical reasoning about the equality of slowing-down spectra from electrons has created a model, which reduces the action of single heavy charged particles to a response function for electrons and photons. The reasoning seems to be valid as long as relatively fast electrons, energetic enough for the binding energies of the molecular electrons to be of minor importance, penetrate into a homogeneous cloud of free electrons, where only the number per unit volume is of major importance. When changing the radiation quality, e.g. into different heavy charged particles, it is, roughly speaking, only the distribution of ionization energy which is changed and consequently the physical stochastics as well. This is possibly the reason why this theoretical approach to determination of relative effectiveness in some way can be treated as independent of the physico-chemical interactions.

From experiments, however, with dye film and alanine reported in this work, it is shown that as long as the mean dose to the medium is kept in the linear region of the response and the specific energy of the heavy ion is above 2 MeV/amu, the medium acts upon irradiation fully in accordance with the theoretical considerations. But at marginal high doses discrepancies appear and uncontrolled physico-chemical processes intervene for which the theoretical model is unable to describe in its current presentation. The change in saturation level, presumably due to a dose-rate effect, in fact implies a change of D_{37} as well. This highly contradicts the conception of D_{37} as being an expression for the radiation sensitivity of a medium. Thus, the irrefutable concept in track structure theory of using a universal characteristic dose, D_{37}, obtained from a fortuitous low-LET irradiation, shows itself to be un-

tenable[136]. The various events, which lead to the final radiation effect in a medium, is influenced by a number of factors, e.g. dose-rate effects, radical-radical interactions, structural changes in the matrix, and annealing. These factors are for the ideal one-hit detector considered negligible. A thorough conception of chemical reaction mechanisms, e.g. a G-value (number of radicals formed per 100 eV imparted energy) could replace the D_{37} concept with advantage. The observations made in this work for the dye film and alanine of increasing respectively decreasing saturation level with excitation and ionization density has also been found by other investigators[107] and emphasize the inadequacy of the D_{37} concept.

It has been shown that good agreement is to be expected mainly at ion velocities well above velocities in the Bragg-peak, i.e. at velocities where the electron slowing-down spectrum is relatively independent of the primary δ-ray energy. At lower ion velocities, however, the electron slowing-down spectrum depends on the primary δ-ray energy, and the consequence for the dye film is too high RE-values. Recent investigations[29] concerning measurements of radiation effects in glutamine and mannose have revealed a decreased effectiveness of very low-energy (< 1 keV) electrons compared to fast electrons, which contradict conclusions of earlier findings[24] of independency of the initial energy of the primary electron and the slowing-down spectrum and number of events per unit energy deposited in water. Other investigations[27,28] have shown a decreased effectiveness for ultra-soft x-rays compared to hard x-rays in dicentric chromosome aberrations of lymphocytes, while an increased effectiveness has been observed for ultra-soft x-rays in cell killing and induced mutations in hamster cells.

These latter observations as well lead to the conviction that it cannot be assumed a priori that there is a unique relation between the absorbed dose from uniform low-LET radiations in general and of the probability of occurrence of the final effect. This means that the folding of the probability function $P(z,\beta,t,a_0,D)$ into the radial dose-distribution calculations does not necessarily mimic correctly the distribution of effect. An ideal situation is achieved when the spectrum of the ion-generated δ-rays and the associated impartation of dose at any position and dose rate is matched by a spectrum of effect obtained for the medium irradiated with electrons with the same spectra in identical volumes. These relationships could be obtained through a careful combination of experiments and calculations. Kalef-Ezra et al.[5] present a modified track structure theory approach to the calculation of relative thermoluminescent response to heavy charged particle irradiation.

In this approach the detector response is not only related to the inhomogeneous dose distribution from the secondary electrons, but also includes the properties of these electrons by using carefully selected low-energy electron spectra as test radiation fields. The electron spectrum is matched as close as possible to the initial energy spectrum of the electrons ejected during the slowing-down of the heavy charged particle. The spectrum in dose-response of the low-energy electrons absorbed in the particular medium is subsequently folded into a calculated point target dose distribution around the ion's path. The relative effectiveness is expressed by the ratio of the response from heavy charged particles to that of low-LET radiation for the same dose. The introduction of test radiation fields has made the concept of the characteristic $D_{s,}$ dose redundant as well as avoiding the use of a sensitive element size. This modified theory shows good agreement with experimental results in predicting relative effectiveness also in regions of the Bragg-peak of the heavy charged particle. In order, however, to establish such a procedure to be incorporated into the model of track structure theory, exhaustive experimental work is necessary, and obviously the ideal situation is virtually impossible to achieve.

In spite of these different variations in radiation effectiveness and the discrepancy at lower ion energies observed in this work, the track structure theory can, by adjusting parameters obtained from experiments, be made to fit radiobiological, experimental data obtained in the Bragg-peak region for kidney cells hypoxic irradiated with carbon and neon ions[137]. This adjustment, however, of parameters is based on a subsequent rationalization and the final result cannot be considered to be a real prediction.

Though the track structure theory is a rather crude model making use of approximations and estimates, the final result of relative radiation effectiveness is rather sensitive to parameters as, e.g., sensitive element size and the probability distribution function. The sensitive element size in theory roughly corresponds to the size of the molecule being the target for radiation. But a change in a_0 by less than an order of magnitude causes RE to become unrealistic. On the other hand, an estimate of the sensitive element size by means of general target theory yields data in good agreement with experimental results. However, fitting of a_0 may be less sensitive for small element sizes of physico-chemical systems than for large element sizes of more complex biological cell systems. Incorporating the sublinear probability function for the dye film by means of the suggested exponent in eq. 6-1, which makes the function mimic experiments, results in comprehensive devia-

tions of the relative effectiveness from measured values. The latter really contradicts the intentions put into the conceptual basis for the convolution of an experimentally obtained probability function into the calculated inhomogeneous dose distribution.

These reflections, in fact, about the apparent arbitrary choice of certain parameters of paramount importance for the results, make the entire theory look rather formal and the results largely based on a fortuitous cancellation of a number of independent errors. It is impossible, on the other hand, from a theoretical point of view to dismiss a theory based on sound thinking of physical mechanisms and which is in good accordance with experiments. At this point it is important to emphasize that the basic theory at present is paramount to any other model attempting to predict the radiation effectiveness for heavy charged particles both for physico-chemical media as for biological systems. In summary it can be stated that the track structure theory provides a model, which over an enormous range of LET (four decades) predicts the dose-response curves for fast (> 2 MeV/amu initial energy) monoenergetic ions in thin targets and to a lesser extent predicts them for thick targets and for slow ions (< 1 MeV/amu).

Apart from implications of the track structure theory to the general understanding of radiation effects from heavy charged particles, an obvious continuation in the future work with the theory should include physical media showing supralinearity in the low-LET dose-response characteristic, thus being characterized as multi-hit detectors. Thermoluminescent dose meters show supralinearity at certain glow peaks, and from previous studies[5] it appears that the track structure theory is applicable in calculation of thermoluminescent properties included by heavy charged particles.

The usage of the track structure theory in thermoluminescence dosimetry will preferably take place in health physics[138] and radiation therapy[139] work, for which neutrons, high-energy protons and α-particles, and fission fragments are common radiation qualities. Calculated predictions of dose-response relationships for heavy charged particles by means of track structure theory are much less time consuming than direct experimental measurements. The theory will have a tremendous impact on personal radiation dosimetry and on mixed field dosimetry for which a given response of a dose meter should be interpreted in terms of dose.

9. ACKNOWLEDGEMENT

I acknowledge with pleasure the support of Risø National Laboratory to implement the present work.

I am indebted to Leif Sarholt-Kristensen, Physical Laboratory II, H.C. Ørsted Institute, University of Copenhagen, for helping me with the formalities in bringing this project into progress, and for the continuous support during the work also in pointing out literature of relevance.

I have enjoyed very much the hospitality at the Department of Radiophysics, the University Hospital of Copenhagen, Herlev, and I am indebted to Kjeld J. Olsen for his careful and precise guidance through this study, and for generously sharing his profound experience and comprehensive knowledge in our discussions.

Special thanks are due to Mads Wille for his skilful construction of the experimental equipment and for his untiring efforts and enthusiasm in the experimental measurements and processing of results. I would as well like to express my sincere appreciation to Ruth Madsen for her patience and endurance in typing the manuscript, and to Jerzy Holcman who as an innocent bystander has given me so much encouragement.

I want to thank the staff at the Niels Bohr Institute, Tandem Accelerator Laboratory, for hospitality and help with equipment and experimental set-up, and I want to express my gratitude to Per Knudsen, Jørn Westergaard, and Per Rex Christensen who have spent time in discussing problems concerning heavy charged particle irradiations.

Thanks are due to Department of Physical Chemistry, University of Aarhus, for lending me the ESR spectrometer, which in fact combined necessary spectroscopy with pleasure.

REFERENCES

1) Kellerer, A.M. and Rossi, H.H., The Theory of Dual Radiation Action. Current Topics in Radiation Research Quarterly 8, 85-158 (1972).

2) Chadwick, K.H. and Leenhouts, H.P., A Molecular Theory of Cell Survival. Phys. Med. Biol. 18, No. 1, 78-87 (1973).

3) Fain, J., Monnin, M. and Montret, M., Spatial Energy Distribution Around Heavy Ion Path. Radiat. Res. 57, 379-389 (1974).

4) Fain, J., Montret, M. and Sanzelle, S., Thermoluminescence and Heavy Ion Microdosimetry. Seventh Symp. on Microdosimetry, Oxford (J. Booz, H.G. Ebert, H.D. Hartfield, Eds.) 807-820, Harwood, England (1980).

5) Kalef-Ezra, J. and Horowitz, Y.S., Heavy Charged Particle Thermoluminescence Dosimetry: Track Structure Theory and Experiments. Int. J. Appl. Radiat. Isot. 33, 1085-1100 (1982).

6) Horowitz, Y.S., Moscowitch, M. and Dubi, A., Response Curves for the Thermoluminescence induced by Alpha Particles: Interpretation Using Track Structure Theory. Phys. Med. Biol. 27, No. 11, 1325-1338 (1982).

7) Butts, J.J. and Katz, R., Theory of RBE for Heavy Ion Bombardment of Dry Enzymes and Viruses. Radiat. Res. 30, 855-871 (1967).

8) Katz, R., Sharma, S.C.and Homayoonfar, M., The Structure of Particle Tracks. In: Topics in Radiation Dosimetry, Supplement 1. (F.H. Attix, Ed.) 317-383. Academic Press, New York. (1972).

9) Katz, R., Track Structure Theory in Radiobiology and in Radiation Detection. Nuclear Track Detection 2, No. 1, 1-28, Pergamon Press, New York (1978).

10) Katz, R., Ackerson, B., Homayoonfar and M., Sharma, S.C., Inactivation of Cells by Heavy Ion Bombardment. Radiat. Res. 47, 402-425 (1971).

11) Katz, R., High LET Constraints on Low LET Survival. Phys. Med. Biol. 23, No. 5, 909-916 (1978).

12) Katz, R. and Sharma S.C., Response of Cells to Fast Neutrons, Stopped Pions, and Heavy Ion Beams. Nucl. Instr. Meth. III, 93-116 (1973).

13) Hansen, J.W., Jensen, M. and Katz, R., The Radiochromic Dye Film Dose Meter as a Possible Test of Particle Track Theory. Seventh Symp. on Microdosimetry, Oxford (J. Booz, H.G. Ebert, H.D. Hartfield, Eds.) Vol. II, 821-830, Harwood, England (1980).

14) Hansen, J.W. and Olsen, K.J., Prediction of High-LET Dose-Response Characteristics From Detector Parameters of Low-LET Radiation. Seventh Meeting in Nordic Society for Radiation Research and Radiation Technology, Gol, Norway, March 8-11 (1981).

15) Hansen, J.W. and Olsen, K.J., High-LET Dose-Response Characteristics Described by Track Structure Theory of Heavy Charged Particles. Risø-M-2308, Risø National Laboratory, Denmark (1981).

16) Olsen, K.J. and Hansen, J.W., High-LET Dose-Response Characteristics of the Dye Film Dose Meter in the Context of Track Structure Theory. Eighth Symp. on Microdosimetry, Jülich (J. Booz, H.G. Ebert, Eds.) 983-992, EUR-8395 (1982).

17) Hansen, J.W. and Olsen, K.J., Experimental Investigation of the Delta Ray Theory for Heavy Ions Applied to Thick Detectors. Proc. Seventh Int. Congress of Radiation Research, Amsterdam (J.J. Broerse, G.W. Barendsen, H.B. Kal, A.J. van der Kogel, Eds.) E1-07, Martinus Nijhoff Pub. (1983).

18) Hansen, J.W. and Olsen, K.J., Experimental and Calculated Response of a Radiochromic Dye Film Dosimeter to High-LET Radiations. Radiat. Res. 97, 1-15 (1984).

19) Hansen, J.W., Wille, M. and Olsen, K.J., Problems Associated with the Use of the Radiochromic Dye Film as a Radiation Dose Meter. Radiat. Phys. Chem. 23, No. 4, 455-462 (1984).

20) Olsen, K.J. and Hansen, J.W., Experimental and Calculated Effectiveness of a Radiochromic Dye Film to Stopping 21 MeV ^{7}Li- and 64 MeV ^{16}O Ions. Nucl. Instr. Meth. B5, 497-504 (1984).

21) Linear Energy Transfer, ICRU Report 16. International Commission on Radiation Units and Measurements. Washington, D.C., USA (1970).

22) Sinclair, W.K., The Relative Biological Effectiveness of 22 Mevp X-Rays, Cobalt-60 Gamma Rays, and 200 kvcp X-rays. Radiat. Res. 16, 394-398 (1962).

23) Olsen, K.J. and Hansen, J.W., Biological Effectiveness and Application of Heavy Ions in Radiation Therapy described by a Physical and Biological Model. Risø-R-477, Risø National Laboratory, Denmark (1982).

24) Hamm, R.N., Wright, H.A., Katz, R., Turner, J.E. and Ritchie R.H., Calculated Yields and Slowing Down Spectra for Electrons in Liquid Water: Implications for Electron and Photon RBE. Phys. Med. Biol.23, No. 6, 1149-1161 (1978).

25) Lehman, C., Interaction of Radiation with Solids and Elementary Defect Production. Vol. 10 of Defects in Crystalline Solids (S. Amelinckx, R. Gevers, J. Nihoul, Eds.), North Holland Publishing Company, Amsterdam, New York, Oxford (1977).

26) Chadderton. L.T., Radiation Damage in Crystals. Methuen's Monographs on Physical Subjects (B.L. Worsnop, Ed.), London, 16-35 (1965).

27) Goodhead, D.T., Cox, R. and Thacker, J., Do Ultrasoft X-Rays Produce Lesions Characteristic of High-LET or Low-LET, or Neither? Seventh Symp. on Microdosimetry, Oxford, (J. Booz, H.G. Ebert, H.D. Hartfield, Eds.), 929-942, Harwood, London (1981).

28) Goodhead, D.T., Virsik, R.P., Harder D., Thacker, J., Cox, R. and Blohm, R., Ultrasolf X-Rays as a Tool to Investigate Radiation-Induced Dicentric Chromosome Aberation. Seventh Symp. on Microdosimetry, Oxford (J. Booz, H.G. Ebert, and H.D. Hartfield, Eds.), 1275-1285, Harwood, London (1981).

29) Ettinger, K.V., Srirath, S., Anunuso, C.J. and Mallard, J.R., Lyoluminescent Dosimetry of Incorporated Low Energy Beta Emitters and of Auger Electrons. Seventh Symp. on Microdosimetry, Oxford (J. Booz, H.G. Ebert, and H.D. Hartfield, Eds.), 1389-1398, Harwood, London (1981).

30) Dertinger, H. and Jung, H., Molecular Radiation Biology. Springer Verlag, New York, USA (1970).

31) Katz, R., Sharma, S.C., and Homayoonfar, M., a) Radical Production in Solid Biological Substances, and b) the Fricke Dosimeter. Third Symp. on Microdosimetry, Stresa (H.G. Ebert, Ed.), Vol. 1, 199-215, EUR 4810 (1971).

32) Sharma, S.C. and Katz, R., The 1-Hit Detector in Measurement of Radiation Quality. Fourth Symp. on Microdosimetry, Pallenza (J. Booz, H.G. Ebert, R. Eickel, A. Waker, Eds.), Vol. 2, 655-688, EUR 5122 (1973).

33) Katz, R., Sharma, S.C. and Homayoonfar, M., Detection of Energetic Heavy Ions. Nucl. Instr. Meth. 100, 13-22 (1972).

34) Rosenstein, M., Eisen, H., Roush, M.L. and Silverman, J., Response of the Hexahydroxyethyl Pararosaniline Cyanide Dosimeter to 3.0 MeV Protons. Int. J. Appl. Radiat. Isot., Vol. 26, 423-426 (1975).

35) Katz, R. and Kobetich, E.J., Response of Nuclear Emulsions to Electron Beams. Nucl. Instr. Meth. 79, 320-324 (1970).

36) Waligorsky, M.P.R., Katz, R., Byrski, E., Sarna, T., Pasenkiewicz-Gierula, M. and Knapczyk, J., Mixed Field Dosimetry in a Cyclotron-Produced Fast Neutron Radiotherapy Beam with Special Emphasis on a Newly Developed Alanine System. Forth Symp. on Neutron Dosimetry, GSF, Munich-Neuherberg, June 1-4 (1981).

37) Katz, R. and Pinkerton, F.E., Response of Nuclear Emulsions to Ionizing Radiations. Nucl. Instr. Meth. 130, 105-119 (1975).

38) Krauter, R.A., The Sigma Integration (unpublished) (1977).

39) Bohr, N., The Penetration of Atomic Particles Through Matter. K. Dan. Vidensk. Selsk Mat.-Fys. Medd. 18, No. 8, Denmark (1948).

40) Barkas, W.H., Nuclear Research Emulsions, Vol. 1. Academic Press, New York, USA (1963).

41) Northcliffe, L.C. and Schilling, R.F., Range and Stopping Power Tables for Heavy Ions. Nucl. Data Tables, A7, 233-463, Academic Press, New York, USA (1970).

42) Burenkov, A.F., Komarov, F.F. Temkin, N.M., Semiclassical Theory for Energy Loss of Heavy Nonrelativistic Ions in Matter. Radiation Effects 46, 59-70 (1980).

43) Shima, K., Ishihara, T. and Mikumo, T., Empirical Formula for the Average Equilibrium Charge-State of Heavy Ions Behind Various Foils. Nucl. Instr. Meth. 200, 605-608 (1982).

44) Nikolaev, V.S., Dmitriev, I.S., On the Equilibrium Charge Distribution in Heavy Element Ion Beams. Phys. Lett. 28A, 277-278 (1968).

45) Ziegler, J.F., Handbook of Stopping Cross-Sections for Energetic Ions in All Elements. Vol. 5 of the Stopping and Ranges of Ions in Matter (Ziegler, Ed.), Pergamon Press, New York, USA (1980).

46) Andersen, H.H. and Ziegler, J.F., Hydrogen Stopping Powers and Ranges in All Elements. Vol. 3 of The Stopping and Ranges of Ions in Matter (J.F. Ziegler, Ed.), Pergamon Press, New York, USA (1977).

47) Ziegler, J.F., Helium Stopping Powers and Ranges in All Elemental Matter. Vol. 4 of The Stopping and Ranges of Ions in Matter (J.F. Ziegler, Ed.), Pergamon Press, New York, USA (1977).

48) Andersen, H.H., Besenbacher, F. and Knudsen, H., Stopping Power and Straggling of 65-500 keV Lithium Ions in H_2, He, CO_2, N_2, O_2, Ne, Ar, Kr and Xe. Nucl. Instr. Meth. 149, 121-127 (1978).

49) Andersen, H.H., Besenbacher, F. and Goddiksen, P., Stopping Power and Straggling of 80-500 keV Lithium Ions in C, Al, Ni, Cu, Se, Ag and Te. Nucl. Instr. Meth. 168, 75-80 (1980).

50) Ziegler, J.F., The Electronic and Nuclear Stopping of Energetic Ions. Appl. Phys. Lett. 31, No. 8, 544-546 (1977).

51) Lindhard, J., Scharff, M. and Schøtt, H.E., Range Concepts and Heavy Ion Ranges. K. Dan. Vidensk. Selsk. Mat.-Fys. Medd. 33, No. 14, Denmark (1963).

52) Bragg, W.H. and Kleeman, R., On the Alpha Particles of Radium and Their Loss of Range in Passing Through Various Atoms and Molecules. Philos. Mag. 10, 318-340 (1905).

53) Thwaites, D.I., Bragg's Rule of Stopping Power Additivity: A Compilation and Summary of Results. Radiat. Res. 95, 495-518 (1983).

54) Bichsel. H., The Stopping Power of a Solid and of a Gas of the Same Composition. Phys. Med. Biol. 27, No. 3, 449-450 (1982).

55) Bethe, H.A. and Ashkin, J., Passage of Radiation Through Matter. In: Experimental Nuclear Physics (E. Segre, Ed.), Vol. 1. John Wiley and Sons, New York, USA (1953).

56) Fain, J., Monnin, M. and Montret, M., Energy Density Deposited by a Heavy Ion Around its Path. Fourth Symp. on Microdosimetry, Pallanza (J. Booz, H.G. Ebert, R. Eickel, A. Water, Eds.),Vol. 1, 169-189, EUR 5122 (1973).

57) Paretzke, H.G., Leuthold, G., Burger, G. and Jacobi, W., Approaches to Physical Track Structure Calculations. Fourth Symp. on Microdosimetry, Pallanza (J. Booz, H.E. Ebert, R. Eickel, A. Waker, Eds.), Vol. 1, 123-140, EUR 5122 (1973).

58) Fain, J., Monnin, M. and Montret, M., Spatial Energy Deposition Around Heavy-Ion Path. Radiat. Res. 57, 379-389 (1974).

59) Gupta, S.K. and Prasad, M.A., Dose Distribution due to Low-Energy Electrons and Delta Rays Produced along the Path of a Heavy Charged Particle in Water. Radiat. Res. 76, 1-14 (1978).

60) Kim, Y.-K. and Inokuti, M., Slow Electrons Ejected from He by Fast Charged Particles. Phys. Rev. A 7, No. 4, 1257-1260 (1973).

61) Toburen, L.H. and Wilson, W.E., Energy and Angular Distribution of Electrons Ejected From Water Vapor by 0.3-1.5 MeV Protons. J. Chem. Phys. 66, No. 11, 5202-5213 (1977).

62) Toburen, L.H. and Wilson. W.E., Secondary Electron Emission in Ion-Atomic Collisions. Proc. Sixth Int. Congress of Radiation Research, Tokyo (S.Okada, M. Imamura, T. Terashima, and H. Yamaguchi, Eds.), 80 (1979).

63) Kim, Y.-K., Angular and Energy Distributions of Secondary Electrons from Helium. Slow Electrons Ejected by Electron Impact. Phys. Rev. a 28, 2, 656-666 (1983).

64) Wilson, W.E. and Toburen, L.H., Delta-Ray Production in Ion-Atom Collisions. Seventh Symp. on Microdosimetry, Oxford (J. Booz, H.G. Ebert and H.D. Hartfield, Eds.), Vol. 1, 435-448, Harwood, London (1980).

65) Cosslett, V.E. and Thomas, R.N., Multiple Scattering of 5-30 keV Electrons in Evaporated Metal Films, II: Range Energy Relations. Brit. J. Appl. Phys. 15, 1283-1300 (1964).

66) Kobetich, E.J. and Katz, R., Electron Depositions by Electron Beams and δ Rays. Phys. Rev. 170, No. 2, 391-396 (1968).

67) Cole, A., Absorption of 20-eV to 50,000-eV Electron Beams in Air and Plastic. Radiat. Res. 38, 7-33 (1969).

68) Iskef, H., Cunningham, J.W. and Watt, D.E., Projected Ranges and Effective Stopping Powers of Electrons with Energy Between 20 eV and 10 keV. Phys. Med. Biol 28, No. 5, 535-545 (1983).

69) Sørensen, H. and Schou, J., Interactions between Solid Nitrogen and 1-3-keV electrons. J. Appl. Phys. 49, 10, 5311-5318 (1978).

70) Everhart, T.E. and Hoff, P.H., Determination of Kilovolt Electron Energy Dissipation vs Penetration Distance in Solid Materials. J. Appl. Phys. 42, 5837-5846 (1971).

71) Holt, P.D., Charged Particle Tracks in Solids and Liquids. Proc. of 2nd L.H. Gray Conference, Cambridge. Published by The Institute of Physics and the Physical Society, Conf. Series No. 8 (1969).

72) Waibel, E. and Grosswendt, B., Spatial Energy Dissipation Profiles, W Values, Backscatter Coefficients, and Ranges for Low-Energy Electrons in Methane. Nucl. Instr. Meth. 211, 489-498 (1983).

73) Berger, M.J., Energy Deposition by Low-Energy Electrons: Delta-Ray Effects in Track Structure and Microdosimetric Event-Size Spectra. Third Symp. on Microdosimetry, Stresa (H.G. Ebert, Ed.), Vol. 1, 157-158, EUR 4810 (1971).

74) Paretzke, H.G. and Berger, M.J., Stopping Power and Energy Degradation for Electrons in Water Vapor. Sixth Symp. on Microdosimetry, Brussels (J. Booz, H.G. Ebert, Eds.), Vol. 2, 749-758, Harwood, London (1978).

75) Ashley, J.C., Energy Losses and Inelastic Mean Free Path of Low-Energy Electrons in Polyethylene. Radiat. Res. 90, 433-436 (1982).

76) Berger, M.J. and Seltzer, S.M., Stopping Power and Ranges of Electrons and Positrons (2nd. Ed.) NBSIR 82-2550-A, U.S. Dept. of Commerce, NBS, Washington, D.C., USA (1983).

77) Varma, M.N., Baum, J.W. and Kuehner, A.V., Stopping Power and Radial Dose Distribution for 42 MeV Bromine Ions. Phys. Med. Biol. 25, No. 4, 651-656 (1980).

78) Baum, J.W., Varma, M.N., Wingate, C.L., Paretzke, H.G. and Kuehner, A.V., Nanometer Dosimetry of Heavy Ion Tracks. Fourth Symp. on Microdosimetry, Pallanza (J. Booz, H.G. Ebert, R. Eickel, A. Waker, Eds.), Vol. I, 93-112, EUR 5122 (1973).

79) Fano, U., Penetration of Protons, Alpha Particles, and Mesons. In: Studies in Penetration of Charged Particles in Matter. Nuclear Science Series, Report No. 39, Publication 1133, National Academy of Sciences-National Research Council, 287-352, Washington, D.C., USA (1964).

80) Jensen, M. and Mathiesen, O., Measured and Calculated Absorptance of Tracks of Fast Heavy Ions in Ilford G5 Emulsion. Physica Scripta 13, 75-82 (1976).

81) Katz, R. and Kobetich, E.J., Formation of Etchable Tracks in Dielectrics. Phys. Rev. 170, 401-405 (1968).

82) Larsson, L. and Katz, R., Supralinearity of Thermoluminescent Dosimeters. Nucl. Instr. Meth. 138, 631-636 (1976).

83) Bermann, F., De Choudens, H. and Descour, S., Application a la Dosimetrie de la Mesure par Resonance Paramagnetique Electronique des Radicaux Libres Crees dans les Acides Amines. In: Advances in Physical and Biological Radiation Detectors, STI/PUB/1269, IAEA-SM-143/50, 311-325, Vienna, Austria (1971).

84) Bermann, F., Adaption of a Free Radical Dosimeter to the Intercomparison of Fast Neutron Beams. Report to IAEA Contract No. 1542/R2/RB, IAEA, Vienna, Austria, July (1978).

85) McLaughlin, W.L. and Kosanic, M., The Gamma-Ray Response of Pararosaniline Cyanide Dosimeter Solutions. Int. J. Appl. Radiat. Isot. 25, 249-262 (1974).

86) McLaughlin, W.L., Solid-Phase Chemical Dosimeters. Int. Conf. on Sterilization by Ionizing Radiation (E.R.L. Gaughran and A.J. Goudie, Eds.), Vienna, Austria. Multiscience Publication Ltd., Montreal, Quebec, Canada, 219-324 (1974).

87) McLaughlin, W.L., Hjortenberg, P.E. and Radak, B.B., Absorbed Dose Measurements with Thin Films. Proc. Symp. Dosimetry in Agriculture, Industry, Biology and Medicine, IAEA, Vienna, Austria, IAEA-SM-160/32, 577-537 (1973).

88) Miller, A., Bjergbakke, E. and McLaughlin, W.L., Some Limitations in the Use of Plastic and Dyed Plastic Dosimeters. Int. J. Appl. Radiat. Isot. 26, 611-620 (1975).

89) McLaughlin, W.L., Miller, A., Fidan, S., Pejtersen, K. and Batsberg Pedersen, W., Radiochromic Plastic Dye Films for Accurate Measurement of Radiation Absorbed Dose and Dose Distributions. Radiat. Phys. Chem. 10, 119-127 (1977).

90) Sporer, A.H., Photoionization of Triarylmethyl Leuconitriles. Trans. Faraday Soc. 57, 983-991 (1961).

91) McLaughlin, W.L. and Chalkley, L., Measurement of Radiation Dose Distributions with Photometric Materials. Radiology 84, 124-125 (1965).

92) Bishop, W.P., Humphereys, K.C. and Randtke, P.T., Poly(halo)styrene Thin-Film Dosimeters for High Doses. Rev. Sci. Instr. 44, No. 4, 443-452 (1973).

93) Dachenko, V., Griffin, G.F. and Brashears, S.S., Delayed Darkening of Radiation-Exposed Radiochromic Dye Dosimeters. IEEE Trans. Nucl. Sci., NS-28, 6, 4156-4160 (1981).

94) McLaughlin, W.L., Humphreys, J.C., Levine, H., Miller, A., Radak, B.B. and Rativanich, N., The Gamma-Ray Response of Radiochromic Dye Films at Different Absorbed Dose Rates. Int. Meeting on Radiation Processing, Tokyo, Japan, Oct. 26-31 (1980).

95) McLaughlin, W.L., The Measurement of Absorbed Dose and Dose Gradients. Radiat. Phys. Chem. 15, 9-38 (1980).

96) Gehringer, P., Eschweiler, H. and Proksch, E., Dose Rate and Humidity Effect on the γ-Radiation Response of Nylon-Based Radiochromic Film Dosimeters. Int. J. Appl. Radiat. Isot. 31, 595-605 (1980).

97) McLaughlin. W.L., Humphreys, J.C., Levine, H., Miller, A., Radak, B.B. and Rativanich, N., The Gamma-Ray Response of Radiochromic Dye Films at Different Absorbed Dose Rates. Radiat. Phys. Chem. 18, 5-6, 987-999 (1981).

98) McLaughlin, W.L., Uribe, R.M. and Miller, A., Megagray Dosimetry or Monitoring of Very Large Radiation Doses. Radiat. Phys. Chem. 22, No. 3-5, 333-362 (1983).

99) Edisburg, J.R., Practical Hints on Absorption Spectrometry. Hilger and Watts Ltd., London, 13-14 (1966).

100) Ayscough, P.B., Electron Spin Resonance in Chemistry. Methuen and Co. Ltd., London, England (1967).

101) Schlichter, C.P., Principles of Magnetic Resonance. Harper and Row, New York, USA (1963).

102) Bradshaw, W.W., Cadena, D.G., Crawford, G.W. and Spetzler H.A.W., The Use of Alanine as a Solid Dosimeter. Radiat. Res. 17, 11-21 (1962).

103) Regulla, D.F. and Deffner, U., A System of Transfer Dosimetry in Radiation Processing. Radiat. Phys. Chem. 22, No. 5, 305-309 (1983).

104) Regulla, D.F. and Deffner, U., Standardization in High-Level Photon Dosimetry Based on ESR Transfer Metrology. Int. Symp. on Biomedical Dosimetry, IAEA-SM-249/84, Paris, France (1980).

105) Regulla, D.F. and Deffner, U., A Practical High-Level Dose Meter Based on Tissue-Equivalent Alanine. Advisory Group Meeting on Standardization and High Dose Intercomparison for Industrial Radiation Processing. IAEA, Vienna, Austria (1978).

106) Regulla, D.F. and Deffner, U., Dosimetry by ESR Spectroscopy of Alanine. Int. J. Appl. Radiat. Isot. 33, 1101-1114 (1982).

107) Müller, A., Schambra, P.E. and Pietsch, E., Comparative ESR-Measurements of Radical Production in Amino Acids by ^{210}Po Alpha- and ^{60}Co Gamma-Radiation. Int. J. Radiat. Biol. 7, No. 6, 587-599 (1964).

108) Ayscough, P.B. and Olsen, K.J., Electron Spin Resonance Studies of Elementary Processes in Radiation- and Photo-Chemistry. J. Chem. Soc., Faraday Trans. I, 68, 1635-1646 (1972).

109) Bjergbakke, E. and Engholm Larsen, E., The 10000 Ci ^{60}Co Facility and the 3000 Ci ^{60}Co Gamma Cell. Risö-M-1651, Danish Atomic Energy Commission, Research Establishment Risö, Denmark (1973).

110) Sehested, K., The Fricke Dosimeter. In Manual on Radiation Dosimetry (N.W. Holm and R.J. Berry, Eds.), 313-316. Marcel Dekker, Inc., New York, USA (1970).

111) Annual Progress Report, Accelerator Department. Risø-M-2348, Risø National Laboratory, Denmark (1981).

112) Brynjolfsson, A. and Thaarup, G., Determination of Beam Parameters and Measurements of Dose Distribution in Materials Irradiated by Electrons in the Range of 6 MeV to 14 MeV. Risö-R-53, Danish Atomic Energy Commission, Research Establishment Risö, Denmark (1963).

113) Fielden, E.M. and Holm, N.W., Dosimetry in Accelerator Research and Processing. In: Manual on Radiation Dosimetry (N.W. Holm and R.J. Berry, Eds.), 261-309. Marcel Dekker, Inc., New York, USA (1970).

114) Holm, N.W., Dosimetry in Industrial Processing, in Radiation Dosimetry (F.H. Attix and E. Tochilin, Eds.), Vol. III, 869-908, Academic Press, New York (1969).

115) Miller, A., McLaughlin, W.L. and Lynggaard, B., A Scanning Spectrophotometer for Reading Thin-Film Dosimeters. Risø-M-1525, Danish Atomic Energy Commission, Research Establishment Risø, Denmark (1972).

116) IAEA, Calibration of Dose Meters Used in Radiotherapy. Technical Report Series No. 185, IAEA, Vienna, Austria (1979).

117) Paretzke, H.G., Comparison of Track Structure Calculations with Experimental Results. Fourth Symp. on Microdosimetry, Pallanza (J. Booz, H.G. Ebert, R. Eickel, and A. Waker, Eds.), Vol. I, 141-165, EUR 5122 (1973).

118) Cook, J.B. and Wyard, S.J., Electron Spin Resonance Studies of Radiation Damage in Deoxyribonucleic Acid. Int. J. Radiat. Biol. 11, 357-365 (1966).

119) Elliott, J.P.and Wyard, S.J., in Effects of Ionizing Radiation on DNA. (J. Hüttermann, W. Köhnlein, and R. Teoule, Eds.), Ch. 5, 80-86, Molecular Biology, Biochemistry, and Biophysics. 27. Springer Verlag Berlin, Heidelberg, New York (1978).

120) McLaughlin, W.L., Kosanic, M.M., Markovic, V.M., Nenadovic, M.T., Holcman, J. and Sehested, K., The Kinetics of Dye Formation by Pulse Radiolysis of Pararosaniline Cyanide in Aqueous or Organic Solution. Risø-M-2202. Risø National Laboratory, Denmark (1979).

121) Rauth, A.M. and Simpson, J.A., The Energy Loss of Electrons in Solids. Radiat. Res. 22, 643-661 (1964).

122) Simmons, J.A., Spectral Changes in Irradiated Glycine. Phys. Med. Biol. 11, No. 4, 597-601 (1966).

123) Henriksen, T., Production of Free Radicals in Solid Biological Substances by Heavy Ions. Radiat. Res. 27, 676-693 (1966).

124) Henriksen, T., Effect of the Irradiation Temperature on the Production of Free Radicals in Solid Biological Compounds Exposed to Various Ionizing Radiations. Radiat. Res. 27, 694-709 (1966).

125) Horan, P.K. and Snipes, W., Free Radical Destruction by Gamma-Irradiation at 77°K. Int. J. Radiat. Biol. 15, No. 2, 157-161 (1969).

126) Snipes, W. and Horan, P.K., Electron Spin Resonance Studies of Free Radical Turn-Over in Gamma-Irradiated Single Crystals of Alanine. Radiat. Res. 30, 307-315 (1967).

127) Rotblat, J. and Simmons, J.A., Dose-Response Relationship in the Yield of Radiation-Induced Free Radicals in Amino Acids. Phys. Med. Biol. 7, 489-497 (1963).

128) Riesz, P., Smitherman, T.C. and Scher, C.D., Hydrogen Transfer From Exhangeable to Carbon-Bound Sites in γ-Irradiated Proteins and Nucleic Acids: The Mechanism of Radical Saturation. Int. J. Radiat. Biol. 17, No. 4, 389-393 (1970).

129) Lea, D.A., Actions of Radiations on Living Cells. Cambridge University Press, 2nd edition (1955).

130) Günther, K. and Schultz, W., Biophysical Theory of Radiation Action. Ch. 1. Akademie-Verlag, Berlin (1983).

131) Marshall, M., Gibson, J.A B. and Holt, P.D., An Analysis of the Target Theory of Lea with Modern Data. Int. J. Radiat. Biol. 18, No. 2, 127-138 (1970).

132) Alper, T., Cellular Radiobiology. Cambridge University Press, (1979).

133) Horowitz, Y.S. and Kalef-Ezra, J., Relative Thermoluminescent Response of LiF-TLD to ^{252}Cf Fission Fragments. Nucl. Instr. Meth. 187, 519-525 (1981).

134) Edwards. A.A., LET,ξ^{*} or z^2/β^2. Which is the Best Specification of Radiation Quality? Seventh Symp. on Microdosimetry, Oxford (J. Booz, H.G. Ebert, and H.D. Hartfield, Eds.), Vol. I, 593-602, Harwood, London (1981).

135) Regulla, D.F. Deffner, U. and Tuschy, H., A Practical High-Level Dosimeter Based on Tissue-Equivalent Alanine. Advisory Group Meeting on Standardization and High Dose Intercomparison for Industrial Radiation Processing, Sept. 25-29, Vienna, Austria (1978).

136) Horowitz, Y.S., The Theoretical and Microdosimetric Basis of Thermoluminescence and Application to Dosimetry. Phys. Med. Biol. 26, No. 4, 765-824 (1981).

137) Roth, R.A. and Katz, R., Prediction of Bevalac Radiobiology. Seventh Symp. on Microdosimetry, Oxford (J. Booz, H.G. Ebert, and H.D. Hartfield, Eds.), Vol. II, 1299-1310, Harwood, London (1981).

138) Katz, R. and Sharma, S.C. Cellular Survival in a Mixed Radiation Invironment. Int. J. Radiat. Biol. 26, 143-146 (1975).

139) Katz, R. and Sharma, S.C., Heavy Particles in Theory. Phys., Med. Biol. 19, 413-435 (1974).

APPENDIX A.

Calculation of the radial dose distribution

To calculate the dose deposited by energetic secondary electrons ejected by the penetrating heavy charge particle in interactions with the atomic electrons of the medium, the theory of Bethe[55,79] is used. Considerations are restricted to δ-rays, i.e. electrons ejected with an energy which is large compared with the ionization potential. The binding energy of the electrons is neglected and the interactions between the heavy charged particle and these free atomic electrons are described by simple Rutherford scattering formalism. Certain additional approximations and simplifications are used as described in section 2.7. The energy of the δ-rays is described by

$$\omega = 2mc^2\beta^2(1-\beta^2)^{-1}\cos^2\Theta \qquad \text{A1-1}$$

where Θ in the laboratory system is the angle with the incident direction for ejection of an electron. The differential cross section for an electron that lies between angle Θ and Θ + dΘ is given by

$$\sigma_\Theta = \frac{2\pi e^4 z^2}{(mc)^2\beta^4} \cdot \frac{\sin\Theta}{\cos^3\Theta}\, d\Theta \qquad \text{A1-2}$$

where z and β are the effective charge and velocity of the heavy charged particle relative to that of light.

Equation A1-1 shows that electrons of the highest energy are preferentially ejected in the forward direction, while those of lowest energy are emitted perpendicular to the ion's path. Equation A1-2 shows that the majority of electrons are ejected at angles above 45°. It turns out, however, that the theory describes the experimental observations to a good approximation as discussed in section 2.7.

The cross section for ejection of an electron with energy between ω and ω + dω is given by

$$\sigma_\omega = \frac{2\pi e^4}{mc^2} \cdot \frac{z^2}{\beta^2} \cdot \frac{d\omega}{\omega^2}$$

and the number of electrons ejected per unit path length of the moving heavy charged particle is the cross section σ_ω multiplied by the number N of elec-

trons per unit volume of the stopping medium

$$dn = N \cdot o_\omega = N \cdot \frac{2\pi e^4}{mc^2} \frac{z^2}{\beta^2} \frac{d\omega}{\omega^2} = C \frac{z^2}{\beta^2} \frac{d\omega}{\omega^2} \qquad \text{A1-3}$$

As described in section 2.7 a fitted power-law range-energy relation is used for the δ-rays and which has the form

$$r = k \cdot \omega^\alpha = \frac{1}{\rho} 5.2 \cdot 10^{-13} \ \omega^{1.67} \ [m] \qquad \text{A1-4}$$

where ρ is the density of the medium and ω is the electron energy in eV.

From this formula the stopping power of the ejected δ-rays is derived as follows: An electron with an initial energy ω_r and corresponding range r will have a residual energy ω_{r-t} given by

$$\omega_{r-t} = (\frac{r-t}{k})^{\alpha^{-1}} = (\frac{r}{k})^{\alpha^{-1}} \cdot (1 - \frac{t}{r})^{\alpha^{-1}} = \omega_r \ (1 - \frac{t}{r})^{\alpha^{-1}}$$

after travelling the distance t. The differential quotient gives the stopping power at the distance t

$$\frac{d\omega_{r-t}}{dt} = -\omega_r \frac{1}{\alpha} \frac{1}{r} (1 - \frac{t}{r})^{(\alpha^{-1} - 1)} \qquad \text{A1-5}$$

The total energy, E(z,β,t), deposited by the ejected δ-rays, in the interval between t and t + dt from the ion's path, is the product of the number of δ-rays and their respective stopping power integrated over all energies. This leads to

$$E(z,\beta,t) = \int_{\omega_t}^{\omega max} \frac{dn}{d\omega} \frac{d\omega_{r-t}}{dt} dt \ d\omega = -C \frac{z^2}{\beta^2} \frac{1}{\alpha} dt \int_{\omega_t}^{\omega max} \frac{1}{\omega_r} \frac{1}{r} (1 - \frac{t}{r})^{(\alpha^{-1} - 1)} d\omega \qquad \text{A1-6}$$

By substituting the δ-ray energy by the corresponding range the integration yields the following expression for the total energy, E(z,β,t), deposited by the δ-rays:

$$E(z,\beta,t) = C \frac{z^2}{\beta^2} \frac{1}{\alpha} \frac{1}{t} dt \ (1 - \frac{t}{t_{max}})^{\alpha^{-1}} \qquad \text{A1-7}$$

and the dose D(z,β,t) deposited in a cylindrical shell of area 2πt dt and of unit length (see Fig. 5) around the ion path then has the form of

$$D(z,\beta,t) = \frac{E}{2\pi t \ dt} = \frac{C}{2\pi} \frac{z^2}{\beta^2} \frac{1}{\alpha} \frac{1}{t^2} (1 - \frac{t}{t_{max}})^{\alpha^{-1}} \qquad \text{A1-8}$$

The maximum range t_{max} of the δ-rays is obtained from eqs. A1-1 and A1-4 for $\cos\theta = 1$. $C = 2.46 \cdot 10^{-12}\ n_e\ \rho/M_w$ joule m^{-1} where n_e, ρ, and M_w is the average number of electrons per molecule, mass density, and molecular weight of the medium, respectively. The effective charge, z, of the heavy charged particle is obtained from eqs. 2-7 to 2-10 in section 2.5. By inserting the distance, t, travelled by the δ-rays in metre, eq. A1-8 expresses the point target dose in Gy.

In the extended target calculation the dose $\bar{D}(z,\beta,t,a_0)$ to the sensitive element is calculated as the average dose deposited in a cylinder of unit length, the axis of which is parallel to the ion path and has the radius a_0. The extended target formulation is derived from simple trigonometric considerations as shown in Fig. 9. The area dA is found from the arc length 2ϕ multiplied by the infinitesimal shell thickness dt, thus

$$dA = 2\phi t\ dt$$

From trigonometry ϕ can be expressed as

$$\phi = 2\ \text{Arctg}\sqrt{\frac{a_0^2-(t_0-t)^2}{(t_0+t)^2-a_0^2}} \quad \text{for } (t_0+t) > a_0$$

$$\phi = \pi \quad \text{for } (t_0+t) \leq a_0 \qquad \text{A1-9}$$

The inequality $(t_0+t) \leq a_0$ in eq. A1-9 arises only for extended target dose calculations within the core by means of the integration procedure.

The average dose to the cylinder can now be calculated as

$$\bar{D}(z,\beta,t,a_0) = \frac{1}{A}\int_{t_0-a_0}^{t_0+a_0} D(z,\beta,t)2\phi t\ dt \qquad \text{A1-10}$$

where $A = \pi\ a_0^2$ is the total area of the sensitive element.

By inserting the expression for the point target dose, eq. A1-8, and the geometry function, eq. A1-9, into A1-10 the expression for the extended target dose is obtained

$$\bar{D}(z,\beta,t,a_0) = \frac{2\ C}{\pi^2\ a_0^2}\ \frac{z^2}{\beta^2}\ \frac{1}{\alpha}\int_{t_0-a_0}^{t_0+a_0}\left[1-\frac{t}{t_{max}}\right]^{\alpha-1}\ \text{Arctg}\sqrt{\frac{a_0^2-(t_0-t)^2}{(t_0+t)^2-a_0^2}}\ \frac{1}{t}\ dt \qquad \text{A1-11}$$

This integration is performed numerically in a computer, and Fig. 10 shows calculated extended target dose distributions for the ions, a) the subtrac-

tion procedure which includes excitation energies, and b) with integration in the core.

At distances from the ion path greater than 3 a_0 the extended target dose approaches that calculated from the point target formula, eq. A1-8, why this formula is used in the calculation procedure for distances extending 3 a_0.

In Appendix 2 is accounted for the calculation procedure and the computer code in Algol to be run at a Burroughs 7800.

APPENDIX B.

Computer programs

This appendix lists the computer program that is used for calculating the results reported in this work. The program language is Algol for the Burroughs 7800 computer at Risø, and the main program "REINT" makes use of four additional programs taken from the Risø computer library. These library programs are: "RISOE/ADAPINT/A" and "RISOE/QG/A" for numerical integration procedures, RISOE/SPLINEVAL/A" for interpolations in data files, and "(BJERGBAKKE)RISOE/SERVOGORPLOT/A" for plotting of point target- and extended target dose profiles. Except for the Risø computer library programs all programs were written in cooperation with Erling Bugge Christensen at the Accelerator Department.

In addition, the main program makes use of a subroutine "ZIEGLERSPLINE", which includes the stopping power data of Andersen and Ziegler[46] for protons in hydrogen, carbon, nitrogen, and oxygen versus energy in the interval of 1 keV/amu to 60 MeV/amu. This routine includes the coefficients necessary for the cubic spline interpolation procedure "RISOE/SPLINEVAL/A".

An independent computer program "ZIEGGEN" (Ziegler spline Generation) computes the interpolation coefficients for the specific stopping power-energy data arrays, and makes use of a Risø computer library program "RISOE/CUBESPLINE/A" for this computation.

The Algol procedure "RISOE/ADAPINT/A" performs numerical quadrature of a function f(x) over an interval (A-B) by an adaptive 7-point formula. The procedure is used by the main program for calculating the extended target dose as a function of distance from the ion's path.

The Algol procedure "RISOE/QG/A" computes the integral function FCT(x), summed over x from A to B, using an n-point gauss-legendre quadrature rule. The procedure is used by the main program for calculation of the activation cross sections in the core and track of the ion.

The Algol procedure "RISOE/SPLINEVAL/A" evaluates a cubic interpolation spline at an arbitrary point. The program is used for calculating an actual proton stopping power value for a given input energy by means of a third-

order polynomium.

In order to obtain significant results in media where the ion energy changes drastically, e.g. in the Bragg-peak region of the slowing down ion, thin segments of the medium must be used. Therefore, the segmentation is performed for which a constant fraction of the ion's input energy to a segment is deposited in the segment. From this follows still thinner segments as the ion emerges into the medium. In the situation, however, where the total thickness of a medium is thin as compared to the range of the ion, a modification is introduced in the calculation procedure such that the initially calculated segment thickness never exceeds the total thickness of the medium.

The use of the numerical integration procedures is optimized with respect to the number of integration intervals in order to cut down on computer time.

The flow diagram below shows the calculation procedure of the main program.

1: Record of input parameters
2: Loop over the segments:
- Calculation of β, z, and LET.
- Calculation of energy loss in the segment.
- Calculation of input parameters for the following segment.
- If the energy is less than 1 keV/amu go to output.
- Calculation of average energy loss in the segment.
- Calculation of average β, z, and LET in the segment.
- Calculation of σ_{track}, σ_{core}, E_{track}, E_{core}, and RE in the segment.
- Calculation of σ_{track}, σ_{core}, E_{track}, E_{core}, LET_{av}, and RE.

3: Read-out of output data on screen or printer.
4: Plotting of radial dose profiles if required.

APPENDIX C.

Derivation of an expression for dose in heavy charged particle experiments.

The absorbed dose in the target samples in heavy charged particle irradiations is obtained through calculations of particle fluence and average electronic stopping power for the ion in question. Derivation of stopping power described in section 2.6, and the derivation of measured particle fluence will be accounted for in this appendix. The experimental set-up for irradiations on the tandem Van de Graaff was described in section 4.3 and schematically shown in Figs. 21 and 22.

With reference to Fig. 23 the infinitesimal target area dA rotates with a velocity

$$v = \omega \cdot r = 2\pi r N \qquad \text{A3-1}$$

where r is the radius for rotation of the target and N is the number of revolutions per unit time. The target area dA stays in the particle beam in a time t_{dA} given by

$$t_{dA} = \frac{\ell}{v} = \frac{\ell}{2\pi r N} \qquad \text{A3-2}$$

where ℓ is the width of the beam defining slit. The total time for dA in the beam during an irradiation time t is

$$t_{tot} = t_{dA} \cdot N \cdot t = \frac{\ell \cdot t}{2\pi r} \qquad \text{A3-3}$$

and the total time for dA to stay in the beam relative to the total time of irradiation is

$$\frac{t_{tot}}{t} = \frac{\ell}{2\pi r} \qquad \text{A3-4}$$

The particle flux $\hat{N}$ in the beam is

$$\hat{N} = \frac{Q_{beam}}{n \cdot e \cdot A_{s\ell} \cdot t} \qquad \text{A3-5}$$

where Q_{beam} is the charge in the beam, n the number of charges carried per particle, e the charge of the electron, and $A_{s\ell}$ is the opening area of the

beam defining slits perpendicular to the beam path. Beam divergence is found to have a negligible influence as the distance between the slits and the target is small, approximately 1 cm.

The particle flux $\dot{N}_{dA}$ to the target is the beam particle flux multiplied by the ratio, eq. A3-4, of the time for the target in the beam and the total irradiation time

$$\dot{N}_{dA} = \dot{N} \frac{t_{tot}}{t} = \frac{Q_{beam} \cdot \ell}{n \cdot e \cdot A_{s\ell} \cdot t \cdot 2\pi r} \qquad A3\text{-}6$$

With a slit opening area $A_{s\ell} = h \cdot \ell$ the particle fluence is expressed as

$$\Phi = \dot{N}_{dA} \cdot t = \frac{Q_{beam}}{n \cdot e \cdot h \cdot 2\pi \cdot r} \qquad A3\text{-}7$$

Q_{cup} is the charge to the Faraday cup that is actually measured. Thus, the ratio between the charge to the cup and charge in the beam must be evaluated. From Fig. 23 it is seen that 4ϕ is the total angle for the clamping signal to be on for one revolution of the wheel. This simply leads to

$$Q_{cup} = \frac{1}{2\pi} \int_0^{4\phi} Q_{beam}\, d\omega + \frac{1}{2\pi} \int_{4\phi}^{2\pi} Q_{beam}\, d\omega \qquad A3\text{-}8$$

where the measured charge from the cup is zero in the interval $0 < \omega \leq 4\phi$ and equals Q_{beam} in the interval $4\phi < Q_{beam} \leq 2\pi$. This leads to

$$Q_{cup} = \frac{1}{2\pi} \int_{4\phi}^{2\pi} Q_{beam}\, d\omega = \frac{1}{2\pi} Q_{beam}\, (2\pi - 4\phi)$$

and

$$\frac{Q_{cup}}{Q_{beam}} = k_1 = \frac{2\pi - 4\phi}{2\pi} \qquad A3\text{-}9$$

This ratio is found geometrically or easily measured either by an oscilloscope coupled to the clamping circuit, or simply by measuring a discharge current to the integrator with and without the clamping signal feed into the charge integrator. The ratio is found to be $k_1 = 0.825$ leading to

$$\Phi = \frac{Q_{cup}}{0.825 \cdot n \cdot e \cdot h \cdot 2\pi r} = 2.5 \cdot 10^{17} \frac{Q_{cup}}{n} [m^{-2}] \qquad A3\text{-}10$$

where $h = 6.6 \cdot 10^{-3}$ m and $r = 7.3 \cdot 10^{-2}$ m and the charge is expressed in coulomb.

The dose to the target is calculated from the track average electronic stopping power S_{av} in the target and the particle fluence of eq. A3-10 as

$$D = \frac{1}{k} S_{av} \cdot \Phi = 4.02 \cdot 10^{-3} S_{av} \frac{Q_{cup}}{n} \text{ [Gy]} \qquad \text{A3-11}$$

with S_{av} expressed in $MeVcm^2g^{-1}$. This equation for dose is valid for any medium exposed to any kind of heavy charged particles in the present experimental equipment.

APPENDIX D.

Listing of computer program

```
100     $ SET INSTALLATION 128
200       BEGIN
300
400          COMMENT ***** NOTICE ! THIS VERSION OF THE PROGRAM USES A SPLINE
500                  INTERPOLATION METHOD AND REQUIRES THE FILE 'ZIEGLERSPLINE'
600                  TO BE PRESENT ON THE USER-PACK;
700
800           COMMENT THIS PROGRAM INCLUDES CALCULATIONS IN FORM2 AND FORM4
900                   (FORM2: EXPONENTIAL RANGE-ENERGY RELATION AND SIMPEL SUB-
1000                  TRACTION OF E-TRACK FROM LET TO GET E-CORE, FORM4:EXPONEN-
1100                  TIAL RANGE-ENERGY RELATION AND INTEGRATION IN THE CORE).
1200                  THE PROGRAM CALCULATES: POINT TARGET DOSE,EXTENDED TAR-
1300                  GET DOSE,CROSS SECTION IN THE CORE AND IN THE TRACK,AND
1400                  RE.THE DETECTOR IS  DIVIDED INTO A NUMBER OF SEGMENTS
1500                  AND ALL CALCULATIONS ARE PERFORMED FOR EACH SEGMENT.
1600                  AVERAGE BETA,AVERAGE ENERGY LOSS,AVERAGE ZEFF,AVERAGE LET
1700                  AND RE ARE CALCULATED IN EACH SEGMENT.THE FINAL RE FOR
1800                  THE COMPLETE DETECTOR IS CALCULATED AS AN AVERAGE OF THE
1900                  INDIVIDUAL SEGMENT-RE'S WHEREBY EACH SEGMENT-RE IS WEIGHTED
2000                  AGAINST THE ENERGY LOST IN THE INDIVIDUAL SEGMENT TO THE
2100                  TOTAL ENERGY LOSS.THE PRINTED OUT RE FOR EACH SEGMENT
2200                  IS BASED ON AVERAGE VALUES FOR THE SEGMENT;
2300    $ INCLUDE "RISOE/PLOTSTART/A"
2400    $ INCLUDE "RISOE/PLOTAXES/A"
2500    $ SET NOASK
2600        INTEGER TYPE,Z,NOSEG,X,I,N1,D,Q,NOFUN,SEGMENTS,PPC,NN;
2700        BOOLEAN EXTENDEDPLOT,PRINT,NEW,PLOTT,PRPLOT,OVERRANGE,REMOTE;
2800        REAL AWEIGHT,ZEFF,ETOT,DENS,THICK,D37,BETA,PI,A0,T,ERG1,ERG2,INENG,
2900             ERROR,TPLL,L,RBE,TAU,ETRACK,ECORE,SIGMT,DCORE,SIGMC,SIGMTOT,ERG,
3000             D37A,ZM,TM,INFLTA,INLET,AVLET,ETRACKR,ECORER,
3100             SIGMTR,SIGMCR,AVLETR,INC,DT,LOWLIMIT,TO,THK,DIST,
3200             DOSEFORSIGMA,DOSEFORTRACK,LETTOT,LETNUCL,PCT,
3300             T1,T2,T3,S1,S2,K1,K2,K3;
3400        FILE REM(KIND=REMOTE,MAXRECSIZE=32),INP(KIND=REMOTE);
3500        DEFINE KEYBRD=INP#,DISP=REM#;
3600        FILE OUT(KIND=PRINTER);
3700        FILE ZIEGLERSPLINE(KIND=DISK,MYUSE=IN,FILETYPE=7);
3800    $ INCLUDE "GAMMERGAARDE)RISOE/SERVOGORPLOT/A"
3900    $ INCLUDE "RISOE/GG/A"
4000    $ INCLUDE "RISOE/ADAPINT/A"
4100    $ INCLUDE "RISOE/SPLINEVAL/A"
4200
4300         READ(ZIEGLERSPLINE,/,NN);
4400         COMMENT **** READ NUMBER OF DATA-POINTS IN SPLINE-FILE ****;
4500           BEGIN
4600            REAL ARRAY E,C,H,N,O,DBC,CCC,DOC,DBH,CCH,DDH,BBN,CCN,DDN,
4700                       EBO,CCO,DDO[0:NN];
4800     COMMENT ************************************************************;
4900
5000        REAL S;
5100        EBCDIC ARRAY TME[0:12];
5200        EBCDIC VALUE ARRAY TPE(" FILM  DYE  NYLON ALANINE");
5300        EBCDIC VALUE ARRAY KIND("FORM 2, SPLINEFORM 4, SPLINE");
5400
5500     COMMENT ************************************************************;
5600
5700        REAL PROCEDURE LET(TYPE,ENERGY);
5800        VALUE TYPE,ENERGY;
5900        INTEGER TYPE;
6000        REAL ENERGY;
6100          BEGIN
6200             REAL D5,F,G,R,S,S5,Z5,F5,D5,R5,D6,E7;
6300              BEGIN
6400                 IF Z=1 THEN
6500                   Z5:=1
6600                 ELSE
6700                 IF Z=2 THEN
6800                   Z5:=((1+7.2762-3*EXP(-(7.6-LN(103*ERG1))**2))
6900                        *(1-EXP(-(0.7446+0.1429*(LN(103*ERG1))+0.01562
7000                        *(LN(ERG1*103))**2-0.00267*(LN(103*ERG1))**3+
7100                        1.3253-6*(LN(103*ERG1))**8)))**2)**2
7200                 ELSE
7300                 IF Z=3 THEN
7400                   Z5:=((1+7.2762-3*EXP(-(7.5-LN(103*ERG1))**2))
7500                        *(1-EXP(-0.7138-2.792*ERG1-1.348*ERG1**2))+3)**2
7600                 ELSE
7700                   Z5:=(7*(1-(EXP(-5.6036*Z**(-2/3)*SQRT(ERG1)-0.0378*
7800                        SIN(8.602*Z**(-2/3)*SQRT(ERG1))))*(1.034-0.1777*
7900                        EXP(-0.08114*Z)))))**2;
```

```
8000
8100            IF (Z=2 OR Z=3) AND ERG1<.15 THEN
8200              ZH:=(Z*(1-(EXP(-5.6036*Z**(-2/3)*SQRT(ERG1)-0.037*
8300                   SIN(8.302*Z**(-2/3)*SQRT(ERG1))))*(1.034-0.1777*
8400                   EXP(-0.08114*Z))))**2
8500            ELSE
8600              ZH:=Z5;
8700              Z5:=MIN(Z5,Z*Z);
8800
8900            COMMENT FOR Z=2 OR Z=3, ZH IS THE SQUARE OF THE RATIO
9000                    OF THE EFFECTIVE CHARGES FOR THE HE- OR LI-ION
9100                    AND THAT OF THE PROTON CALCULATED FROM THE GE-
9200                    NERAL FORMULA FOR ZEFF.ZH IS ONLY USED FOR THESE
9300                    IONS IN HYDROGEN TARGETS AT ENERGIES < .15 MEV/U;
9400
9500            COMMENT FOR Z=2, Z5 IS THE SQUARE OF THE RATIO BETWEEN
9600                    THE EFFECTIVE CHARGES OF THE HELIUM ION AND THE
9700                    PROTON AT THE SAME VELOCITY WHEN ENTERING A
9800                    SEGMENT;
9900
10000           COMMENT FOR Z=3, Z5 IS THE SQUARE OF THE RATIO BETWEEN
10100                   THE EFFECTIVE CHARGES OF THE LITIUM ION AND THE
10200                   PROTON AT THE SAME VELOCITY WHEN ENTERING A
10300                   SEGMENT;
10400
10500           COMMENT Z5 IS THE SQUARE OF THE RATIO BETWEEN THE EFFECTIVE
10600                   CHARGES OF THE ION AND THE PROTON AT THE SAME
10700                   VELOCITY WHEN ENTERING A SEGMENT;
10800
10900           COMMENT HERE STARTS THE SPLINE INTERPOLATION ON STOPPING
11000                   POWER TABLES IN ORDER TO OBTAIN LET FOR THE DESIRED
11100                   MATERIAL,FILM,DYE,NYLON OR ALANINE;
11200           IF ERG1<=1 THEN
11300             BEGIN
11400               E7:=65060*ERG1*AWEIGHT/(Z*(AWEIGHT+12)*
11500                   SQRT(Z**(2/3)+3.302));
11600               P5:=0.5*LN(1+E7)*2548.3*Z*AWEIGHT/((E7+0.107818*E7**
11700                   0.37544)*(AWEIGHT+12)*SQRT(Z**(2/3)+3.302));


11800             END
11900               ELSE P5:=0;
12000             COMMENT P5 IS THE NUCLEAR STOPPING POWER OF THE ION IN
12100                     CARBON;
12200           P:=SPLINEVAL(NN,ENERGY,E,C,BBC,CCC,DDC)*Z5;
12300             COMMENT P IS THE COLLISION STOPPING POWER OF THE ION IN
12400                     CARBON INTERPOLATED FROM ZIEGLER-DATA;
12500           IF ERG1<=1 THEN
12600             BEGIN
12700               E7:=32530*ERG1*AWEIGHT/(Z*(AWEIGHT+1)*
12800                   SQRT(Z**(2/3)+1));
12900               Q5:=0.5*LN(1+E7)*5096.7*Z*AWEIGHT/((E7+0.107818*
13000                   E7**0.37544)*(AWEIGHT+1)*SQRT(Z**(2/3)+1));
13100             END
13200               ELSE Q5:=0;
13300             COMMENT Q5 IS THE NUCLEAR STOPPING POWER OF THE ION IN
13400                     HYDROGEN;
13500           Q:=SPLINEVAL(NN,ENERGY,E,H,BBH,CCH,DDH)*ZH;
13600             COMMENT Q IS THE COLLISION STOPPING POWER OF THE ION IN
13700                     HYDROGEN INTERPOLATED FROM ZIEGLER-DATA;
13800           IF ERG1<=1 THEN
13900             BEGIN
14000               E7:=65060*ERG1*AWEIGHT/(Z*(AWEIGHT+14)*
14100                   SQRT(Z**(2/3)+3.6593));
14200               R5:=0.5*LN(1+E7)*2548.3*Z*AWEIGHT/((E7+0.107818*
14300                   E7**0.37544)*(AWEIGHT+14)*SQRT(Z**(2/3)+3.6593));
14400             END
14500               ELSE R5:=0;
14600             COMMENT R5 IS THE NUCLEAR STOPPING POWER OF THE ION IN
14700                     NITOGEN;
14800           R:=SPLINEVAL(NN,ENERGY,E,N,BBN,CCN,DDN)*Z5;
14900             COMMENT R IS THE COLLISION STOPPING POWER OF THE ION IN
15000                     NITROGEN INTERPOLATED FROM ZIEGLER-DATA;
15100           IF ERG1<=1 THEN
15200             BEGIN
15300               E7:=65060*ERG1*AWEIGHT/(Z*(AWEIGHT+16)*
15400                   SQRT(Z**(2/3)+4));
15500               S5:=0.5*LN(1+E7)*2548.3*Z*AWEIGHT/((E7+0.107818*
15600                   E7**0.37544)*(AWEIGHT+16)*SQRT(Z**(2/3)+4));
15700             END
15800               ELSE S5:=0;
15900             COMMENT S5 IS THE NUCLEAR STOPPING POWER OF THE ION IN
16000                     OXYGEN;
16100           S:=SPLINEVAL(NN,ENERGY,E,O,BBO,CCO,DDO)*Z5;
16200             COMMENT S IS THE COLLISION STOPPING POWER OF THE ION IN
16300                     OXYGEN INTERPOLATED FROM ZIEGLER-DATA;
16400           IF TYPE=0 THEN D5:=.63792*P+.09484*Q+.1212*R+.14405*S ELSE
16500           IF TYPE=1 THEN D5:=.8644*P+.07266*Q+.09689*R+.1661*S ELSE
16600           IF TYPE=2 THEN D5:=.6372*P+.0971*Q+.1239*R+.1416*S ELSE
16700           D5:=.4065*P+.0778*Q+.1573*R+.3663*S;
16800             COMMENT D5 IS THE COLLISION STOPPING POWER IN MEVCM**2/G
16900                     FOR THE ION IN THE TARGET MATERIAL;
17000           LET:=D5*1.602*10-6*DENS;
```

```
17100                 COMMENT LET IS THE COLLISION STOPPING POWER IN ERG/CM
17200                         FOR THE ION IN THE TARGET MATERIAL;
17300               IF TYPE=0 THEN D6:=0.63992*P5+0.054P4*05+0.1212*R5+
17400                                  0.14405*S5 ELSE
17500               IF TYPE=1 THEN D6:=0.6644*P5+0.07256*05+0.09689*R5+
17600                                  0.1661*S5 ELSE
17700               IF TYPE=2 THEN D6:=0.6372*P5+0.0973*05+0.1239*R5+


17800                                  0.1416*S5 ELSE
17900               D6:=0.4065*P5+0.0778*05+0.1573*F5+0.3663*S5;
18000               LETNUCL:=D6;
18100                 COMMENT D6 AND LETNUCL ARE THE NUCLEAR STOPPING POWER
18200                         IN MEVCM**2/G FOR THE ION IN THE TARGET MATERIAL;
18300               LETTOT:=(05+D6)*1.602*10-6*DENS;
18400                 COMMENT LETTOT IS THE TOTAL STOPPING POWER IN ERG/CM
18500                         FOR THE ION IN THE TARGET MATERIAL;
18600                 COMMENT LETTOT IS USED FOR THE ENERGY CALCULATION OF
18700                         THE SLOWING DOWN OF THE ION, WHILE LET IS USED
18800                         FOR THE DOSE DEPOSITION OF THE DELTA RAYS;
18900             END
19000         END;
19100     COMMENT ***********************************************************;
19200
19300        REAL PROCEDURE EPOINT(T);
19400
19500            COMMENT WHEN THE DISTANCE TO THE ION'S PATH IS GREATER
19600                    THAN THREE TIMES THE RADIUS OF THE SENSITIVE ELEMENT,THE
19700                    DOSE IS CALCULATED BY THE POINT TARGET APPROXIMATION
19800                    FORMULA EPOINT(T).BELOW THIS DISTANCE THE DOSE IS
19900                    CALCULATED AS AN EXTENDED TARGET FORMULA EBAR(T);
20000
20100        VALUE T;
20200        REAL T;
20300
20400          BEGIN
2[illegible]
20600            EPOINT:=1.2632-8*DENS*(ZEFF/BETA/T)**2*
20700            (MAX(10-5,(1-DENS/BT/.5668*T)))**.6
20800            COMMENT ERG/CM**3;
20900          ELSE
21000            EPOINT:=1.282-8*DENS*(ZEFF/BETA/T)**2*
21100            (MAX(10-5,(1-DENS/BT/.5668*T)))**.6;
21200            COMMENT ERG/CM**3;
21300          END;
21400     COMMENT ***********************************************************;
21500
21600
21700        REAL PROCEDURE EEXT(T);
21800            COMMENT EEXT(T) IS THE ENERGY EXPRESSION TO BE USED FOR
21900                    THE EXTENDED TARGET DOSE CALCULATION OF EBAR;
22000
22100        VALUE T;
22200        REAL T;
22300          BEGIN
22400            REAL ALFA;
22500            T:=MIN(T,TAU);
22600            IF(T0+T<=A0) THEN ALFA:=PI/2 ELSE
22700            ALFA:=ARCTAN(SQRT(ABS((A0**2-(T0-T)**2)/((T0+T)**2-A0**2))));
22800            EEXT:=(MAX(10-5,1-DENS/BT/.5668*T))**.6/T*ALFA;
22900          END;
23000
23100        REAL PROCEDURE EBAR(ZEFF,BETA,T,A0,DENS);
23200        VALUE ZEFF,BETA,T,A0,DENS;
23300        REAL ZEFF,BETA,T,A0,DENS;
23400          BEGIN
23500            COMMENT EXTENDED TARGET DOSE CALCULATION.EBAR IS THE DOSE IN
23600                    ERG/CM**3 DEPOSITED IN A CYLINDER WITH LENGTH AND
23700                    DIAMETER EQUAL TO 2*A0.EEXT(T) IS INTEGRATED FROM


23800                    T0=A0 TO T0+A0 BY MEANS OF THE COMPUTERCODE ADAPINT;
23900
24000            T0:=T;
24100          IF TYPE=3 THEN
24200            EBAR:= IF T<=3*A0 THEN (1.6083-8*(ZEFF/A0/BETA)**2*DENS*
24300            ADAPINT(EEXT,MAX(LOWLIMIT,T-A0),T+A0,.1,150,
24400            NOFUN,ERROR)) ELSE EPOINT(T)
24500            COMMENT ERG/CM**3;
24600          ELSE
24700
24800            EBAR:= IF T<=3*A0 THEN (1.632-08*(ZEFF/A0/BETA)**2*DENS*
24900            ADAPINT(EEXT,MAX(LOWLIMIT,T-A0),T+A0,.1,150,
25000            NOFUN,ERROR)) ELSE EPOINT(T);
25100            COMMENT ERG/CM**3;
25200          END;
25300     COMMENT ***********************************************************;
25400     FORMAT FMT2(/"************  RELATIVE EFFECTIVENESS  ************"
25500                 /"KIND OF CALCULATIONS          : ",A14
25600                 /"DETECTOR TYPE                 : ",A7
25700                 /"DETECTOR DENSITY              : ",F6.2," G/CM**3"
25800                 /"DETECTOR THICKNESS            : ",E10.3," CM"
25900                 /"PARTICLE ATOMIC NUMBER        : ",I3
26000                 /"PARTICLE ATOMIC WEIGHT        : ",F6.2," AMU"
```

```
26100                /"INITIAL ENERGY                    : ",E10.3," MEV/AMU"
26200                /"INITIAL BETA                      : ",E11.4
26300                /"INITIAL LET                       : ",E11.4,
26400                " MEV*CM**2/G"
26500                /"RADIUS OF SENSITVE ELEMENT        : ",E10.3," CM"
26600                /"D37                               : ",F5.1," MRAD"
26700                /" "/
26800                " "/
26900                 "RL                                : ",F6.3/
27000                 "AVERAGE ETRACK                    : ",E10.3," ERG/CM"/
27100                 "AVERAGE ECORE                     : ",E10.3," ERG/CM"/
27200                 "AVERAGE SIGMATRACK                : ",E10.3," CM**2"/
27300                 "AVERAGE SIGMACORE                 : ",E10.3," CM**2"/
27400                 "AVERAGE LET                       : ",E11.4," MEV*CM**2/G"/
27500                 "PCT. DEP. PR SEGMENT              : ",F7.2," %"/
27600                 "NUMBER OF SEGMENTS IN TARGET      : ",I5>;
27700        LIST LIST2(KIND[SIGN(PPC)+1],TPE[TYPE+1],DENS,THICK,Z,AWEIGHT,
27800      INERG,INBETA,INLET,A0,D37A,RBE,ETRACK,ECORE,SIGMT,SIGMC,AVLET,PCT,
27900       SEGMENTS);
28000      FORMAT FMT3<"RANGE OF THE ION               : ",E10.3," CM">;
28100      LIST LIST3(DLST);
28200        REMOTE:=MYJOB.STACKNO=MYSELF.STACKNO;
28300        IF NOT REMOTE THEN FCM.KIND:=VALUE(PRINTER);
28400        REPLACE TME BY(S:=TIME(7)).[47:12] FOR 4 DIGITS,"-",S.[35:6] FOR 2
28500              DIGITS,"-",S.[29:6] FOR 2 DIGITS,"  ",S.[23:6] FOR 2 DIGITS,
28600              ":",S.[17:6] FOR 2 DIGITS,":",S.[11:6] FOR 2 DIGITS;
28700        COMMENT TME IS "YYYY-MM-DD  HH:MM:SS";
28800              FOR I:=0 STEP 1 UNTIL NN DO
28900                BEGIN
29000                  READ(ZIEGLERSPLINE,/,BBC[I]);
29100                  READ(ZIEGLERSPLINE,/,CCC[I]);
29200                  READ(ZIEGLERSPLINE,/,DDC[I]);
29300                END;
29400              FOR I:=0 STEP 1 UNTIL NN DO
29500                BEGIN
29600                  READ(ZIEGLERSPLINE,/,BBH[I]);
29700                  READ(ZIEGLERSPLINE,/,CCH[I]);

29800                  READ(ZIEGLERSPLINE,/,DDH[I]);
29900                END;
30000              FOR I:=0 STEP 1 UNTIL NN DO
30100                BEGIN
30200                  READ(ZIEGLERSPLINE,/,BBN[I]);
30300                  READ(ZIEGLERSPLINE,/,CCN[I]);
30400                  READ(ZIEGLERSPLINE,/,DDN[I]);
30500                END;
30600              FOR I:=0 STEP 1 UNTIL NN DO
30700                BEGIN
30800                  READ(ZIEGLERSPLINE,/,BBO[I]);
30900                  READ(ZIEGLERSPLINE,/,CCO[I]);
31000                  READ(ZIEGLERSPLINE,/,DDO[I]);
31100                END;
31200              FOR I:=0 STEP 1 UNTIL NN DO
31300                BEGIN
31400                  READ(ZIEGLERSPLINE,/,E[I]);
31500                  READ(ZIEGLERSPLINE,/,C[I]);
31600                  READ(ZIEGLERSPLINE,/,H[I]);
31700                  READ(ZIEGLERSPLINE,/,N[I]);
31800                  READ(ZIEGLERSPLINE,/,O[I]);
31900                END;
32000              CLOSE(ZIEGLERSPLINE);
32100        PI:=3.14159265;
32200        WRITE(REM,<"ENTER 1 OR 2 FOR DEFAULT TO FILM OR ALANINE, ELSE 0">);
32300        READ(INP,/,Z);
32400        CASE Z OF
32500        BEGIN
32600      1: TYPE:=0; DENS:=1.13;A0:=10-7;PPC:=0;LOWLIMIT:=10-8;D37:=3.729D9;
32610                  D37A:=33;
32700      2: TYPE:=3;DENS:=1.21;A0:=10-7;PPC:=0;LOWLIMIT:=10-8;D37:=1.27139;
32710                  D37A:=10.5;
32800      ELSE:
32900        WRITE(REM,<"DETECTOR TYPE? FILM=0,DYE=1,NYLON=2,ALANINE=3">);
33000        READ(INP,/,TYPE);
33100        WRITE(REM,<"DENSITY OF DETECTOR ?">);
33200        READ(INP,/,DENS);
33300        WRITE(REM,<"RADIUS OF SENSITIVE ELEMENT,(CM) ?">);
33400        READ(INP,/,A0);
33500        WRITE(REM,<"NUMBER OF POINTS IN THE CORE-INTEGRATION">);
33600        WRITE(REM,<"VALID INPUTS ARE: 0,8,10,12,16,24,32,48,64.">);
33700        WRITE(REM,<"A 0 CAUSES CALC. OF ECORE BY SUBTRACTION OF">);
33800        WRITE(REM,<"ETRACK FROM LET.">);
33900        READ(INP,/,PPC);
34000        WRITE(REM,<"LOWER LIMIT FOR INTEGRATION (1E-8) ">);
34100        READ(INP,/,LOWLIMIT);
34200        END;
34300        WRITE(REM,<"DETECTOR THICKNESS IN CM ?">);
34400        READ(INP,/,THICK);
34500        WRITE(REM,<"D37 IN MRAD">);
34600        READ(INP,/,D37A);
34700        D37:=D37A*1.30E-9*DENS;
34800        WRITE(REM,<"NUMBER OF SEGMENTS IN DETECTOR ?">);
34900        READ(INP,/,NOSEG);
35000        WRITE(REM,<"INITIAL ENERGY OF PARTICLE IN MEV/AMU ?">);
```

```
35100         READ(INP,/,ERG1);
35200         INERG:=ERG1;
35300         WRITE(REM,<"ATOMIC NUMBER OF PARTICLE?">);
35400         READ(INP,/,Z);
35500         WRITE(REM,<"ATOMIC WEIGHT OF PARTICLE?">);



35600         READ(INP,/,AWEIGHT);
35700         WRITE(REM,<"IF PLOT:  ENTER 1, LPPLOT 2, NO PLOT 3">);
35800         READ(INP,/,I);
35900         CASE I OF
36000           BEGIN
36100     1:      PRPLOT:=FALSE;
36200             PLOTT:=TRUE;
36300             TERMINALPLOT;
36400     2:      PRPLOT:=PLOTT:=TRUE;
36500             LPPLOT;
36600     ELSE:   PRPLOT:=PLOTT:=FALSE;
36700         END;
36800          PCT:=100*(EXP(LN(ERG1/E[0])/(NOSEG*0.95))-1);
36900          COMMENT  PCT IS THE PERCENTUAL ENERGY LOSS PER SEGMENT.
37000                   PCT IS USED FOR CALCULATING THE SEGMENT THICKNESS;
37100
37200         TPLL:=A0*LOWLIMIT;
37300         IF PLOTT THEN
37400           BEGIN
37500             WRITE(REM,
37600     <"IF PLOT, EXTENDED TARGET:1,POINT TARGET:0">);
37700             READ(INP,/,I);
37800             EXTENDEDPLOT:=I=1;
37900         WRITE(REM,<"MAX DOSE ON DOSE-AXIS IN UNITS OF LOG(MRAD)">);
38000         READ(INP,/,D);
38100           END;
38200         N1:=2*PPC+112+(IF NOT EXTENDEDPLOT THEN 5 ELSE
38300           IF PPC>0 THEN 0 ELSE 2);
38400         WRITE(REM,<"IF PRINTED OUTPUT :     ENTER 1, ELSE 0">);
38500         READ(INP,/,I);
38600         IF I=1 THEN PRINT:=TRUE ELSE PRINT:=FALSE;
38700           BEGIN
38800             LABEL OUTPUT;
38900             REAL ARRAY ETR,LT,ECR,STR,SCR,DELTAE,R3[0:NOSEG];
39000             REAL ARRAY  EXTENDEDDOSE,POINTDOSE,EXTENDEDT,
39100                         PCINTT[0:NOSEG,0:N1];
39200             ARRAY REFERENCE DOS,TA[1,0];
39300      COMMENT ***************************************************;
39400
39500             REAL PROCEDURE BCD(T);
39600               COMMENT THE SIGMA-TRACK INTEGRATION FUNCTION BCD(T) MAKE
39700               USE OF THE EXTENDED TARGET DOSE FORMULATION EBAR(T).
39800               BCD(T) IS USED IN THE SIGMA INTEGRATION CALCULATION;
39900             VALUE T;
40000             REAL T;
40100               BEGIN
40200                 DOSEFORSIGMA:=EBAR(ZEFF,BETA,T,A0,DENS);
40300                   COMMENT ERG/CM**3;
40400                 EXTENDEDDOSE[0,I]:=LOG(DOSEFORSIGMA/DENS*10-8);
40500                   COMMENT EXTENDEDDOSE[0,I] IS ONLY USED FOR PLOTTING OF THE
40600                           EXTENDED TARGET DOSE PROFILE AND IS EXPRESSED IN
40700                           LOG(MRAD);
40800                 DOSEFORSIGMA:=*/037;
40900                 BCD:=(IF DOSEFORSIGMA<10-3 THEN DOSEFORSIGMA
41000                 ELSE (1-EXP(-DOSEFORSIGMA)))*T;
41100                 EXTENDEDT[0,I]:=LOG(T);
41200                 I:=*+1;
41300               END;
41400      COMMENT ***************************************************;
41500



41600             REAL PROCEDURE ABC(T);
41700               COMMENT THE ETRACK INTEGRATION FUNCTION ABC(T) MAKE USE OF THE
41800               POINT TARGET DOSE FORMULATION EPOINT(T). ABC(T) IS USED
41900               IN THE DOSE TO THE TRACK ETR INTEGRATION CALCULATION;
42000             VALUE T;
42100             REAL T;
42200               BEGIN
42300                 DOSEFORTRACK:=EPOINT(T);
42400                   COMMENT ERG/CM**3;
42500                 POINTDOSE[0,I]:=LOG(DOSEFORTRACK/DENS*10-8);
42600                   COMMENT POINTDOSE[0,I] IS ONLY USED FOR PLOTTING OF THE
42700                   POINT TARGET DOSE PROFILE AND IS EXPRESSED IN LOG(MRAD);
42800                 ABC:=DOSEFORTRACK*T;
42900                 PCINTT[0,I]:=LOG(T);
43000                 I:=*+1;
43100               END;
43200      COMMENT ***************************************************;
43300
43400             ETOT:=0;DIST:=0;
43500             IF PRINT THEN
43600               WRITE(OUT,<A17//
43700       "  ENERGY  DELTA E     BETA      ZEFF      LETIOT      LETNUCL      RE
43800          THICK     DIST    ECORE    ETRACK SIGMACORE SIGMATRACK"/>,TME);
43890               WRITE(OUT,<A17//"/>,TME);
43900               WRITE(OUT,<A17//
```

```
43910       "         MEV/AMU                                        MEVCM**2/G
43920                                                                    CM**/>,TME);
44000             INBETA:=SQRT(2*INERG/931.8);
44100             SEGMENTS:=NOSEG;
44200             OVERRANGE:=FALSE;
44300             Q:=1;
44400             WHILE ERG1>E[0] DO
44500               BEGIN
44600                 COMMENT HERE STARTS THE LOOP OVER THE SEGMENTS IN THE
44700                         DETECTOR;
44800                 BETA:=SQRT(2*ERG1/931.8);
44900                 IF Z=1 THEN
45000                   ZEFF:=1-EXP(-6.3246*SQRT(ERG1)-1.2*ERG1-14.43*ERG1**2)
45100                 ELSE
45200                 IF Z=2 THEN
45300                   ZEFF:=((1+7.2762-3*EXP(-(7.6-LN(123*ERG1))**2))
45400                        *(1-EXP(-(0.7446+0.1429*(LN(123*ERG1))+0.01562
45500                      *(LN(ERG1*123))**2-0.00267*(LN(123*ERG1))**3+
45600                      1.3253-6*(LN(123*ERG1))**6)))**2)*
45700                   (1-EXP(-6.3246*SQRT(ERG1)-1.2*ERG1-14.43*ERG1**2))
45800                 ELSE
45900                 IF Z=3 THEN
46000                   ZEFF:=(1+7.2732-3*EXP(-(7.6-LN(123*ERG1))**2))
46100                        *(1-EXP(-0.7136-2.792*ERG1-1.348*ERG1**2))**3
46200                        *(1-EXP(-6.3246*SQRT(ERG1)-1.2*ERG1-14.43*ERG1**2))
46300                 ELSE
46400                   ZEFF:=Z*(1-(EXP(-5.6036*SQRT(ERG1)*7**(-2/3)-0.0372*
46500                        SIN(8.802*SQRT(ERG1)*Z**(-2/3))))*(1.034-0.1777*
46600                        EXP(-0.08114*Z)))*(1-EXP(-6.3246*SQRT(ERG1)-
46700                        1.2*ERG1-14.43*ERG1**2));
46800                   ZEFF:=MIN(Z,ZEFF);
46900                 L:=LET(TYPE,ERG1);
47000                 IF Q=1 THEN INLET:=LETTOT/1.6022-6/DENS;
47100                 THK:=PCT/100*ERG1*AWEIGHT/6.2422E5/L;
47200                 DIST:=*+THK;



47300                 IF DIST>THICK THEN
47400                   BEGIN
47500                     THK:=THICK-DIST-THK;
47600                     OVERRANGE:=TRUE;
47700                     DIST:=THICK;
47800                   END;
47900       COMMENT   THE SEGMENT THICKNESS IS CALCULATED SO THAT (PCT)% OF THE
48000                 SEGMENT INPUT ENERGY WILL BE DEPOSITED IN THE SEGMENT. IF
48100                 THIS, HOWEVER, CAUSES CALCULATIONS BEYOND THE THICKNESS OF
48200                 THE TARGET, THE THICKNESS OF THE LAST SEGMENT IS ADJUSTED
48300                 ACCORDINGLY;
48400                   IF Q=1 THEN
48500                     BEGIN
48600                       DELTAE[Q]:=L*THK/AWEIGHT*6.2422E5;
48700                       T1:=0;
48800                       S1:=L;
48900                     END
49000                   ELSE
49100                   IF Q=2 THEN
49200                     BEGIN
49300                       T2:=DIST-THK;
49400                       DELTAE[Q]:=THK*(L+(L-S1)/T2*THK/2);
49500                       DELTAE[Q]:=*/AWEIGHT*6.2422E5;
49600                       S2:=L;
49700                     END
49800                   ELSE
49900                     BEGIN
50000                       T3:=DIST-THK;
50100                       K3:=(L-S1-(S2-S1)*(T3-T1)/(T2-T1))/
50200                            (T3*T3-T1*T1-(T2*T2-T1*T1)*(T3-T1)/(T2-T1));
50300                       K2:=(S2-S1-K3*(T2*T2-T1*T1))/(T2-T1);
50400                       K1:=S1-K3*T1*T1-K2*T1;
50500                       DELTAE[Q]:=K1*THK+0.5*K2*(2*T3*THK+THK*THK)+K3/3*
50600                                  (3*THK*T3*(T3+THK)+THK*THK*THK);
50700                       DELTAE[Q]:=*/AWEIGHT*6.2422E5;
50800                       DELTAE[Q]:=MAX(0,DELTAE[Q]);
50900                       S1:=S2;
51000                       S2:=L;
51100                       T1:=T2;
51200                       T2:=T3;
51300                     END;
51400                   COMMENT  THE DEPOSITED ENERGY IN EACH SEGMENT IS THE
51500                            INTEGRAL OF LET OVER THE THICKNESS OF THE
51600                            SEGMENT. THIS INTEGRAL IS APPROXIMATED WITH A
51700                            INTEGRAL OF A PARABOLIC EXTRAPOLATION OF THE
51800                            LET DATA. SUCH AN EXTRAPOLATION IS, HOWEVER,
51900                            NOT POSSIBLE FOR THE FIRST TWO SEGMENTS.
52000                            A MORE CRUDE METHOD IS APPLIED TO THESE TWO
52100                            SEGMENTS;
52200                 ERG2:=ERG1-DELTAE[Q];
52300                 ETOT:=*+DELTAE[Q];
52400                 IF ERG2<=E[0] THEN
52500                   BEGIN
52600                     SEGMENTS:=Q;
52700                     OVERRANGE:=TRUE;
52800                       COMMENT "NOSEG" IS USED FOR CALCULATING AVERAGE VALUES
52900                               OF THE SUMMARIZED RESULTS FOR ALL SEGMENTS WHEN
53000                               THE ION RANGE IS BIGGER THAN THE TARGET THIC-
53100                               NESS.FOR TARGET THICNESS' BIGGER THAN THE ION
53200                               RANGE "SEGMENTS" IS USED AND PUT EQUAL TO THE
```

```
                    NUMBER OF SEGMENTS PENETRATED;
      GO TO OUTPUT
    END;
  COMMENT  ERG IS THE AVERAGE ENERGY LOSS,BETA IS THE AVERAGE
           RELATIVE VELOCITY,AND ZEFF IS THE AVERAGE CHARGE
           IN THE SEGMENT;
ERG:=(ERG1+ERG2)/2;
BETA:=SQRT(2*ERG/931.8);
IF Z=1 THEN
  ZEFF:=1-EXP(-6.3246*SQRT(ERG)-1.2*ERG-14.43*ERG**2)
ELSE
IF Z=2 THEN
  ZEFF:=((1+7.2763-3*EXP(-(7.6-LN(133*ERG))**2))
       *(1-EXP(-(0.7446+0.1429*(LN(133*ERG))+0.01562
     *(LN(ERG*133))**2-0.00267*(LN(133*ERG))**3+
      1.325E-6*(LN(133*ERG))**8)))**2)*
  (1-EXP(-6.3246*SQRT(ERG)-1.2*ERG-14.43*ERG**2))
ELSE
IF Z=3 THEN
  ZEFF:=(1+7.2763-3*EXP(-(7.6-LN(133*ERG))**2))
       *(1-EXP(-0.7138-2.792*ERG-1.348*ERG**2))*3
       *(1-EXP(-6.3246*SQRT(ERG)-1.2*ERG-14.43*ERG**2))
ELSE
  ZEFF:=Z*(1-(EXP(-5.6036*SQRT(ERG)*Z**(-2/3)-0.0378*
       SIN(9.802*SQRT(ERG)*Z**(-2/3))))*(1.034-0.1777*
       EXP(-0.08114*Z)))*(1-EXP(-6.3246*SQRT(ERG)-1.2*
       ERG-14.43*ERG**2));
    ZEFF:=MIN(Z,ZEFF);
L:=LET(TYPE,ERG);
  COMMENT L IS THE AVERAGE COLLISION STOPPING POWER IN
          THE SEGMENT IN ERG/CM;
LT[Q]:=LETTOT/1.6022-6/DENS;
  COMMENT LT[Q] IS THE AVERAGE TOTAL STOPPING POWER IN
          THE SEGMENT IN MEVCM**2/G;
BT:=(BETA**2/(1-BETA**2))**1.67;
TAU:=0.5668/DENS*BT;
  IF TAU<5.01*A0 THEN
    BEGIN
      IF TAU<=TPLL THEN
        BEGIN
      COMMENT IF THE RANGE OF THE DELTA RAYS DOES NOT
              EXCEED RANGE OF THE SENSITIVE ELEMENT
              (TAU<A0),THE CALCULATIONS OF ETRACK AND
              SIGMA-TRACK ARE OMITTED;
          I:=1;
          STR[Q]:=0;
          ETR[Q]:=0;
        END
      ELSE
        BEGIN
          I:=1;
          STR[Q]:=2*PI*QG(16,TPLL,TAU,BCD);
          I:=1;
          ETR[Q]:=2*PI*QG(16,TPLL,TAU,ABC);
        END
    END
  ELSE
BEGIN
I:=1;
  COMMENT INC IS THE INCREMENT IN DISTANCE T FROM THE
          CENTER OF THE ION'S PATH.INC IS EQUIDISTANT
          STEPS IN A LOGARITHMIC SYSTEM;
INC:=EXP(LN(TAU/(3*A0))/3);
  COMMENT STR IS THE INTEGRATION OF THE POISSON PROBA-
          BILITY DISTRIBUTION FORMULA IN THE TRACK GIVING
          SIGMA,THE CROSS-SECTION IN THE TRACK;
STR[Q]:=2*PI*(QG(16,TPLL,3*A0,BCD)+QG(32,3.001*A0,3*INC*A0,
       BCD)+QG(32,3.001*INC*A0,3*INC**2*A0,BCD)+QG(32,3.001*
       INC**2*A0,TAU,BCD));
  COMMENT CM**2;
I:=1;
  COMMENT ETR IS THE INTEGRATION OF THE POINT TARGET
          DOSE GIVING THE TOTAL POINT TARGET DOSE DEPO-
          SITED IN THE TRACK;
ETR[Q]:=2*PI*(QG(16,TPLL,3*A0,ABC)+QG(32,3.001*A0,3*INC*A0,
       ABC)+QG(32,3.001*INC*A0,3*A0*INC**2,ABC)+QG(32,3.001*
       A0*INC**2,TAU,ABC));
  COMMENT ERG/CM;
END;
  COMMENT PPC IS THE NUMBER OF INTEGRATION STEPS IN THE CORE
  AREA.IF PPC=0 THE DOSE TO THE CORE IS CALCULATED AS A
  SUBTRACTION OF ETRACK FROM LET.SIGMA-CORE IS FOUND FROM
  AN ANALYTIC EXPRESSION INCLUDING DOSE TO THE CORE AS A
  CONSTANT.IF PPC#0 THE DOSE TO THE CORE IS CALCULATED AS
  AN INTEGRATION OF EBAR IN THE SAME WAY AS THE DOSE TO THE
  TRACK WITH LOWER LIMIT OF INTEGRATION EQUAL TO "LOWLIMIT".
  SIGMA-CORE IS CALCULATED AS SIGMA-TRACK;
IF PPC=0 THEN
BEGIN
ECR[Q]:=L-ETR[Q];
  COMMENT ERG/CM;
DCORE:=ECR[Q]/(PI*A0**2)/DENS*1E-08;
  COMMENT MRAD;
EXTENDEDDOSE[Q,113]:=EXTENDEDDOSE[Q,114]:=LOG(MAX(DCORE,
```

```
62700                EXTENDEDDOSE[0,113]:=EXTENDEDDOSE[0,114]:=LOG(MAX(DCORE,
62800                                    10-40));
62900                EXTENDEDT[0,113]:=-8;EXTENDEDT[0,114]:=LOG(.9999*A0);
63000                IF (DCORE/D37A)>20 THEN DCORE:=D37A*20;
63100                SCR[0]:=(1-EXP(-DCORE/D37A))*PI*A0**2;
63200                END
63300                ELSE
63400                BEGIN
63500                  COMMENT SCR[0] IS THE INTEGRATION OF THE POISSON PROBA-
63600                          BILITY DISTRIBUTION FORMULA IN THE CORE GIVING
63700                          SIGMA,THE CROSS-SECTION IN THE CORE;
63800                SCR[0]:=2*PI*(QG(PPC,LOWLIMIT,SQRT(A0*LOWLIMIT),BCD)+
63900                          QG(PPC,SQRT(A0*LOWLIMIT),A0,BCD));
64000                  COMMENT CM**2;
64100                I:=113;
64200                ECR[0]:=2*PI*(QG(PPC,LOWLIMIT,SQRT(A0*LOWLIMIT),ABC)+
64300                          QG(PPC,SQRT(A0*LOWLIMIT),A0,ABC));
64400                  COMMENT ERG/CM;
64500                END;
64600                IF NOT EXTENDEDPLOT THEN FOR TO:=-8 STEP 0.2 UNTIL -7.1
64700                DO ABC(10**TO);
64800
64900                RB[0]:=(SCR[0]+STR[0])*D37/L;
65000                IF PRINT THEN
65100                WRITE(OUT,<F,.4,F9.4,E11.4,F9.4,E11.4,E11.4,F6.3,E11.4,E11.4
65110                          ,E9.2,E9.2,E9.2,E9.2>
65200                ,ERG1,DELTAE[0],BETA,ZEFF,LT[0],LETMUCL,RB[0],THK,DIST,
65210                ECR[0],ETR[0],SCR[0],STR[0]);
65300                ERG1:=ERG2;
65400                    COMMENT ERG2 IS THE INPUT ENERGY FOR THE NEXT SEGMENT;
65500                  ETR[0]:=**THK;
65600                  ECR[0]:=**THK;
65700                  STR[0]:=**THK;
65800                  SCR[0]:=**THK;
65900                  LT[0]:=**THK;
66000                  IF OVERRANGE THEN GO TO OUTPUT;
66100          COMMENT  THIS IS TO ENSURE THAT NO CALCULATIONS ARE MADE BEYOND
66200                   THE PHYSICAL END OF THE TARGET;
66300                0:=*+1;
66400              END;
66500    OUTPUT: ETRACK:=ECORE:=SIGMT:=SIGMC:=AVLET:=RBE:=0;
66600            SEGMENTS:=0;
66700            FOR 0:=1 STEP 1 UNTIL SEGMENTS DO
66800              BEGIN
66900                COMMENT THE SEGMENT RBE IS WEIGHTED AGAINST THE ENERGY LOST
67000                        BY THE ION IN THE SEGMENT TO THE TOTAL ENERGY LOSS;
67100
67200                ETRACK:=*+ETR[0];
67300                ECORE:=*+ECR[0];
67400                SIGMT:=*+STR[0];
67500                SIGMC:=*+SCR[0];
67600                AVLET:=*+LT[0];
67700                RBE:=*+RB[0]*DELTAE[0];
67800              END;
67900            ETRACK:=ETRACK/DIST;
68000            ECORE:=ECORE/DIST;
68100            SIGMT:=SIGMT/DIST;
68200            SIGMC:=SIGMC/DIST;
68300            AVLET:=AVLET/DIST;
68400            RBE:=RBE/ETOT;
68500            IF REMOTE THEN
68600              BEGIN
68700                WRITE(REM,<4"18270C",120(4"00")>);
68800                WRITE(REM,FMT2,LIST2);
68900              IF THICK>=DIST THEN
69000            WRITE(REM,FMT3,LIST3);
69100              END REMOTE;
69200            IF PRINT OR NOT REMOTE THEN
69300              BEGIN
69400                WRITE(OUT,<A1>,4"0C");
69500                COMMENT OUTPUT ON PRINTER;
69600                WRITE(OUT,FMT2,LIST2);
69700              IF THICK>=DIST THEN
69800            WRITE(OUT,FMT3,LIST3);
69900              END;
70000
70100                  COMMENT HERE STARTS THE PLOTTING SECTION;
70200
70300            IF PLOTT THEN
70400              BEGIN
70500                LABEL ERR,OPIGEN,NOPLOT,KOMORE,PICKENGANG;
70600
70700                  IF EXTENDEDPLOT THEN
70800                  BEGIN
70900                    DOS:=EXTENDEDDOSE;TA:=EXTENDEDT
71000                  END
71100                  ELSE
71200                  BEGIN
71300                    DOS:=POINTDOSE;TA:=POINTT
71400                  END;
```

```
71500                 DELTAX:=DELTAY:=.005;
71600                 SETORIGC(8,-(D-13));
71700                 PLOTAXES(-8,(D-13),-8,-2,(D-13)+8,1,1);
71800                 PAPERHEIGHT:=29;
71900                 PAPERWIDTH:=21;
72000                 LEFTMARGIN:=1.5;
72100                 LOWERMARGIN:=1.5;
72200                 FOR I:=ENTIER(D/2)+2 STEP-2 UNTIL (D-13) DO
72300                 PLOTSTRING((STRINGBUFFER+),<I3>,I),-8.5,I-.075,.3);
72400                 FOR I:=-8 STEP 2 UNTIL-2 DO
72500                 PLOTSTRING((STRINGBUFFER+),<I2>,I),I-.15,(D-13)-0.2,0.3);
72600                 PLOTSTOP;
72700     NOKENGANG:  WRITE(REM,
72800                       <"IF PLOT WITH NO AXIS, ENTER 1, AXIS 2, NO PLOT 0">);
72900                 READ(INP,/,I);
73000                 IF I=1 THEN GO TO OKIGEN ELSE
73100                 IF I=0 THEN GO TO NOPLOT;
73200                 SERVOGORPLOT(1,FALSE);
73300     OKIGEN:     SETORIGO(8,-(D-13));
73400     ERR:        WRITE(REM,<"SEGMENT NUMBER FOR DOSE-PROFILE PLOT ?">);
73500                 READ(INP,/,X);
73600                 IF X>SEGMENTS THEN
73700                   BEGIN
73800                     WRITE(REM,<"INVALID SEGMENT NUMBER, MAX NUMBER",I4>,
73900                           SEGMENTS);
74000                     GO TO ERR;
74100                   END;
74200                   BEGIN
74300                     INTEGER X1;
74400      COMMENT ***************************************************;
74500
74600                     PROCEDURE OUTPROC(B,A);
74700                     VALUE B;
74800                     BOOLEAN B;
74900                     ARRAY A[0];
75000                       BEGIN
75100                         IF NOT B THEN
75200                           BEGIN
75300                             TA[X,X1:=X1+1]:=A[0];
75400                             DOS[X,X1]:=A[1];
75500                           END;
75600                       END;
75700      COMMENT ***************************************************;
75800
75900                     BOOLEAN PROCEDURE INPROC(A);
76000                     ARRAY A[0];
76100                     IF AUTINPROC:=(X1:=X1-1)<1 THEN
76200                       BEGIN
76300                         A[0]:=TA[X,Y1];
76400                         A[1]:=DOS[X,X1];
76500                       END;
76600      COMMENT ***************************************************;
76700
76800                     BOOLEAN PROCEDURE CMP(A,B);
76900                       ARRAY A,B[0];
77000                       CMP:=A[0]<B[0];



77100      COMMENT ***************************************************;
77200
77300                     X1:=N1+1;
77400                     SORT(OUTPROC,INPROC,0,CMP,2);
77500                   END;
77600                 PLOTMOVE(MAX(TA[X,1],-8),DOS[X,1]);
77700                 FOR I:=2 STEP 1 UNTIL N1 DO
77710                 BEGIN
77720                     IF TA[X,I]=0 THEN GO TO NOPORE;
77800                 IF DOS[X,I]>(D-13) THEN PLOTDRAW(MAX(TA[X,I],-8),DOS[X,I])
77900                  ELSE IF DOS[X,I-1]>(D-13) THEN PLOTDRAW (TA[X,I-1],D-13);
77910                 END;
78000                 PLOTMOVE(0,0);
78100       NOMORE:   PLOTSTOP;
78200                 IF REMOTE THEN SERVOGORPLOT(0,FALSE);
78300                 WRITE(REM,<"TABLE OF PROFILES; ENTER 1 ELSE 0">);
78400                 READ(INP,/,I);
78500                 IF I=1 THEN
78600                   BEGIN
78700                     WRITE(OUT,<//"    T [CM]    DOSE [MRAD]"/>);
78800                     FOR I:=1 STEP 2 UNTIL N1 DO
78900                     WRITE(OUT,<2E12.5>,10**TA[X,I],10**DOS[X,I]);
79000                   END;
79100                   COMMENT PRINTED DATA ARE DOSE [MRAD] AS A FUNCTION OF
79200                           THE DISTANCE T [CM] FROM THE IONS PATH;
79300                 GO TO NOKENGANG;
79400       NOPLOT:   IF PLOTFIL.OPEN AND NOT PRPLOT THEN
79500                 IF REMOTE THEN CLOSE(PLOTFIL,PURGE) ELSE
79600                 LOCK(PLOTFIL,CHUNCH);
79700               END;
79800             END;
79900           END;
80000       $ INCLUDE "RISCE/PLOTSLOT/A"
80100     END.
80200
```

Table I

Dose as a function of radial distance for a 42 MeV bromine ion in tissue-equivalent unit-density material.

t[nm]	D[Gy][a]	D[Gy][b], %	D_1[Gy], %	D_2[Gy], %
0.5	$3.9 \cdot 10^7$	$5.0 \cdot 10^7$, +28	$9.2 \cdot 10^7$, +136	$5.5 \cdot 10^7$, +41
1.05	$1.5 \cdot 10^7$	$1.3 \cdot 10^7$, -13	$2.1 \cdot 10^7$, + 39	$1.2 \cdot 10^7$, -17
2.1	$4.8 \cdot 10^6$	$3.5 \cdot 10^6$, -27	$5.2 \cdot 10^6$, + 7	$3.1 \cdot 10^6$, -36
4.2	$1.1 \cdot 10^6$	$9.2 \cdot 10^5$, -16	$1.3 \cdot 10^6$, + 15	$7.6 \cdot 10^5$, -31
8.4	$2.6 \cdot 10^5$	$2.3 \cdot 10^5$, - 8	$3.0 \cdot 10^5$, + 17	$1.8 \cdot 10^5$, -30
16.8	$5.6 \cdot 10^4$	$5.3 \cdot 10^4$, - 5	$7.0 \cdot 10^4$, + 25	$4.2 \cdot 10^4$, -26
25.2	$1.6 \cdot 10^4$	$1.7 \cdot 10^4$, + 6	$2.9 \cdot 10^4$, + 78	$1.7 \cdot 10^4$, + 4
33.7	$7.0 \cdot 10^3$	$7.2 \cdot 10^3$, + 3	$1.5 \cdot 10^4$, +107	$8.2 \cdot 10^3$, +17
42.1	$2.9 \cdot 10^3$	$3.2 \cdot 10^3$, +10	$8.3 \cdot 10^3$, +187	$4.5 \cdot 10^3$, +54
50.5	$1.4 \cdot 10^3$	$1.6 \cdot 10^3$, +14	$5.1 \cdot 10^3$, +267	$2.5 \cdot 10^3$, +77
70.9	$6.0 \cdot 10^2$	$5.2 \cdot 10^2$, -13	$1.8 \cdot 10^3$, +200	0
root mean square deviation:		5%	39%	12%

[a] experimental data of Varma et al[77].

[b] data obtained from continuous slowing down approximation calculations by Paretzke[77].

D_1 = dose calculated from eq. 2-14.

D_2 = dose calculated from eq. 2-15.

The percent deviation: $\frac{\text{Calc.-Exp.}}{\text{Exp.}} \cdot 100$

Table II

Dose as a function of radial distance for different ions in water.

	90 MeV/amu Fe ion			2 MeV/amu C ion			8.1 MeV/amu Ne ion		
t[nm]	D^a [Gy]	D^b [Gy]	%[c]	D^a [Gy]	D^b [Gy]	%[c]	D^a [Gy]	D^b [Gy]	%[c]
0.3	$4.12 \cdot 10^6$	$5 \cdot 10^6$	+21	$7.23 \cdot 10^6$	$1.0 \cdot 10^7$	+38	$5.66 \cdot 10^6$	8.10^6	+42
1.0	$5.2 \cdot 10^5$	$4.5 \cdot 10^5$	-14	$9.2 \cdot 10^5$	$9.0 \cdot 10^5$	- 2	$7.2 \cdot 10^5$	$7.3 \cdot 10^5$	- 1
3.0	$8.4 \cdot 10^4$	$5 \cdot 10^4$	-40	$1.45 \cdot 10^5$	$1.0 \cdot 10^5$	-31	$1.15 \cdot 10^5$	$8 \cdot 10^4$	-30
10	$7.7 \cdot 10^3$	$4.5 \cdot 10^3$	-42	$1.24 \cdot 10^4$	$8.9 \cdot 10^3$	-28	$1.05 \cdot 10^4$	$7.2 \cdot 10^3$	-31
30	$6.1 \cdot 10^2$	$5 \cdot 10^2$	-18	$1.0 \cdot 10^3$	$9.7 \cdot 10^2$	- 3	$8.5 \cdot 10^2$	$8 \cdot 10^2$	- 6
100	$5.0 \cdot 10^1$	$4.5 \cdot 10^1$	-10	$7 \cdot 10^1$	$8.1 \cdot 10^1$	+16	$6.9 \cdot 10^1$	$7.2 \cdot 10^1$	+ 4
300	5.5	5.0	- 9				7.7	7.8	+ 2
10^3	$5 \cdot 10^{-1}$	$4.5 \cdot 10^{-1}$	-10				$6.2 \cdot 10^{-1}$	$6.6 \cdot 10^{-1}$	+ 6
$3 \cdot 10^3$	$5.8 \cdot 10^{-2}$	$5 \cdot 10^{-2}$	-16						
10^4	$5.5 \cdot 10^{-3}$	$4.4 \cdot 10^{-3}$	-20						
$3 \cdot 10^4$	$6 \cdot 10^{-4}$	$4.8 \cdot 10^{-4}$	-20						
10^5	$3.4 \cdot 10^{-5}$	$3.9 \cdot 10^{-5}$	+16						
root mean square deviation			6%			10%			8%

[a] calculated data of Fain et al.[56].

[b] calculated from eq. 2-15.

[c] the percent deviation: $\frac{D^b - D^a}{D^a} \cdot 100$.

Table III

Experimental values of RE for the dye film compared to calculated RE with a D_{37} value of $1.7 \cdot 10^5$ Gy and $3.3 \cdot 10^5$ Gy.

	$RE_{exp.}$	RE_1, %	RE_2, %
^{60}Co γ-rays	1.00	1.00	
10 MeV electrons	1.00		1.00
16 MeV protons	1.00	0.92, - 8.0	0.96, - 4.0
3 MeV protons	0.81	0.65, -19.8	0.76, - 6.2
10 Mev α-particles	0.55	0.47, -14.6	0.52, - 5.5
21 MeV ^{7}Li ions	0.47	0.42, -10.6	0.46, - 2.1
64 MeV ^{16}O ions	0.36	0.36, 0	0.38, + 5.6
42 MeV ^{14}N ions	0.28	0.31, +10.7	0.32, +14.3
root mean square deviation:		5%	2.9%

$RE_{exp.}$: RE derived from the initial slope of the dose-response characteristics.

RE_1 : RE calculated for $D_{37} = 1.7 \cdot 10^5$ Gy.

RE_2 : RE calculated for $D_{37} = 3.3 \cdot 10^5$ Gy.

The percent deviation: $\frac{\text{Calc.-Exp.}}{\text{Exp.}} \cdot 100.$

Table IV

Experimental values of RE for the dye film compared to calculated RE based on a linear and a power-law range-energy relation for the δ-rays. $D_{3,7} = 3.3 \cdot 10^5$ Gy.

	$RE_{exp.}$	RE_{1a}, %	RE_{2a}, %
10 MeV electrons	1.00		
16 MeV protons	1.00	0.97, - 3.0	0.96, - 4.0
3 MeV protons	0.81	0.80, - 1.2	0.76, - 6.2
10 MeV α-particles	0.55	0.64, +16.4	0.52, - 5.5
21 MeV ^{7}Li ions	0.47	0.57, +21.3	0.46, - 2.1
64 MeV ^{16}O ions	0.36	0.48, +33.3	0.38, + 5.6
42 MeV ^{14}N ions	0.28	0.44, +57.1	0.32, +14.3
root mean square deviation:		11.9%	3%

$RE_{exp.}$: RE derived from the initial slope of the dose-response characteristics.

RE_{1a} : RE calculated by means of the linear relation.

RE_{2a} : RE calculated by means of the power-law relation.

The percent deviation: $\frac{\text{Calc.-Exp.}}{\text{Exp.}} \cdot 100.$

Table V

Experimental values of RE for alanine compared to calculated RE for $a_0 = 3 \cdot 10^{-9}$ m and $D_{37} = 1.05 \cdot 10^5$ Gy.

	$RE_{exp.}$	$RE_{calc.}$, %	$LET_{init.}$ [a]	$LET_{av.}$ [a]	$(z^2/\beta^2)_{init.}$	$(z^2/\beta^2)_{av.}$
^{60}Co γ-rays						
16 MeV protons	1.00	0.99, - 1.0	27	38	29	39
6 MeV protons	0.86	0.85, - 1.2	68	119	78	130
20 MeV α-particles	0.58	0.60, + 3.4	311	534	373	621
21 MeV ^{7}Li ions	0.37	0.40, + 8.1	1026	1582	1375	2247
64 MeV ^{16}O ions	0.32	0.31, - 3.1	5274	7349	6598	10176
80 MeV ^{32}S ions	0.25	0.23, - 8.0	20200	20780	27792	37869

root mean square deviation: 2.0%

the percent deviation: $\frac{\text{Calc.-Exp.}}{\text{Exp.}} \cdot 100.$

[a] : MeVcm^2/g.

Table VI

Experimental values of RE for the dye film compared to calculated RE with a radius of the radiation sensitive element of $1 \cdot 10^{-9}$, $1.3 \cdot 10^{-9}$, and $1.8 \cdot 10^{-9}$ m. $D_{37} = 3.3 \cdot 10^{5}$ Gy.

	$RE_{exp.}$	RE_{1b}, %	RE_{2b}, %	RE_{3b}, %
10 MeV electrons	1.00			
16 MeV protons	1.00	0.96, - 4.0	0.98, - 2.0	1.00, 0
3 MeV protons	0.81	0.76, - 6.2	0.83, - 2.5	0.90, +11.1
10 MeV α-particles	0.55	0.52, - 5.5	0.55, 0	0.64, +16.4
21 MeV ^{7}Li ions	0.47	0.46, - 2.1	0.48, + 2.1	0.54, +14.9
64 MeV ^{16}O ions	0.36	0.38, + 5.6	0.38, + 5.6	0.39, + 8.3
42 MeV ^{14}N ions	0.28	0.32, +14.3	0.32, +14.3	0.34, +21.4
root mean square deviation:		3%	2.6%	5.6%

$RE_{exp.}$: RE derived from the initial slope of the dose-response characteristics.

RE_{1b} : RE calculated by means of $a_0 = 1 \cdot 10^{-9}$ m.

RE_{2b} : RE calculated by means of $a_0 = 1.3 \cdot 10^{-9}$ m.

RE_{3b} : RE calculated by means of $a_0 = 1.8 \cdot 10^{-9}$ m.

The percent deviation: $\frac{\text{Calc.-Exp.}}{\text{Exp.}} \cdot 100$.

Table VII

Experimental values of RE in dye film compared to initial and average values of LET and z^2/β^2.

	$RE_{exp.}$	$LET_{init.}$ [a]	$LET_{av.}$ [a]	$(z^2/\beta^2)_{init.}$	$z^2/\beta^2)_{av.}$
^{60}Co γ-rays	1.00				
10 MeV electrons	1.00	2.1	2.1		
16 MeV protons	1.00	28	28	29.1	29.3
3 MeV protons	0.81	120	135	155	180
10 MeV α-particles	0.55	551	628	740	910
21 MeV ^{7}Li ions	0.47	1058	1228	1375	1651
64 MeV ^{16}O ions	0.36	5434	6740	6598	8835
42 MeV ^{14}N ions	0.28	5087	6689	6611	9845

[a] : $MeVcm^2g^{-1}$

$D_{37} = 3.3 \cdot 10^5$ Gy

$a_0 = 1 \cdot 10^{-9}$ m

LIST OF FIGURES

Fig. 8. Schematic representation of the radiation sensitive elements around the path of an ion for calculation of the extended target dose.

Fig. 9. Deriving the geometric function $A(t,a_0)$ from simple trigonometric considerations.

$$dA_1 = 4\ \mathrm{Arctg}\ \sqrt{(a_0^2-(t_0+t)^2)/((t_0+t)^2-a_0^2}\cdot t\,dt \quad \text{for } (t_0+t) > a_0$$

$$dA_2 = 2\pi t\,dt \quad \text{for } (t_0+t) \leq a_0$$

Fig. 10. Average dose to the sensitive element (extended target dose) as a function of distance from the ion's path calculated from eq. 2-17. The dose distribution profiles of a 64 MeV ^{16}O ion in a 0.5 μm thick segment of dye film is calculated as: a) the subtraction procedure, and b) the integration procedure in the core with a lower integration limit of 10^{-10} m.

Fig. 11 Schematical representation of the radial distribution of delta rays and subsequent dose around the path of a heavy charged particle.

Fig. 12. Light absorption spectra of the dye film irradiated with (1) ^{60}Co γ-rays; (2) UV-light at 250 nm, and (3) 3 MeV protons. (4) Spectrum for unirradiated film.

Fig. 13. Light absorption spectra of the dye film showing the time dependent decay of primary formed species at 412 nm and the build-up of dye at 604 nm after irradiation with 10 MeV electrons. The film is conditioned 24 hours in vacuum before irradiation in vacuum.

Fig. 14. Time dependent change in relative ΔOD/mm at 510 nm after irradiation in air to different doses of ^{60}Co γ-rays with a dose rate of 14 Gy s^{-1}. The response is normalized with respect to maximum absorption.

Fig. 15. Saturation optical density as a function of dose rate for the FWT 60 radiochromic dye film measured at 510 nm.

Fig. 16. Temperature effect on dose-response measured at absorbed doses of 10 and 100 kGy for the FWT 60 radiochromic dye film.

Fig. 17. ESR spectra of L-α-alanine irradiated with ^{60}Co γ-rays, 10 MeV electrons, 16 MeV protons to a dose of 5 kGy, and with 64 MeV ^{16}O ions to a dose of 19 kGy yielding the same ESR signal size. The adjustment of the ESR spectrometer is the same for the four signals.

Fig. 18. Equipment layout for irradiation with 10 MeV electrons in the bent beam mode on the conveyor.

Fig. 19. Relative depth-dose curve for 10 MeV electrons perpendicular into a water phantom. Narrow beam geometry. t_c corresponds to the thickness of the water calorimeter and t_a is the depth corresponding to average dose in the calorimetric body.

Fig. 20. Equipment layout for irradiation with 10 MeV electrons in the straight ahead beam mode.

Fig. 21. Equipment layout for irradiation on the tandem Van de Graaff accelerator.

Fig. 22. Experimental set-up for particle irradiations on the tandem Van de Graaff. (1) Target sample; (2) rotating wheel with slits; (3) optical coupler; (4) high-potential shield; (5) 0.5 T magnet, and (6) beam-defining slits.

Fig. 23. Schematic representation for dose calculations in heavy ion irradiations.

a) The target of area A_T passes the slit area A_{sl} with a velocity $v = \omega r$. The target diameter $d < h$.

b) The beam charge Q_{beam} enters through the slit, the charge Q_T hits the target, and the charge Q_{cup} is collected by the Faraday cup.

Fig. 24. Spectrophotometric scan of dye film. (a) Homogeneously irradiated with ^{60}Co γ-rays, and (b) part of the film irradiated with 16 MeV protons. The full-scale optical density is 0.2 for both scannings. Figure b shows the background signal of the unirradiated film.

Fig. 25. ESR spectra of L-α-alanine irradiated with ^{60}Co γ-rays to doses of 10^2, 10^4, and $4.5 \cdot 10^5$ Gy.

Fig. 26. Dose-response characteristics of the FWT 60 radiochromic dye film dose meter measured at the wavelength of 510 nm for different radiation qualities.

Fig. 27. Initial part of the dose-response characteristics of Fig. 26 shown in a linear plot.

Fig. 28. Calculated relative effectiveness, RE, versus the radius, a_0, of the sensitive element for the investigated particles in the dye film. Error bars indicate 95% confidence level on experimental values.

Fig. 29. Dose-response curves for a thin (5 μm) radiochromic dye film FWT 60-20 irradiated with ^{60}Co γ-rays and 10 MeV electrons with a dose rate of 14 and $5 \cdot 10^7$ Gy s^{-1}, respectively. The optical density is measured at the wavelength of 604 nm.

Fig. 30. Average absorbed dose in the FWT 60-20 film segments as a function of penetration depth and energy of ^{7}Li ions. (1) measured from film response and low-LET dose-response calibration curve; (2) calculated from LET and particle fluence. Bars indicate 95% confidence level.

Fig. 31. Average absorbed dose in the FWT 60-20 film segments as a function of penetration depth and energy of ^{16}O ions. (1) measured from film response and low-LET dose-response calibration curve; (2) calculated from LET and particle fluence. Bars indicate 95% confidence level.

Fig. 32. Average relative effectiveness (RE) in the FWT 60-20 film segments as a function of average LET of a ^{7}Li ion with an initial energy of 21 MeV. (1) calculated from theory; (2) measured from film response and low-LET calibration curve.

Fig. 33. Average relative effectiveness (RE) in the FWT 60-20 film segments as a function of average LET of a ^{16}O ion with an initial energy of 64 MeV. (1) calculated from theory; (2) measured from film response and low-LET calibration curve.

Fig. 34. Ratio of calculated to experimental RE values as a function of the specific energy of ^{7}Li- and ^{16}O ions. Solid lines indicate the 95% confidence level of the data for a ratio of unity independent of the energy.

Fig. 35. Dose-response characteristics of L-α-alanine measured as the change in ESR-response per unit weight of irradiated alanine for different radiation qualities.

Fig. 36. Calculated relative effectiveness, RE, versus the radius, a_0, of the sensitive element for the investigated particles in alanine. Error bars indicate 95% confidence level on experimental values.

Fig. 37. Average dose to the sensitive element (extended target dose) as a function of distance from the ion's path calculated from eq. 2-17. The profiles are for the investigated ions penetrating into dye film and for the first segment with a thickness of 0.5 μm. The dose close to the ion's path should be seen in relation to the characteristic dose, D_{37}.

Fig. 38. RE as a function of LET and z^2/β^2, curve 1 and 2, respectively, for a ^{14}N ion with an initial energy of 42 MeV being completely stopped in the FWT 60 radiochromic dye film.

Fig. 39. Average dose to the sensitive element as a function of distance from the ion's path of a 42 MeV ^{14}N ion and a 0.66 MeV α-particle having the same average $z^2/\beta^2 = 6630$ in a 0.5 μm thick segment of the dye film.

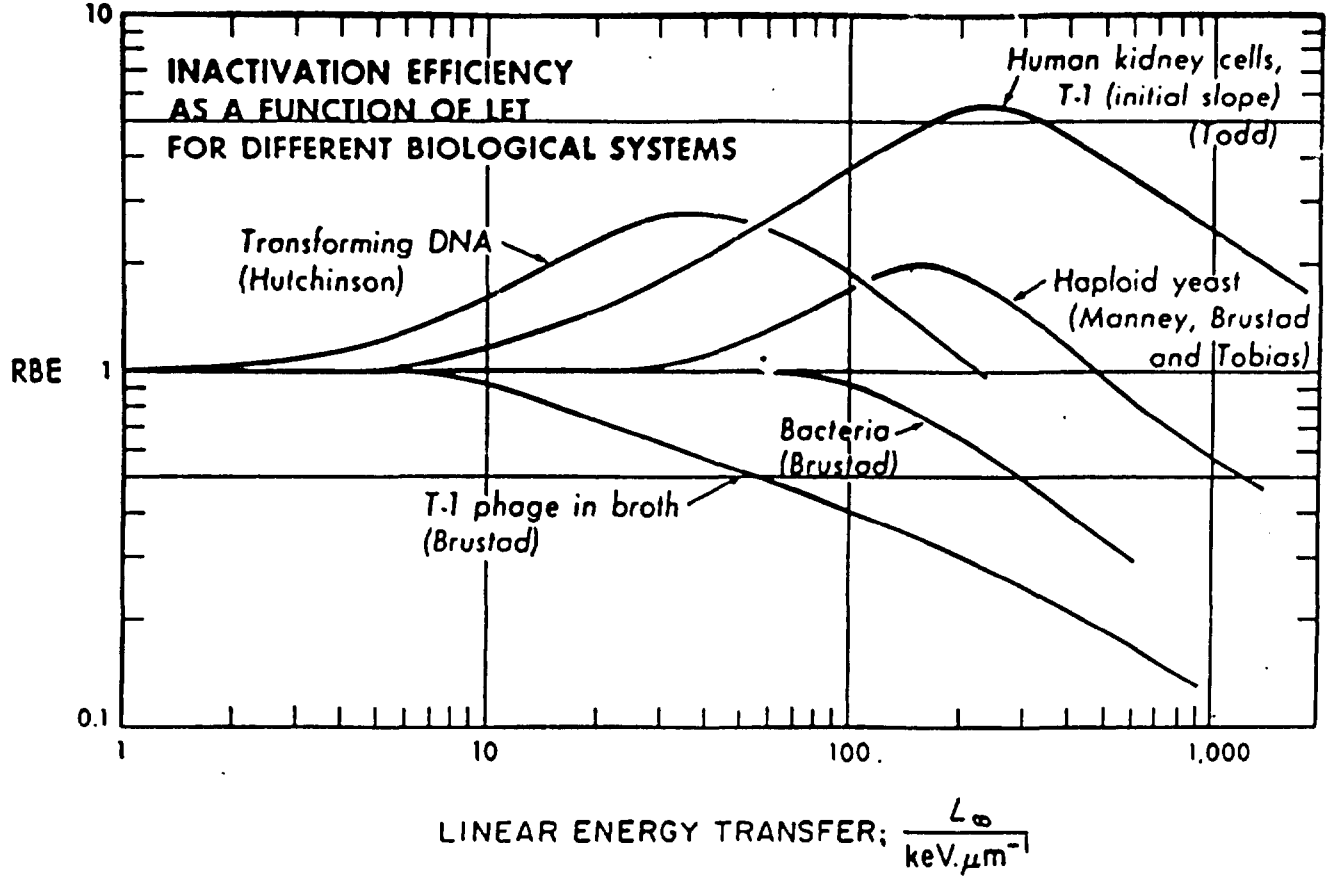
INACTIVATION EFFICIENCY
AS A FUNCTION OF LET
FOR DIFFERENT BIOLOGICAL SYSTEMS
Human kidney cells, T-1 (initial slope) (Todd)
Transforming DNA (Hutchinson)
Haploid yeast (Manney, Brustad and Tobias)
Bacteria (Brustad)
T-1 phage in broth (Brustad)
RBE
10
1
0.1
1
10
100
1,000
LINEAR ENERGY TRANSFER; $\frac{L_\infty}{keV.\mu m^{-1}}$

Fig. 1.

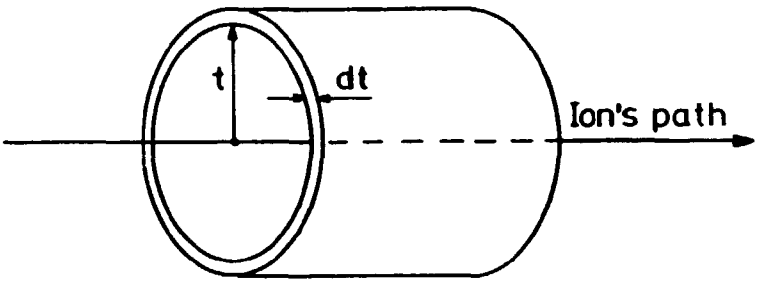
t
dt
Ion's path

Fig. 2.

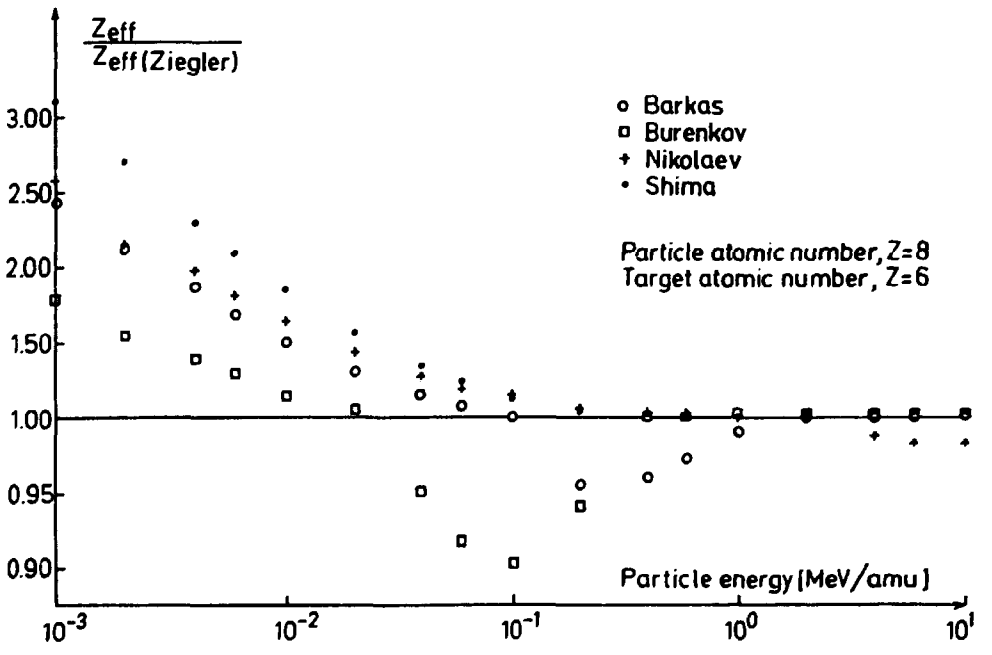
Zeff / Zeff(Ziegler)
3.00
2.50
2.00
1.50
1.00
0.95
0.90
10-3
10-2
10-1
100
101
Barkas
Burenkov
Nikolaev
Shima
Particle atomic number, Z=8
Target atomic number, Z=6
Particle energy (MeV/amu)

Fig. 3.

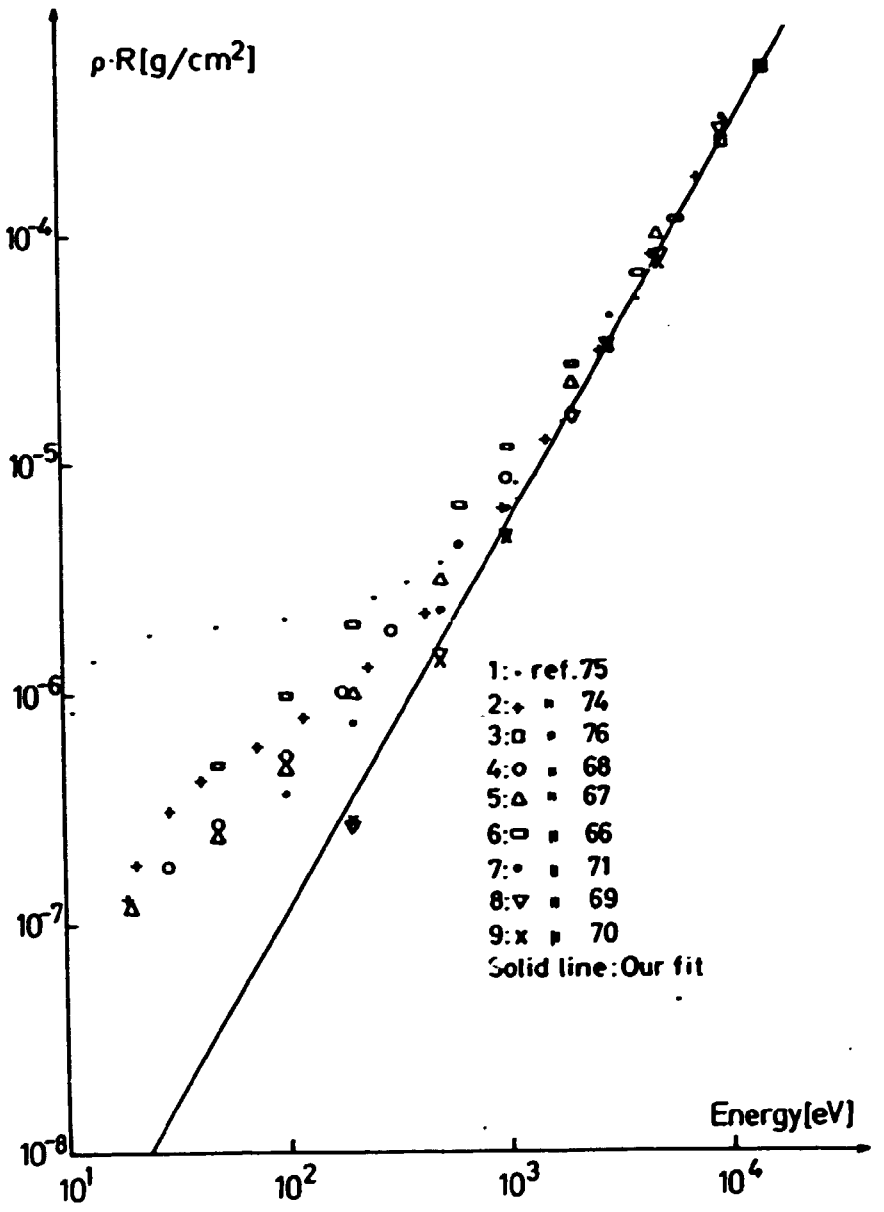
ρ·R[g/cm²]
10⁻⁴
10⁻⁵
10⁻⁶
10⁻⁷
10⁻⁸
10¹
10²
10³
10⁴
Energy[eV]
1:· ref.75
2:+ ▪ 74
3:□ ▪ 76
4:○ ▪ 68
5:△ ▪ 67
6:▭ ▪ 66
7:• ▪ 71
8:▽ ▪ 69
9:x ▪ 70
Solid line:Our fit

Fig. 4.

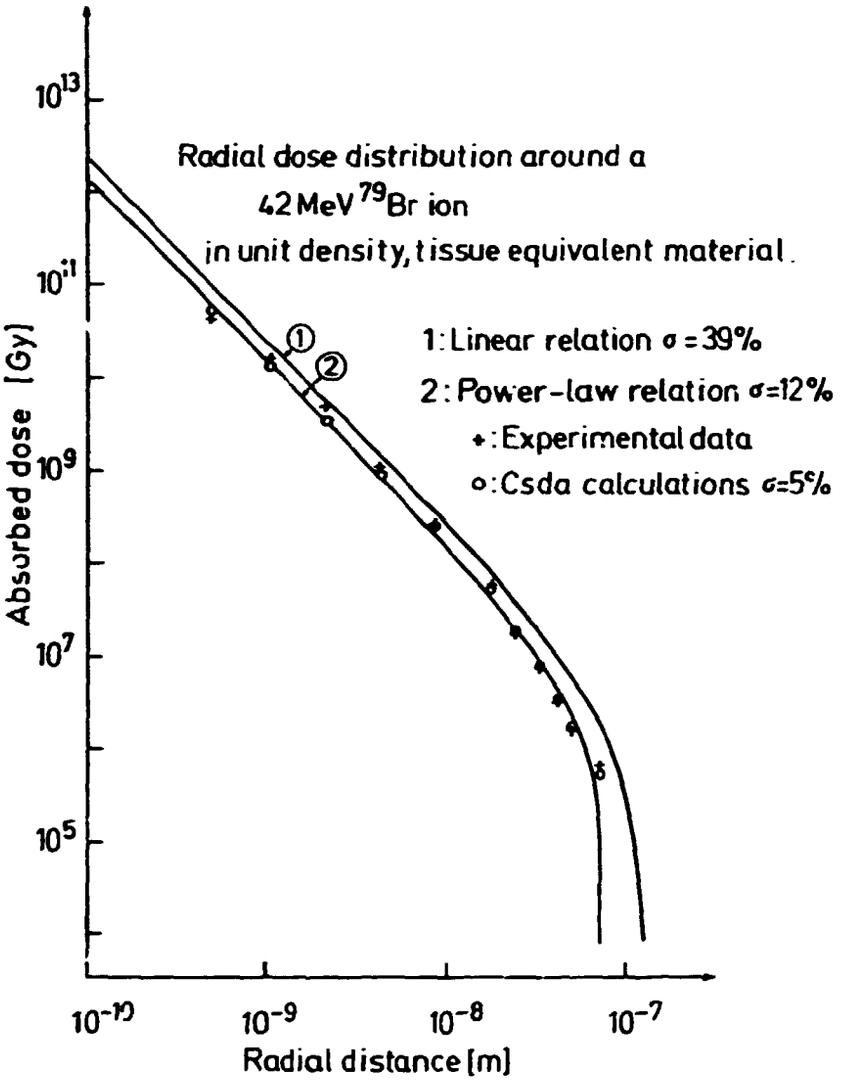
Radial dose distribution around a
42 MeV ^{79}Br ion
in unit density, tissue equivalent material.
1: Linear relation σ = 39%
2: Power-law relation σ=12%
•: Experimental data
o: Csda calculations σ=5%
Absorbed dose [Gy]
10^{13}
10^{11}
10^{9}
10^{7}
10^{5}
10^{-10}
10^{-9}
10^{-8}
10^{-7}
Radial distance [m]

Fig. 5.

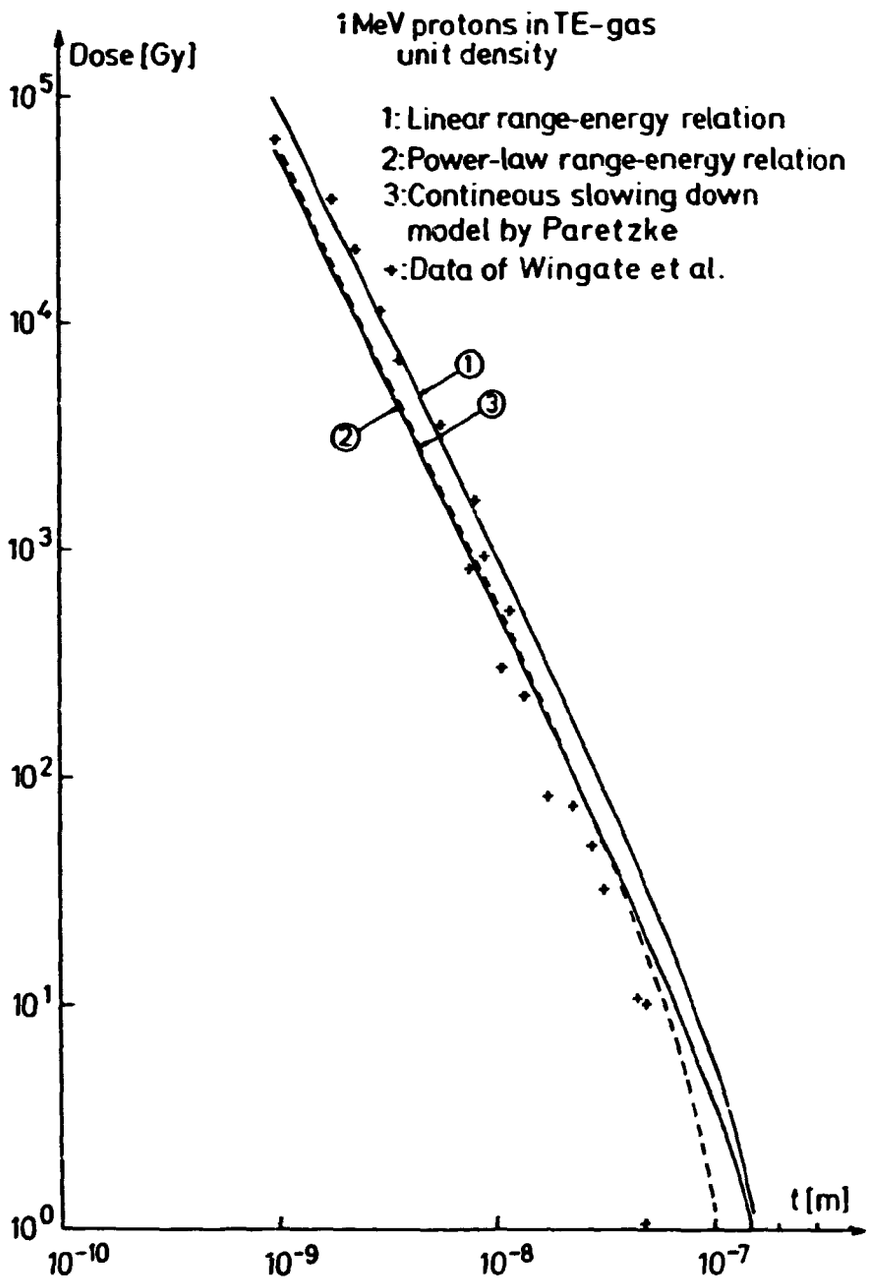
1 MeV protons in TE-gas
unit density
Dose [Gy]
1: Linear range-energy relation
2: Power-law range-energy relation
3: Contineous slowing down
model by Paretzke
+: Data of Wingate et al.
10^5
10^4
10^3
10^2
10^1
10^0
10^{-10}
10^{-9}
10^{-8}
10^{-7}
t [m]

Fig. 6.

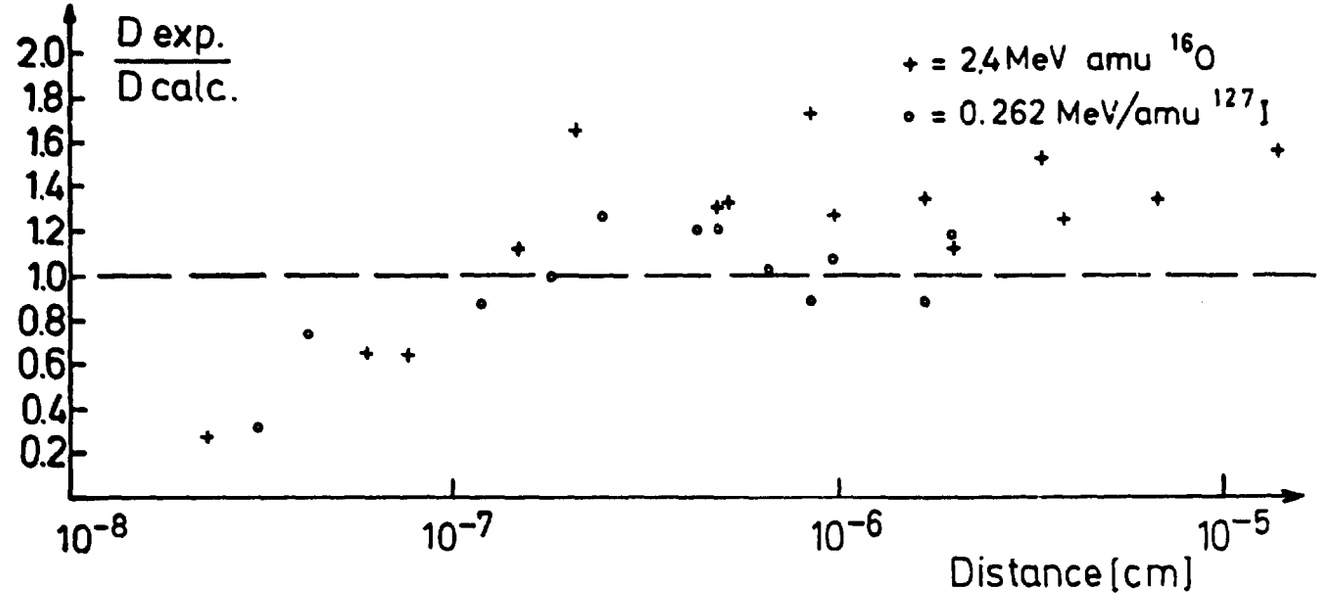
D exp.
D calc.
2.0
1.8
1.6
1.4
1.2
1.0
0.8
0.6
0.4
0.2
+ = 2.4 MeV amu ^{16}O
∘ = 0.262 MeV/amu ^{127}I
10^{-8}
10^{-7}
10^{-6}
10^{-5}
Distance [cm]

Fig. 7.

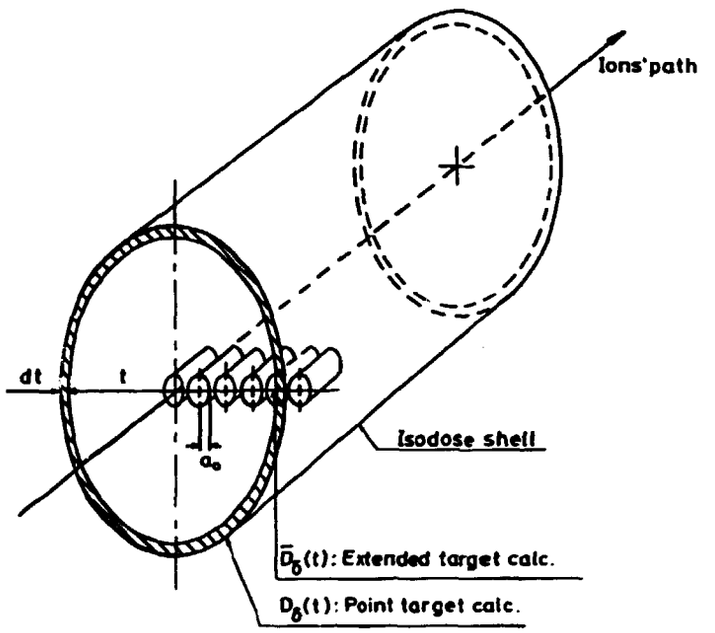

Fig. 8.

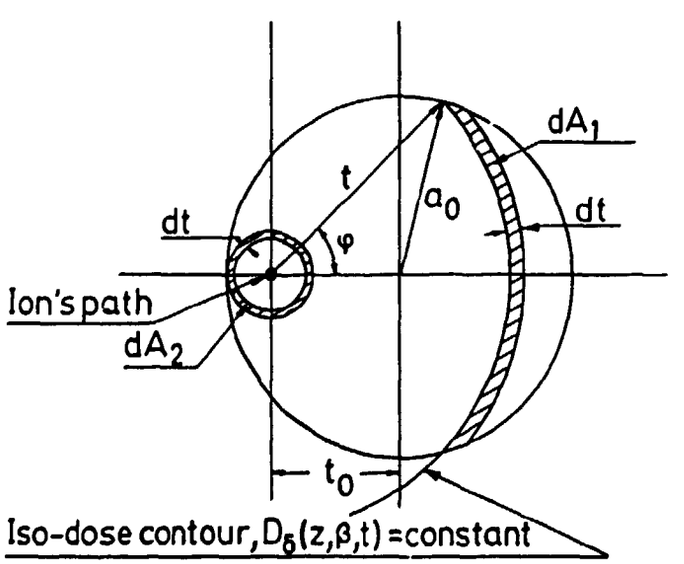

Ion's path is perpendicular into the drawing

Fig. 9.

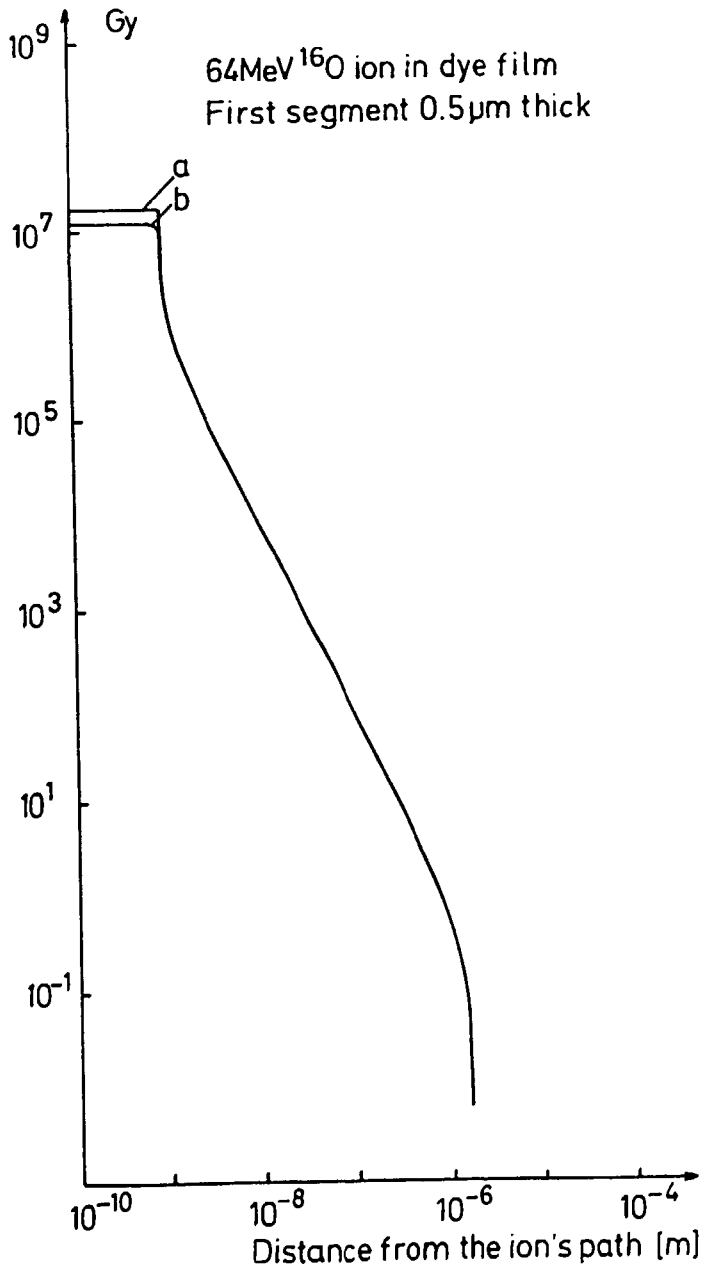
Gy
64MeV ^{16}O ion in dye film
First segment 0.5μm thick
a
b
10^{9}
10^{7}
10^{5}
10^{3}
10^{1}
10^{-1}
10^{-10}
10^{-8}
10^{-6}
10^{-4}
Distance from the ion's path [m]

Fig. 10.

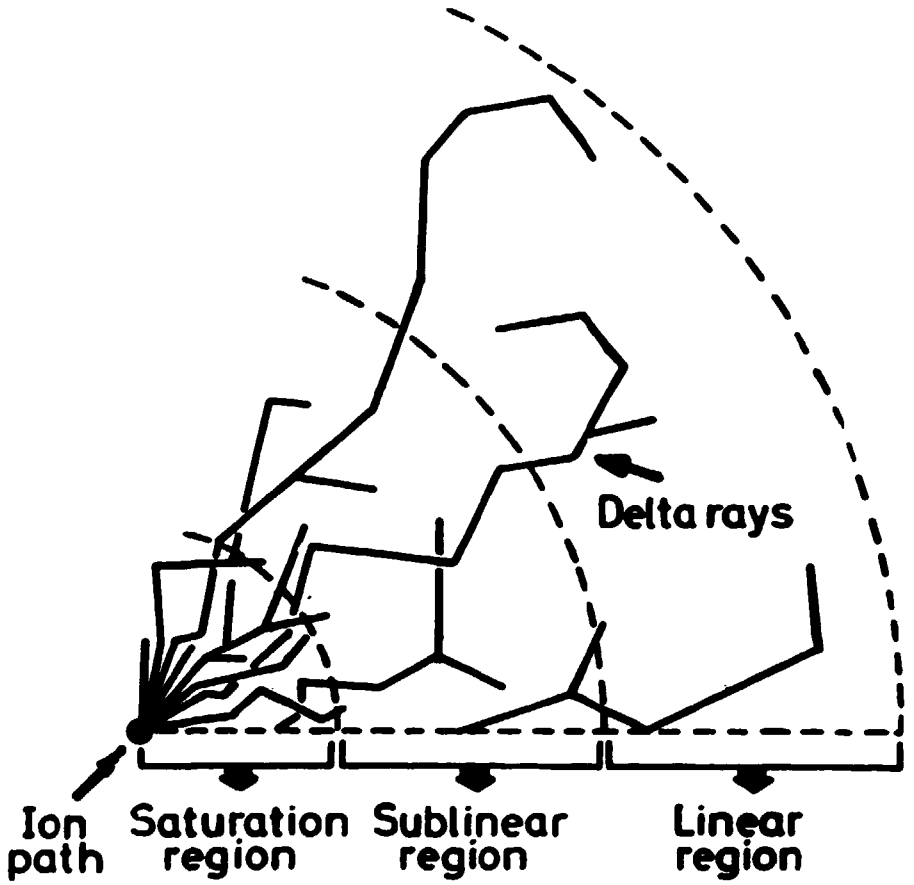
Delta rays
Ion path
Saturation region
Sublinear region
Linear region

Fig. 11.

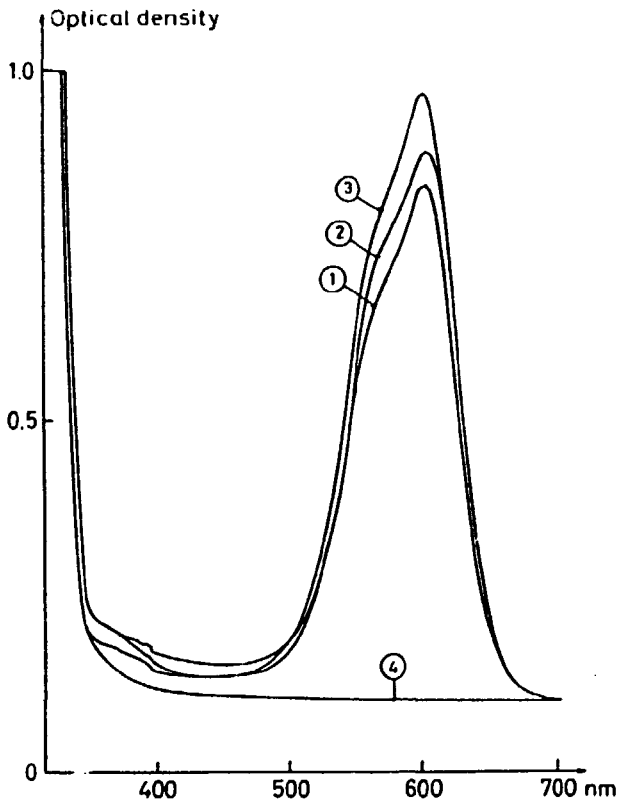
Optical density
1.0
0.5
0
400
500
600
700 nm
1
2
3
4

Fig. 12.

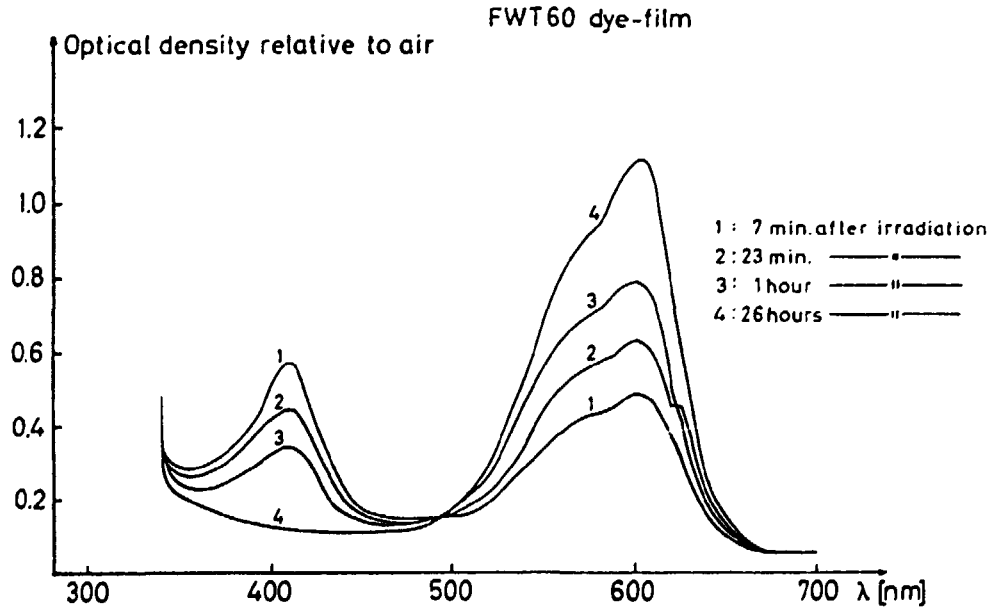
FWT60 dye-film
Optical density relative to air
1.2
1.0
0.8
0.6
0.4
0.2
300
400
500
600
700 λ [nm]
1 : 7 min. after irradiation
2 : 23 min.
3 : 1 hour
4 : 26 hours

Fig. 13.

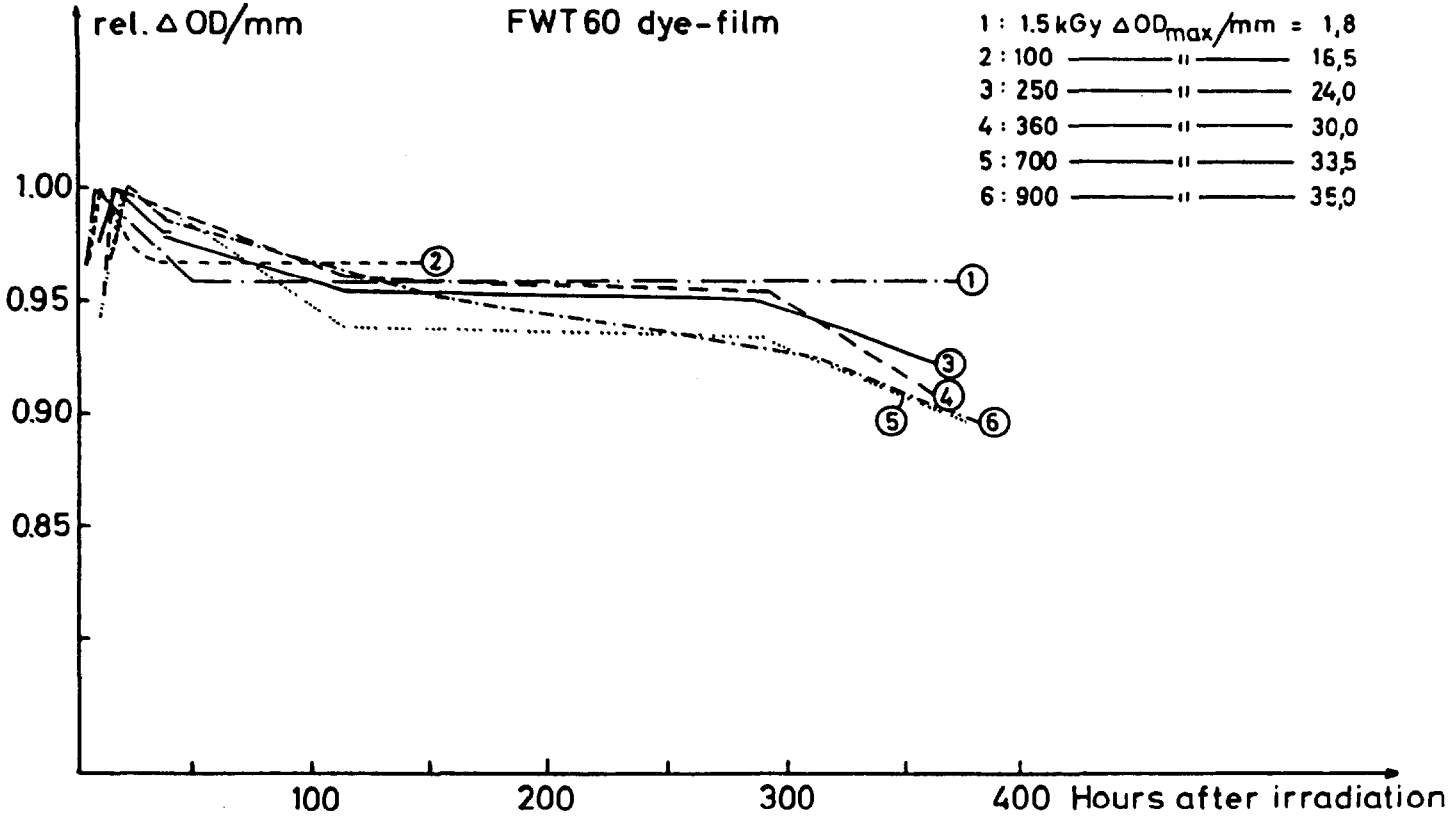
rel. Δ OD/mm
FWT60 dye-film
1 : 1.5 kGy ΔOD$_{max}$/mm = 1,8
2 : 100 " 16,5
3 : 250 " 24,0
4 : 360 " 30,0
5 : 700 " 33,5
6 : 900 " 35,0
1.00
0.95
0.90
0.85
100
200
300
400 Hours after irradiation

Fig. 14.

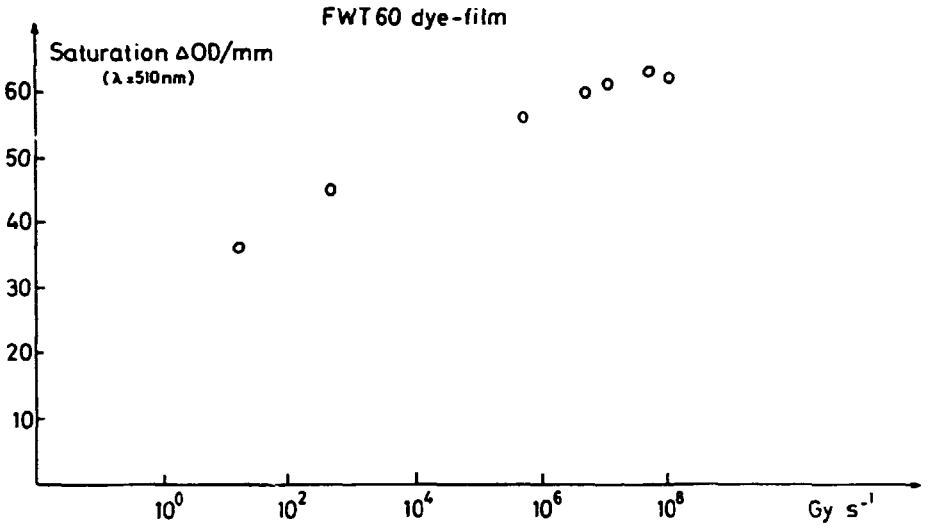
FWT 60 dye-film
Saturation ΔOD/mm
(λ=510nm)
60
50
40
30
20
10
10^0
10^2
10^4
10^6
10^8
Gy s^{-1}

Fig. 15.

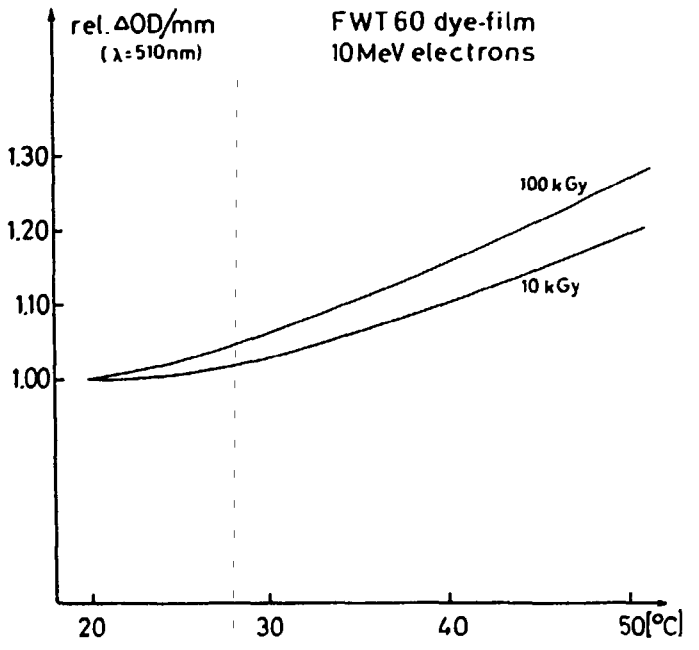
rel. ΔOD/mm
(λ=510nm)
FWT 60 dye-film
10MeV electrons
1.30
1.20
1.10
1.00
100 kGy
10 kGy
20
30
40
50[°C]

Fig. 16.

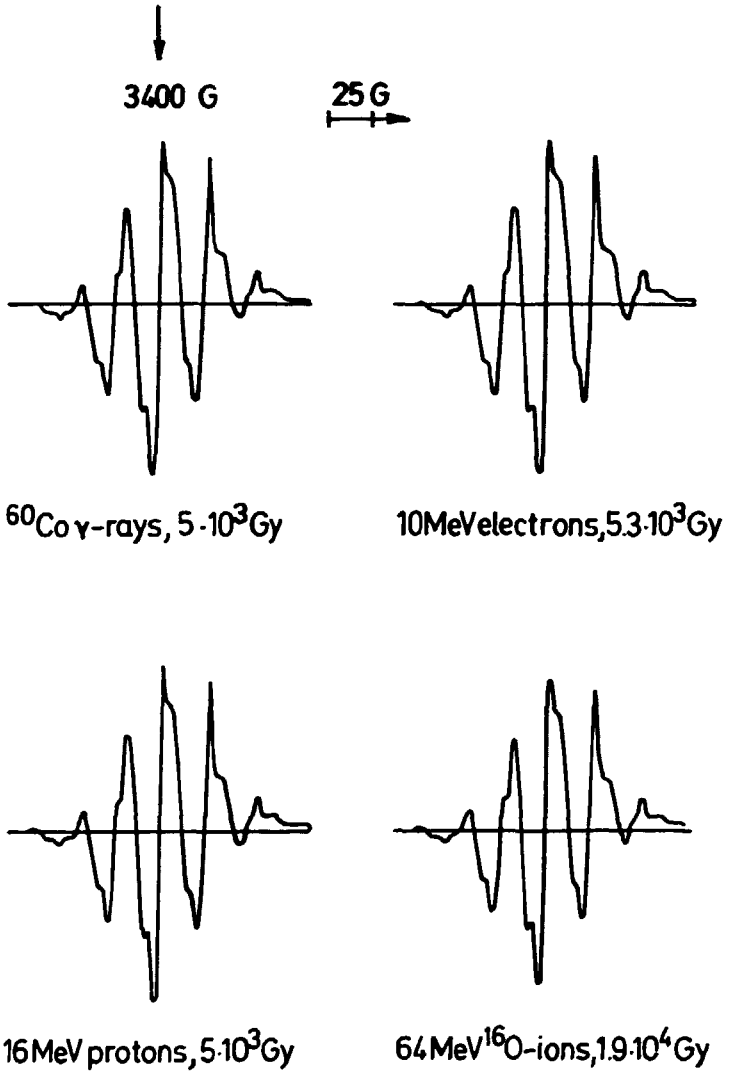
3400 G
25 G
^{60}Co γ-rays, 5·10^{3}Gy
10MeV electrons, 5.3·10^{3}Gy
16MeV protons, 5·10^{3}Gy
64MeV ^{16}O-ions, 1.9·10^{4}Gy

Fig. 17.

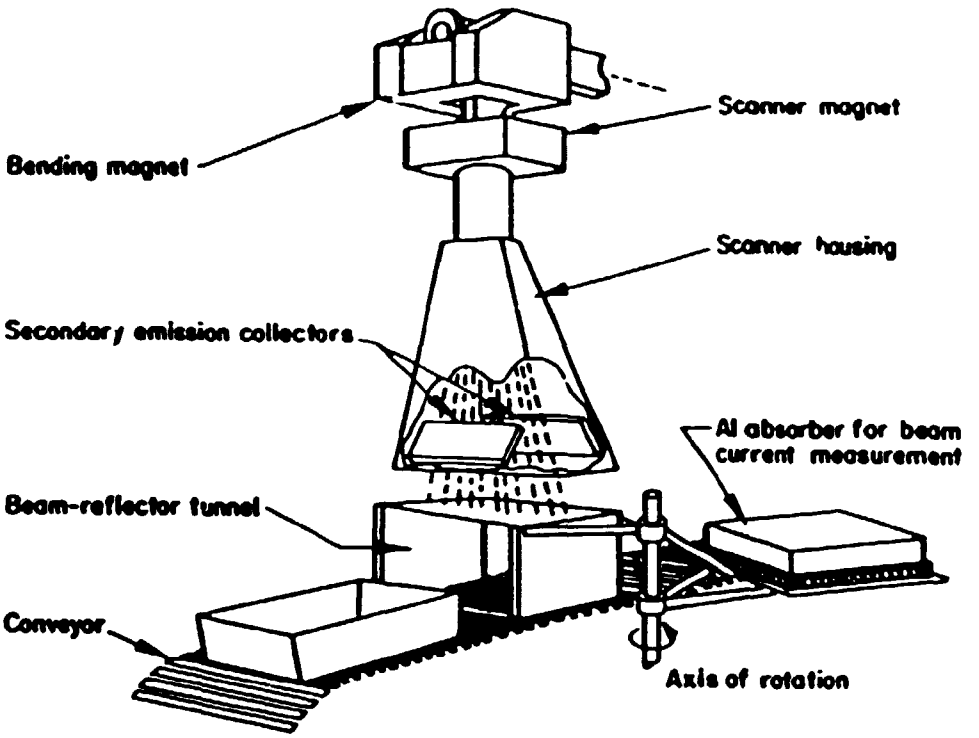
Scanner magnet
Bending magnet
Scanner housing
Secondary emission collectors
Al absorber for beam current measurement
Beam-reflector funnel
Conveyor
Axis of rotation

Fig. 18.

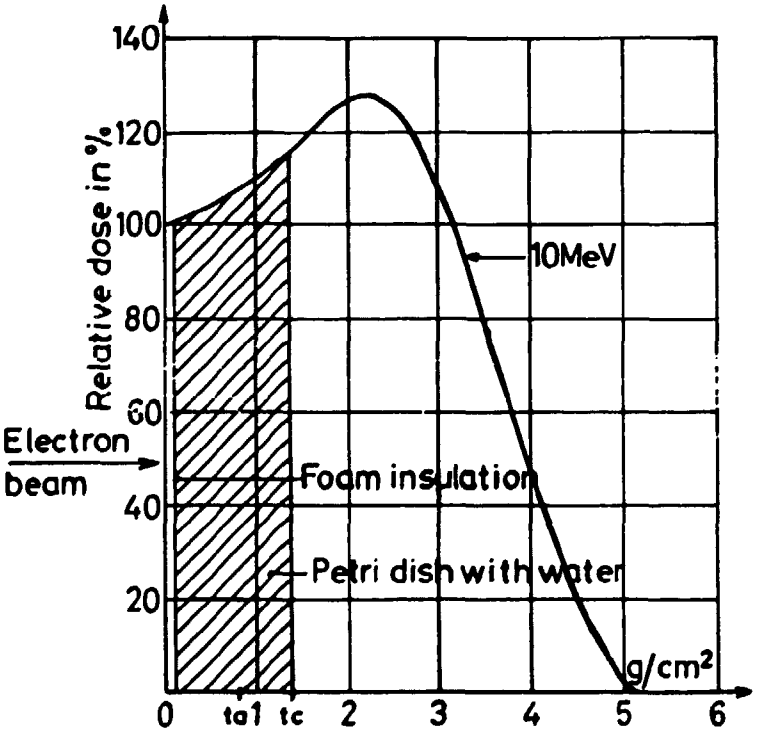
140
120
100
80
60
40
20
Relative dose in %
10MeV
Electron beam
Foam insulation
Petri dish with water
g/cm²
0
ta1
tc
2
3
4
5
6

Fig. 19.

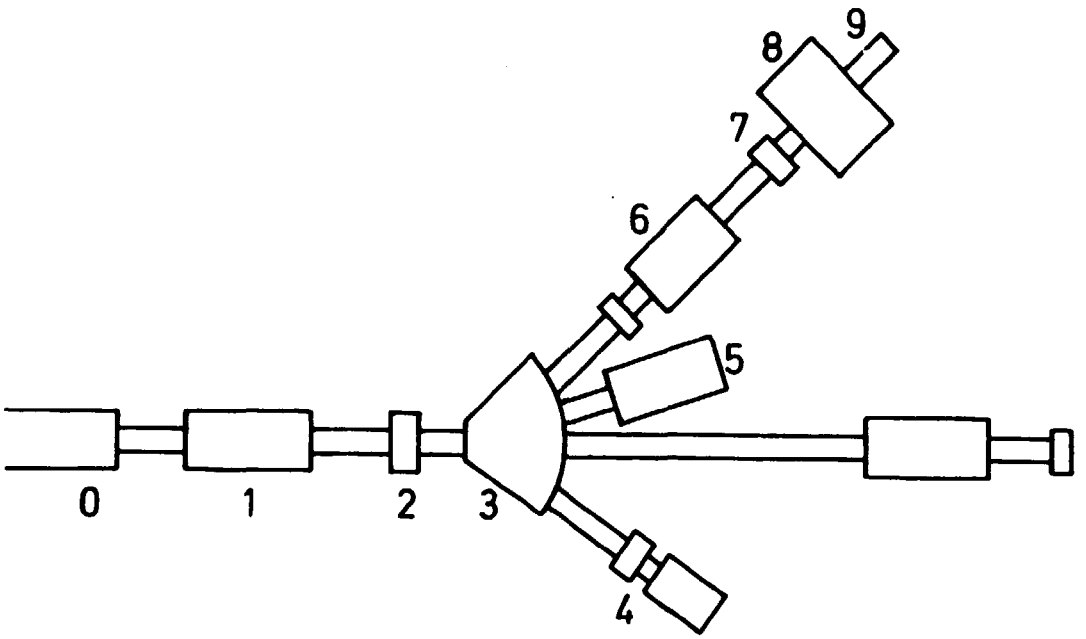

0) linear accelerator, 1) 90° bending magnet,
2) beam position and beam current monitor,
3) switching magnet and energy spectrometer,
4) energy analyzing slit, 5) high-power Faraday cup, 6) doublet quadrupole magnet, 7) beam defining slits, 8) irradiation chamber, and
9) Faraday cup.

Fig. 20.

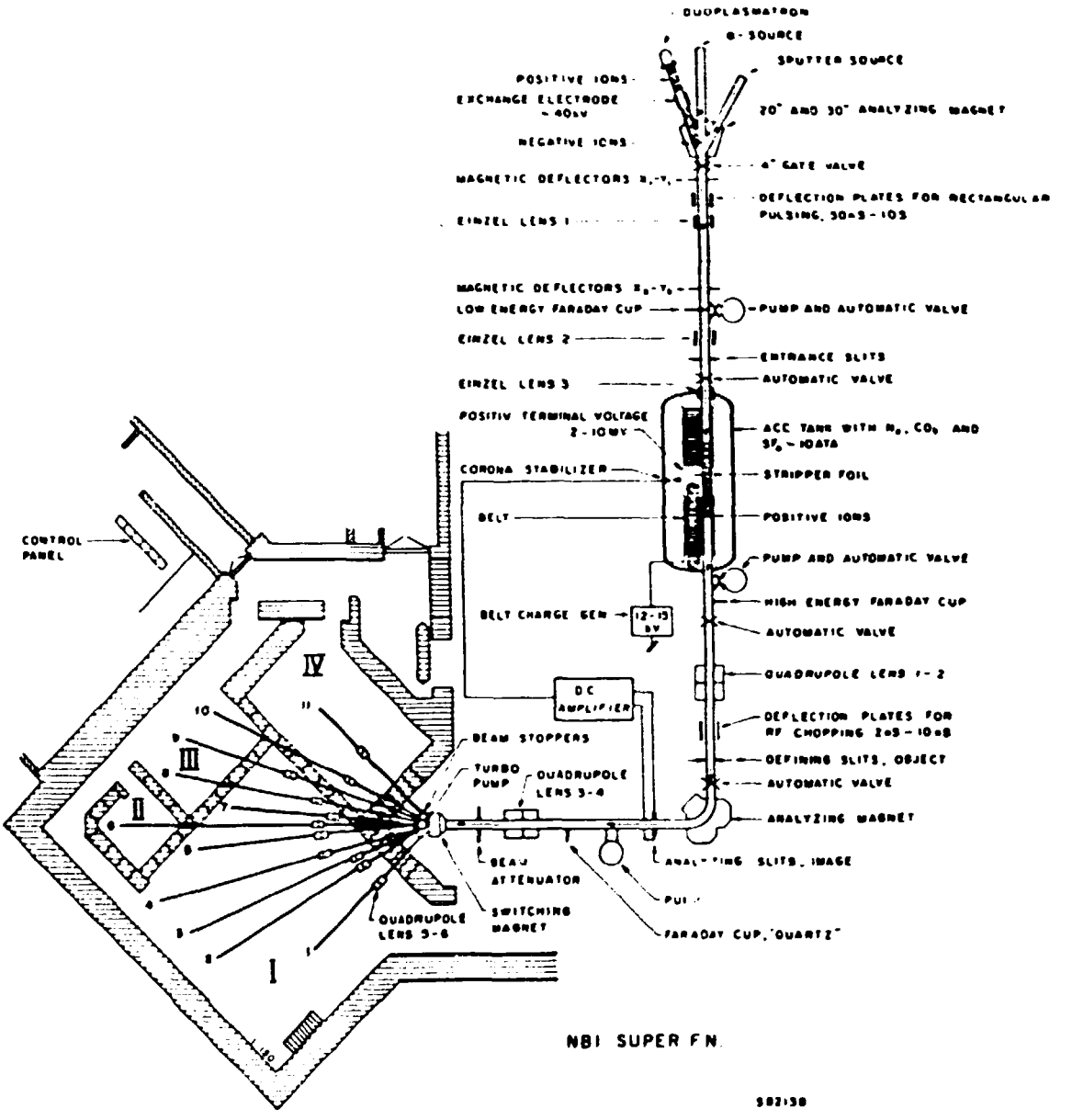
DUOPLASMATRON
CS-SOURCE
SPUTTER SOURCE
POSITIVE IONS
EXCHANGE ELECTRODE
~40kV
NEGATIVE IONS
20° AND 30° ANALYZING MAGNET
4" GATE VALVE
MAGNETIC DEFLECTORS
DEFLECTION PLATES FOR RECTANGULAR PULSING, 30nS - 10S
EINZEL LENS 1
MAGNETIC DEFLECTORS
LOW ENERGY FARADAY CUP
PUMP AND AUTOMATIC VALVE
EINZEL LENS 2
ENTRANCE SLITS
EINZEL LENS 3
AUTOMATIC VALVE
POSITIV TERMINAL VOLTAGE
2 - 10MV
ACC TANK WITH
CORONA STABILIZER
STRIPPER FOIL
BELT
POSITIVE IONS
PUMP AND AUTOMATIC VALVE
CONTROL PANEL
BELT CHARGE GEN
12 - 15 kV
HIGH ENERGY FARADAY CUP
AUTOMATIC VALVE
QUADRUPOLE LENS 1 - 2
DC AMPLIFIER
DEFLECTION PLATES FOR RF CHOPPING
BEAM STOPPERS
DEFINING SLITS, OBJECT
TURBO PUMP
QUADRUPOLE LENS 3-4
AUTOMATIC VALVE
ANALYZING MAGNET
BEAM ATTENUATOR
ANALYZING SLITS, IMAGE
PULSER
SWITCHING MAGNET
FARADAY CUP, "QUARTZ"
QUADRUPOLE LENS 5-6
I
II
III
IV
NBI SUPER FN
S82138

Fig. 21.

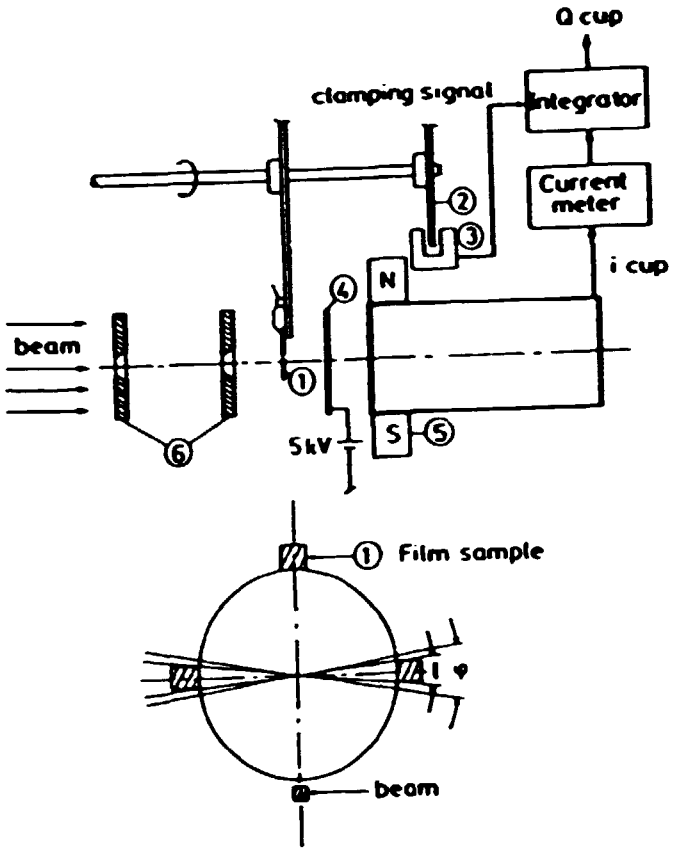
Q cup
clamping signal
integrator
Current meter
i cup
N
S
5kV
beam
① Film sample
beam

Fig. 22.

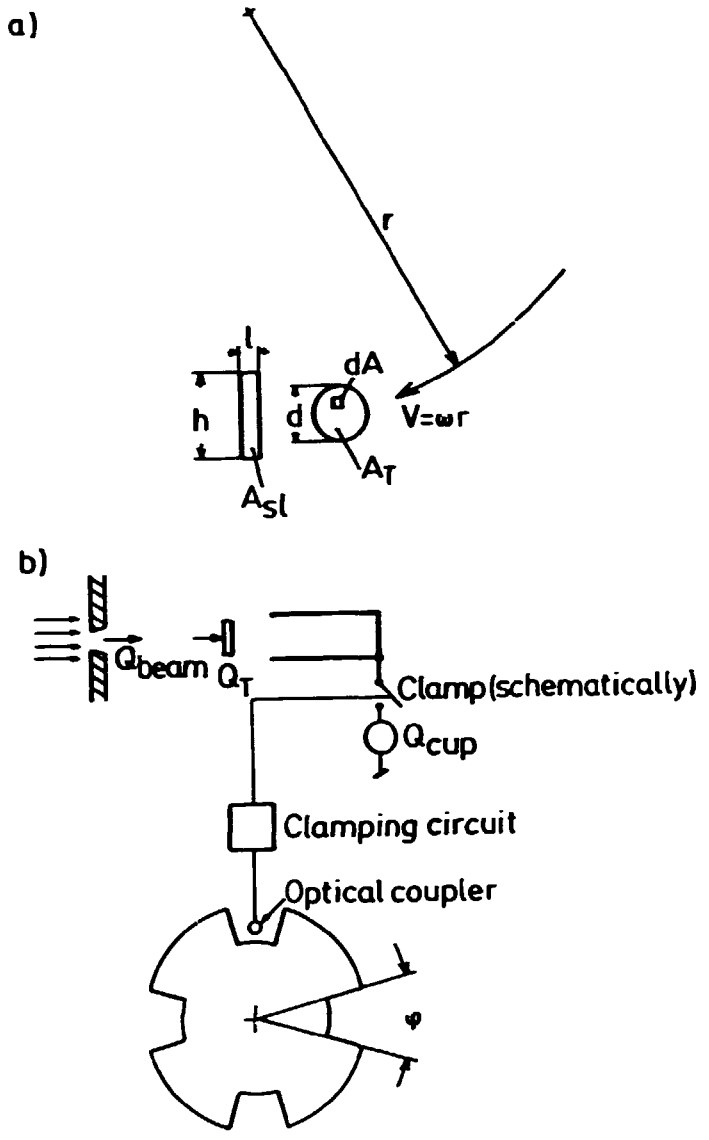
a)
r
l
dA
h
d
V=ωr
A_T
A_{Sl}
b)
Q_{beam}
Q_T
Clamp(schematically)
Q_{cup}
Clamping circuit
Optical coupler
φ

Fig. 23.

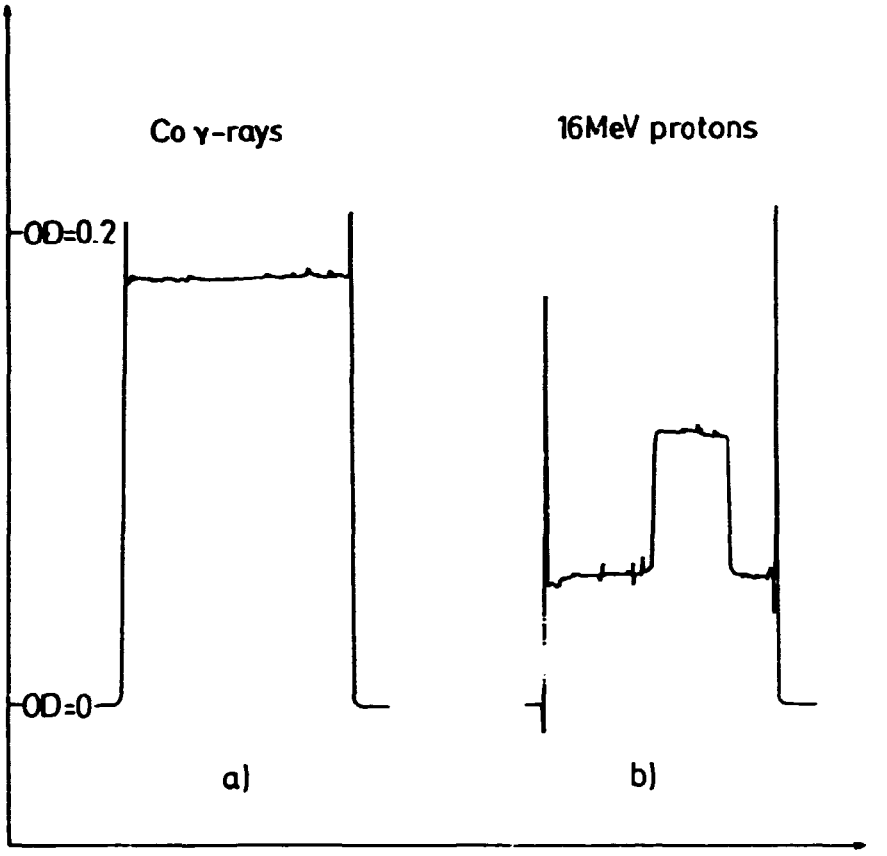

Fig. 24.

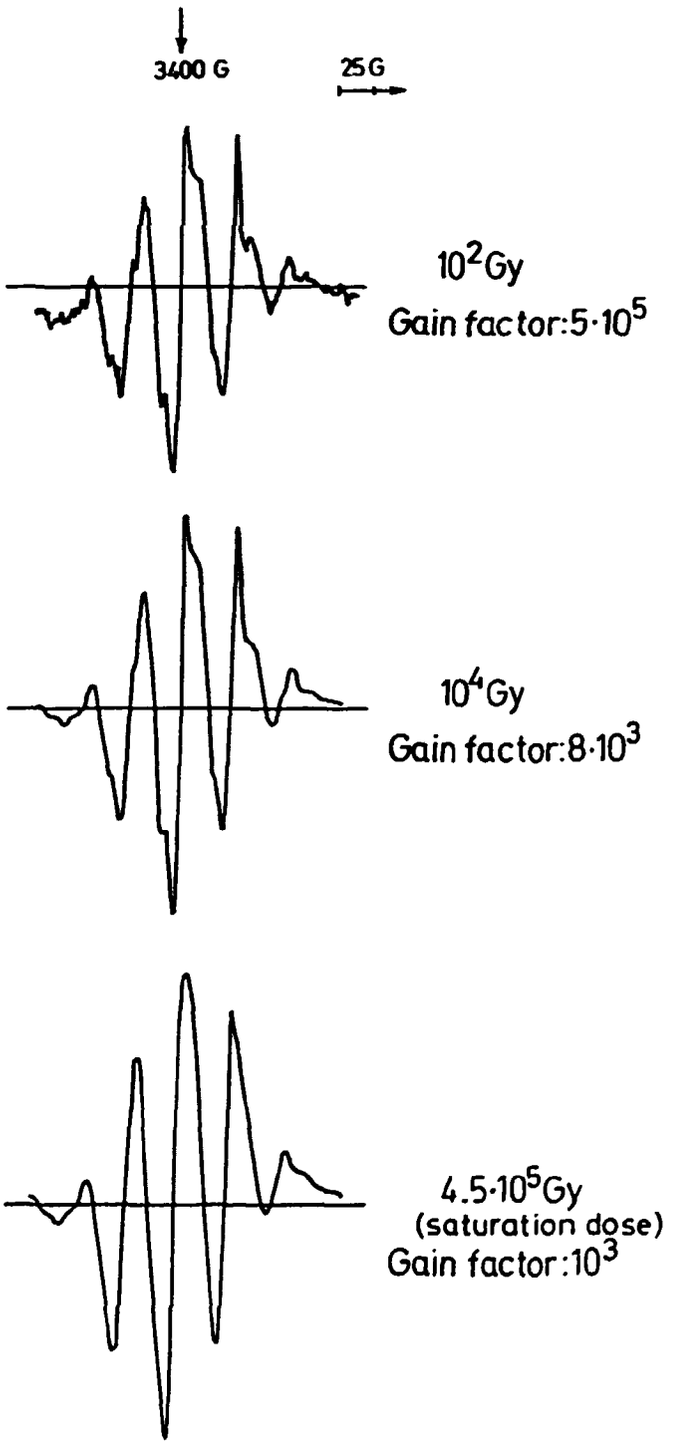
3400 G
25G
10^2Gy
Gain factor:$5 \cdot 10^5$
10^4Gy
Gain factor:$8 \cdot 10^3$
$4.5 \cdot 10^5$Gy
(saturation dose)
Gain factor:10^3

Fig. 25.

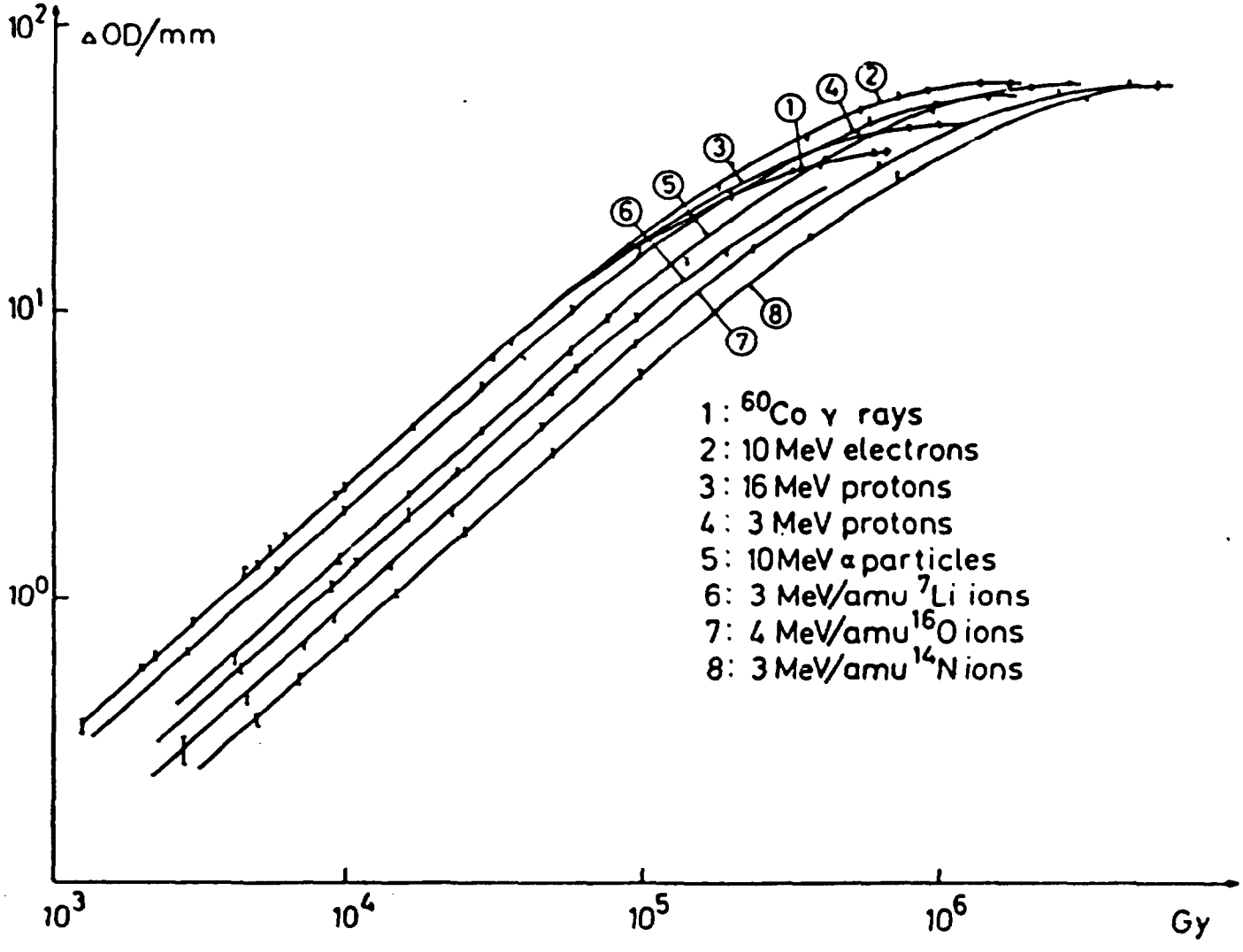
10^2
ΔOD/mm
10^1
10^0
10^3
10^4
10^5
10^6
Gy
1 : ^{60}Co γ rays
2 : 10 MeV electrons
3 : 16 MeV protons
4 : 3 MeV protons
5 : 10 MeV α particles
6 : 3 MeV/amu ^{7}Li ions
7 : 4 MeV/amu ^{16}O ions
8 : 3 MeV/amu ^{14}N ions

Fig. 26.

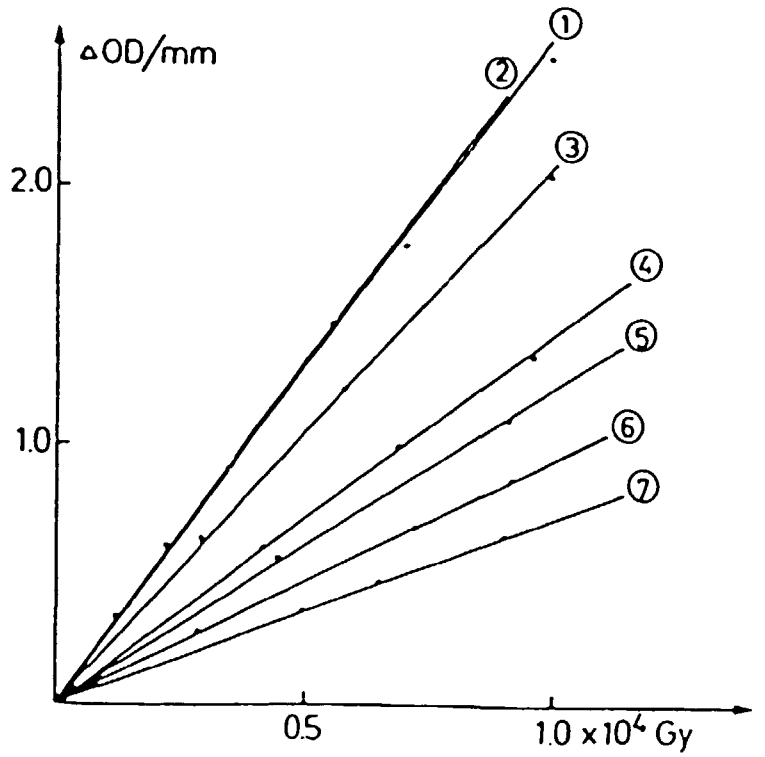
ΔOD/mm
2.0
1.0
0.5
1.0 x10⁴ Gy
①
②
③
④
⑤
⑥
⑦

Fig. 27.

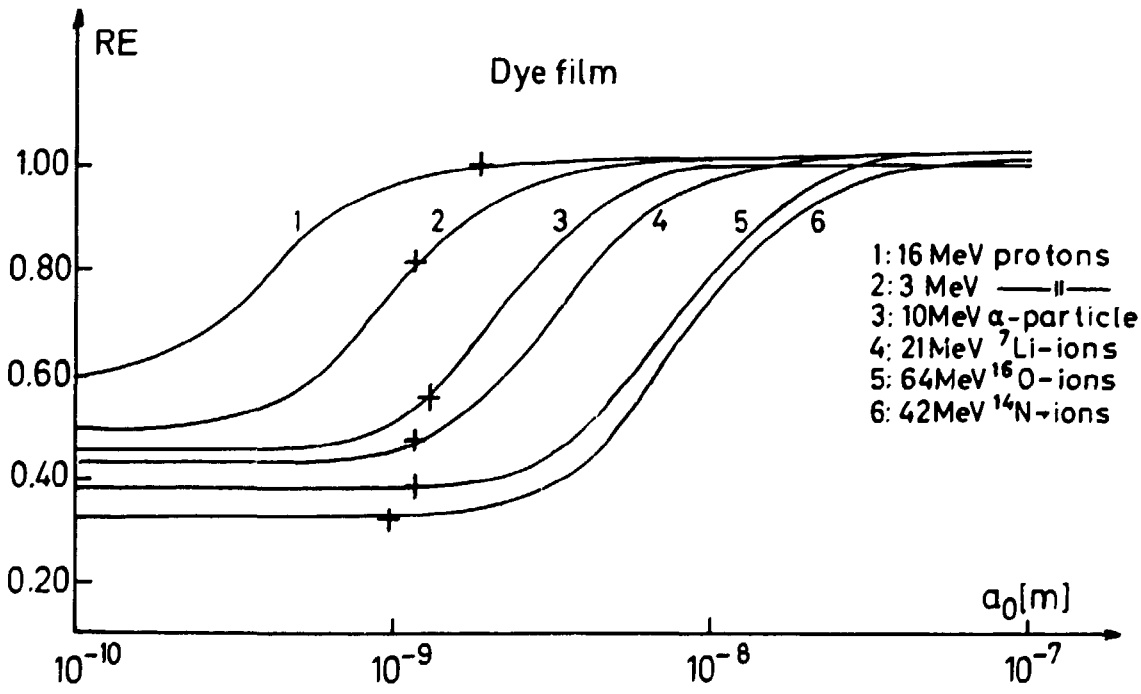
RE
Dye film
1.00
0.80
0.60
0.40
0.20
10⁻¹⁰
10⁻⁹
10⁻⁸
10⁻⁷
a₀[m]
1
2
3
4
5
6
1: 16 MeV protons
2: 3 MeV —"—
3: 10MeV α-particles
4: 21MeV ⁷Li-ions
5: 64MeV ¹⁶O-ions
6: 42MeV ¹⁴N-ions

Fig. 28.

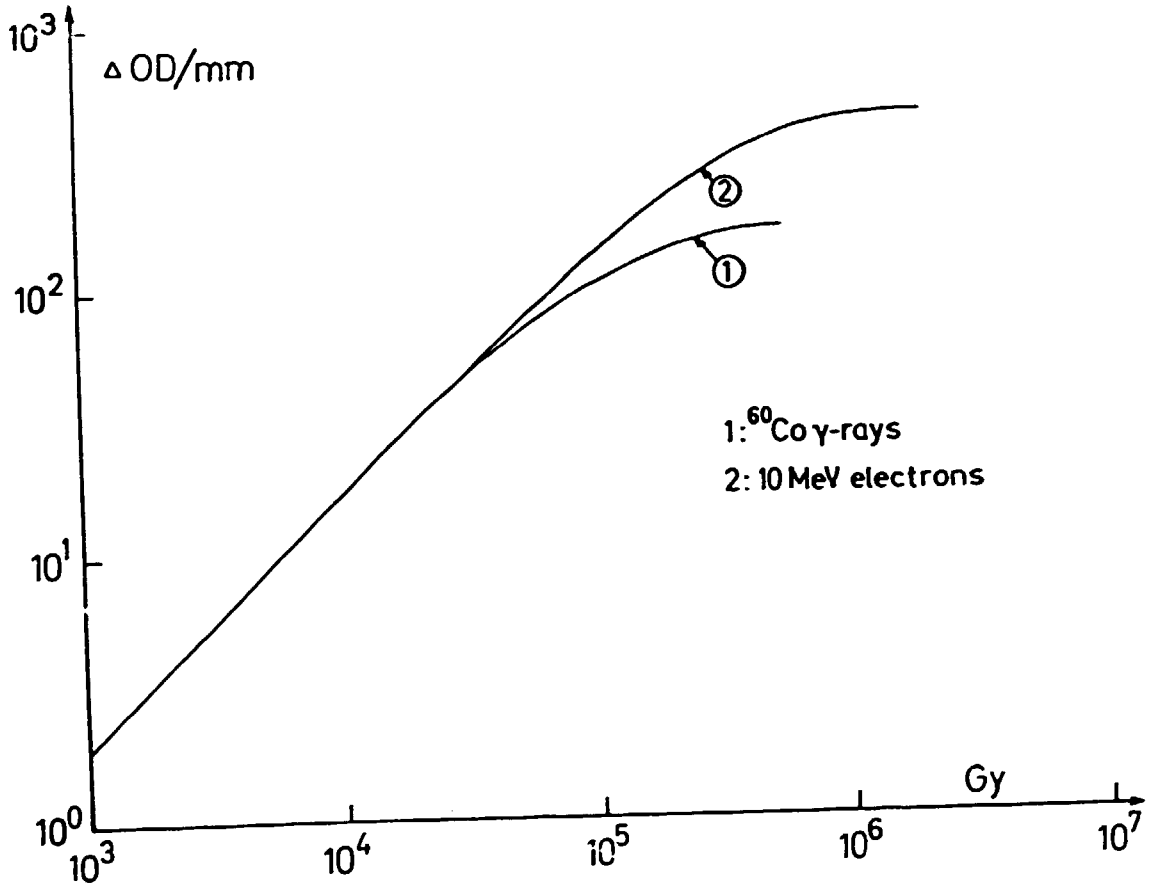
10^3
Δ OD/mm
10^2
10^1
10^0
10^3
10^4
10^5
10^6
10^7
Gy
②
①
1: ^{60}Co γ-rays
2: 10 MeV electrons

Fig. 29.

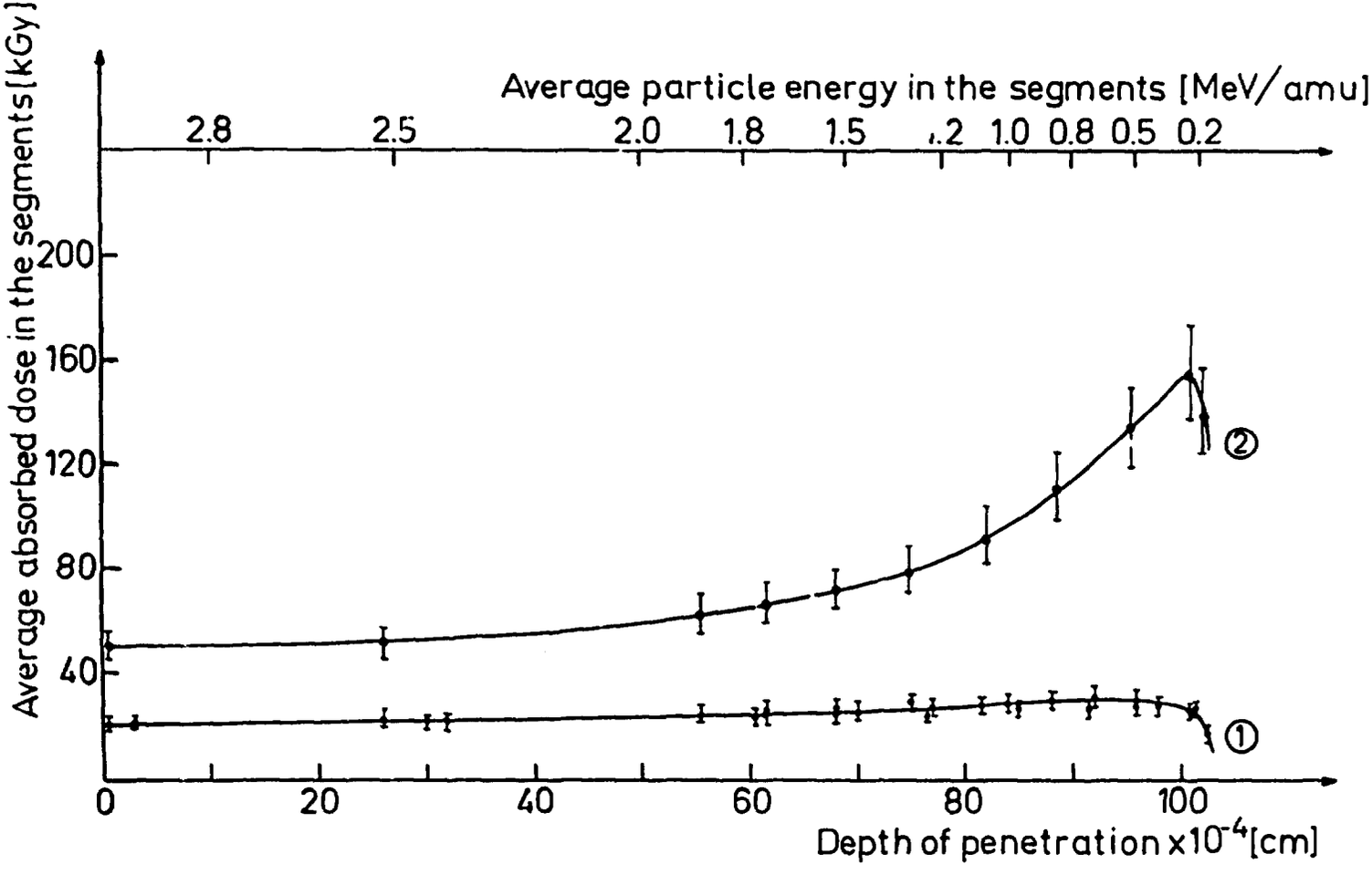
Average particle energy in the segments [MeV/amu]
2.8
2.5
2.0
1.8
1.5
1.2
1.0
0.8
0.5
0.2
Average absorbed dose in the segments [kGy]
200
160
120
80
40
0
20
40
60
80
100
Depth of penetration x10⁻⁴[cm]
②
①

Fig. 30.

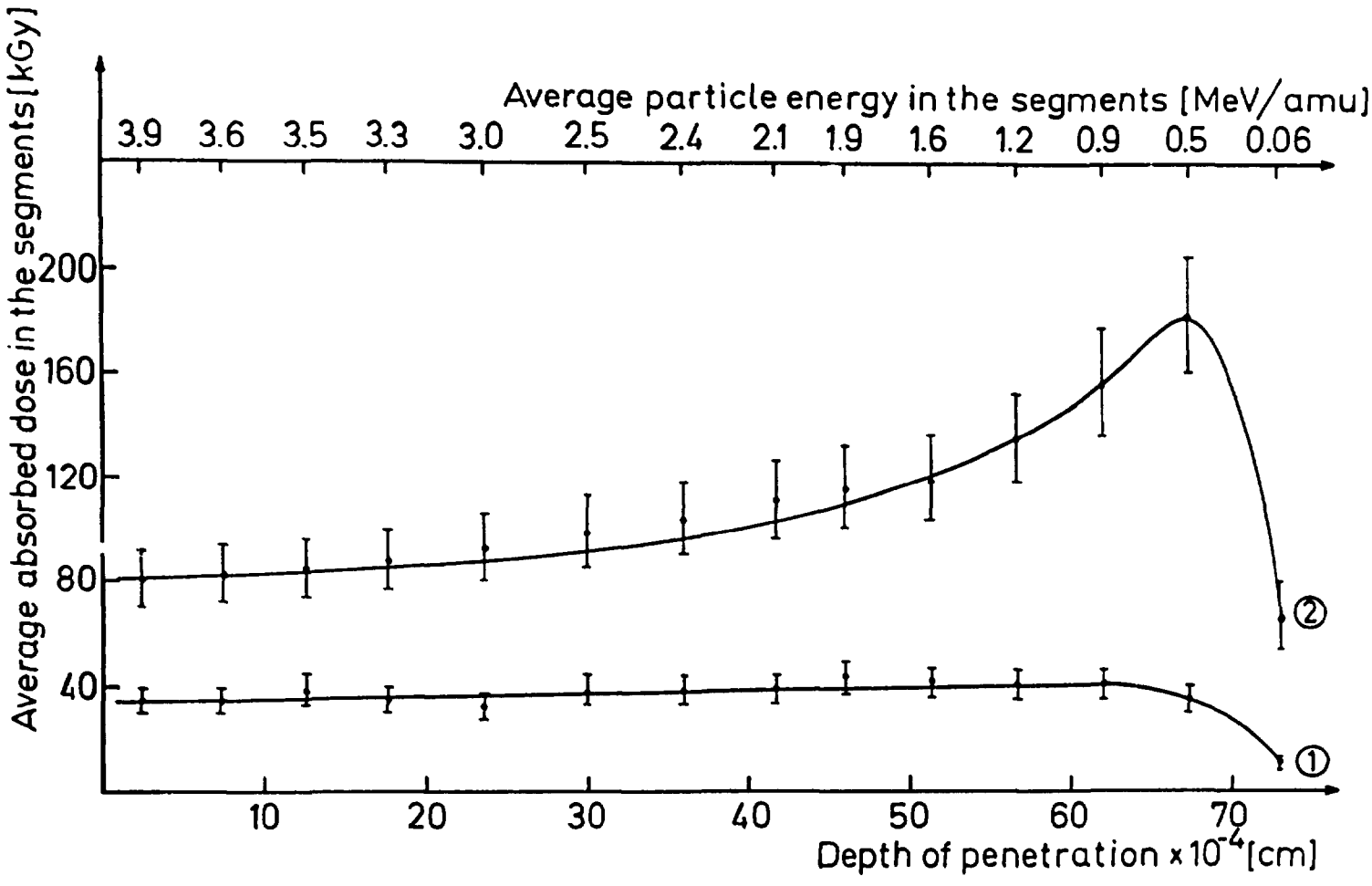
Average particle energy in the segments [MeV/amu]
3.9 3.6 3.5 3.3 3.0 2.5 2.4 2.1 1.9 1.6 1.2 0.9 0.5 0.06
Average absorbed dose in the segments [kGy]
200
160
120
80
40
10 20 30 40 50 60 70
Depth of penetration x 10^-4 [cm]
②
①

Fig. 31.

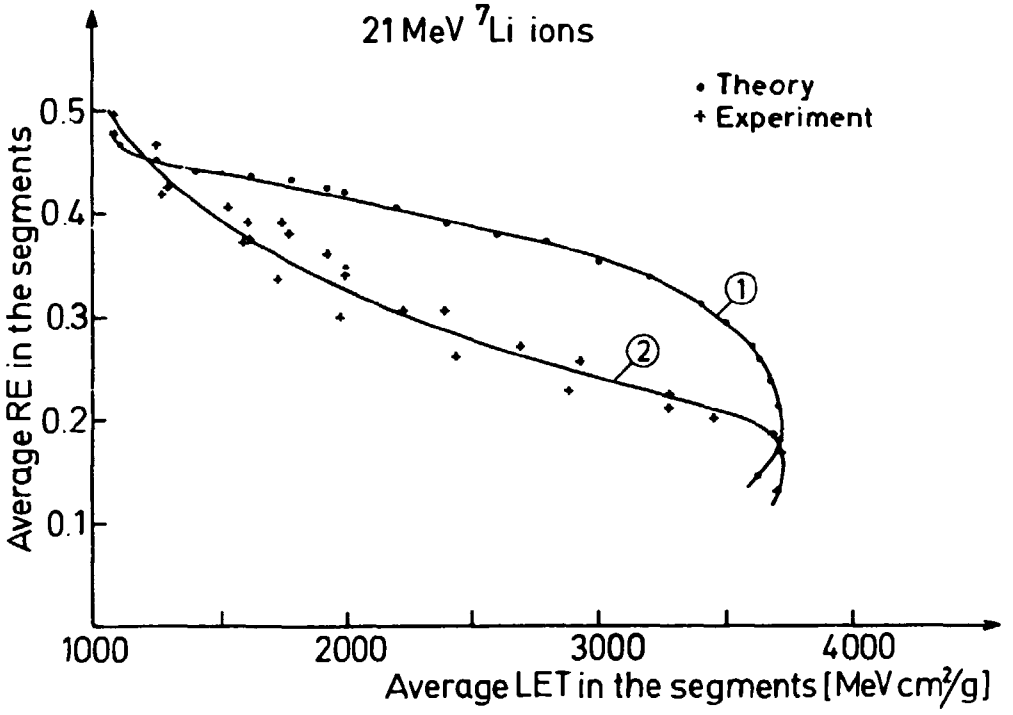
21 MeV ^{7}Li ions
• Theory
+ Experiment
Average RE in the segments
0.5
0.4
0.3
0.2
0.1
1000
2000
3000
4000
Average LET in the segments [MeV cm²/g]
①
②

Fig. 32.

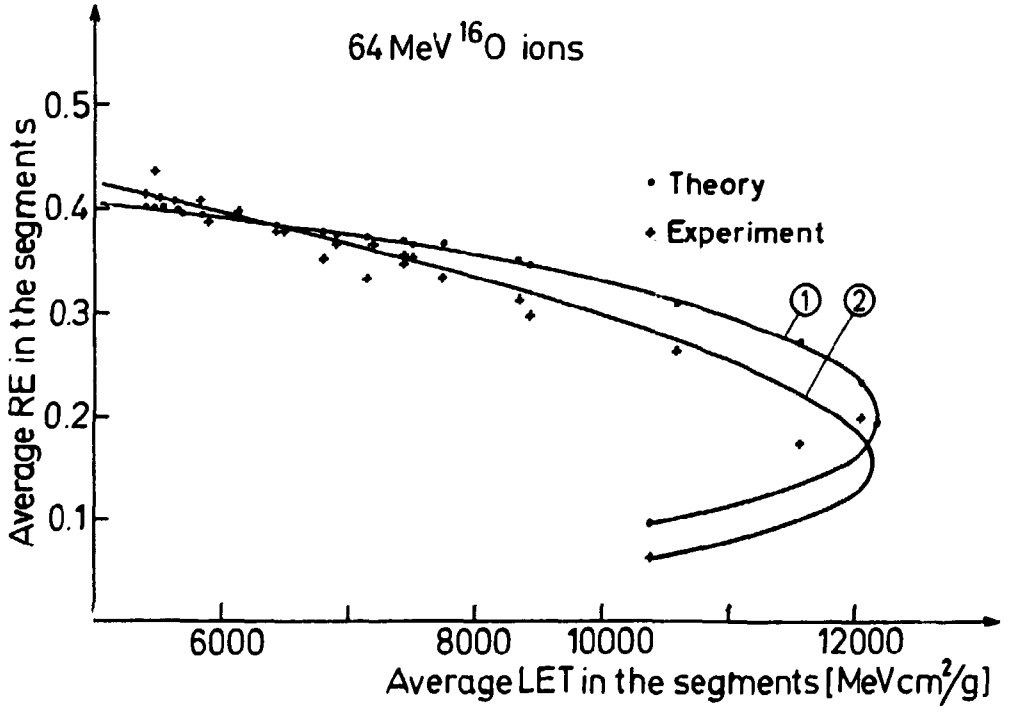
64 MeV ^{16}O ions
• Theory
+ Experiment
Average RE in the segments
0.5
0.4
0.3
0.2
0.1
6000
8000
10000
12000
Average LET in the segments [MeV cm²/g]
①
②

Fig. 33.

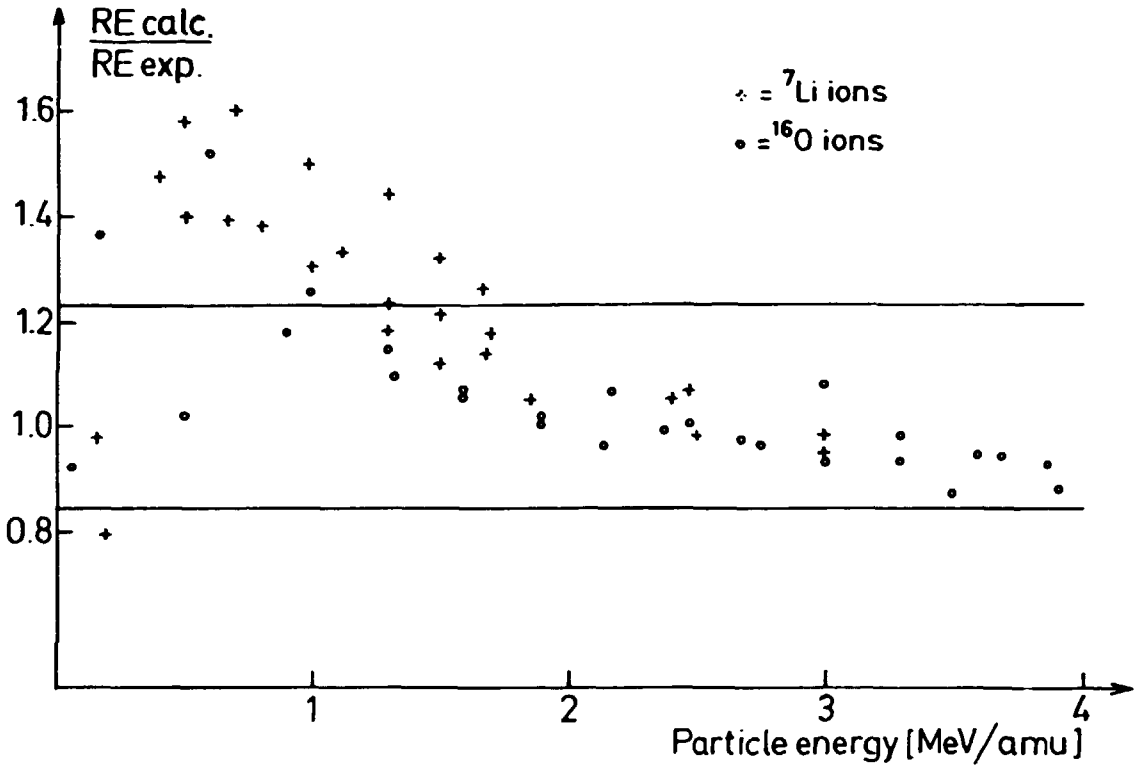
RE calc.
RE exp.
1.6
1.4
1.2
1.0
0.8
+ = ^{7}Li ions
• = ^{16}O ions
1
2
3
4
Particle energy [MeV/amu]

Fig. 34.

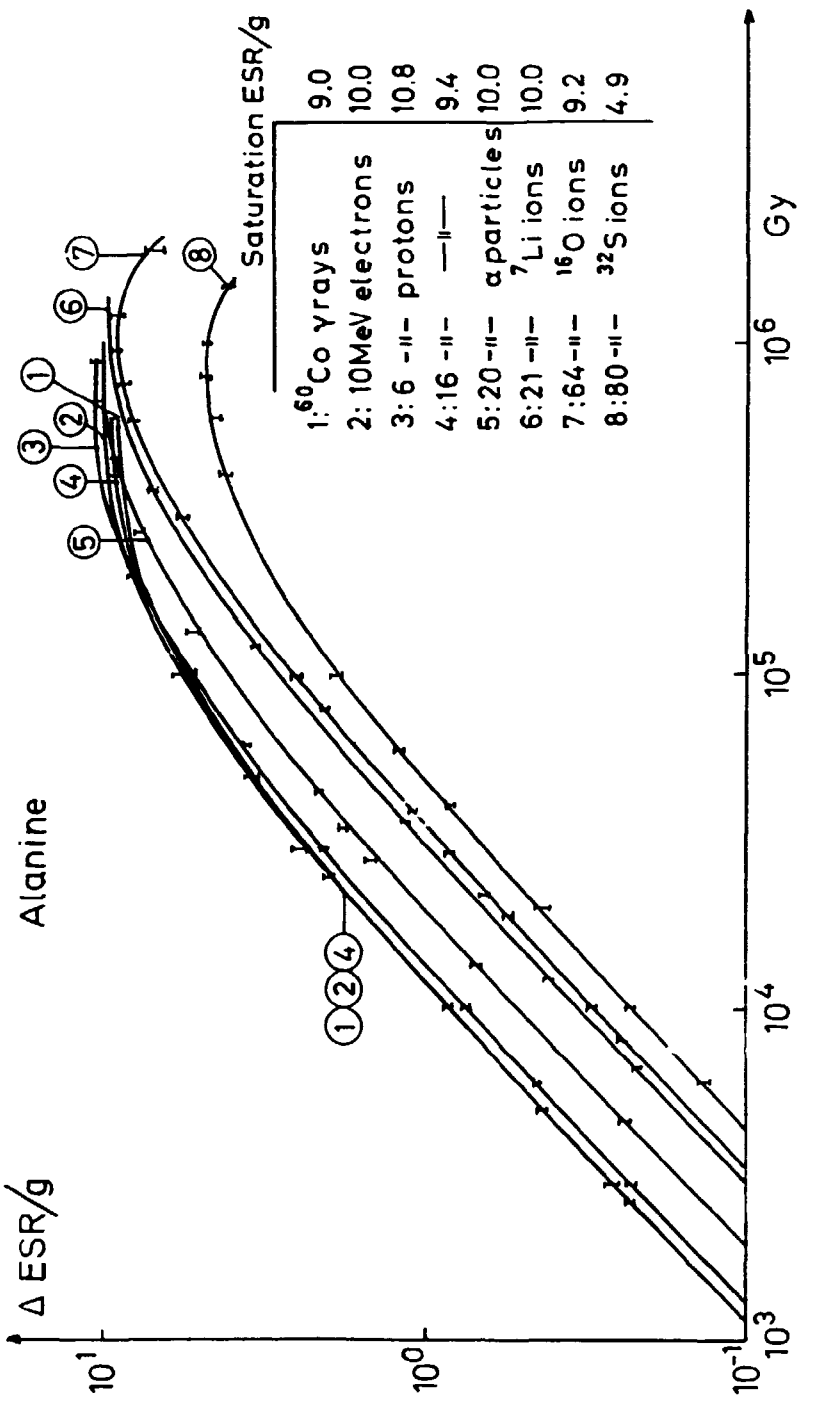
Alanine
Δ ESR/g
10^1
10^0
10^{-1}
10^3
10^4
10^5
10^6
Gy
Saturation ESR/g
1: ^{60}Co γrays 9.0
2: 10MeV electrons 10.0
3: 6 -"- protons 10.8
4: 16 -"- —"— 9.4
5: 20 -"- α particles 10.0
6: 21 -"- ^{7}Li ions 10.0
7: 64 -"- ^{16}O ions 9.2
8: 80 -"- ^{32}S ions 4.9

Fig. 35.

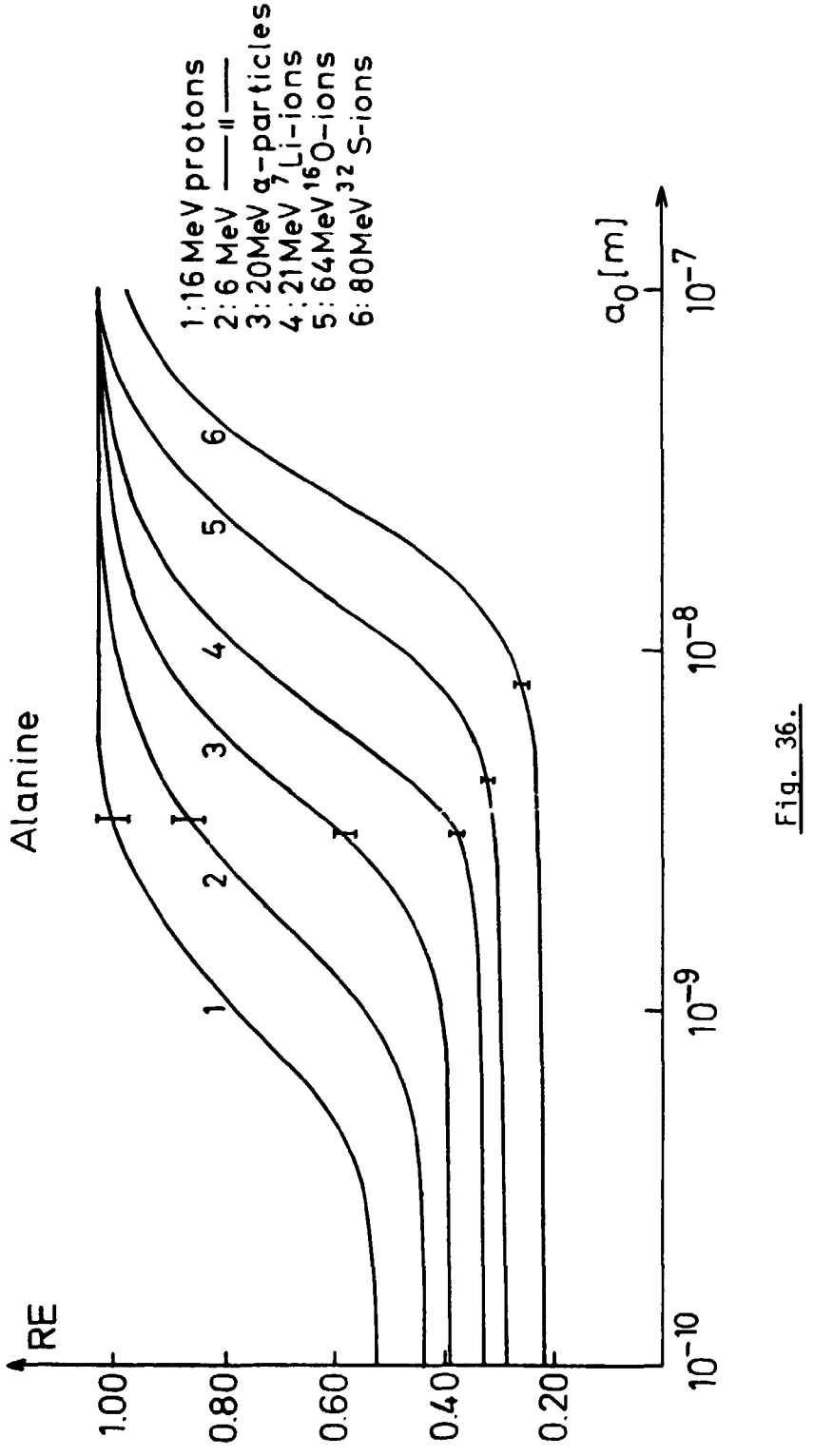
Alanine
RE
1.00
0.80
0.60
0.40
0.20
10^{-10}
10^{-9}
10^{-8}
10^{-7}
a_0 [m]
1
2
3
4
5
6
1: 16 MeV protons
2: 6 MeV —"—
3: 20MeV α-particles
4: 21MeV ^{7}Li-ions
5: 64MeV ^{16}O-ions
6: 80MeV ^{32}S-ions

Fig. 36.

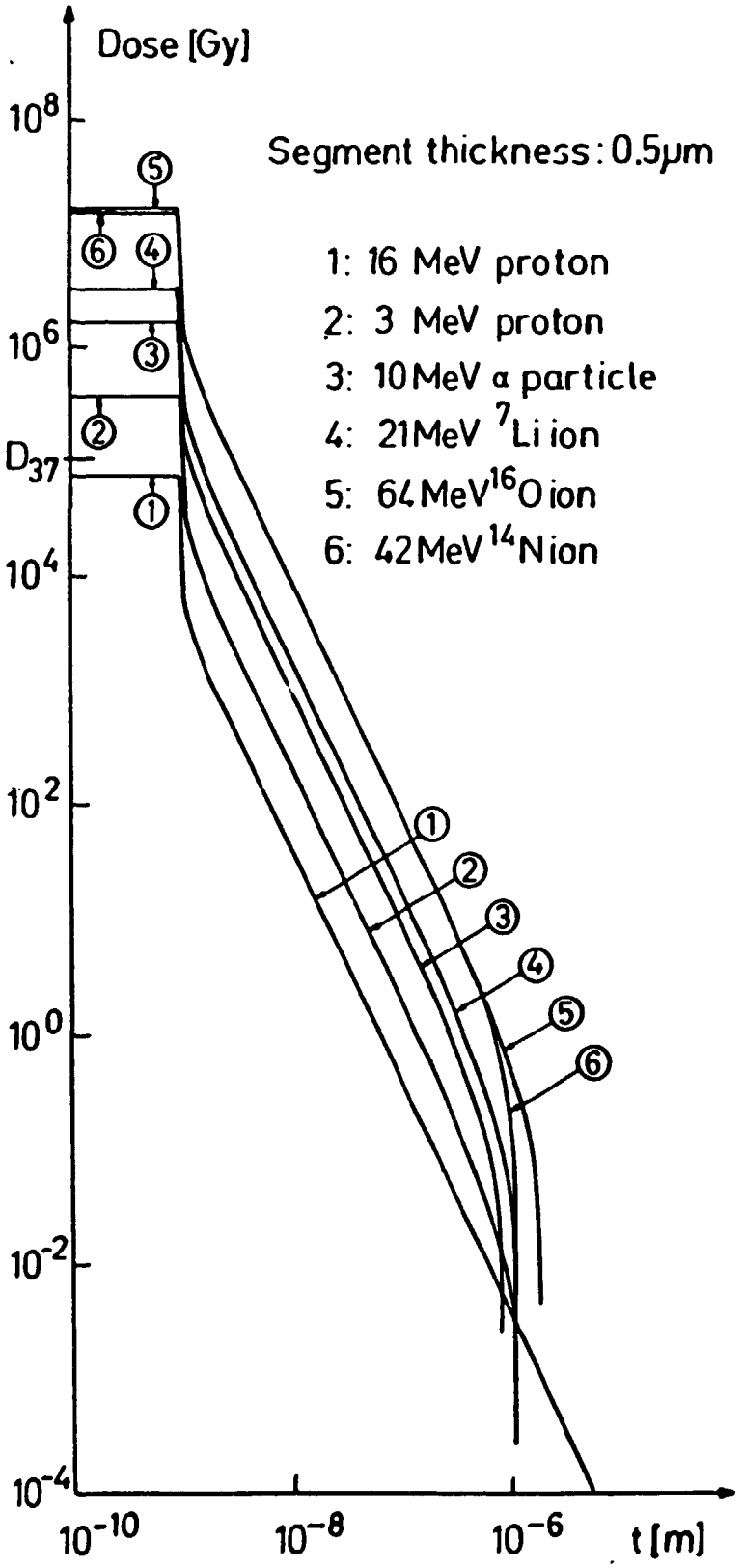
Dose [Gy]
10^8
10^6
D_{37}
10^4
10^2
10^0
10^{-2}
10^{-4}
10^{-10}
10^{-8}
10^{-6}
t [m]
Segment thickness: 0.5μm
1: 16 MeV proton
2: 3 MeV proton
3: 10 MeV α particle
4: 21 MeV ^{7}Li ion
5: 64 MeV ^{16}O ion
6: 42 MeV ^{14}N ion

Fig. 37.

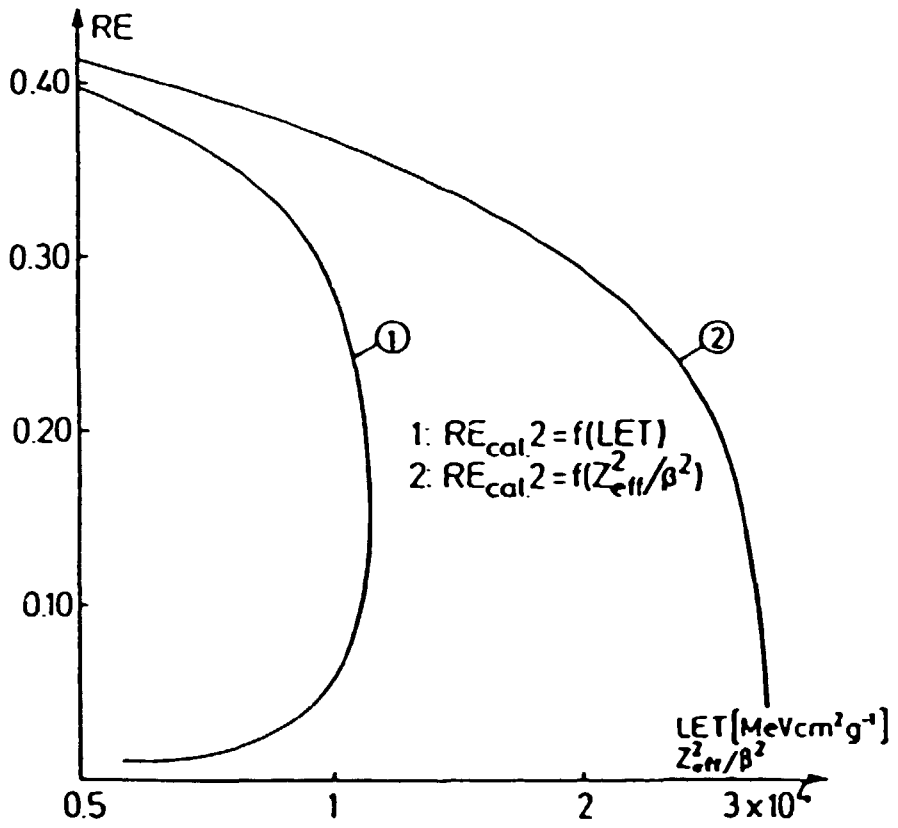
RE
0.40
0.30
0.20
0.10
0.5
1
2
3x10
1: RE_cal.2 = f(LET)
2: RE_cal.2 = f(Z²_eff/β²)
LET [MeVcm²g⁻¹]
Z²_eff/β²

Fig. 38.

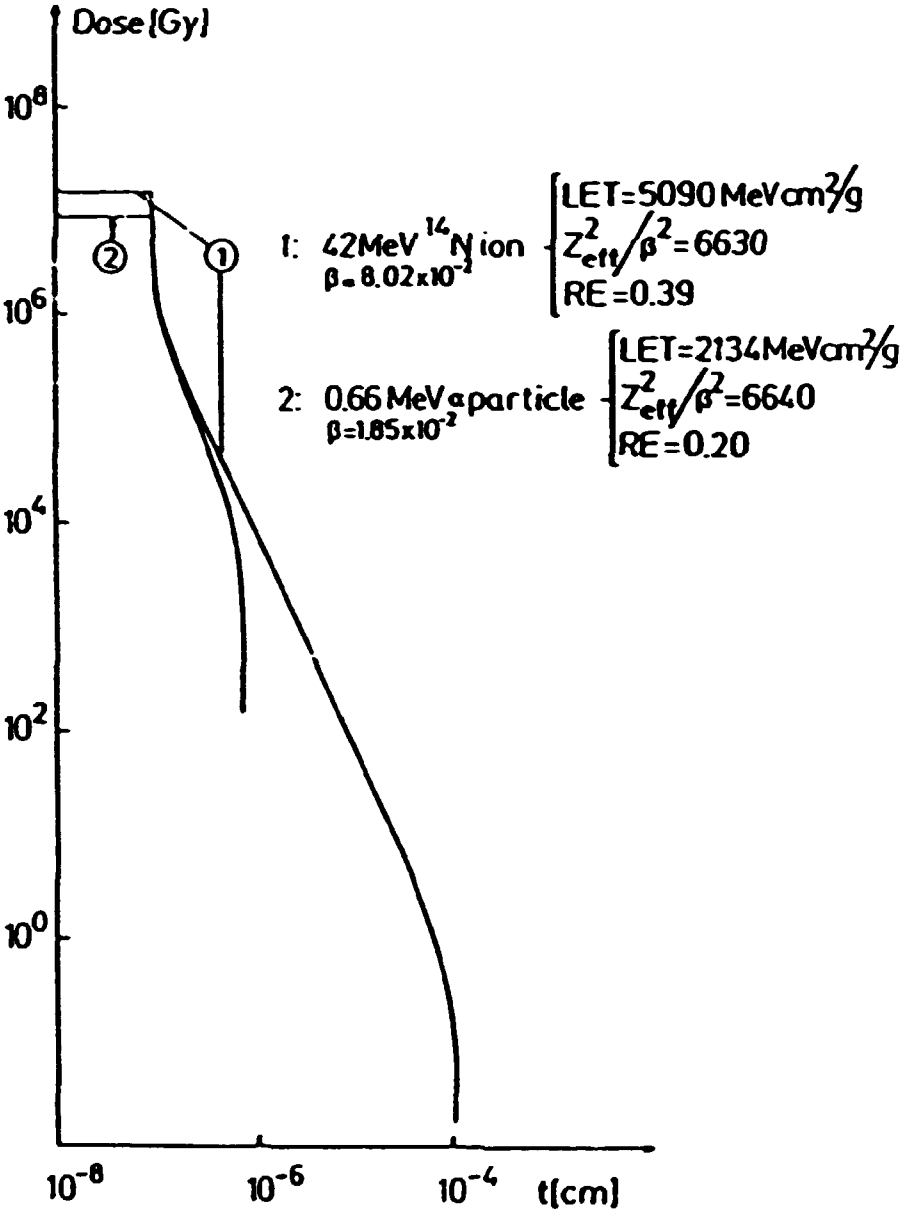
Dose [Gy]
10^8
10^6
10^4
10^2
10^0
1: 42MeV ^{14}N ion
$\beta = 8.02 \times 10^{-2}$
LET=5090 MeVcm²/g
$Z^2_{eff}/\beta^2 = 6630$
RE=0.39
2: 0.66 MeV α particle
$\beta = 1.85 \times 10^{-2}$
LET=2134 MeVcm²/g
$Z^2_{eff}/\beta^2 = 6640$
RE=0.20
10^{-8}
10^{-6}
10^{-4}
t[cm]

Fig. 39.

COMMISSION OF THE EUROPEAN COMMUNITIES

radiation protection

Eighth Symposium on Microdosimetry

Kernforschungsanlage Jülich GmbH
Jülich, Federal Republic of Germany
27 September - 1 October 1982

Proceedings edited by
J. BOOZ and H.G. EBERT

Directorate-General
Science, Research and Development
Radiation Protection

1983

EUR 8395 EN

High-LET Dose Response Characteristics of the Dye Film Dose Meter in the Context of Track Structure Theory.

K.J. Olsen
Department of Radiophysics
Københavns Amts Sygehus
DK 2730 Herlev, Denmark

J.W. Hansen
Accelerator Department
Risø National Laboratory
DK 4000 Roskilde, Denmark

ABSTRACT

Experimental dose-response characteristics of both low- and high-LET radiation for a radiochromic dye film dose meter have been compared with calculations based on the track structure theory of Katz et al. The low-LET radiation was ^{60}Co γ-rays and 10 MeV electrons while the high-LET radiation was beams of 16 MeV protons, 10 MeV α-particles, 21 MeV ^{7}Li-, 42 MeV ^{14}N- and 64 MeV ^{16}O-ions covering a range in initial LET of 31-5500 MeV $cm^2 g^{-1}$.

The effectiveness of the ion beams relative to the low-LET radiation was determined both from the initial slope of the dose-response curves in a linear plot and from the parallel displacement of the curves in a log-log plot.

The effectiveness decreased monotonically with increasing z^2_{eff}/β^2 but not with increasing LET. The experimental values were 0.93, 0.52, 0.48, 0.35 and 0.29 for protons, α-particles, ^{7}Li-, ^{16}O- and ^{14}N-ions, respectively.

The radial dose distribution around the ion path was calculated using two different range-energy relations for the δ-rays, $r=k_1 \cdot \omega$ and $r=k_2 \cdot \omega^{\alpha}$ with r-range and ω-energy of the δ-rays. The calculated effectiveness was in good agreement (~ 6%) with experimental values when the exponential range-energy relation was used with $\alpha=1.67$. The linear expression gave values which deviated considerably from experimental values at the highest LET.

INTRODUCTION

The track structure theory of Katz et al. (1) ascribes the difference in effectiveness between low- and high-LET radiation as due to the highly inhomogeneous dose distribution around the particle path. From the theory it is possible to calculate the effectiveness of high-LET radiation relative to low-LET radiation once the dose-response characteristics for low-LET radiation are known.

This is, however, only strictly valid for ideal detectors. An ideal physical detector is predicted from the theory to have the following properties: 1) no dose rate effect, 2) linear dose-response up to doses comparable to the characteristic dose of the detector, 3) in a log-log plot all dose-response curves will be 45^{o} lines, 4) the maximum response is the same for all types of radiation and 5) the effectiveness decreases monotonically with increasing Z^2_{eff}/β^2.

Two previous studies of the response of the dye film to high-LET radiation using 3 MeV protons (2) and 16 MeV protons and 64 MeV ^{16}O-ions (3) have indicated that the dye film behaves almost as an ideal physical detector and that the effectiveness to a certain extent is in agreement with calculations based on track structure theory.

The dye film is a suitable test system for the theory since the sensitive element is very small, ~ 1 nm, and the characteristic dose high which means that the detector can be studied over a wide range in LET.

EXPERIMENTAL

The radiation detector is a 55 μm thick film of hexahydroxyethyl pararosaniline embedded in a nylon matrix. The film develops an absorption at 600 nm upon exposure to either UV or ionizing radiation. The colouration may be expressed as increase in optical density per unit film thickness, ΔOD/mm, which is measured in a photospectrometer calibrated against a National Bureau of Standards gray scale. The film thickness is measured individually with an electronic gauge unit with a precision better than 1 μm.

The ion-beam irradiations are carried out with a tandem Van de Graff accelerator (4). The absorbed dose is calculated from the particle fluence and stopping power. The average dose rate is between $0.8 \cdot 10^5$ and $5 \cdot 10^5$ rad/s depending on the ions used. The particle fluence is measured by integration of the ion current in a Faraday cup and the charge state of the ions is determined by an analyzing spectrometer.

The reference radiation is ^{60}Co γ-rays from a 10 kCi source with a dose rate of $1.4 \cdot 10^3$ rad/s and 10 MeV electrons from a linear accelerator with a dose rate of $5 \cdot 10^9$ rad/s (4). Both radiation facilities are calibrated against a Fricke dose meter.

The stopping power of the ion beams is calculated from published proton stopping data (5,6) as $S(Z_{eff},\beta) = S(Z_p,\beta) \cdot Z_{eff}^2/Z_p^2$ where $S(Z_{eff},\beta)$ is the stopping power of the ion with atomic number Z moving at speed β relative to the speed of light and $S(Z_p,\beta)$ is the stopping power of a proton moving at same speed. Z_{eff} and Z_p are the effective charges of the ion and proton, respectively. The effective charge is calculated from the formula of Barkas (7): $Z_{eff} \sim Z(1-\exp(-125\beta\, Z^{-2/3}))$. The proton stopping power is calculated from the atoms constituting the detector using Bragg's additivity rule (8).

The dosimetry in low-LET irradiations is accurate within ±2% and the uncertainty of the low-LET dose-response measurements is 3.2% given as the root mean square (RMS) of the uncertainties of the various measurements involved in an experimental datum point.

The accuracy of the dose-response measurements with ion beams is ±5.2% given as the RMS of the individual uncertainties and statistical scatter.

The uncertainty of the proton stopping power data is from 1 to 15%, highest at low energies, and the uncertainty introduced by using Bragg's additivity rule may be of same magnitude (8).

RESULTS

The dose-response characteristics of the radiation qualities used in the present study are shown in figs. 1 and 2. The two

low-LET radiation qualities ^{60}Co γ-rays and 10 MeV electrons show identical dose-response below 5 Mrad, but at higher doses the two curves deviate considerably.

The characteristic dose, D_{37}, may be found as the dose which corresponds to 63% of the saturation optical density. From fig. 1 D_{37} is found to be 33 Mrad for 10 MeV electrons and 16.8 Mrad for ^{60}Co γ-rays.

The dose-response curves in fig. 1 are parallel but have an initial slope slightly less than 45°. The saturation optical density for the ^{14}N- and ^{16}O-beams is the same as for 10 MeV electrons while 16 MeV protons show a dose-response curve almost identical to the ^{60}Co γ-ray curve with the curve of 10 MeV α-particles between the two extremes.

The relative effectiveness of the ion beams may be found both from the parallel displacement of the curves in fig. 1 and from the initial slope of the curves as shown in fig. 2.

The relative effectiveness (RBE) may be calculated from track structure theory. The calculations use as parameters D_{37} and a_o, the radius of the sensitive elements in the dye film. a_o is taken as 1 nm corresponding to the approximate size of a dye molecule. Two different range-energy relations for the δ-rays have been used. The linear relation $r=k_1 \cdot \omega$ with r=range and ω=energy of the δ-rays leads to a point-target dose expression

$$D_\delta(t) = \frac{C}{2\pi} \cdot \frac{Z_{eff}^2}{\beta^2} \cdot \frac{1}{t^2} \cdot \left[1 - \frac{t}{t_{max}}\right]$$

with t = distance from the particle path, t_{max} = maximum range of the δ-rays, $C = \frac{2\pi N e^4}{mc^2} = 1.34 \cdot 10^{-7} \cdot \rho$ erg/cm, and ρ = density. $k_1 = 10^{-8}$ g/cm^2/eV as used in the work of Katz et al. (1). The exponential relation $r=k_2 \cdot \omega^\alpha$ leads to

$$D_\delta(t) = \frac{C}{2\pi} \cdot \frac{1}{\alpha} \cdot \frac{Z_{eff}^2}{\beta^2} \cdot \frac{1}{t^2} \cdot \left[1 - \frac{t}{t_{max}}\right]^{1/\alpha}$$

In the calculations α is taken as 1.67 and $k_2 = 5.11 \cdot 10^{-11}$ g/cm^2/eV$^\alpha$ is found by fitting to the data of Paretzke et al. (9).

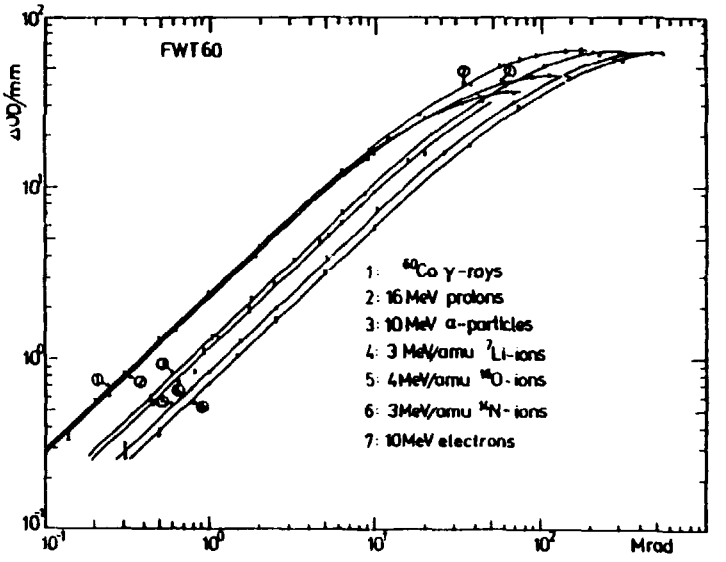

Fig. 1. Dose-response characteristics of the radiation qualities under investigation.

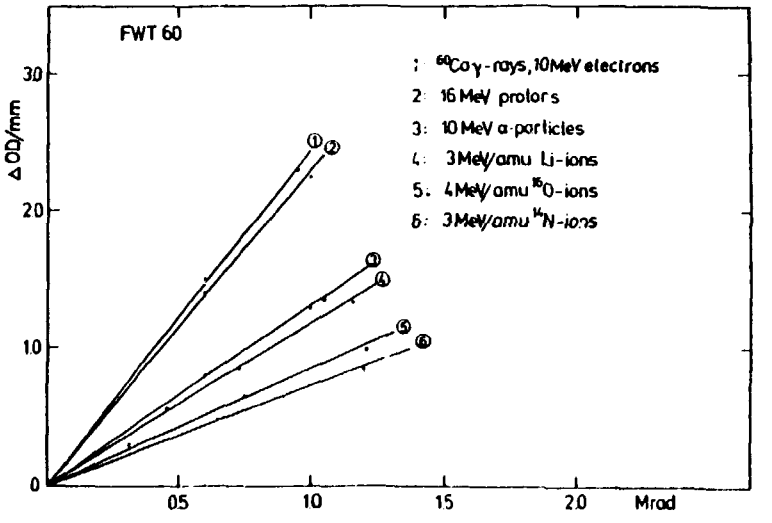

Fig. 2. Initial slope of the dose-response characteristics shown in fig. 1.

In the extended target dose calculations (1) used for determination of cross-section the dose at $t \leq a_o$ is assumed to be constant and is mainly due to the part of the energy loss of the ion deposited as excitational energy (4). The energy deposited at $t \leq a_o$ is found from the total energy loss of the ion less the energy deposited at $t > a_o$ which may be calculated by integration of the point-target formula given. The calculated values of RBE are shown in table I.

The calculated RBE values are dose-weighted mean-values over the detector taking into account the change in LET, Z_{eff} and β during passage of the ion through the detector. The experimental RBE values are shown in table II together with initial and average values of LET and Z^2_{eff}/β^2.

The overall uncertainty in experimental RBE's are ±6% disregarding the uncertainty in LET. Since identical values of LET are used in the calculations and in experiments the uncertainty in LET does not influence the comparison of experimental and theoretical values.

The fittedness of the calculations involving the two range-energy relations have been tested by comparison with the experimental data of Varma et al. (10) for 42 MeV ^{79}Br ions. The mean deviation of calculated and experimental doses are +40% for the linear relation and +3% for the exponential range-energy relation.

Fain et al. (11) have calculated the dose distribution around the path of a 2 MeV/amu C-ion using a different method. The mean deviations are in this case +34% and +8% for the linear and exponential case, respectively.

DISCUSSION

The dose response curves in fig. 1 show that the dye film deviates in at least two respects from an ideal physical detector. The maximum response differs for various radiation qualities and the curves are not 45^o lines at low doses in a log-log plot. Both effects may be ascribed to the complex chemical reactions involved in converting the leucocyanide into the final dye molecule. Both in solutions (12) and in the solid matrix (13) an

intermediate species is formed which is converted into the dye molecule over a period of several hours at room temperature (13). The intermediate and the dye molecule may thus react with electrons or other radicals with ensuing reduction in yield depending on the dose rate.

The two low-LET radiations give different D_{37} values. The relative low dose rate of the ^{60}Co γ-source necessitates long exposures to obtain the value of maximum optical density. During this exposure back reactions, reactions with the intermediate species and changes in matrix structure due to radiation are very likely to take place leading to a too low maximum optical density and correspondingly low D_{37} value. For this reason we prefer to use the D_{37} value for 10 MeV electrons obtained with comparatively short exposure times. The D_{37} being related to the radiation sensitivity of the detector must by definition be the same for the two low-LET radiations as reflected in the identical values of the initial slope shown in figures 1 and 2.

The exponential range-energy relation improves the agreement between calculated and experimental RBE's considerably. This is presumably due to that the exponential relation is a much better fit to the actual range-energy relation for the low-energy δ-rays. In comparison with the calculations of Paretzke et al. (9) the exponential relation underestimates the range of very low-energy electrons (E < 100 eV). At low energies, however, where binding effects play a role the Bethe energy-distribution of the δ-rays is not correct.

The method used for calculating extended target radial dose distributions in the present work compensates for this by considering an area of radius a_o, which corresponds to the range of 100 eV δ-rays, around the ion path separately from the rest of the particle track. In this way we also take account of the fact that a large part of the ion energy loss is due to primary excitation energy (11).

The data in table II underline the point made by Katz (1) and Edwards (14) that Z^2_{eff}/β^2 is a better parameter than LET for description of the effect of high-LET radiation since the ^{14}N-ions have a lower LET and a lower RBE, but a higher Z^2_{eff}/β^2 than the ^{16}O-ions.

CONCLUSION

The results demonstrate that despite some deviation of the dye film from an ideal physical detector the effectiveness of the dye film to high-LET radiation may be quantitatively described by the track structure theory. An exponential range-energy relation for the δ-rays improves the model, but a further development should include effects as e.g. dose rate, which will permit predictions of dose-response also at saturation doses.

REFERENCES

1. Katz, R., Sharma, S.C., Homayoonfar, M., in Topics of Radiation Dosimetry, Supplement 1. (Ed. F.H. Attix), Academic Press, N.Y. (1972) 314.
2. Rosenstein, M., Eisen, H., Roush, M.L., Silverman, J., Int. Jour. of Applied Radiation and Isotopes (1975), Vol. 26, 423.
3. Hansen, J.W., Jensen, M., Katz, R., Seventh Symp. on Microdosimetry (1980), Vol. II, 821.
4. Hansen, J.W., Olsen, K.J., Experimental and Predicted Effectiveness of a Radiochromic Dye Film Dose Meter to High-LET Radiation (to be published).
5. Northcliff, L.C., Schilling, R.F., Nuclear Data Tables, A7, Academic Press (1970), 233.
6. Barkas, W.H., Berger, M.J., Nuclear Science Series, Rep. No. 39. NAS-NRC Publication 1133 (1964), 103-172.
7. Barkas, W.H., Nuclear Emulsions, Vol. 1, Academic Press N.Y. (1963).
8. Bichsel, H., Phys. Med. Biol. (1982), Vol. 27, No. 3, 449.
9. Paretzke, H.G., Berger, M.J., Sixth Symp. on Microdosimetry (1978), Vol. II, 749.
10. Varma, M.N., Baum, J.W., Kuehner, A.V., Phys. Med. Biol. (1980), Vol. 2, No. 4, 651.
11. Fain, J., Monnin, M., Montret, M., Fourth Symp. on Microdosimetry, Vol. I (1974), 169.
12. McLaughlin, W.L., Kosanic, M.M., Markovic, V.M., Nenadovic, M.T., Holcman, J., Sehested, K. (1979) Risø-M-2202, Risø National Laboratory, Denmark.
13. Dachenko, V., Griffin, G.F., Brashears, S.S., IEEE Trans. on Nucl. Science (1981), Vol. NS28, No. 6.
14. Edwards, A.A., Seventh Symp. on Microdosimetry (1980), Vol. I, 593.

Table I

	$RBE_{exp.}$	$RBE_{cal.}^{1}$	$RBE_{cal.}^{2}$	$RBE_{cal.}^{1a}$	$RBE_{cal.}^{2a}$
^{60}Co γ-rays	1.00	1.00		1.00	
10 MeV electrons	1.00		1.00		1.00
16 MeV protons	0.94	0.89	0.95	0.95	0.98
10 MeV α-particles	0.52	0.43	0.49	0.60	0.67
21 MeV ^{7}Li-ions	0.48	0.41	0.45	0.56	0.61
42 MeV ^{14}N-ions	0.29	0.29	0.30	0.41	0.45
64 MeV ^{16}O-ions	0.35	0.34	0.37	0.46	0.49

$RBE_{exp.}$: RBE derived from the initial slope of the dose-response characteristics.

$RBE_{cal.}^{1}$: RBE calculated with exponential range-energy relation, D_{37} = 16.8 Mrad.

$RBE_{cal.}^{2}$: RBE calculated with exponential range-energy relation, D_{37} = 33 Mrad.

$RBE_{cal.}^{1a}$: RBE calculated with linear range-energy relation, D_{37} = 16.8 Mrad.

$RBE_{cal.}^{2a}$: RBE calculated with linear range-energy relation, D_{37} = 33 Mrad.

Table II

	$RBE_{exp.}$[1]	$LET_{init.}$	$LET_{av.}$	$z^2_{eff}/\beta^2_{init.}$	$z^2_{eff}/\beta^2_{av.}$
^{60}Co γ-rays	1.00				
10 MeV electrons	1.00	2.1	2.1		
16 MeV protons	0.94	31.4	31.5	29.1	29.3
10 MeV α-particles	0.52	564	686	740	923
21 MeV ^{7}Li-ions	0.48	1079	1272	1375	1660
42 MeV ^{14}N-ions	0.29	5227	6658	6660	9963
64 MeV ^{16}O-ions	0.35	5496	7191	6653	8982

LET in $MeVcm^2/g$.

RADIATION RESEARCH 97, 1–15 (1984)

Experimental and Calculated Response of a Radiochromic Dye Film Dosimeter to High-LET Radiations

J. W. HANSEN

Risø National Laboratory, DK 4000 Roskilde, Denmark

AND

K. J. OLSEN

Department of Radiophysics, University Hospital of Copenhagen, DK 2730 Herlev, Denmark

HANSEN, J. W., AND OLSEN, K. J. Experimental and Calculated Response of a Radiochromic Dye Film Dosimeter to High-LET Radiations. *Radiat. Res.* 97, 1–15 (1984).

Dose–response characteristics were measured for the FWT 60 nylon-base radiochromic dye film dosimeter irradiated with ion beams of 3- and 16-MeV protons, 10-MeV α particles, and 21-MeV ^{7}Li, 42-MeV ^{14}N, and 64-MeV ^{16}O ions. These characteristics were compared with the response to reference low-LET radiations, i.e., ^{60}Co γ rays and 10-MeV electrons. The ion beams covered an initial LET range of 28–5430 MeV cm^2 g^{-1} corresponding to an average LET in the detector of 28–6740 MeV cm^2 g^{-1}. The experimental relative effectiveness (RE) decreased monotonically with z^2_{eff}/β^2 from 1.00 for 16-MeV protons to 0.81, 0.55, 0.47, 0.36, and 0.28 for 3-MeV protons, α particles, and ^{7}Li, ^{16}O, and ^{14}N ions, respectively. The radial dose distribution around the ion path was calculated using two different range–energy relations for the δ rays: a linear relation $r = k_1 \cdot \omega$ and a power-law relation $r = k_2 \cdot \omega^n$, where r is the range and ω the energy of the δ rays. Calculations of theoretical RE values, based on the track structure theory of Katz and co-workers, were in good agreement with experimental results. The best agreement (−6.2 to +14.3%) was obtained by using a power-law range–energy relation.

INTRODUCTION

The dose–response characteristics of biological systems and physical detectors change with the linear energy transfer (LET) of the impinging charged particle, so that the response to high-LET radiation may be either larger or smaller relative to the response to low-LET radiation for the same absorbed dose. Most physical detectors in fact show a decrease in relative response with increase in z^2_{eff}/β^2. Once two or three parameters can be obtained from low LET radiation experiments with a given detector, the theory of track structure (*1*) predicts its high-LET dose–response characteristics. The theory is based on the assumption that the ratio in response for high-LET particles to that for low-LET radiations, relative effectiveness (RE), is due mainly to the inhomogeneous dose distribution around the particle's path. The radiation effects of interest are due primarily to the absorbed dose of the δ rays ejected from the ion path. Radiation effects from low LET radiation, e.g., γ rays and high-energy electrons, are also due to absorbed dose from δ rays, i.e., low-energy electrons.

0033-7587/84 $3.00

The present work is focused on the dose response of a radiochromic dye film dosimeter (*2*) to ionizing radiation in the context of track structure theory. This dosimeter is considered here as a one-hit detector the response of which to both low- and high-LET radiation can be described by Poisson statistics (*3*), such that the probability for activation of a radiation sensitive element is

$$P(z, \beta, t, a_0) = 1 - \exp(-\bar{D}(z, \beta, t, a_0)/D_{37}) \quad (1)$$

where z is the effective charge of the moving ion, β is the ion velocity relative to the velocity of light, t is the radial distance perpendicular to the ion path, a_0 is the radius of the sensitive element, $\bar{D}(z, \beta, t, a_0)$ is the average absorbed dose to the sensitive element, and D_{37} is a characteristic dose (*3*). a_0 is, in the track structure theory, a fitted parameter which together with D_{37} for low-LET radiation determines the radiation sensitivity of the detector. For a physical–chemical detector, e.g., the dye film, a_0 is the approximate physical size of the molecule which responds to the absorbed radiation dose. The D_{37} value is the dose at which 63% of the maximum (saturation) effect is reached and is obtained from the measured low-LET dose–response characteristic. To consider the total effect of a given high-LET radiation on sensitive elements at all distances from the primary particle path, an integration of the probabilities must be made over the detector volume being affected by the δ rays generated by the primary ion. This integration yields the total activation cross-section

$$\sigma_T(z, \beta, a_0) = 2\pi \int_0^{t_{max}} P(z, \beta, t, a_0) t\, dt \quad (2)$$

where t_{max} is the maximum range of the most energetic δ rays. The radiosensitivity of a detector to heavy ions is defined as σ_T/E_T, where E_T is the total energy deposited by the ion per unit path length, and the radiosensitivity of a detector to low-LET radiation is given by $1/D_{37}$. RE is defined as the ratio between the radiation sensitivities for heavy ions and low-LET radiation and can be expressed as $RE = \sigma_T \cdot D_{37}/E_T$, where E_T is equal to LET_∞ of the stopping ion. In a one-hit detector the activation of a sensitive element proceeds directly from a single event of energy deposition above a characteristic threshold, e.g. the ionization potential or bond energy.

In the theory of track structure (*1*) only electromagnetic interactions are taken into account, whereas effects arising from nuclear interactions are assumed to be negligible. The theory does not incorporate fading, annealing, or dose-rate effects.

The radiochromic dye film dosimeter is an appropriate detector for testing the theory, since the sensitive elements are small and the film is relatively insensitive to radiation. This makes it possible to study the dose response over a wide range of LET. Two previous investigations of the dye film using 3-MeV protons (*4*) and 16-MeV protons and 64-MeV ^{16}O ions (*5*) have indicated that the dye film displays an effectiveness to high-LET radiation as predicted by the theory.

EXPERIMENTAL

The radiation detector in these experiments is a thin-film plastic dosimeter type FWT 60[1] developed for measurements of high absorbed doses in the kilogray range (*2*). The host material is a form of nylon,

[1] Commercially available from Far West Technology, Goleta, CA.

$(C_{12}H_{22}N_2O_2)_n$, which contains 10–15% of a colorless radiochromic dye precursor hexahydroxyethyl pararosaniline leucocyanide, $(C_6H_4N(C_2H_4OH)_2)_3C\text{-}CN$, and which attains a blue color upon irradiation with exciting or ionizing radiation. The formed dye has a broad optical absorption band with a maximum at 604 nm. The dosimeter response is expressed as increase of optical density per unit film thickness, $\Delta OD/mm$, measured at 510 nm, which is off the maximum at the edge of the absorption band. This wavelength was chosen to allow measurement at doses where the detector response shows saturation, since the optical densities at the absorption maximum become too large for ready analysis.

The average film thickness is 55 μm and the density 1.13 g cm^{-3}. The thicknesses were measured individually with an electronic transducer gauge unit and the optical densities were measured in a recording spectrophotometer designed to read spatial variations in optical density across the field. The spectrophotometer was calibrated against a gray scale (National Bureau of Standards).

The stopping powers of the ions in the film were calculated from published proton stopping power data (6, 7) as

$$S(z_{eff}, \beta) = S(z_p, \beta)\cdot(z_{eff}^2/z_p^2) \tag{3}$$

where $S(z_{eff}, \beta)$ is the stopping power of the ion with atomic number Z moving at a velocity β relative to the velocity of light, $S(z_p, \beta)$ is the stopping power of a proton moving at the same velocity, and z_{eff} and z_p are the effective charges of the ion and proton, respectively. The effective charge was calculated from the formula of Ziegler (7).

$$z_{eff} = Z_p\cdot Z[1 - \exp(-A)\cdot(1.034 - 0.177\cdot\exp(-0.08114\cdot Z))] \tag{4}$$

$$Z_p = 1 - \exp(-0.2\sqrt{E} - 0.0012\cdot E - 1.443\cdot 10^{-3}\cdot E^2) \tag{5}$$

$$A = 0.1772\cdot Z^{-2/3}\cdot\sqrt{E} + 0.0378\cdot\sin(0.2783\cdot Z^{-2/3}\cdot\sqrt{E})$$

where Z_p is the effective charge of the proton and E is the energy of the ion in keV/a.m.u.

The proton stopping powers were calculated by Bragg's additivity rule (8) from the weight fractions of the atoms constituting the detector.

The reference low-LET radiations were γ rays from a $3.7\cdot 10^{14}$-Bq ^{60}Co source with a dose rate of 14 Gy sec^{-1} and 10-MeV electrons from a linear accelerator with an average dose rate of $5\cdot 10^7$ Gy sec^{-1}. These radiation fields were calibrated with Fricke dosimetry (9) and water calorimetry (10), respectively.

The ion-beam irradiations were carried out on a tandem Van de Graaff accelerator with an average dose rate of $\sim 10^3$ Gy sec^{-1}. The absorbed dose in the detector was calculated from particle fluence and stopping-power values. The particle fluence was determined from an integration of the ion current to a Faraday cup, and the charge state of the ions was measured in an analyzing spectrometer placed in front of the irradiation chamber. During ion-beam irradiation three samples of dye film were mounted around the periphery of a rotating wheel carrying it through the beam path. When the samples were in the beam path the integration of the current from the Faraday cup was interrupted, thus avoiding corrections for change in charge state of the primary ion during passage of the film, particle number attenuation, scattering from the film edges, large-angle scattering, and secondary electrons escaping from the back side of the detector. The interruption was controlled by cutting off the light path in an optical coupler by another wheel running synchronously to the wheel on which the film samples were mounted (see Fig. 1). The wheel was rotated with $\sim$200 rpm which made the intervals between irradiation of the samples and measurement of the beam current very short, thus diminishing influence from fluctuations in beam current with time. Irradiation of three film samples at each run ensured agreement between measured film response and measured charge.

The electric charge, Q_{beam}, transported by the ion beam into the irradiation chamber is obtained from a measurement of integrated current to the Faraday cup, charge Q_{cup}, as

$$Q_{beam} = Q_{cup}\frac{2\pi}{2\pi - p\phi} \tag{6}$$

where ϕ is the pulse length in terms of radians of the signal from the optical coupler, and p is the number of pulses per revolution of the wheel (see Fig. 1). The ratio between particles hitting the film sample and those entering the irradiation chamber is $l/2\pi$, where l is the width of the film sample in terms of radians.

The particle fluence Φ [cm^{-2}] hitting the film sample is determined by

$$\Phi = Q_{cup}\cdot\frac{l}{n\cdot e\cdot A\cdot(2\pi - p\phi)} \tag{7}$$

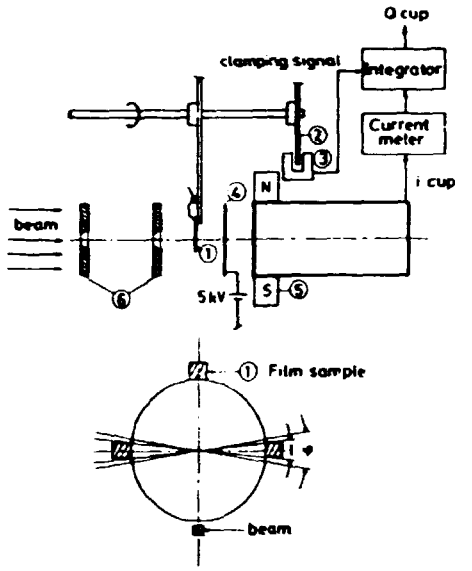

FIG. 1. Experimental set-up for particle irradiations on the tandem Van de Graaff. (1) Film sample, (2) rotating wheel with slits, (3) optical coupler, (4) high-potential shield, (5) 0.5 T magnet, and (6) beam-defining slits.

where n is the charge state of the ions, e the charge of the electron, and A the irradiated area on the film defined by the width l of the film and the vertical dimension of the beam collimator. From measurement of the size of the irradiated area on the film, beam divergence was found to be negligible. The absorbed dose in the film can then be calculated from the track average stopping power in the film S_w and the particle fluence Φ as

$$D = \frac{1}{k} S_w \cdot \Phi = \frac{S_w \cdot Q_{cup} \cdot l}{k \cdot n \cdot e \cdot A \cdot (2\pi - p\phi)} \tag{8}$$

with $k = 6.24 \cdot 10^9$ MeV g^{-1} Gy^{-1} as a conversion constant.

To ensure beam homogeneity on the irradiated area, the particle beam was dispersed by a magnetic field and collimated by two sets of thin collimators, 3×3 mm^2, positioned so that secondary electrons and scattered ions originating from the slit edges are prevented from reaching the film. To limit effects arising from secondary electrons escaping from the Faraday cup, a magnetic field of 0.5 T perpendicular to the beam axis was applied at the entrance to the cup. Additionally an electron shield ring with a potential of +5 kV was mounted between the film sample and the Faraday cup.

Irradiations with ^{60}Co γ rays and 10-MeV electrons were in open air, whereas irradiations with heavy particles took place in a vacuum. The film response for a given dose was found to be independent of these two irradiation conditions (*11, 12*).

RESULTS

Experimental dose–response characteristics for the different radiations are given in Figs. 2 and 3. At doses below $5 \cdot 10^4$ Gy the curves for 10-MeV electrons and ^{60}Co γ rays are identical, but the maximum optical density is considerably higher for the 10-MeV electrons than for ^{60}Co γ rays. The D_{37} values are $3.3 \cdot 10^5$ and $1.7 \cdot 10^5$ Gy, respectively.

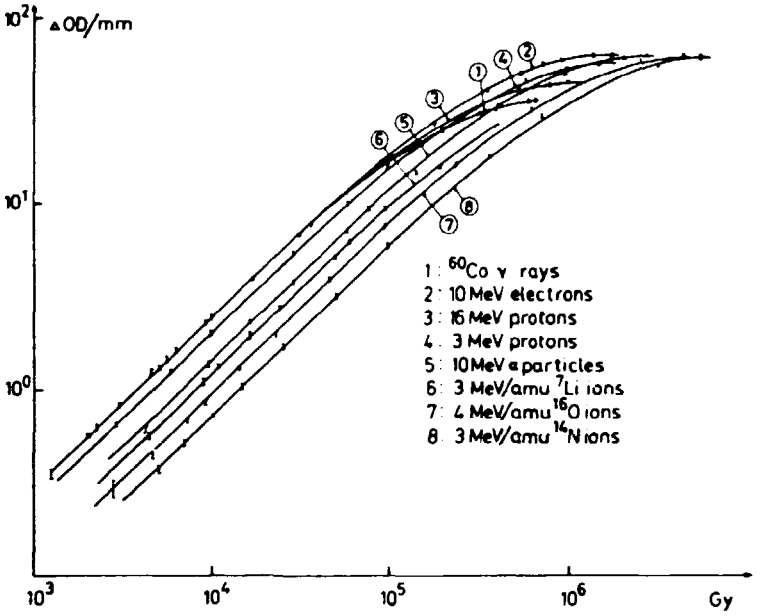

FIG. 2. Dose-response characteristics of the FWT 60 radiochromic dye film dosimeter measured for different radiation qualities.

The dose-response curves in Fig. 2 are all parallel at least up to approximately ΔOD/mm = 10, with a slope of 43°. The saturation optical density for the ^{14}N and ^{16}O ions is the same as for 10-MeV electrons.

The measured effectiveness of the ions, RE, can be found from the initial slope of the curves (see Fig. 3), or from the parallel displacement of the response curves in Fig. 2. Any minor difference between the two sets of results is insignificant. The

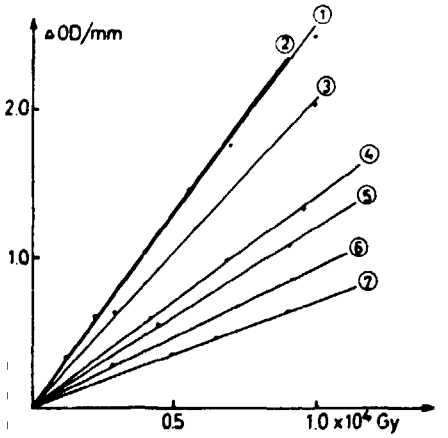

FIG. 3. Initial part of the dose-response characteristics shown in Fig. 2. (1) ^{60}Co γ rays, 10-MeV electrons; (2) 16-MeV protons; (3) 3-MeV protons; (4) 10-MeV α particles; (5) 3 MeV/a.m.u. ^{7}Li ions; (6) 4 MeV/a.m.u. ^{16}O ions; and (7) 3 MeV/a.m.u. ^{14}N ions.

uncertainty in a given RE value depends on several factors which will be described below.

The dosimetry for the ^{60}Co γ rays and the 10-MeV electrons has an uncertainty of dose within $\pm 2\%$, and the precision of the low-LET dose–response measurements is $\pm 5.5\%$ [total random uncertainty at 95% confidence level (*13*)] determined from the uncertainties associated with the individual measurements involved in an experimental data point. The accuracy of the particle fluence data is difficult to determine because a contamination of the ion beam with secondary electrons from the beam collimators and escaping secondary electrons from the Faraday cup may introduce systematic errors, although certain precautions against these sources of error have been taken as described above. The precision of the dose–response measurements for ions is $\pm 7.4\%$ (determined as for the low-LET dose–response measurements). The uncertainty in the proton stopping power is less than 1% for energies above 400 keV and $\pm 10\%$ for lower energies (*6*), and the method of calculating the stopping power for the ions in a compound material may introduce an additional error of about 10% (*14*). Based on these considerations the overall uncertainty at about 95% confidence level of experimental RE values is $\pm 12.2\%$ calculated as recommended by IAEA (*13*).

The uncertainty in stopping power data influences the determination of absorbed dose to the film and consequently the dose–response characteristics of the ions and measured RE. RE decreases proportionally to increasing stopping power. The influence on calculated RE from uncertainties in stopping power is most noticeable at those values of stopping power causing a RE much less than unity. A 10% increase in stopping power causes a 2% decrease in RE for the 16-MeV protons, 6% for the 3-MeV protons, and 10% for the 4-MeV/a.m.u. ^{16}O ions. A comparison between experimental and calculated RE is then for small RE unaffected by the uncertainty in stopping power data. The RE for the ion beams has been calculated from the track structure theory taking the radius of the sensitive element, a_0, equal to 1 nm. The dose distribution around the ion path is calculated from the Bethe energy distribution formulation for δ rays and the stopping power for low-energy electrons. Due to considerable uncertainties in the Bethe formula at low energies a cut-off in the calculations of the absorbed dose by the δ rays is made at 100 eV by having an area of radius a_0 with the center at the ion path considered separately. The energy absorbed over this area is calculated by a subtraction of the energy deposited in the track outside the central area from the total energy deposited by the moving ion. This method restricts the use of the Bethe formula to energies above 100 eV, and allowance is also made for that part of the energy which is deposited as primary excitation energy close to the ion path (*15*).

Two different range–energy relations for low-energy electrons have been used in the dose distribution calculations. The linear relation $r = k_1 \cdot \omega$ with r = range and ω = energy, leads to a point-target dose distribution, $a_0 \sim 0$, given by

$$D(z,\beta,t) = \frac{C}{2\pi} \cdot \frac{z_{eff}^2}{\beta^2} \cdot \frac{1}{t^2}\left[1 - \frac{t}{t_{max}}\right] \tag{9}$$

where $C = 2\pi \cdot N \cdot e^4/mc^2 = 1.34 \cdot 10^{-12} \cdot \rho$ J m^{-1}, t is the distance from the center of the ion path, and $t_{max} = k_1 \cdot \omega_{max} \cdot \rho^{-1}$ is the maximum range of the δ rays in the film of density ρ. $\omega_{max} = 2mc^2\beta^2(1 - \beta^2)^{-1}$ is the maximum energy of the δ rays

ejected by the ion of velocity β relative to the velocity of light. $k_1 = 10^{-8}$ g cm^{-2} eV^{-1} is used in the work of Kobetich and Katz (*16*). $N = A_0 \cdot n_e \cdot \rho \cdot \mathrm{Mw}^{-1}$ is the electron density of the film, where A_0 is the Avogadro number, n_e is the number of electrons per molecule, and Mw is the molecular weight. z_{eff} is the effective charge of the moving ion of relative velocity β. The effective charge was obtained from the formula given by Ziegler (*7*).

The power-law relation $r = k_2 \cdot \omega^{\alpha}$ leads to a point-target dose distribution, $a_0 \sim 0$, given by

$$D(z,\beta,t) = \frac{C}{2\pi} \cdot \frac{z_{\mathrm{eff}}^2}{\beta^2} \cdot \frac{1}{\alpha} \cdot \frac{1}{t^2} \left[1 - \frac{t}{t_{\max}}\right]^{\alpha^{-1}} \tag{10}$$

where $\alpha = 1.67$ and $k_2 = 5.22 \cdot 10^{-11}$ g cm^{-2} eV$^{-\alpha}$ is found by fitting to published data (*17–19*).

The calculated radial dose distributions have been tested by comparison with experimental data (*20*) and continuous slowing down model calculations (*20*) for 42-MeV ^{79}Br ions in a tissue-equivalent unit-density gas (Rossi-type). The results are shown in Fig. 4 and Table I. The percentage deviation of calculated values using Eq.

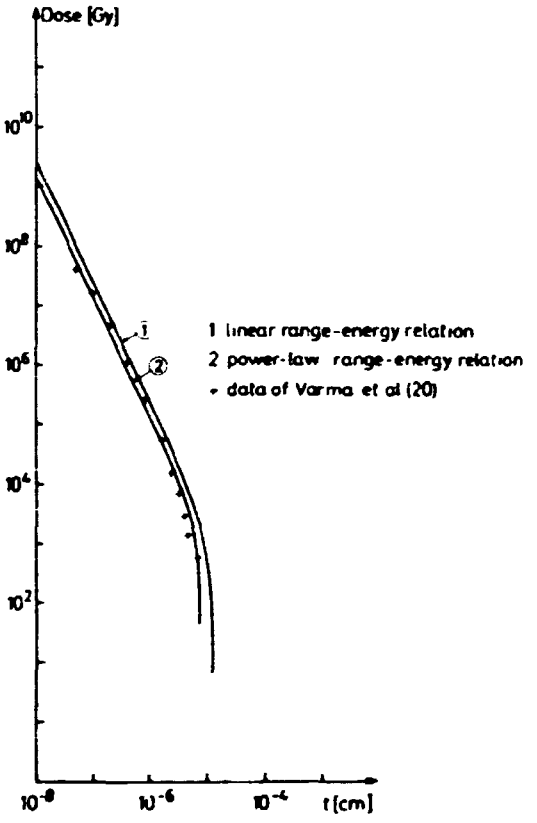

FIG. 4. Dose as function of distance from the ion's path of a 42-MeV ^{79}Br ion in a tissue-equivalent unit-density material calculated from Eqs. (9) and (10) and compared with published experimental data (*20*).

TABLE I

Dose as a Function of Radial Distance for a 42-MeV Bromine Ion in Tissue-Equivalent Unit-Density Material

t (nm)	D (Gy)[a]	D (Gy[b], %[c])	D_1[d] (Gy, %[c])	D_2[e] (Gy, %[c])
0.5	$3.9 \cdot 10^7$	$5.0 \cdot 10^7$, +28	$9.2 \cdot 10^7$, +136	$5.5 \cdot 10^7$, +41
1.05	$1.5 \cdot 10^7$	$1.3 \cdot 10^7$, −13	$2.1 \cdot 10^7$, +39	$1.2 \cdot 10^7$, −17
2.1	$4.8 \cdot 10^6$	$3.5 \cdot 10^6$, −27	$5.2 \cdot 10^6$, +7	$3.1 \cdot 10^6$, −36
4.2	$1.1 \cdot 10^6$	$9.2 \cdot 10^5$, −16	$1.3 \cdot 10^6$, +15	$7.6 \cdot 10^5$, −31
8.4	$2.6 \cdot 10^5$	$2.3 \cdot 10^5$, −8	$3.0 \cdot 10^5$, +17	$1.8 \cdot 10^5$, −30
16.8	$5.6 \cdot 10^4$	$5.3 \cdot 10^4$, −5	$7.0 \cdot 10^4$, +25	$4.2 \cdot 10^4$, −26
25.2	$1.6 \cdot 10^4$	$1.7 \cdot 10^4$, +6	$2.9 \cdot 10^4$, +78	$1.7 \cdot 10^4$, +4
33.7	$7.0 \cdot 10^3$	$7.2 \cdot 10^3$, +3	$1.5 \cdot 10^4$, +107	$8.2 \cdot 10^3$, +17
42.1	$2.9 \cdot 10^3$	$3.2 \cdot 10^3$, +10	$8.3 \cdot 10^3$, +187	$4.5 \cdot 10^3$, +54
50.5	$1.4 \cdot 10^3$	$1.6 \cdot 10^3$, +14	$5.1 \cdot 10^3$, +267	$2.5 \cdot 10^3$, +77
70.9	$6.0 \cdot 10^2$	$5.2 \cdot 10^2$, −13	$1.8 \cdot 10^3$, +200	0
Standard deviation σ =		5%	39%	12%

[a] Experimental data of Varma *et al.* (*20*).

[b] Data obtained from continuous slowing down model calculations by Paretzke (*20*).

[c] The percentage deviation: $\frac{\text{Calc.} - \text{Exp.}}{\text{Exp.}} \cdot 100$.

[d] Dose calculated from Eq. (9).

[e] Dose calculated from Eq. (10).

(9) from those experimentally obtained varied from +267 to +7%, with a standard deviation of 39% over the range of distances from the ion path of 0.5 to 70 nm. Results obtained by using Eq. (10) varied from +77 to −36%, with a standard deviation of 12%. Radial dose distributions calculated by means of Eq. (10) agree with published calculated data (*15*) for 2-MeV/a.m.u. C ions, 8-MeV/a.m.u. Ne ions, and 90-MeV/a.m.u. Fe ions with a standard deviation of 10, 9, and 6%, respectively, over the range of distances from 0.3 to 10^5 nm.

In the calculation of the activation cross section σ_T and the RE, an average dose deposited in the sensitive element in the film must be calculated. The average dose $\bar{D}(z,\beta,t,a_0)$ to the sensitive element with radius a_0 positioned at a distance t from the path of the ion of effective charge z and relative velocity β is given by

$$\bar{D}(z,\beta,t,a_0) = \frac{1}{\pi a_0^2} \int_{t-a_0}^{t+a_0} D(z,\beta,l) \cdot A(t,a_0)\,dl \tag{11}$$

where $A(t,a_0)$ is a geometry function determined by the shape of the sensitive volume element. This element is in our calculations considered as a cylinder of radius and length equal to a_0, and positioned with the axis of symmetry parallel to the ion's path, thus leading to $A(t,a_0) = 4\,Arctg\sqrt{[a_0^2 - (t_0 - t)^2]/[(t_0 + t)^2 - a_0^2]}$. t_0 is the distance from the ion's path to the center of the sensitive element. a_0 is a fitted parameter the value of which determines the calculated RE. We have chosen a value of 10^{-7} cm corresponding to an estimated size of the dye molecule which also gives the best fit of the calculated RE to the experimentally obtained RE. The extended target dose

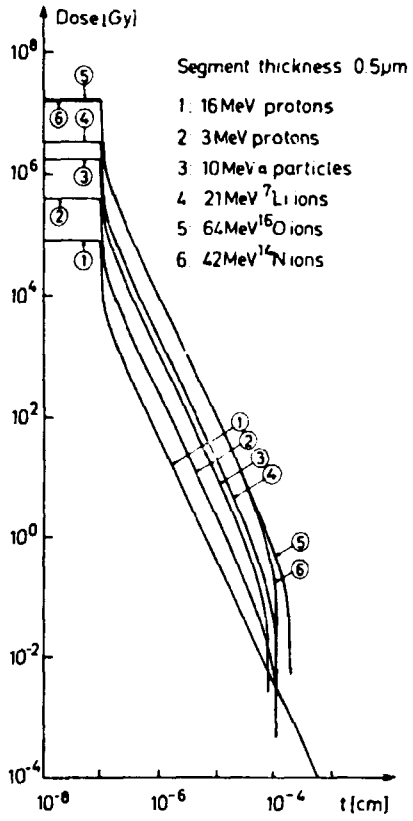

FIG. 5. Average dose to the sensitive element in the FWT 60 radiochromic dye film as a function of distance from the ion path calculated from Eq. (11). The dose profiles are for the investigated ions and for the first segment of calculation.

distribution $\bar{D}(z,\beta,t,a_0)$ calculated by means of Eqs. (10) and (11) is shown in Fig. 5.

The average RE of the ions in the dye film has been calculated by dividing the 55-μm-thick film into a number of segments and in each segment determining average values of z_{eff}, β, σ_T, and RE. The number of segments used is large enough so that the RE converges; e.g., for the ^{14}N ions 100 segments are used. The RE value for each segment is weighted against the ratio of the dose deposited in that segment to the total dose deposited in the film. The results are given in Tables II and III, while experimental RE and initial and average values of LET and z_{eff}^2/β^2 are given in Table IV.

The values of RE shown in Tables II and III are calculated using the Poisson statistics for a one-hit detector. The results shown in Fig. 2 indicate that the expression should be modified with an exponent m as

$$P(z,\beta,t,a_0) = (1 - \exp(-\bar{D}(z,\beta,t,a_0)/D_{37}))^m \qquad (12)$$

without taking variations in maximum optical density into consideration. $m = 0.945$

is a fitted parameter. The values of RE obtained from this modification differ insignificantly from the values given in Tables II and III.

DISCUSSION

The results in Table II reveal a remarkable agreement between theory and experiment. Taking $D_{37} = 3.3 \times 10^5$ Gy, theory and experiment agree within experimental uncertainty, which must be considered as a major success of the track structure theory and taking the wide range in LET and z^2_{eff}/β^2 into account.

The power law for the range–energy relation leads to a radial dose distribution (Eq. (10)) around the ion path in good agreement with published data (*15, 20*) at ranges above 0.3 nm corresponding to δ-ray energies above 50 eV. The disagreement below 50 eV is certainly due to an underestimation of the range in our exponential fit to the published range–energy data (*17–19*) and to the uncertainty in the Bethe energy distribution formula at low energies. These discrepancies have a limited influence on our calculations, because of the splitting of the dose to the central core and the dose to the track as described in the previous section. The comparison of experimental and calculated RE values shows the improvement introduced by the use of the power-law range–energy relation in Eq. (10). REs calculated from the linear range–energy relation, Eq. (9), deviate considerably from those determined experimentally at high LET as shown in Table III.

If we consider the relative effectiveness as a function of either initial or average LET as shown in Table IV, no monotonic decrease in RE is found with increasing LET. The 64-MeV ^{16}O ions have both higher initial and average LET than the 42-MeV ^{14}N ions, and also a higher RE. This may be explained by reference to the curves in Fig. 6. In the case of 42-MeV ^{14}N ions the Bragg peak lies within the dye film, and since z^2_{eff}/β^2 increases smoothly through the Bragg peak, the average z^2_{eff}/β^2 in the film will be much higher than the average LET. With 64-MeV ^{16}O ions the Bragg peak is not reached in the dye film, and LET and z^2_{eff}/β^2 increase continuously

TABLE II

Experimental Values of RE Compared to Calculated RE Based on Eq. (10) with a D_{37} Value of $1.7 \cdot 10^5$ and $3.3 \cdot 10^5$ Gy

	RE_{exp}[a]	RE_{cal} 1[b], %[c]	RE_{cal} 2[d], %[c]
^{60}Co γ rays	1.00	1.00	
10-MeV electrons	1.00		1.00
16-MeV protons	1.00	0.92, −8.0	0.96, −4.0
3-MeV protons	0.81	0.65, −19.8	0.76, −6.2
10-MeV α particles	0.55	0.47, −14.6	0.52, −5.5
21-MeV ^7Li ions	0.47	0.42, −10.6	0.46, −2.1
64-MeV ^{16}O ions	0.36	0.36, 0	0.38, +5.6
42-MeV ^{14}N ions	0.28	0.31, +10.7	0.32, +14.3

[a] RE derived from the initial slope of the dose-response characteristics.

[b] RE calculated by means of Eq. (10) for $D_{37} = 1.7 \cdot 10^5$ Gy.

[c] The percentage deviation: $\frac{\text{Calc.} - \text{Exp.}}{\text{Exp.}} \cdot 100$.

[d] RE calculated by means of Eq. (10) for $D_{37} = 3.3 \cdot 10^5$ Gy.

TABLE III

Experimental Values of RE Compared to Calculated RE Based on Eq. (9) with a D_{37} Value of $1.7 \cdot 10^5$ and $3.3 \cdot 10^5$ Gy

	RE_{exp}[a]	RE_{calc} 1a[b], %[c]	RE_{calc} 2a[d], %[c]
^{60}Co γ rays	1.00	1.00	
10-MeV electrons	1.00		1.00
16-MeV protons	1.00	0.97, −3.0	0.99, −1.0
3-MeV protons	0.81	0.80, −1.2	0.88, +8.6
10-MeV α particles	0.55	0.64, +16.4	0.71, +29.1
21-MeV ^{7}Li ions	0.47	0.57, +21.3	0.65, +38.3
64-MeV ^{16}O ions	0.36	0.48, +33.3	0.60, +66.7
42-MeV ^{14}N ions	0.28	0.44, +57.1	0.48 +71.4

[a] RE derived from the initial slope of the dose-response characteristics.
[b] RE calculated by means of Eq. (9) for $D_{37} = 1.7 \cdot 10^5$ Gy.
[c] The percentage deviation: $\frac{\text{Calc.} - \text{Exp.}}{\text{Exp.}} \cdot 100$.
[d] RE calculated by means of Eq. (9) for $D_{37} = 3.3 \cdot 10^5$ Gy.

during passage of the film. With increasing z^2_{eff}/β^2 the range of the δ rays decreases, and relatively more energy is deposited in a region of saturation close to the ion path with a resulting decrease in RE (*21*), see Fig. 7.

That RE also depends on β (*22*) is illustrated by curves 1 and 2 in Fig. 7, where two ions with the same average $z^2_{eff}/\beta^2 = 6630$, but with different average relative velocity, $\beta = 8.02 \cdot 10^{-2}$ and $1.85 \cdot 10^{-2}$, have an RE of 0.39 and 0.20, respectively.

The experimental results in Fig. 2 show that the dye film is not an ideal detector with a dose–response characteristic in accordance with Eq. (1). The response is slightly sublinear and does not have a constant saturation level for the different investigated radiation qualities. This may be due to several factors. The chemical reactions leading to the final dye formation have not yet been established in detail, although it is known that the reaction takes place in at least two steps, the latter being fairly slow in solids (*11, 23*). An intermediate product may react with the primary radicals and ions in an as yet unknown fashion and simultaneous bleaching may compete slightly with

TABLE IV

Experimental Values of RE Compared to Initial and Average Values of LET and z^2_{eff}/β^2

	RE_{exp}	LET_∞[a]	LET_{av}[a]	$(z^2_{eff}/\beta^2)_{init}$	$(z^2_{eff}/\beta^2)_{av}$
^{60}Co γ rays	1.00				
10-MeV electrons	1.00	2.1	2.1		
16-MeV protons	1.00	28	28	29.1	29.3
3-MeV protons	0.81	120	135	155	180
10-MeV α particles	0.55	551	628	740	910
21-MeV ^{7}Li ions	0.47	1058	1228	1375	1651
64-MeV ^{16}O ions	0.36	5434	6740	6598	8835
42-MeV ^{14}N ions	0.28	5087	6689	6611	9845

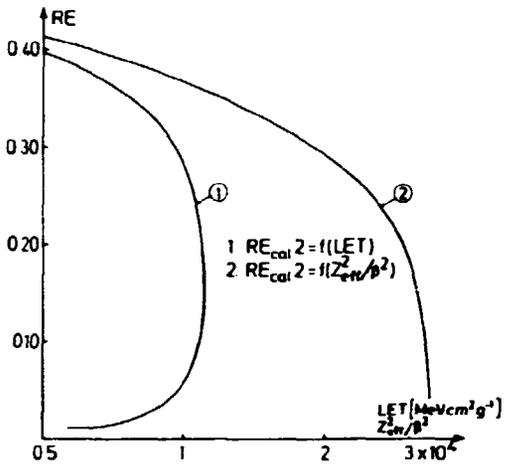

FIG. 6. RE as a function of LET and z^2_{eff}/β^2 for a ^{14}N ion with an initial energy of 42 MeV being completely stopped in the FWT 60 radiochromic dye film.

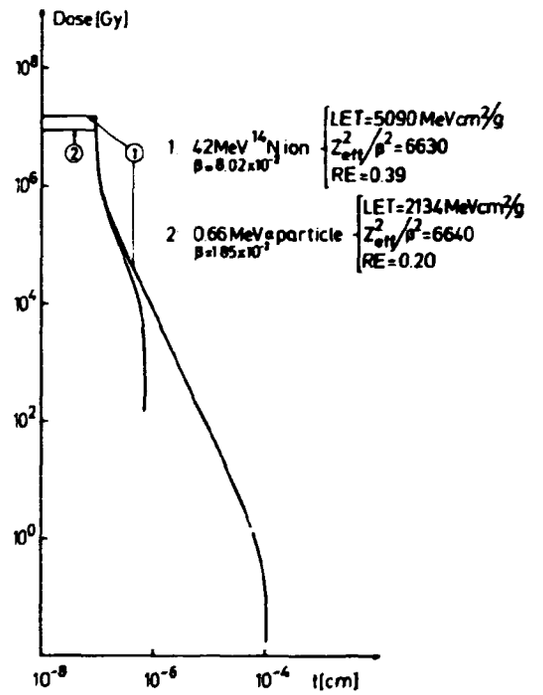

FIG. 7. Average dose to the sensitive element as a function of distance from the ion's path for a 42-MeV ^{14}N ion and a 0.66-MeV α particle having the same average $z^2_{eff}/\beta^2 = 6630$ in a 0.5-μm-thick segment of the dye film.

dye formation. Likewise, the nylon matrix may be seriously deformed at the high doses employed, and if this deformation takes place at the same time as irradiation proceeds, the effectiveness of the irradiation may change as well. An investigation of the mechanisms controlling the dye formation and bleaching effects is beyond the scope of the present work.

The difference in saturation optical density can be due to dose-rate effects at high doses. Previous publications have shown the film to be dose-rate independent at low to medium doses (*24*) except at very low dose rates, <1 Gy sec^{-1}, (*25*). The dose rate for ^{60}Co γ rays is 14 Gy sec^{-1}, but $5 \cdot 10^7$ Gy sec^{-1} for the 10-MeV electrons. The dose rate for the ions expressed as an average dose rate calculated from absorbed dose and irradiation time is approximately 10^3 Gy sec^{-1}. Taking the highly inhomogeneous dose distribution for high-LET particles into account by considering an average dose rate in microvolumes around the ion path, a more appropriate dose rate is obtained. A 64-MeV ^{16}O ion penetrating the film has an effective average dose rate in the track of 10^7 Gy sec^{-1}, if the energy is absorbed within 1 μsec corresponding to the length of the 10-MeV linac electron pulse. This dose rate is comparable to that of the 10-MeV electrons. Similar calculations for the 16-MeV protons give an effective average dose rate of 500 Gy sec^{-1}, which is only an order of magnitude higher than for ^{60}Co γ rays. These considerations agree with the experimental findings, which show the saturation optical density to be an increasing function of dose rate.

D_{37} expresses the radiation sensitivity of a detector and in the theory (*1, 2*) is related to the response at saturation dose for low-LET radiation. When the response at saturation is dose-rate dependent, D_{37} appears to be dose-rate dependent as well. By expanding the Poisson distribution function (Eq. (1)) in a Taylor series, P will at low doses be equal to $\bar{D}/D_{37}$, indicating that D_{37} is related to the average energy required to create a dye molecule. Since ^{60}Co γ rays and 10-MeV electrons have the same effectiveness at low doses, D_{37} must be the same for the two radiation qualities, and the apparent difference in D_{37} is due only to variations in the maximum optical density. This variation is probably due to dose-rate effects. At present, however, the theory cannot compensate for such dose-rate effects, which forces us to choose a D_{37} value from a low-LET radiation with a dose rate corresponding to the dose rate of the investigated radiation qualities. This reasoning indicates that the D_{37} value for the 10-MeV electrons is the most appropriate value to use, and the agreement between calculations and experiments is then very good indeed, within −6.2 and +14.3%. These arguments invoked for the D_{37} value also suggest that the initial slope of the dose-response characteristics in Fig. 3 should be used when determining the experimental values of RE.

CONCLUSION

In this work we have shown that the track structure theory of Katz and co-workers is quantitatively capable of predicting dose-response characteristics of high-LET particles in a FWT 60 radiochromic dye film dosimeter. We have introduced a power-law range–energy relation for the δ rays generated by the impinging ion, which makes the dose distribution around the ion path in agreement with published data and improves the predictions of the theory. Though the detector is not ideal as implied by the theory, dose response at low and medium doses can be calculated with an

accuracy of −6 to +14%. We find that, for the dye film dosimeter exposed to radiations having an initial LET range of 28–5440 MeV cm^2 g^{-1}, prediction of RE is not very sensitive to variations in the low-LET D_{37} value.

The track structure theory cannot at present account for dose-rate effects at high doses and accordingly does not predict dose response of the dye film dosimeter at saturation doses.

ACKNOWLEDGMENTS

The authors are indebted to The Niels Bohr Institute, Risø, for providing irradiation time at the tandem Van de Graaff accelerator, to M. Wille for his skillful help in construction of the experimental equipment and for the read-out of the irradiated film samples, and to E. Haugaard for typing the manuscript.

RECEIVED: September 21, 1982; REVISED: March 29, 1983; RE-REVISED: May 23, 1983

REFERENCES

1. R. KATZ, S. C. SHARMA, and M. HOMAYOONFAR, The structure of particle tracks. In *Topics in Radiation Dosimetry* (F. H. Attix, Ed.), Supplement 1, pp. 317–383. Academic Press, New York, 1972.
2. W. L. MCLAUGHLIN, P. E. HJORTENBERG, and B. B. RADAK, Absorbed dose measurements with thin films. In *Dosimetry in Agriculture, Industry, Biology and Medicine*, pp. 577–597. International Atomic Energy Agency, Vienna, 1973.
3. H. DERTINGER and H. JUNG, *Molecular Radiation Biology*. Springer-Verlag, New York/Heidelberg/Berlin, 1970.
4. M. ROSENSTEIN, H. EISEN, M. L. ROUSCH, and J. SILVERMAN, Response of the hexahydroxyethyl pararosaniline cyanide dosimeter to 3 MeV protons. *Int. J. Appl. Radiat. Isot.* **26**, 423–426 (1975).
5. J. W. HANSEN, M. JENSEN, and R. KATZ, The radiochromic dye film dose meter as a possible test of particle track theory. In *Seventh Symposium on Microdosimetry, Oxford* (J. Booz, H. G. Ebert, and H. D. Hartfiel, Eds.), pp. 821–830. Commission of the European Communities, Harwood, London, 1981.
6. H. H. ANDERSEN and J. F. ZIEGLER, *Hydrogen Stopping Powers and Ranges in All Elements*. Pergamon, New York, 1977.
7. J. F. ZIEGLER, *Handbook of Stopping Cross-Sections of Energetic Ions in All Elements*. Pergamon, New York, 1980.
8. H. A. BETHE and J. ASHKIN, Passage of radiations through matter. In *Experimental Nuclear Physics* (E. Segre, Ed.) Vol. 1, p. 205. Wiley, New York, 1953.
9. K. SEHESTED, The Fricke Dosimeter. In *Manual on Radiation Dosimetry* (N. W. Holm and R. J. Berry, Eds.), p. 313. Dekker, New York, 1970.
10. A. BRYNJOLFSSON and G. THAARUP, *Determination of Beam Parameters and Measurements of Dose Distribution in Materials Irradiated by Electrons in the Range of 6 MeV to 14 MeV*. Risø Report No. 53, Risø National Laboratories, Denmark, 1963.
11. J. W. HANSEN, M. WILLE, and K. J. OLSEN, Problems associated with the use of the radiochromic dye film as a radiation dose meter. *Radiat. Phys. Chem.* **23** (1984), in press.
12. W. L. MCLAUGHLIN, Radiochromic dye-cyanide dosimeters. In *Manual on Radiation Dosimetry* (N. W. Holm and R. J. Berry, Eds.), p. 377. Dekker, New York, 1970.
13. IAEA, *Calibration of Dose Meters used in Radiotherapy*. Technical Report Series No. 185, International Atomic Energy Agency, Vienna, 1979.
14. H. BICHSEL, The stopping power of a solid and a gas of the same composition. *Phys. Med. Biol.* **27**, 449–450 (1982).
15. J. FAIN, M. MONNIN, and M. MONTRET, Energy density deposited by a heavy ion around its path. In *Proceedings of the Fourth Symposium on Microdosimetry, Verbania-Pallanza* (J. Booz, H. G. Ebert, R. Eickel, and W. Walker, Eds.), pp. 169–188. Commission of the European Communities, Luxembourg, 1974.

16. E. J. KOBETICH and R. KATZ, Energy deposition by electron beams and δ-rays. *Phys. Rev.* **170**, 391–396 (1968).
17. H. G. PARETZKE and M. J. BERGER, Stopping power and energy degradation for electrons in water vapor. In *Sixth Symposium on Microdosimetry, Brussels, Belgium* (J. Booz and H. G. Ebert, Eds.), pp. 749–758. Commission of the European Communities, Harwood, London, 1978.
18. J. C. ASHLEY, Energy losses on inelastic mean free path of low-energy electrons in polyethylene. *Radiat. Res.* **90**, 433–436 (1982).
19. A. COLE, Absorption of 20-eV to 50,000-eV electron beams in air and plastic. *Radiat. Res.* **38**, 7–33 (1969).
20. M. N. VARMA, J. W. BAUM, and A. V. KUEHNER, Stopping power and radial dose distribution for 42 MeV bromine ions. *Phys. Med. Biol.* **25**, 651–656 (1980).
21. A. A. EDWARDS, LET, ξ^* or z^2/β^2. Which is the best specification of radiation quality? In *Seventh Symposium on Microdosimetry, Oxford* (J. Booz, H. G. Ebert, and H. D. Hartfiel, Eds.), pp. 593–602. Commission of the European Communities, Harwood, London, 1981.
22. R. KATZ, Track structure theory in radiobiology and in radiation detection. *Nuclear Track Detection* **2**, 1–29 (1978).
23. V. DANCHENKO, G. F. GRIFFIN, and S. S. BRASHEARS, Delayed darkening of radiation-exposed radiochromic dye dosimeters. *IEEE Trans. Nucl. Sci.* **NS-28**, 4156–4160 (1981).
24. W. L. MCLAUGHLIN, J. C. HUMPHREYS, H. LEVINE, A. MILLER, B. B. RADAK, and N. RATIVANICH, The gamma-ray response of radiochromic dye films at different absorbed dose rates. *Radiat. Phys. Chem.* **18**, 987–999 (1981).
25. P. GEHRINGER, H. ESCHWEILER and E. PROKSCH, Dose rate and humidity effects on the γ-radiation response of nylon-based radiochromic film dosimeters. *Int. J. Appl. Radiat. Isot.* **31**, 595–605 (1980).

Radiat. Phys. Chem. Vol. 23, No. 4, pp. 455–462, 1984
Printed in Great Britain

0146-5724/84 $3.00 + .00
Pergamon Press Ltd

PROBLEMS ASSOCIATED WITH THE USE OF THE RADIOCHROMIC DYE FILM AS A RADIATION DOSE METER

JOHNNY W. HANSEN and MADS WILLE
Accelerator Department, Riso National Laboratory, DK-4000 Roskilde, Denmark

and

KJELD J. OLSEN
Department of Radiophysics, Copenhagen University Hospital, Herlev, DK-2730 Herlev, Denmark

(*Received* 4 *January* 1983)

Abstract—A thorough investigation has been made of the problems involved in using a dye film dose meter for precision dosimetry at high doses, using both low- and high-LET radiation. The study includes: time course of coloration following irradiation at various dose levels; dose response after irradiation in vacuum or at atmospheric pressure; dose response dependency of temperature during irradiation and dose rate effects at high doses. The dose response characteristics have been measured mainly at 510 nm and over a dose range from 1 kGy to 10^4 kGy, which ranges from the lowest detectable dose to saturation of coloration. The dose response has been found to depend strongly on: the time span between irradiation and measurement; the irradiation temperature; and the dose rate at doses above 50 kGy for low-LET radiation. Irradiation in vacuum (1 P.) and in air produced the same dose response. This work supplements previous investigations of the dye film, which were mainly carried out at lower doses.

INTRODUCTION

DURING AN investigation[1] of a theory of particle track structure[2] by the use of the radiochromic dye film dose meter as a detector, it was found that the knowledge of the behaviour of the dose meter was lacking in several respects. Previous investigations of the dye film have mostly been concerned with dose levels at which the response is linear. We have now exposed the dose meter to doses up to 1–2 MGy, which saturates the formation of dye molecules with low-LET radiation. The film has been irradiated with both ^{60}Co γ-rays, 10 MeV electrons and heavy charged particles covering a range in initial LET of 31–5500 MeV cm^2 g^{-1}. Our investigations have covered: The optical absorption spectrum at various dose levels and radiation qualities; the kinetics of build-up and fading of coloration after exposure to high and low doses; the saturation dose response level; bleaching at very high doses; the dose response after irradiation in air or vacuum; dose rate effects at high doses; and the temperature dependence of the dose response.

This investigation of the dye film at high doses and high LET is a supplement to previous investigations,[3–14] but is of importance to users of the radiochromic dye film when high precision dosimetry is needed.

DOSE METER SYSTEM

The dose meter used in this work is the nylon-based FWT 60, commercially available from Far West Technology Inc., 330 Kellog, Goleta, California, U.S.A. This thin-film radiochromic dye dose meter contains a leucocyanide (hexahydroxyethyl pararosaniline) which is transformed into a coloured state, a dye, by absorption of energy from ionizing or exciting radiation. The radiochromic leucocyanide is dissolved in a nylon matrix at a concentration of 10–15% by weight. The dye has a broad absorption band in a part of the visible spectrum with a maximum at 604 nm. In this work the response to radiation is mostly measured at the wavelength of 510 nm, which is on the edge of this absorption peak. The dose meter is supplied in pieces of 1 × 1 cm^2 with an approximate thickness of 55 μm. For some of our experiments, a very thin film has been used with a thickness of 5 μm but with the same materials and the same content of leucocyanide.

EXPERIMENTAL

The response of the irradiated film samples was measured by means of a scanning photospectrometer[15] with a high spatial resolution. The instrument is calibrated up to an optical density of 3.5 by means of a photographic step tablet supplied by the U.S. National

Bureau of Standards. The light absorption spectra were measured with a Pye Unicam SP8-400 photospectrometer. The thickness of each film sample was carefully measured by means of an electronic gauge unit with a resolution better than 1 μm. The γ-irradiations were carried out on a 3.7×10^{14} Bq ^{60}Co γ-ray facility calibrated[18] against a Fricke dose meter surrounded by a nylon container with a wall thickness of 1 cm providing electron equilibrium. The film samples were irradiated in the same nylon container.

For electron irradiations a pulsed 10 MeV linear electron accelerator was used. The pulse length was 4 μs with a pulse repetition rate of 50 pulses per sec. The dose rate in the pulse was 5×10^{7} Gy s^{-1}. The film samples were irradiated either by passage on a conveyor under a scanned beam or by a straight-ahead collimated beam. In the scanned beam mode the dose was determined by routine water calorimetry,[17] which has been compared to measurements with a Fricke dose meter.[19] A maximum of 50 kGy was given to the film in the scanned beam mode, because a higher dose would involve elevated temperatures influencing the measurements.

In the straight-ahead beam mode the film was placed behind a thick collimator with a circular hole, $d = 7$ mm, determining the beam area on the film. The collimator consisted of a layer of light material, aluminium, thick enough to stop the electrons, and a thick layer of lead to attenuate the produced bremsstrahlung to an insignificant level. The electron beam, which is negligibly influenced from penetrating the thin film, was picked up by a Faraday cup and the integrated charge flux measured. Dose response data obtained at low doses in the straight-ahead beam mode were compared with data obtained at low doses in the calibrated scanned beam mode and a proportionality factor was found for transforming measured integrated charge into dose at high dose levels.

The investigation of the influence of pressure and temperature on the dose response was carried out in an experimental equipment used for irradiation of the film with heavy charged particles. This equipment includes a chamber and Faraday cup, which can be evacuated to less than 10^{-4} Pa or be flushed with a gas at different temperature. This equipment is described in Ref. 1.

The dose absorbed by the film when irradiated with heavy charged particles was calculated from the average stopping power and particle fluence. The dose calculations are described in Ref. 1.

The dose calibration of the ^{60}Co γ-rays and the 10 MeV electrons is accurate within ±2% and the precision of dose interpretation is ±3.2% determined as the root mean square of the uncertainties of the individual measurements involved in an experimental data point. The precision of the heavy charged particle dose measurements including statistical scatter amounts to ±5.2%, but the accuracy of the dose determination depends on the tabulated proton stopping power data[19, 20] and the calculation of stopping power for heavy ions in a compound material.[21] The uncertainty on the proton stopping power data is from 1 to 15%, highest for the lower energies,[19, 20] and the uncertainty on the heavy ion stopping power in a compound material is of the same order of magnitude.[22]

RESULTS AND DISCUSSION

Spectrum

The light absorption spectrum of the dye film has been measured for an unirradiated film sample and samples irradiated with low- and high-LET radiation (Fig. 1). The position of the maximum absorption changes slightly from one batch of film to the other. Irradiation with different radiation qualities to the same medium-range light absorption level causes the same shape of the spectrum. This shows that the formation of dye is independent of how the energy is deposited in the film, either by homogeneously distributed ionizations and excitations as from γ-ray photons and fast electrons or by highly inhomogeneously distributed δ-rays from high-LET particles, or by excitation alone as from UV-light.

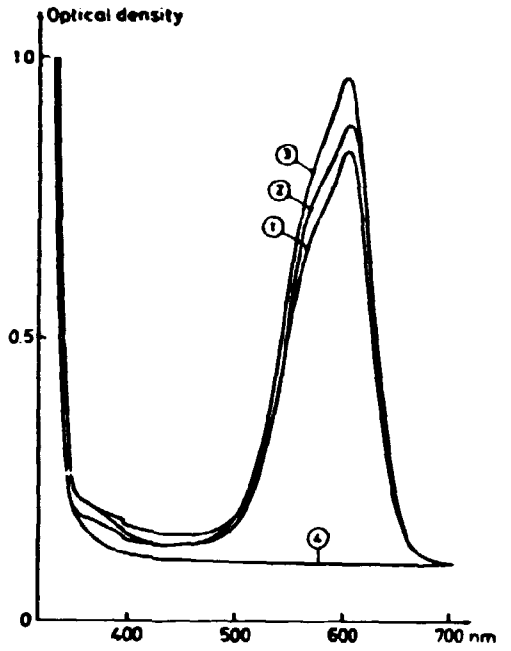

FIG. 1. Light absorption spectra of the dye film irradiated with (1) ^{60}Co γ-rays, (2) UV-light at 250 nm, (3) 3 MeV protons, (4) Spectrum for unirradiated film.

The shape of the spectrum changes when the film is irradiated to very high doses, where saturation and bleaching of the response occurs (Fig. 2). This change in shape implies that different processes take place at the wavelength of 510 and 604 nm and that there is no longer proportionality between response measured at the two wavelengths. From Fig. 1 it appears that the light absorption around 600 nm consists of at least two overlapping peaks with a maximum for the dye at 604 nm.

Changes in colouration after irradiation

The leucocyanide does not change into the coloured state immediately upon irradiation, but intermediate species are formed with an absorp-

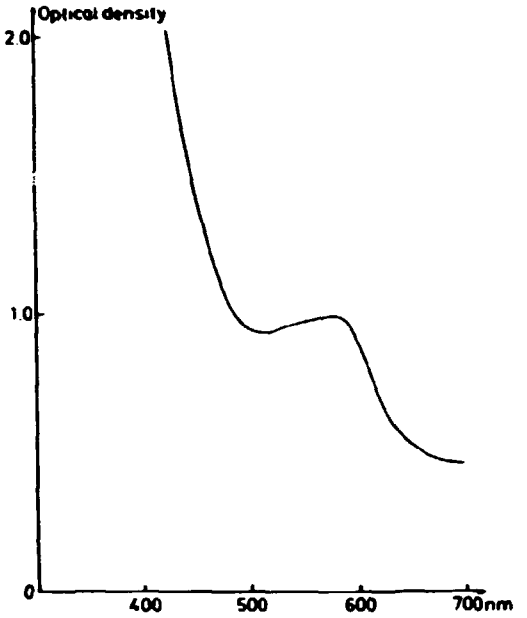

FIG. 2. Light absorption spectrum of the dye film irradiated to a dose of 30 MGy with 64 MeV ^{16}O-ions.

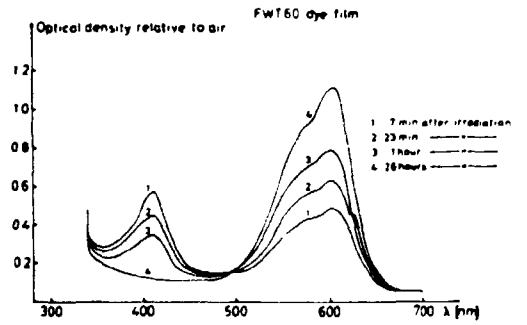

FIG. 3. Light absorption spectrum of the dye film showing the time dependent decay of primary formed species at 412 nm and the build-up of dye at 604 nm after irradiation with 10 MeV electrons. The film is conditioned 24 h in vacuum before irradiation in vacuum.

tion maximum at 412 nm.[11, 23] These rather short-lived species decay and the blue coloured dye is formed with an absorption maximum at 604 nm. In Fig. 3 it is shown how the change in the light absorption spectrum takes place within a time span of 24 h. If the film is preconditioned in vacuum for several hours before irradiation in vacuum, but measured in open air, the time dependent change in spectrum is very pronounced. Under these circumstances the rate of colour formation will presumably be determined by diffusion of oxygen and water into the film material. As the formation of dye is the response to absorbed dose it is very important to measure the optical density when the kinetics in the film have stabilized.

We have investigated the build-up of dye in the film irradiated with γ-rays and 10 MeV electrons under environmental conditions of: open air, preconditioning in 24 h and irradiation in vacuum (~ 1 Pa), nitrogen atmosphere, and vacuum of ~ 1 Pa without preconditioning at doses ranging from 15 to 2000 kGy (Figs. 4–6). The temperature during storage, irradiation and measurement has been kept as close as possible to room temperature (20°C) and the relative humidity has been between 50 and 60%.

Build-up and subsequent fading of the dye after ^{60}Co γ-irradiations at doses from 1.5 to 900 kGy is shown in Fig. 4. The response is expressed in relative change in optical density per unit film thickness. The build-up takes place within the first 20 h after irradiation with a relative rate slowest

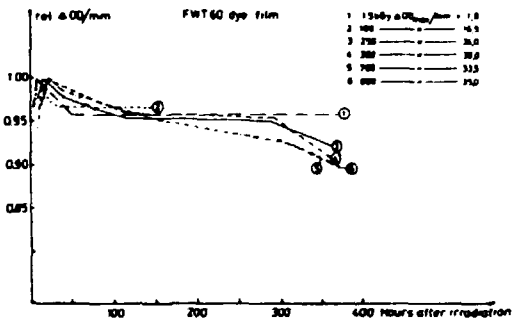

FIG. 4. Time dependent change in relative ΔOD/mm at 510 nm after irradiation in air to different doses of ^{60}Co γ-rays with a dose rate of 14 Gy s^{-1}. The response is normalized with respect to maximum absorption.

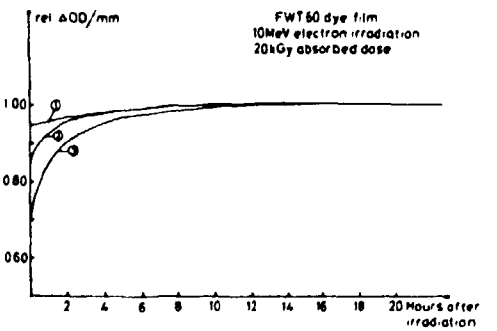

FIG. 5. Time dependent build-up of colour after irradiation in (1) air, (2) N_2-atmosphere, (3) vacuum with preconditioning in 24 h. Absorbed dose of 20 kGy from 10 MeV electrons with a dose rate of 5×10^7 Gy s^{-1}.

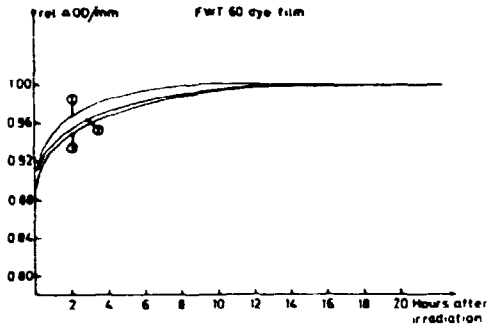

FIG. 6. Time dependent build-up of colour after irradiation in vacuum without preconditioning with 10 MeV electrons to absorbed doses of 0.14, 0.4 and 2 MGy with dose rate of 5×10^7 Gy s^{-1}.

for the highest absorbed doses. Thereafter a decline in a response is observed until about 100 h after irradiation. A plateau is reached 4–5% below maximum response, which for the lowest doses ((0.1 MGy) appears to be constant for a period of time exceeding 350 h, whereas the response for the higher absorbed doses declines further at times exceeding 350 h. The difference ($\sim$2%) in the relative response at the plateau following the maximum may be due to scatter in the individual measurements but the subsequent fading after the peak in build-up is significant.

Build-up of colouration in the first hours following irradiation with 10 MeV electrons to a dose of 20 kGy with a dose rate of 5×10^7 Gy s^{-1} has been monitored for irradiations in air, N_2-atmosphere, and vacuum with preconditioning for 24 h (Fig. 5). The films were measured in open air. The build-up is most pronounced for the film irradiated in vacuum, changing from 30 to 50% below maximum shortly after irradiation ($\sim$ 10 min) until maximum was obtained 15–20 h later. The build-up following irradiations in air and nitrogen amounts to 10–20%, respectively, shortly after irradiation and maximum is achieved after about 10 h.

The rate of build-up of colour after irradiation is dose and dose rate dependent and the build-up depends further on the content of oxygen and water in the film material during irradiation. Previous investigations[13] at low doses and dose rates have also shown a dose rate dependency.

To simulate a situation most common for the use of the dose meter in a vacuum environment the film was kept under normal air storage conditions but irradiated in vacuum with 10 MeV electrons at doses ranging from 0.14–2 MGy. The build-up of colouration is shown in Fig. 6. It is seen that despite the big dose range and subsequent different time of exposure to vacuum, the build-up of coloration peaks after a period of 10–20 h.

Absolute optical density readings of film samples irradiated in open air and in vacuum has been compared at doses of 10, 100 and 500 kGy. No significant difference in dose response was found, but a tendency of recording slightly higher response (4%) at high doses ($\sim$ 500 kGy) for samples irradiated in vacuum was recorded. This, we believe, is due to a higher temperature in the film during irradiation in vacuum, because in this case the heating caused by the irradiation can only be dissipated through heat radiation.

Dose-response characteristics

From the light absorption spectrum of the dye film (Fig. 1), it is seen that any wavelength 350–650 nm can be used as the characteristic wavelength for calibration of the dose meter. The highest sensitivity to radiation is obtained at 604 nm, which mainly reflects light absorption of the pure dye. The broad peak around 600 nm consists of two overlapping peaks, which is seen from the bump on the leading edge of the peak. This in fact indicates that more than one single reaction takes place following irradiation. Dose response has been measured at 600, 510 and 494 nm (Fig. 7). The manufacturer of the film recommends measurements at 600 nm for γ-ray and electron doses below 30 kGy and at 510 nm at higher doses. The wavelength of 494 nm has been chosen because of being an isosbestic point[24] (Fig. 3), which is stable in time within the first 24 h after irradiation and thus independent of build-up of colour. Though the sensitivity of the film to

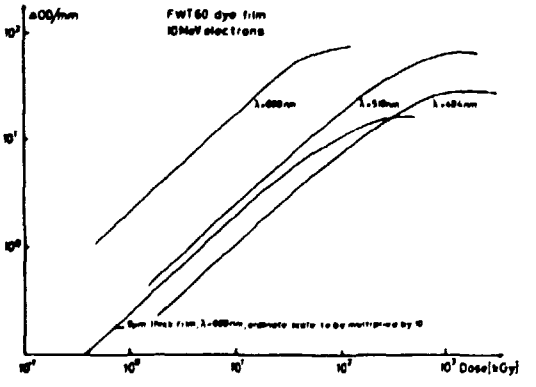

FIG. 7. Dose response characteristics of the dye film irradiated with 10 MeV electrons and measured at the wavelength of 600, 510 and 494 nm. The ordinate scale has to be multiplied by 10 for the 5 μm thick film.

irradiation is down by a factor of about 2.5 at 494 nm as compared to measurements at 510 nm, the 494 nm should be preferred to 510 nm. The shape of the dose response characteristics in Fig. 7 are the same except for the 600 nm response at saturation. This difference may be caused by the photospectrometer as the optical density is more than 4. The slope in the log–log plot of the dose-response is less than 45° indicating sublinearity.

A single mechanism of response to irradiation, such as breaking of a double bond in the leucocyanide molecule, shall according to hit- and target-theory[25] show a dose response characteristic, which follows a Poisson distribution function for a one-hit detector. This means that a single ionizing or exciting event with an energy deposition above a certain threshold (3.8 eV) may lead to the formation of a coloured dye molecule. The Poisson distribution function can for the dye film dose meter be expressed as $\Delta OD/mm = \Delta OD/mm_{max} \times (1 - \exp(-D/D_0))$, where $\Delta OD/mm_{max}$ is the maximum obtainable coloration and D_0 is a characteristic dose at which 63% of maximum coloration is achieved. This distribution function is linear at low doses and has a slope of 45° in a log–log plot.

We have investigated the very thin, 5 μm, FWT 60 film in order to see whether the dose response measured at the wavelength of 600 nm follows a Poisson distribution function up to saturation doses (Fig. 7). The thin film can be measured at the absorption maximum even at saturation optical density. The shape and slope of the dose response characteristic is the same as for the thick film measured at 510 nm, showing the same sublinearity and response at saturation doses. This shows that the difference in shape of the dose respone for the thick film measured at 600 and 510 nm is due to saturation of the photospectrometer.

Dose-response characteristics of the dye film have been obtained for various radiation qualities: 3 and 16 MeV protons, 10 MeV α-particles, 21 MeV ^{7}Li-, 42 MeV ^{14}N-, and 64 MeV ^{16}O-ions covering a range in initial LET of 31–5500 MeV cm^2 g^{-1} corresponding to an average LET in the film of 31–7200 MeV cm^2 g^{-1}. The dose response characteristics measured at the wavelength of 510 nm are shown in a log–log plot (Fig. 8), together with the dose response characteristics obtained for ^{60}Co γ-rays and 10 MeV electrons. All the curves are parallel at low doses with the same slope up to approximately ΔOD/mm = 10, but the saturation optical densities are different. At doses below 50 kGy the curves

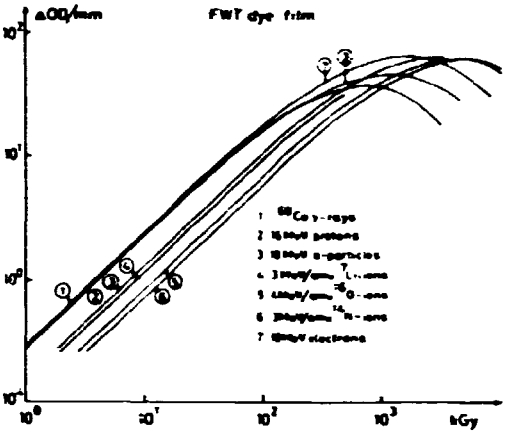

FIG. 8. Dose response characteristics of the dye film irradiated with ^{60}Co γ-rays, 10 MeV electrons, and heavy charged particles of varying radiation quality.

for ^{60}Co γ-rays and 10 MeV electrons are identical, but the maximum optical density is considerably higher for the 10 MeV electrons than for ^{60}Co γ-rays. The saturation optical density for the 42 MeV ^{14}N- and 64 MeV ^{16}O-ions is the same as for the 10 MeV electrons, whereas the saturation optical density for the 3 and 16 MeV protons and the 10 MeV α-particles is between the saturation optical density for ^{60}Co γ-rays and 10 MeV electrons. The parallel displacement of the curves relative to the curve for ^{60}Co γ-rays and 10 MeV electrons reflects the relative effectiveness, RBE, of the different radiation qualities.[1]

The leucocyanide content in the film is ~10% by weight (information from manufacturer). With an extinction coefficient of approximately 10^4 l mol^{-1} cm^{-1}[21,26] a theoretical saturation optical density at the wavelength of 604 nm is calculated to OD ≈ 120 for a 55 μm thick film. This value of optical density at 604 nm is by no means obtained for the 55 μm thick film showing that not all leucocyanide molecules are converted into the coloured dye at saturation. At a 10% content by weight the concentration of leucocyanide molecules is 1.1×10^{20} molecules/g if they are homogeneously distributed in the film. If an event size of 60 eV[27] is estimated, the number of event sites per gram of film is 2.1×10^{20} at a saturation dose of 2 MGy. This consideration leads to the conclusion that all existing leucocyanide molecules in average experience 2 hits if all the energy is absorbed by the leucocyanide molecules, and that the maximum obtainable optical density theoretically should be achieved. If the energy is homogeneously distributed on both leucocyanide

and nylon molecules calculations show that only 20% of the existing leucocyanide molecules are hit once at a dose of 2 MGy. If this is the case no saturation in dye formation would be observed in the investigated dose range.

Sublinearity in the dose response can be due to several reaction mechanisms one of which is the destruction of latent colour centers.[29,29a] Another possible explanation is that a reduction in radiation induced radical yield is due to annealing effect.[30a] In a previous section it has been shown that the reaction leading to the dye formation takes place in at least two steps, the latter being fairly slow. The intermediate product may react with the primary radicals and ions in a way annealing the otherwise formed coloured carbonium ion.

The shape of the curves in Fig. 8 are almost identical showing that the same reaction mechanisms take place independent of whether the energy is deposited homogeneously as from ^{60}Co γ-rays and 10 MeV electrons or highly inhomogeneous as from the heavy charged particles.

Bleaching effects

From the dose-response characteristic in Fig. 8 it is seen that irradiating the film into doses above saturation causes a bleaching effect. This destruction of the formed dye at high doses is not unexpected because radiation in addition to producing colour centers also can destroy colour centers. The nylon matrix may be seriously deformed at the high doses employed, and if this deformation takes place at the same time as irradiation proceeds the effectiveness of the radiation may change as well. At doses above saturation the shape of the spectrum changes (Fig. 2) and the peak at 604 nm starts to decrease before the optical density at 510 nm decreases.

Attempts[12] to explain the sublinearity as due to a bleaching effect and trials to accomplish linearity by adding a dose response curve for bleaching to the dose response curve for colour formation fail. This is because the saturation optical density and bleaching as a function of dose are not constant for different radiation qualities (Fig. 8). We have irradiated the dye film (55 μm) into saturation with UV-light of different wavelength and with sunlight (broad UV-spectrum). The maximum optical density was dependent on the wavelength of the UV-light and on whether the film was irradiated from one or two sides. Two-sided irradiation with 254 and 340 nm UV-light gave a saturation optical density of ΔOD/mm ~ 25 and ~ 40, respectively. Irradiation with sunlight gave a ΔOD/mm ~ 50. By subsequent irradiation with 10 MeV electrons the optical density at first increased to the same level as if the film was irradiated with electrons from blanc. ΔOD/mm ~ 62, and then decreased as shown in Fig. 8.

Dose rate dependence

Previous investigations[4-6,9] have shown the film to be dose rate independent at low to medium doses except at very low dose rates, < 1 Gy s^{-1}.[11,13,14] The difference in saturation optical density (Fig. 8) may, however, be due to dose rate effects at high doses. At doses below 50 kGy the curves for ^{60}Co γ-rays and 10 MeV electrons are identical, but the maximum optical density is considerably higher for the 16 MeV electrons than for ^{60}Co γ-rays. The dose rate for ^{60}Co γ-rays is 14 Gy s^{-1}, but 5×10^{7} Gy s^{-1} for the 10 MeV electrons. The average dose rate for the ions is approx. 10^{5} Gy s^{-1}. Taking, however, the highly inhomogeneous dose distribution for high-LET particles into account by considering an average dose rate in microvolumes around the path of the moving ion,[1,2,31] a more appropriate dose rate is obtained. A 64 MeV ^{16}O-ion penetrating the film has an average dose rate in the track of 10^{7} Gy s^{-1} if the energy is absorbed within 4 μs corresponding to the length of the 10 MeV linac electron pulse. This dose rate is comparable to the dose rate of the 10 MeV electrons. Similar calculations for the 16 MeV protons give an effective average dose rate of approximately 500 Gy s^{-1}, which is an order of magnitude higher than for ^{60}Co γ-rays. These considerations are in agreement with the experimental observations, which show the saturation optical density to be an increasing function of the dose rate (Fig. 9).

Temperature dependence

In the present work the temperature dependency of the dye film has been monitored at the photospectrometer wavelength of 510 nm. The effect

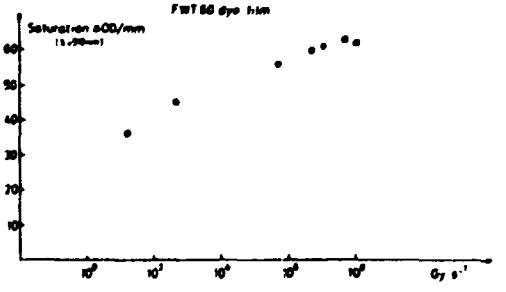

FIG. 9. Saturation optical density as a function of dose rate.

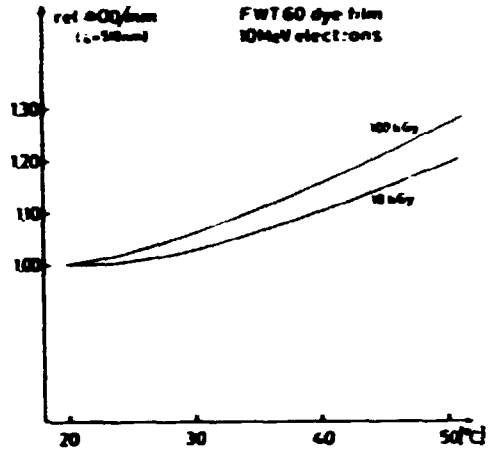

FIG. 10. Temperature effect on dose-response measured at absorbed doses of 10 and 100 kGy.

of increased temperature during irradiation with 10 MeV electrons on dose response was investigated without preconditioning of the film samples. The film samples were placed in the irradiation chamber, which was flushed with heated air, the temperature of which was monitored by means of a thermistor placed close to the film. The dose response dependence on temperature was measured in the temperature range of 20–50°C and at dose levels of 10 and 100 kGy (Fig. 10). The increase in dose response with temperature was in average 0.6 and 0.9%/°C for the dose levels of 10 and 100 kGy, respectively. The temperature effect on dose response is thus dependent on dose, which makes corrections for irradiation temperature complicated. A previous investigation at a dose of 20 kGy[13] has shown dose response to be dependent on temperature with an average of 0.5%/°C in the temperature range of 20–50°C.

CONCLUSION

The experiments described in the present work show that great care must be taken when using radiochromic dye films for more exact ($< \pm 10\%$) dose measurements. Careful measurements of the thickness is important, because film thickness varies within a batch of films, and small surface irregularities can change the final dose reading drastically. The rate of build-up of colour after irradiation is dose- and dose-rate-dependent and depends further on the content of oxygen and water in the film during irradiation. At doses corresponding to a change in optical density per millimeter film thickness > 10 at $\lambda = 510$ nm, the dose response is strongly dose rate dependent. The dose response is temperature dependent, the rate of which is a function of absorbed dose. Readings of optical density at high doses can with advantage be made at an isosbestic point of wavelength, thus avoiding build-up of colour. This point, however, must be measured for the individual batch of film because the isosbestic point changes from batch to batch, as does the wavelength for maximum light absorption in the region of 600 nm.

REFERENCES

1. J. W. Hansen and K. J. Olsen, Experimental and predicted effectiveness of a radiochromic dye film dose meter to high-LET radiation. *Radiat. Res.* To be published.
2. R. Katz, S. C. Sharma and M. Homayoonfar, in *Topics of Radiation Dosimetry*, Supplement 1 (Edited by F. M. Attix), pp. 314–383. Academic Press, New York, 1972.
3. W. L. McLaughlin, *Int. Conf. on Sterilization by Ionizing Radiation*, pp. 219–324. Vienna, Austria, 1974.
4. W. L. McLaughlin, P. E. Hjortenberg and B. B. Radak, *Proc. Symp.*, pp. 577–597. Vienna, IAEA, Vienna, 1973.
5. A. Miller, E. Bjergbakke and W. L. McLaughlin, *Int. J. Appl. Rad. Isotopes* 1975, **26**, 611.
6. W. L. McLaughlin, A. Miller, S. Fidan, K. Pejtersen and W. Batsberg Pedersen, *Radiat. Phys. Chem.* 1977, **10**, 119.
7. A. H. Spiers, *Trans. Faraday Soc.* 1961, **57**, 983.
8. W. L. McLaughlin and L. Chalkley, *Radiology*, 1965, **84**, 124.
9. W. P. Bishop, K. C. Humphreys and P. T. Randtke, *Rev. Sci. Inst.* 1973, **44**, 443.
10. W. L. McLaughlin and M. Kosanic, *Int. J. Appl. Rad. Iso.* 1974, **25**, 249.
11. V. Danchenko, G. F. Griffin and S. S. Brashears, *IEEE Trans. Nucl. Sci.* 1981, **NS-28**, 4156.
12. W. L. McLaughlin, J. C. Humphreys, H. Levine, A. Miller, B. B. Radak and N. Rativanich, *Int. Meet. Radiat. Process.* Tokyo, Japan, 1980.
13. P. Gehringer, H. Eschweiler and E. Proksch, *Int. J. Appl. Radiat. Iso.* 1980, **31**, 595.
14. W. L. McLaughlin, J. C. Humphreys, H. Levine, A. Miller, B. B. Radak and N. Rativanich, *Radiat. Phys. Chem.* 1981, **18**, 5–6, 987.
15. A. Miller, W. L. McLaughlin and B. Lyngaard, *A Scanning Spectrophotometer for Reading Thin-Film Dosimeters*. Risø-M-1525. Risø National Laboratory, 1972.
16. E. Bjergbakke and E. Engholm Larsen, *The 10,000-Ci ^{60}Co Facility and the 3,000-Ci ^{60}Co Gamma Cell*. Risø-M-1651. Risø National Laboratory, 1973.
17. E. M. Fielder, and N. W. Holm, Dosimetry in Accelerator Research and Processing, in *Manual on Radiation Dosimetry* (Edited by N. W. Holm and R. J. Berry), Part 1, pp. 297–300. Marcel Dekker, New York, 1970.
18. K. Sehested, *Manual on Radiation Dosimetry* (Edited by N. W. Holm and R. J. Berry), Part 2, pp. 313–317. Marcel Dekker, New York, 1970.
19. L. C. Northcliffe and R. F. Schilling, *Nuclear Data Tables* 1970, **A7**, 233.

20. W. H. BARKAS and M. J. BERGER *Nuclear Science Series, Rep. No.* 39, NAS-NRC Publication 1133, pp. 103–172.
20. W. H. BARKAS and M. J. BERGER, *Nuclear Science Series, Rep. No.* 39, NAS-NRC Publication 1133, pp. 103–172, 1964.
21. W. H. BRAGG and R. KLEEMAN, *Phil. Mag.* 1905, **10**, 318.
22. H. BICHSEL, *Phys. Med. Biol.* 1982, **27**, 449.
23. W. L. MCLAUGHLIN, M. M. KOSANIC, V. M. MARKOVIC, M. T. NENADOVIC, J. HOLCMAN and K. SEHESTED, *The Kinetics of Dye Formation by Pulse Radiolysis of Pararosaniline cyanide in Aqueous or Organic Solution.* **Risø-M-2202**. Risø National Laboratory, Denmark, 1979.
24. J. R. EDISBURG, *Practical Hints on Absorption Spectrometry*, pp. 13–14. Hilger and Watts, London, 1966.
25. H. DERTINGER and H. JUNG, *Molecular Radiation Biology*, pp. 12–37. Springer Verlag, New York, 1970.
26. W. L. MCLAUGHLIN and M. KOSANIC, *Int. J. Appl. Rad. Iso.* 1974, **25**, 249.
27. A. M. RAUTH and J. A. SIMPSON, *Radiat. Res.* 1964, **22**, 643–661.
28. T. HENRIKSEN, *Radiat. Res.* 1966, **27**, 676.
29. T. HENRIKSEN, *Radiat. Res.* 1966, **27**, 694.
30. J. A. SIMMONS, *Phys. Med. Biol.* 1966, **11**, 597.
31. J. W. HANSEN, M. JENSEN, R. KATZ, *The Radiochromic Dye Film Dose Meter as a Possible Test of Particle Track Theory.* **Risø-M-2243**, Risø National Laboratory, Denmark, 1980.

Nuclear Instruments and Methods in Physics Research B5 (1984) 497–504
North-Holland, Amsterdam

EXPERIMENTAL AND CALCULATED EFFECTIVENESS OF A RADIOCHROMIC DYE FILM TO STOPPING 21 MeV ^{7}Li AND 64 MeV ^{16}O IONS

Kjeld J. OLSEN

Department of Radiophysics, University Hospital of Copenhagen, DK-2730 Herlev, Denmark

Johnny W. HANSEN

Accelerator Department, Risø National Laboratory, DK-4000 Roskilde, Denmark

Received 30 November 1983 and in revised form 9 July 1984

Relative radiation effectiveness, RE, of 21 MeV ^{7}Li and 64 MeV ^{16}O ions being completely stopped in a tissue equivalent film dose meter has been measured as a function of penetration depth and energy, and the results have been compared with calculations based on a δ-ray theory for heavy charged particles developed by Katz et al. The experiment was designed to test calculations particularly in the Bragg-peak region of the slowing down particles where significant deviation between theory and experiment was found. Fitting of the characteristic D_{37} dose and the size of the radiation sensitive element in the detector, which are important parameters in the theoretical model, does not improve the overall correlation between theory and experiment. It is concluded that disagreement between theoretical and experimental RE-values below 1.5 MeV/amu is partly due to lack of equivalence between the δ-ray spectrum and the slowing down spectrum of electrons from low-LET radiation, and partly from approximations in the calculated distribution of energy deposition of the δ-rays.

1. Introduction

The dose-response characteristics of physical detectors exposed to beams of heavy charged particles change considerably with the linear energy transfer (LET) of the particles. The only theory at present which allows a prediction of this change is the δ-ray theory of track structure developed by Katz et al. [1]. This theory considers a detector to be made of sensitive elements, which are activated through interaction processes with δ-rays (secondary electrons) ejected from the path of the heavy ion. The size of the radiation sensitive element is characteristic for the detector, which is assumed to respond with equal effectiveness for a given end-point to this spectrum of δ-rays as to the slowing down spectrum of electrons from a beam of fast electrons or γ-ray photons (low-LET radiation). The difference in dose-response characteristics between low- and high-LET irradiation of the detector is in the theory ascribed to the very inhomogeneous dose distribution around the path of a high-LET particle.

The inhomogeneous dose distribution may be calculated from a knowledge of the δ-ray distribution, differential in angle and energy [2], and from the primary excitation energy deposited very close to the ion path [3]. It has been shown [4] that the radial distribution of dose due to ionizing interactions as calculated from the Bethe theory [5] is in good agreement with experimentally obtained data [6,7] and data obtained from Monte Carlo calculations in continuous slowing down approximation [6,7]. The Bethe formulation of the energy spectrum of δ-rays generated by a heavy ion of velocity β relative to the velocity of light and effective charge z is expressed as $N(\omega) = C(z^2/\beta^2)d\omega/\omega^2$, where $N(\omega)$ is the number of δ-rays per unit pathlength having energies between ω and $\omega + d\omega$, and C is a constant proportional to the number of electrons per unit volume of the penetrated medium. The maximum energy, which can be transferred to an electron from a heavy ion, is obtained from kinematics as $\omega_{max} = 2mc^2\beta^2(1-\beta^2)^{-1}$, where m is the electron rest mass and c the velocity of light. The δ-ray dose distribution may now be calculated from the energy distribution, angular distribution, and stopping power of the δ-rays. For ease of calculation of dose in track segments the angular distribution has been approximated by assuming ejection of δ-rays perpendicular to the track. The range and a subsequent effective stopping power of the δ-rays have been obtained from fitting to experimental [8,9] and theoretical [10,11] range–energy data, from which a power-law range–energy relation of $r = 5.22 \times 10^{-11}\,\omega^{1.67}$ g/cm^2 has been obtained, where r is the range and ω the energy of the electrons in eV. This relation yields improved dose distribution data as compared with a linear relation $r = 10^{-8}\,\omega$ g/cm^2 proposed by Katz.

According to the δ-ray theory the radiation sensitive

0168-583X/84/$03.00

elements grouped around the path of the ion will respond to the local dose deposited there by the generated δ-rays, as if the elements were part of a larger system uniformly irradiated with low-LET radiation to the same dose. Thus, the dose-response characteristic, which is experimentally obtained for the detector irradiated with low-LET radiation, is used to correlate the calculated dose in the elements with a produced effect. The probability that a sensitive element is activated by an ion is given by the Poisson distribution function as $P(z,\beta,t,a_0,D_{37}) = 1 - \exp(-\bar{D}(z,\beta,t,a_0)/D_{37})$, where $P(z,\beta,t,a_0,D_{37})$ represents the fraction of sensitive elements of radius a_0 activated by the incoming ion of relative velocity β, and which are lying at a distance t from the track axis. $\bar{D}(z,\beta,t,a_0)$ is the average dose deposited in the sensitive element at a distance t from the track axis, and is found from a calculation of dose distribution around the ion path. D_{37} is the dose of low-LET radiation at which 37% or e^{-1} of the sensitive elements are not activated by the radiation. The total effect produced by a single ion or a beam of ions is found from an integration of $P(z,\beta,t,a_0,D_{37})$ over all distances t from the axis of the ion's path to the maximum range of the δ-rays. This integration yields the total activation cross section $\sigma(z,\beta,a_0,D_{37})$.

Relative effectiveness, RE, of high-LET radiation to low-LET radiation is defined as the ratio of the doses of the radiations being compared, which produce the same response under identical conditions. RE may as well be derived from the ratio between the radiation sensitivities of the medium towards the radiations involved. The sensitivity of a detector towards low-LET radiation is given by $1/D_{37}$, and the sensitivity towards high-LET radiation is defined [12] as $\sigma(z,\beta,a_0,D_{37})/\mathrm{LET}$, which is the ratio of the total cross section to the average energy deposited by the moving ion per unit pathlength in a unit density medium. The relative effectiveness can then be expressed as $\mathrm{RE} = k\sigma(z,\beta,a_0,D_{37})/\mathrm{LET}$. For D_{37} in Gy and LET in $\mathrm{MeVcm^2g^{-1}}$ the conversion constant k equals $6.24 \times 10^9\ \mathrm{MeVGy^{-1}g^{-1}}$.

Knowing the relative effectiveness, RE, of the ion in the detector as a function of energy (velocity β), the high-LET dose-response characteristic may be calculated. The size of the sensitive element is a parameter in this calculation, which may either be approximately calculated by means of classical target theory [12–14] or by fitting to experimental high-LET data for the detector. For the radiochromic dye film a sensitive element size, a_0, of 10^{-7} cm has been used

The δ-ray theory is proposed to be applicable to "ideal" detectors, which for most physico-chemical detectors means a one-hit response, i.e. only interaction energies above a certain threshold lead to the end-point, whereas accumulation of interaction energies below the threshold cannot take place. An ideal one-hit detector has the following properties [12]: 1) a linear dose-response up to doses comparable to D_{37}, 2) absence of dose rate effect since the sensitive element may be activated by a single electron, and fading or recombination of formed radicals is disregarded, 3) in a double logarithmic plot all dose-response curves will be 45° lines independent of the radiation quality, and 4) the effectiveness, i.e. the response per unit dose for a given end-point will decrease monotonically as a function of LET and the particle velocity.

In our previous study [4] of the response of the radiochromic dye film, FWT-60, to beams of ions ranging from 16 MeV protons (initial LET = 28 $\mathrm{MeVcm^2g^{-1}}$) to 64 MeV oxygen ions (initial LET = 5434 $\mathrm{MeVcm^2g^{-1}}$) we found very good agreement between theoretical predictions of the dose response curves and experiments except in the case of 42 MeV nitrogen ions, which were completely stopped in the film. For the nitrogen ions the difference between theory and experiment was greater than the experimental uncertainty at 95% confidence level.

The results indicated that the theory might not be applicable at low specific ion energies. We thus decided to investigate the energy range for application of the δ-ray theory by using a stack of very thin radiochromic dye films (nominally 5 μm thick) of the same composition as the nominally 55 μm thick ones as used previously. This work should indicate the specific ion energy below which the various approximations in the δ-ray theory break down.

2. Experimental

The radiochromic FWT-60 dye film consists of a form of nylon $(C_{12}H_{22}N_2O_2)_n$, which contains approximately 10% of a colourless radiochromic dye precursor hexahydroxyethyl pararosaniline leucocyanide $(C_6H_4N(C_2H_4OH)_2)_3C\text{-}CN$ which attains a blue colour upon irradiation with exciting or ionizing radiation [15]. The dye formed has a broad optical absorption band with a maximum at 604 nm. The dose meter response is expressed as increase in optical density per unit film thickness, ΔOD/mm, measured at 604 nm.

The actual film thickness varied from 4–8 μm, but in the case of 21 MeV ^{7}Li ions a 53 μm thick film was used in the stack due to the longer penetration depth of this ion. The thicknesses were measured individually with an electronic transducer gauge unit, and the optical densities were obtained in a recording spectrophotometer designed to read spatial variations in optical density across the field.

The stopping power of the ions in the film was calculated from published stopping power data for protons [16] as $S(z_{eff},\beta) = S(z_p,\beta)(z_{eff}/z_p)^2$. $S(z_{eff},\beta)$ is the stopping power of the ion with atomic number Z moving at a velocity β relative to the velocity of light.

$S(z_p,\beta)$ is the stopping power of a proton moving at the same velocity, and z_{eff} and z_p are the effective charges of the ion and the proton, respectively, calculated from the formulas of Ziegler [17]. In order, however, to fit with experimental stopping power data [18,19], z_{eff} for ^{7}Li ions in hydrogen was calculated by means of the specialized expression for lithium ions as proposed by Ziegler [17] only at energies above 0.15 MeV/amu, whereas the general expression for z_{eff} for all ions was used below this energy. The stopping power for the ions in the film material was calculated by Bragg's additivity rule [20] from the weight fractions of the atoms (H, C, N, and O) constituting the detector. The reference low-LET radiations were γ-rays from a ^{60}Co source with a dose rate of 14 Gy s^{-1} and 10 MeV electrons from a linear accelerator with an average dose rate in the pulse of 5×10^7 Gys^{-1}, while the high-LET radiations were beams from a tandem Van de Graaff accelerator with dose rate of approximately 10^3 Gys^{-1}. By calculating an average dose rate in the track of the moving ion in the 55 μm film, a dose rate of approximately 10^7 Gys^{-1} and 10^8 Gys^{-1} is obtained for the ^{7}Li- and ^{16}O ions, respectively. Detailed description of the irradiation technique for low- and high-LET radiations has already been published [4].

The determination of dose of the low-LET radiations has an uncertainty within 2%, and the precision of the low-LET dose-response measurements is 14.3% (total random uncertainty at 95% confidence level [21]) determined from the uncertainty associated with the individual measurements involved in an experimental data point. The precision of the dose-response measurements for ions is ±15.1% (determined as for the low-LET dose-response measurements). The uncertainty in the proton stopping power is less than 1% for energies above 400 keV and approximately ±10% for lower energies [16], and the method of calculating the stopping power for the ions in a compound material may introduce an error of about 10% [22]. While the expression for the effective charge of the ions is an empirical fit relating stopping power of protons to experimental stopping power data of heavy ions of the same velocity, the expression is used as well in the δ-ray energy distribution formula for which we do not really know its applicability. With reference to calculated and measured ranges of the ions (see next section), the uncertainty of the absolute energy of the ion as a function of residual range is considered to be less than the stated error on stopping power. Based on these considerations the overall uncertainty at 95% confidence level of experimental RE values is ±18.7% calculated as

$$U = \left(\sum_i x_i^2 + 1.13 \sum_i x_i^2 \right)^{1/2},$$

where x_i is the random uncertainty and x_i is the estimated maximum systematic error of the individual data points.

3. Results

The dose-response characteristics of the 5 μm thick dye film to low-LET radiations of ^{60}Co γ-rays and 10 MeV electrons are shown in fig. 1. The end-point considered is the colouration of the film measured as change in optical density per unit film thickness at 604 nm, which is the wavelength at maximum absorption. At doses below 30 kGy the response is identical for the two radiation qualities, while at higher doses the response to 10 MeV electrons is higher than to ^{60}Co γ-rays. This is in correspondence with observations made for the 55 μm thick FWT-60 film measured at 510 nm and the effect is ascribed to the difference in dose rate [15]. The low-LET dose-response curves of the 5 μm and 55 μm thick films measured at 604 nm are parallel up to doses that cause optical densities above the measuring range of the photospectrometer. For the 55 μm thick films the wavelength at 510 nm was chosen to allow studies of the film at very high absorbed doses [15].

For calculation of the activation cross-sections of colour formation in the film the curves in fig. 1 may be described by the expression $\Delta OD/mm = (\Delta OD/mm)_{max}(1 - \exp(-D/D_{37}))^{0.94}$, which does not correspond to an ideal one-hit detector as described by the classical target theory. The exponent of 0.94 does not reflect the hit-number, which must be an integer, but is rather a parameter which takes into account nonlinearity of the detector due to fading or recombination

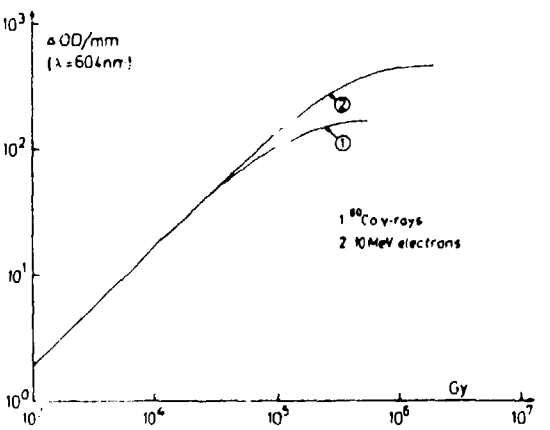

Fig. 1. Dose-response curves for a thin (nominally 5 μm) radiochromic dye film FWT 60-20 irradiated with ^{60}Co γ-rays and 10 MeV electrons with a dose rate of 14 and 5×10^7 Gy s^{-1}, respectively. The optical density is measured at the wavelength of 604 nm

effects or possible radiation damage of latent leuco centers. The observed D_{37}-value and maximum response were 110 kGy and 165, respectively, for ^{60}Co γ-rays, and 330 kGy and 480 for 10 MeV electrons. The D_{37}-value measured at 604 nm for the 5 μm thick film irradiated with ^{60}Co γ-rays is identical to the value for the 55 μm thick film measured at 510 nm.

The average absorbed dose in the thin dye films irradiated in stacks with 3 MeV/amu ^{7}Li and 4 MeV/amu ^{16}O ions is shown in figs. 2a and b as a function of depth and ion energy. Curve number 1 shows the dose determined from the measured optical density and the low-LET calibration curve in fig. 1. For comparison curve number 2 shows the dose calculated from the stopping power and particle fluence. The error bars indicate 95% confidence level of experimental values. The penetration depth calculated from the continuous slowing down of the ion taking nuclear stopping into account is 107 and 77 μm for 3 MeV/amu ^{7}Li and 4 MeV/amu ^{16}O ions, respectively. The measured range taken as the depth at the center of the last film in the stack giving a response significantly different from zero is 108 and 73 μm for ^{7}Li and ^{16}O ions, respectively.

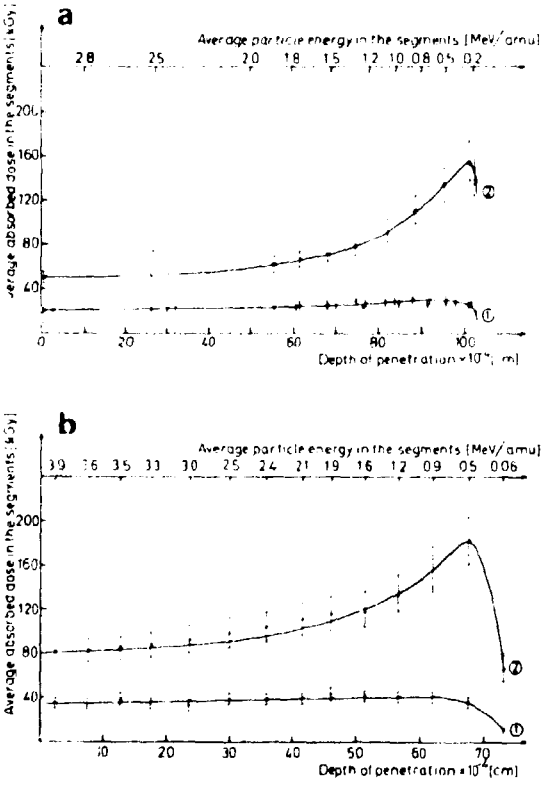

Fig. 2. (a) Average absorbed dose in the FWT 60-20 film segments as a function of penetration depth and energy of ^{7}Li ions with an initial energy of 21 MeV, curve 1: measured from film response and low-LET dose-response calibration curve; curve 2: calculated from LET_∞ and particle fluence. Bars indicate 95% confidence level. (b) Average absorbed dose in the FWT 60-20 film segments as a function of penetration depth and energy of ^{16}O ions with an initial energy of 64 MeV, curve 1: measured from film response and low-LET dose-response calibration curve; curve 2: calculated from LET_∞ and particle fluence. Bars indicate 95% confidence level.

Theoretical values of the relative effectiveness (RE) of the two ion beams relative to 10 MeV electrons have been calculated using D_{37} = 330 kGy and a radius of the radiation sensitive element, a_0, equal to 10^{-7} cm. In the calculations the calibration curve for 10 MeV electrons is used since the dose rates for the high-LET beams and the electron beam are comparable [4]. A difference in response at saturation doses for the film irradiated with ^{60}Co γ-rays and 10 MeV electrons is ascribed to the dose rate, since an intermediate product is formed upon irradiation [15]. This intermediate is over a time scale of some hours transformed into the coloured dye and may participate in back reactions, if the exposure is prolonged as for ^{60}Co γ-irradiations, where several hours of exposure are needed at the highest dose level. The value of a_0 is chosen as it already has been shown [4] to give a good fit to experimental data for the 55 μm films exposed to 3 and 16 MeV protons, 10 MeV α-particles, 21 MeV ^{7}Li, and 64 MeV ^{16}O ions. Experimental and theoretical values are shown in figs. 3a and b for the two ions as a function of the average LET in the stacked dye films and indicate deviations between experimental and theoretical RE values at low ion energies. For ease of comparison the ratio of calculated to experimental RE values is given in fig. 4 both for ^{7}Li and ^{16}O ions as function of the specific energy of the ions. Also indicated is the 95% confidence level for a ratio of unity independent of the energy.

Due to the longer penetration range of the ^{7}Li ions a similar 53 μm thick dye film was interspersed in the beginning of the dye film stack irradiated with 3 MeV/amu ^{7}Li ions. The measured and calculated RE value for this film agreed with previous work [4] within 5% taking a slight change of RE into account as due to a difference in stopping power values used in the two investigations. Similarly for the first 53 μm of the ^{16}O stack the experimental and theoretical RE agreed both with previous data and with each other within 5%.

The radial dose distribution used in the present investigation is given by

$$D(z,\beta,t) = \frac{C}{2\pi}\frac{z^2}{\beta^2}\frac{1}{a}\frac{1}{t^2}\left[1-\frac{t}{t_{max}}\right]a^{-1}$$

for $a_0 = 0$. This is the expression for the point-target dose distribution, where t is the distance from the ion path, while the other parameters have been discussed above. The average value of dose to the sensitive elements is found from averaging the point-target dose expression over the size of the sensitive element. A

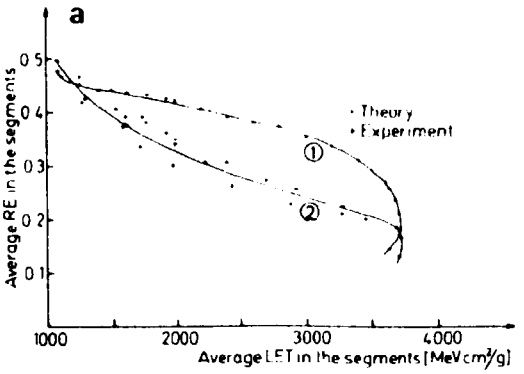

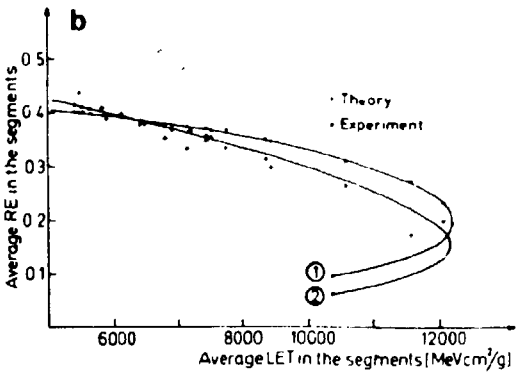

Fig. 3. (a) Average relative effectiveness (RE) in the FWT 60-20 film segments as a function of average LET_∞ of ^7Li ions with an initial energy of 21 MeV, curve 1: calculated from theory; curve 2: measured from film response and low-LET calibration curve. (b) Average relative effectiveness (RE) in the FWT 60-20 film segments as a function of average LET_∞ of ^{16}O ions with an initial energy of 64 MeV, curve 1: calculated from theory; curve 2: measured from film response and low-LET calibration curve.

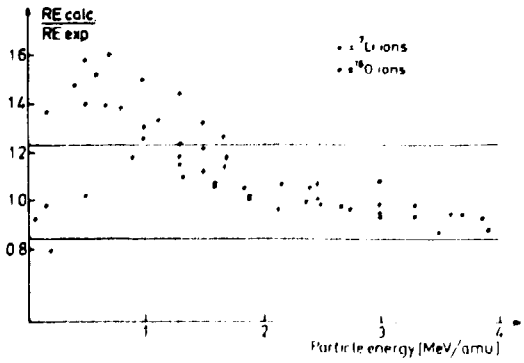

Fig. 4. Ratio of calculated to experimental RE values as a function of the specific energy of ^7Li and ^{16}O ions. Solid lines indicate the 95% confidence level of the data for a ratio of unity independent of the energy.

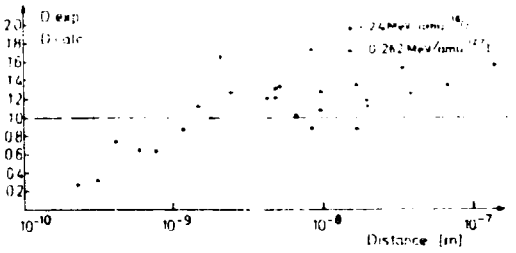

Fig. 5. Ratio of experimental [12] to calculated dose as a function of the distance from the particle track of a 2.4 MeV/amu ^{16}O ion and a 0.262 MeV/amu ^{127}I ion.

detailed description may be found elsewhere [4].

The accuracy of the point-target dose expression has been investigated by calculating radial dose distributions in tissue-equivalent unit-density gases for 0.262 MeV/amu ^{127}I and 2.4 MeV/amu ^{16}O ions and comparing the calculations to experimental data of Baum et al. [6]. This comparison has as well been made for 0.53 MeV/amu ^{79}Br ions of Varma et al. [7].

The ratio of experimental to calculated doses as a function of the distance from the particle track is shown in fig. 5. In the experiments the effective charge was calculated from the formula of Nikolaev and Dmitriev [23]. The formula given by Ziegler [17] gives almost identical z_{eff} for 2.4 MeV/amu ^{16}O ions but about 10% lower z_{eff} for ^{127}I. This difference has been corrected for in the calculations shown in fig. 5.

The two parameters in the theory D_{37} and a_0 have been varied from the stated values of 330 kGy and 10^{-7} cm, respectively. A reduction of D_{37} will lead to a decrease in calculated RE values. The decrease in RE will be slightly lower at high specific energies (> 2 MeV/amu) than at low energies (< 1 MeV/amu), but the difference was not sufficient to obtain a significantly better correlation between experiment and theory than shown in fig. 4. The effect of changing the size of the sensitive element a_0 is more complicated since it depends on the stopping power, and it has not been possible to obtain better agreement between theory and the present experimental results by varying a_0.

4. Discussion

The experimental technique used in the present investigation is very similar to that used with 55 μm thick films [4], but there are differences which may be of importance. The films are irradiated in stacks, the optical density is measured at the absorption maximum at 604 nm instead of 510 nm as used with the 55 μm films, and the dye content of the thin and thick films might be slightly different. The various tests reported for com-

parison show that the thin and thick films give identical results and that conclusions drawn from experiments with thick films may be used on thin films as well.

In the previous work [4] too high calculated RE values were found for the stopping 3 MeV/amu ^{14}N ions corresponding to a ratio of calculated to experimental RE values above unity. The data shown in fig 4 give an explanation of this finding since this ratio is considerable above unity at energies below 1.5 MeV/amu. 1.5 MeV/amu is just the residual energy of 4 MeV/amu ^{16}O ions after passage of a 53 μm thick dye film, and thus the effect was not observed for 4 MeV/amu ^{16}O ions in our previous work. It must be mentioned here that the calculation of RE-values are only valid for the linear part of the dose-response characteristic where overlap of the tracks is negligible. The leveling-off of the response at high doses is due to overlapping tracks.

As outlined in the introduction the relative effectiveness is calculated from a convolution of a probability function into a radial dose distribution. This dose distribution is in good agreement with experimental data for 0.262 MeV/amu ^{127}I and 2.4 MeV/amu ^{16}O ions as shown in fig. 5. The larger discrepancy for 2.4 MeV/amu ^{16}O data is partly due to the experimental data being approximately 20% too high due to a too high assumed value for W as discussed by Baum et al. [6]. Below 1 nm experimental data are too low due to lack of charge equilibrium. Previous calculations of radial dose distributions using the present method [4] have shown to be in good agreement with experimental and theoretical data for 0.53 MeV/amu ^{79}Br ions [7] and theoretical calculations for 2 MeV/amu ^{12}C ions [24].

The good agreement between calculated and experimental radial dose distributions for 0.262 MeV/amu ^{127}I ions, 0.53 MeV/amu ^{79}Br ions, and 2.4 MeV/amu ^{16}O ions indicates that in spite of simplified assumptions mentioned in the introduction, the procedure yields reasonable results in the energy range considered in the present work.

The present δ-ray theory assumes that all δ-rays are ejected perpendicular to the ion path. The angular distribution has been observed [2,25] to be nearly isotropic for low-energy δ-rays, while higher-energy δ-rays are ejected at an angle of approximately 45–60° to the ion path. This observation is equivalent to an increase in dose close to the ion path relative to calculations. The deviation of the energy distribution from the Bethe δ-ray energy distribution formula becomes important at δ-ray energies below 30 eV according to Wilson and Toburen [25]. In this energy region the chemical composition of the target material also plays a role. This effect will have a big impact on dose distribution only at very low specific ion energies.

The range-energy relation used, $r = k\omega^n$, underestimates the range of low-energy δ-rays at energies below 200 eV according to Waibel and Grosswendt [26] and Ashley [27]. This implies a too high calculated dose close to the track. The good agreement between calculated and experimental dose distributions indicates that the various approximations involved in our calculations only have a minor influence and that these three effects taken together to some extent cancel each other.

The effective charge of the ion has a strong influence on the dose distribution since the dose is proportional to the square of z_{eff}. z_{eff} may be calculated from different formulas [17,23,28,29] giving widely varying results below 2 MeV/amu. The z_{eff} used in the present work in combination with stopping power for protons yields ion stopping power data which are in good agreement with experimental stopping power data for ^{7}Li ions down to 80 keV/amu and for ^{16}O ions down to 200 keV/amu in solid media. Despite its frequent application, the procedure of using the effective charge is rather problematic, since there are several effective charges to be discriminated among in this context, e.g. effective charge for stopping power calculations, charge distribution after passage of the ion through the medium, and effective charge for emission of secondary electrons. The empirical expression used in this work is a versatile description of effective charge independent of the kind of stopping medium. The expression, however, has been developed in order to describe stopping power of a penetrating ion and may not necessarily describe accurately the effective charge to be used in the expression for dose deposition from δ-rays ejected by the ion.

The good agreement between calculated and measured range of the ions implies that no large errors are present in the LET calculations though the Bragg additivity rule is used for determination of the LET of the compound material. Above 80 keV/amu for ^{7}Li ions and 200 keV/amu for ^{16}O ions, LET of the individual material components is stated to be accurate within 5% [17–19]. A larger uncertainty below 200 keV/amu will have little influence on the total range, but will have a large effect on the calculated and experimental RE values. A shift in position of 1 μm for a 5 μm film placed with the center corresponding to 180 keV/amu of a ^{7}Li ion will change the calculated RE by 20%. Such a shift may be introduced both by the LET calculations and by measurements of the film thicknesses.

Fig. 4 shows that deviation between theory and experiments above what may be ascribed to the experimental uncertainty is observed both for ^{7}Li and ^{16}O ions below approximately 1.5 MeV/amu. Since the calculated radial dose distribution appears to give reasonable fits to experimental data at both high and low specific energies, this deviation points to that the effect is due to the crucial assumption in the theory that the response of the detector to the δ-ray spectrum is equivalent to the response from the slowing-down spectrum of high-energy electrons from low-LET radiations of either

fast electrons or ^{60}Co γ-rays. Ettinger [30] reported a RE of 0.88 and 0.92 for ^{3}H and ^{14}C β-rays in sucrose compared to ^{60}Co γ-rays, while the low energy Auger electrons from the ^{125}I isotope had an even lower RE of 0.66. At low energies B' increases [26] which will lead to a decrease in effectiveness for a detector more sensitive to ionizations than to excitations. Variations of the two parameters D_{37} and a_0 are not able to reconcile the calculations with the experimental data. RE at low ion energies (< 1.5 MeV/amu) cannot be decreased by choosing appropriate values of D_{37} and a_0 without decreasing RE at higher ion energies where theory and experiments are in very good agreement.

D_{37} has previously [31] been observed to vary with the dose rate. This is due to various competing reactions occurring only at very high absorbed doses [15] as has also been observed in some amino acids [32]. In a previous study [15] of the 55 μm thick dye film the saturation optical density has been found to be dependent on the average dose rate in the track of the heavy charged particles as well as on dose rate in low-LET irradiations. At doses below the saturation range no dose rate dependency has been observed. A change in response at saturation doses changes the D_{37} value accordingly and leads to D_{37} values of 300 and 310 kGy to be used in the calculations of relative effectiveness for the ^{7}Li and ^{16}O ions, respectively. Better agreement, however, between theory and experiment cannot be obtained using other values of D_{37}.

5. Conclusion

The results of the present investigation show considerable deviation between predictons based on the δ-ray theory for track structure and experimental data for ^{7}Li and ^{16}O ions in the radiochromic dye film at energies below 1.5 MeV/amu. Above 1.5 MeV/amu theoretical and experimental data agree within the experimental uncertainty over a large range in LET as has been found previously [4] for the radiochromic dye film.

The observations made point to that deviation between theoretical and experimental data for relative effectiveness is not associated with the LET of the particles or with calculations of radial dose distribution around the ion path, but should merely be found in the assumption of equivalence in radiation effect of the δ-ray spectra and the spectra from the low-LET ^{60}Co γ-rays. The usefulness of the δ-ray theory in predicting the dose-response of physical detectors irradiated with heavy charged particles could be improved by including the dose-response from low-energy electrons in the actual detector.

References

[1] R. Katz, S.C. Sharma, and M. Homayoonfar, in: Topics of radiation dosimetry, Supplement 1, ed. F.H. Attix (Academic Press, New York, 1972) p. 317.

[2] L.H. Toburen and W.E. Wilson, J. Chem. Phys. 66 (11) (1977) 5202.

[3] J. Fain, M. Monnin, and M. Montret, Rad. Res. 57 (1974) 379.

[4] J.W. Hansen and K.J. Olsen, Rad. Res. 97 (1984) 1.

[5] H.A. Bethe and J. Ashkin, in: Experimental nuclear physics, ed., E. Segre, Vol. 1. (John Wiley and Sons, New York, 1953) p. 166.

[6] J.W. Baum, M.N. Varma, C.L. Wingate, H.G. Paretzke, and A.V. Kuehner, 4th Symp. on Microdosimetry, Pallanza, eds., J. Booz, H.G. Ebert, R. Eickel and A. Waker, Vol. 1, EUR 5122 (1973) p. 93.

[7] M.N. Varma, J.W. Baum, and A.V. Kuehner, Phys. Med. Biol. 25 (4) (1980) 651.

[8] H. Sørensen and J. Schou, J. Appl. Phys. 49 (10) (1978) 5311.

[9] A. Cole, Rad. Res. 38 (1969) 7.

[10] T.E. Everhart, and P.H. Hoff, J. Appl. Phys. 42 (1971) 5837.

[11] P.D. Holt, Proc. of 2nd L.H. Gray Conference, Cambridge (Institute of Physics and the Physical Society, Conf. Series No. 8, 1969).

[12] H. Dertinger and H. Jung, Molecular radiation biology (Springer Verlag, New York, 1970) ch. 5.

[13] K. Günther and W. Schultz, Biophysical theory of radiation action (Akademie-Verlag, Berlin, 1983) ch. 1.

[14] M. Marshall, J.A.B. Gibson, and P.D. Holt, Int. J. Radiat. Biol. 18 (2) (1970) 127.

[15] J.W. Hansen, M. Wille, and K.J. Olsen, Radiat. Phys. Chem. 23 (4) (1984) 455.

[16] H.H. Andersen and J.F. Ziegler, Hydrogen stopping powers and ranges in all elements, vol. 3 of The stopping and ranges of ions in matter, (Pergamon Press, New York, 1977).

[17] J.F. Ziegler, Handbook of stopping cross-sections of energetic ions in all elements, vol. 5 of The stopping and ranges of ions in matter (Pergamon Press, New York, 1980).

[18] H.H. Andersen, F. Besenbacher and P. Goddiksen, Nucl. Instr. and Meth. 168 (1980) 75.

[19] H.H. Andersen, F. Besenbacher, and H. Knudsen, Nucl. Instr. and Meth. 149 (1978) 121.

[20] W.H. Bragg and R. Kleeman, Phil. Mag. 10 (1905) 318.

[21] IAEA, Calibration of dose meters used in radiotherapy, Technical Report Series No. 185 (IAEA, Vienna, 1979).

[22] D.I. Thwaites, Rad. Res. 95 (1983) 495.

[23] V.S. Nikolaev and I.S. Dmitriev, Phys. Lett. 28A (1968) 277.

[24] J. Fain, M. Monnin, and M. Montret, 4th Symp. on Microdosimetry, Pallanza, eds., J. Booz, H.G. Ebert, R. Eickel and A. Waker, Vol. 1, EUR 5122 (1983) p. 169.

[25] W.E. Wilson and L.H. Toburen, 7th Symp. on Microdosimetry, Oxford, eds., J. Booz, H.G. Ebert and H.D. Hartfield, Vol. 1 (Harwood, London, 1980) p. 435.

[26] E. Waibel and B. Grosswendt, Nucl. Instr. and Meth. 211 (1983) 489.

[27] J.C. Ashley, Rad. Res. 90 (1982) 433.
[28] W.H. Barkas, Nuclear Research Emulsions, Vol. 1, (Academic Press, New York, 1963).
[29] L.C. Northcliffe and R.F. Schilling, Nucl. Data Tables, A7 (Academic Press, New York, 1970) 233.
[30] K.V. Ettinger, S. Srirath, C.J. Anunuso, and J.R. Mallard, 7th Symp. on Microdosimetry, Oxford, eds., J. Booz, H.G. Ebert, and H.D. Hartfield (Harwood, London (1981) p. 1389.
[31] W.L. McLaughlin, R.M. Uribe, and A. Miller, Radiat. Phys. Chem. 22 (3–5) (1983) 333.
[32] W. Snipes and P.K. Horan, Rad. Res. 30 (1967) 307.

Sales distributors:
G.E.C. Gad Strøget
Vimmelskaftet 32
DK-1161 Copenhagen K, Denmark

Available on exchange from:
Risø Library, Risø National Laboratory,
P.O.Box 49, DK-4000 Roskilde, Denmark

ISBN 87-550-1049-0
ISSN 0106-2840